11-1-2022

Polymer Mimetics for Soil Modeling and Detection of Biomarkers

Md Ragib Hasan
Louisiana State University and Agricultural and Mechanical College

POLYMER MIMETICS FOR SOIL MODELING AND DETECTION OF BIOMARKERS

A Dissertation

Submitted to the Graduate Faculty of the
Louisiana State University and
Agricultural and Mechanical College
in partial fulfillment of the
requirements for the degree of
Doctor of Philosophy

in

The Department of Chemistry

by
Md Ragib Hasan
BS, University of Dhaka, 2014
MS, University of Dhaka, 2016
December 2022

To my family

Mother Habibun Nahar

Father Md Delwar Hossain

Sister Ayesha Zerin

Acknowledgments

First, I would like to express my deepest appreciation to my advisor, Dr. David Spivak, for providing me with consistent direction, unparalleled support, valuable advice, and belief in me during my doctoral studies. Without his skilled and inventive advice, as well as his compassion, kindness, and patience, it would be impossible for me to triumph over the challenges that I faced in my research.

I would like to extend my gratitude to Dr. John Pojman, Dr. Robert Cook, and Dr. Aixin Hou, whom I am honored to have on my committee. Dr. Cook's guidance on the collaborative soil project and Dr. Pojman's resourceful polymer class helped me a lot. I would like to thank Dr. Thomas K Weldeghiorghis for the assistance with solid-state NMR, Dr. Rafael Cueto and Dr. Kerry Dooley for their assistance with TGA, Dr. Fabrizio Donnarumma for MALDI-TOF MS analysis, and Dr. Carlos Astete for the assistance with HPLC.

I would like to thank my colleagues, Dr. Arjun Pandey, Dr. Ghada Abdalla, and Dr. Nicholas Gariano, for their help, mentorship, and constructive advice. I am thankful to my lab mate Harry Spencer for his continuous assistance. I would like to thank Dr. Benjamin Haywood, Dr. MP Hayes, and Dr. Emmanuel Ampiah for their assistance with the HPLC. I am thankful to the Chemistry department, especially to Ms. Kim Mollere for her continuous support and care.

Finally, I would like to convey my gratitude to my family and friends, especially my mother and father. I would never have been able to finish my studies without their unwavering support and motivation throughout the years.

Table of Contents

List of Tables

List of Figures

List of Schemes

Abbreviations

A_t	Adsorption percentage of test substance at a specific time t (%)
C_{aq}	Concentration of sorbate remaining in the aqueous phase (mg/L)
C_s	Concentration of sorbate present on the sorbent (mg/kg)
k'	Capacity factors
t_R	Retention time of the analyte
t_V	Void volume
AA	Acrylic acid
ABF	Acetylbenzylfentanyl
ACs	Agricultural Chemicals
APS	Ammonium persulphate
ARGET	Activators Regenerated by Electron Transfer
ATRP	Atom Transfer Radical Polymerization
BBF	Benzoylbenzylfentanyl
Bfen	Benzylfentanyl
CDC	Center for Disease Control and Prevention
CP	Cross-polarization
CRP	Controlled Radical Polymerization
DBU	1,8-diazabicyclo[5.4.0]undec-7-ene
DCM	Dichloromethane
DD	Dipolar decoupling
DEA	Drug Enforcement Agencies

DP_n	Degree of Polymerization
EGDMA	Ethylene glycol dimethacrylate
ELISA	Enzyme-linked immunosorbent assays
ESSs	Engineered Soil Surrogates
FAS	Fentanyl Analog Screening
FDA	Food and Drug Administration
FTS	Fentanyl Test Strip
GHG	Greenhouse gases
Gt	Gigaton
HOC	Hydrophobic Organic Compound
HPLC	High Performance Liquid Chromatography
ICAR	Initiators for Continuous Activator Regeneration
IF	Imprinting factor
IHSS	International Humic Substances Society
IMS	Ion Mobility Spectroscopy
K_F	Freundlich sorption coefficient
Koc	Organic carbon distribution coefficient (L/kg)
Kp	Distribution coeeficient (L/kg)
LFA	Lateral Flow Immunoassays
LOD	Limit of Detection
MAA	Methacrylic acid
m_{aq}	Mass of test substance remaining in solution after time t (µg)
MAS	Magic Angle Spinning

MBAm	N,N’-methylenebisacrylamide
MeCN	Acetonitrile
MIP	Molecularly Imprinted Polymer
m_o	Initial mass of test substance at the beginning of the experiment (µg)
m_s	Mass of test substance adsorbed on the soil after time t (µg)
NFP	Non-pharmaceutical fentanyl
NIPAAm	N-isopropylacrylamide
NMR	Nuclear Magnetic Resonance
NOM	Natural Organic Matter
OECD	Organization for Economic Cooperation and Development
PAMS	4-acetoxy-3-methoxy styrene
PAS	4-acetoxy styrene
PMDETA	N,N,N’,N’’,N’’-pentamethyldiethylenetriamine
RDRP	Reversible-Deactivation Radical Polymerization
SELEX	Systematic Evolution of Ligands by Exponential enrichment
SOC	Soil Organic Carbon
SOM	Soil Organic Matter
TFMAA	Trifluoromethacrylic acid
TGA	Thermogravimetric Analysis
TOF	Total Organic Fractions

Abstract

The population of the world is increasing day by day and is expected to reach 9.8 billion by the year 2050. The ever-increasing demand for agricultural products is putting an unprecedented strain on the world's soils as the human population continues to expand. Soil degradation caused by over-farming and the agrochemicals (fertilizers, pesticides, etc.) used in agriculture is a growing problem, although its causes remain murky. In addition, little is understood about the molecular-level interactions of substances that are subsequently introduced to soils, such as agricultural chemicals (ACs). Therefore, it is expected that these constraints may be circumvented by the synthesis of natural mimics of soil, known as Engineered Soil Surrogates (ESSs), to associate their bulk attributes with structure compositions. A series of polymeric ESSs were synthesized and the sorption behavior of Norflurazon as the ACs was observed and compared to the sorption behavior of a natural soil, Pahokee peat.

On the other hand, the world is currently dealing with the drug overdose epidemic mainly due to the illicit use of synthetic opioids, primarily fentanyl. More than 70000 people died due to fentanyl overdose in 2021, which is often mixed with other drugs such as heroin, cocaine, etc. with or without the knowledge of the end-users. Therefore, the detection of fentanyl by law enforcement agencies and end-users is of utmost importance. Molecularly Imprinted Polymer (MIP) based sensors can be a solution to this problem. A MIP was made by using methacrylic acid (MAA), and ethylene glycol dimethacrylate (EGDMA) as the functional monomer and cross-linking monomer respectively, and benzyl fentanyl as the target template. Binding sites that are complementary to the analyte in size and shape are revealed after the template has been removed. Selectivity studies comprising various drugs such as heroin, cocaine, and methamphetamine showed that the synthesized MIP can selectively detect benzyl fentanyl.

Finally, a molecularly imprinted hydrogel employing diffraction grating techniques was developed to detect microRNA. The hydrogels imprinted with the miR-21 DNA target were sensitive to the target sequence's reintroduction and selective among comparable nucleotide sequences.

Chapter 1. Comparison of the Sorption Behavior of Agricultural Chemical (AC) with Engineered Soil Surrogates (ESSs) and Real Soil (Pahokee Peat)

1.1 Introduction and Significance

1.1.1 Soil

Soil plays a vital role in the complex ecosystem of the world by providing around 98.8% of the global food supply.[1] Soil is also crucial for carbon storage, greenhouse gas control, flood mitigation, waste recycling, and pest regulation.[1, 2] It is a finite resource, and the soil type varies from location to location. As a consequence of attempts to boost food production while using less land per capita, the soil has become the most stressed of the earth's ecosystems. Agricultural practices have led to the transformation of a significant section of the landmass that comprises our planet. In fact, it has been estimated that about 37% of the land mass of our world is being used for agricultural purposes at present, and as much as 67% of that land mass is being used for combined agricultural purposes and grazing, which is now comparable to the area that is occupied by forests.[3] The reduction in the amount of land that is accessible for agricultural use is a consequence of the expansion of both urban and industrial areas (e.g., land for housing, roads, industrial and commercial buildings). Also, recent changes in land use include cutting down tropical forests to grow biofuels.[4] The rapid intensification of agricultural practices has led to unsustainable soil degradation, such as loss of organic matter, the release of greenhouse gases, overuse of fertilizer, pollution, and loss of biodiversity, which will eventually reduce the soil's long-term capability to serve humans and causes environmental damage.

Soil mainly consists of minerals, organic matter, water, air, and organisms.[5] Typically, soil contains small amounts of organic matter of about 5%, whereas it has 45% minerals, 20-30% water, and 20-30% air by volume.[6] The decay of living things contributes to the formation of soil organic matter (SOM), whereas the weathering of rocks on earth is responsible for the formation

of the mineral component of soil. Plants take in the nutrients that are generated as a byproduct of the breakdown of organic compounds. These nutrients are then taken up by animals and eventually returned to the soil via the process of decomposition. Soil is also home to a wide variety of organisms, including bacteria, fungi, etc.

1.1.2 Soil Air

The air in the soil is a direct descendant of the air in the atmosphere. In contrast to the other components, it is in a perpetual state of mobility, moving both into and out of the soil's pores and the air around them. This continual movement or flow of air inside the soil mass, which results in the regeneration of its component gases, is referred to as soil aeration.[7] The air in the soil has a greater concentration of carbon dioxide and a lower concentration of oxygen compared to the air in the atmosphere that is directly above it. For instance, one liter of dry air contains approximately 20.9% oxygen and 0.03% carbon dioxide, whereas a similar volume of aerobic soil contains approximately 18–20.5% oxygen and 0.3–3% carbon dioxide.[8, 9] In addition, unless it has become very dry, the soil will often maintain a humidity level of close to 100%. However, the concentrations of CO_2 and O_2 may shift a little depending on the water-filled porosity of the rock and the biological demand for oxygen from plant roots and other macro- and microbes. It is common for soil O_2 levels to drop while soil CO_2 levels rise when there is less air exchange between the soil and the atmosphere, as occurs in moist or compacted soils. Soil that has been properly aerated should contain enough oxygen and moisture for aerobic organisms to carry out their breathing processes (i.e., aerobes). For optimum microbial development in soil, the soil's pore space should be moistened by water to the tune of 50-60% (the remaining pore space should be air).[10] Modifications to soil aeration affect the microorganism population. Both oxygen and its absence are necessary for the growth of facultative anaerobes, but microaerophiles and obligatory anaerobes have different preferences and needs.[11] Soil microbial communities are very sensitive

to variations in aeration and may undergo dramatic shifts when conditions alter.

Aeration in the soil is very sensitive to soil conditions, especially soil porosity, soil moisture, and soil depth. Diffusion is influenced by both the texture and structure of the soil. Diffusion is slowed in soils with a high proportion of clay because clay has a fine texture. Larger holes will be introduced throughout the aggregation process, creating an optimal balance of pore sizes that improve gas diffusion. Aeration is high in sandy (coarse texture) soils because diffusion is quick in the comparatively wide pores around the bigger sand particles. The diffusion of oxygen via soil is also affected by the moisture content of the soil. In the air, oxygen diffuses at a rate of 0.198 $cm^2sec^{-1,}$ while in water, it diffuses at a rate of 1.9 x 105 cm^2sec^{-1}.[12] Simply said, the diffusion rate of O_2 via water is about 10,000 times slower than through air. Consequently, under respiration-favorable circumstances, CO_2 levels will increase, and O_2 levels will fall when pores are completely filled with water. Clay-rich soils are more likely to have poor aeration than sandy ones because of the increased quantity of tiny pores, which are more prone to be water-filled, particularly when weakly aggregated. The soil's aeration is also influenced by its depth. Oxygen content in soils often decreases with depth, particularly in clay-rich soils.[10]

1.1.3 Soil Water

In nutrient management, the right balance between soil water and soil air is very important since most processes that put nutrients into the soil need both water and air. In nutrient control, soil water is especially crucial. In addition to maintaining life on Earth, soil water contains dissolved nutrients that are immediately accessible for plant absorption. Therefore, it is essential to maintain adequate soil moisture levels.[13, 14]

The hydrogen bonding capabilities of water have a significant impact on how water is retained and distributed in soils. For example, water sticks to the minerals and SOM found in soil. Ion-dipole interaction causes water molecules to be drawn to the edges of minerals and the surfaces

of organic matter because these surfaces have negative charges.[9, 15] A thin layer of tightly adhered water molecules (about 1.7×10^{-3}% of particle diameter) known as hygroscopic water is the result of this rather strong contact.[16] This form of water cannot be used by plants since it never solidifies and is never labile as a liquid.[16] In a soil environment that is saturated with water, hygroscopic water is encased in an additional layer of water molecules, which are kept together cohesively by intermolecular forces of attraction. This water, which travels from one particle to another and is a readily accessible water supply in soils, is known as capillary water.[16] Capillary water is surrounded by gravitational water when there is an excess of water in the soil that is more than its optimal capacity. Typically, this kind of water will fill the larger pores in the soil, and it will then migrate downhill due to gravity or hydrostatic pressure.[14, 16] The soil's water holding capacity is determined by the size of the spaces between the soil particles and the capillary force that draws water into the soil. In sand, both the particles and the pores are big. However, the capacity to retain water is limited in materials with wide pores. This causes an overflow of water from sandy soils. Conversely, clay-based soils have microscopic particles and narrow pores. Clay soils often have a high-water retention capacity because their narrow pores are better able to store water. The Physico-chemical distribution of water in the soil acts as a hydration buffer, meaning that it mitigates the effects of circumstances in the soil that are either very dry or extremely inundated.

1.1.4 Soil Inorganic Matrix

In the soil, the inorganic or mineral components are formed by weathering of the rocks. There are two distinct kinds of particles found in the mineral component of soil. Primary particles are distinct individual particles, while secondary particles are the aggregation of those particles. Sand, silt, and clay are the three kinds of soil particles. The forms of soil particles vary greatly; as a result, they are classified based on their "effective diameter". The diameter of clay particles is less than 0.002 millimeters. The size limitations of sand and silt vary; however, the top limit of sand is 2 mm in

all cases. Greater than 2 mm diameter particles are classified as pebbles (2 mm to 7.5 cm), cobbles (7.5 to 25 cm), stones (25 to 60 cm), and boulders (>60 cm). These particles are often not regarded to be soil components due to their little impact on soil fertility and production. However, certain soils may have a significant proportion of stones.[17]

Minerals may be categorized as either "primary" or "secondary," depending on how they were formed. Primary minerals are those that crystallize directly from magma or lava during the solidification process, whereas secondary minerals are those that form from alterations to primary minerals or from resynthesis and recrystallization processes that occur during weathering.[17] Sulfides, oxides and hydroxides, halides, carbonates, nitrates, borates, sulfates, phosphates, and silicates are the most general chemical categories of minerals.[18] Silicon and oxygen are two of the most common elements in the Earth's crust and make up the bulk of most minerals. Consequently, silicates are by far the most common mineral found in earth's rocks.[17]

Primary minerals, such as metal oxides and oxyhydroxide-type minerals, have charges on their surfaces as a consequence of pH-dependent proton transfer reactions of surface O^{2-} and OH- sites in aqueous solutions. Examples include quartz (SiO_2), gibbsite ($Al(OH)_3$), and goethite (α-FeOOH).[18] Additionally, clays have both stable and fluctuating negative charges that provide ionic molecules with interaction sites. Similar to the aforementioned fundamental minerals, the edges of clays (such as aluminum oxides) have negative charges that change depending on pH and ionic strength.[19] Tetrahedral sheets, in which silicon is covalently coupled with four oxygens, and octahedral sheets, in which Al^{3+} is bound to O^{2-} or OH- ions in an octahedral configuration, alternately make up the layers of clay minerals.[9, 15] As an example, montmorillonite, a 2:1 type clay mineral with a chemical structure of $MO\text{-}7Al_2O_3\text{-}22SiO_2\text{-}nH_2O$, where M is either sodium or calcium, has two tetrahedral sheets and one octahedral sheet.[15] On the other hand, kaolinite is a

straightforward 1:1 mixture with the formula $Al2O_3$-$2SiO_2$-nH_2O (where n=0 or 2).[20] The "isomorphic substitution" process, which occurs during clay formation and involves the replacement of higher charge cations with lower charge cations (e.g., Mg^{2+}, Al^{3+}), results in the permanent negative charge in clays.[9] Unlike other clay minerals, kaolinite does not experience this kind of isomorphic replacement. The cation exchange capacity is correlated with the number of these negative charges in minerals and clays.[20] Therefore, the existence of persistent negative charges might encourage complexation and cation exchange, which aids in the adsorption of cationic contaminants.[15] However, because of charge repulsion, anionic organic contaminants are less likely to sorb on mineral surfaces and may consequently combine with nearby cations. Therefore, the following list of potential HOC sorption processes on mineral surfaces may apply: complexation of organocations; hydrogen bonding, in which a lone pair of oxygen serves as a proton acceptor; n-π bonding, in which oxygen's lone pair act as electron donors to aromatic pi systems lacking in electrons; and cation-π bonding, in which aromatic π act as electron donors.

1.1.5 Soil Organic Matter (SOM)

Soil organic matter (SOM) plays a large role in preserving the nutrients and water in the soil, which is crucial for microbial, plant, and animal life, as well as critical for maintaining soil fertility and long-term agricultural sustainability. The major component, approximately 60-70%, of SOM, which is known as humus, is a complex mixture of aliphatic and aromatic organic compounds formed by humification, chemical decay, transformation, and recalcitrant residues originating from the decomposition of plant, animal, and microbial materials at various stages.[21] The humus has three defined fractions, which are also known as humic substances: humic acid (water-soluble at pH above 2), fulvic acid (water-soluble at all pH conditions), and humin (not soluble in water at any pH value).[22] Humic and fulvic acids are typically similar in structure but vary in molecular weight and the content of elemental and functional groups.[23] Humic acids are higher molecular

weight organic materials with phenol, catechol, quinone, and sugar moieties, while fulvic acids are lower molecular weight than humic acids containing carboxyl, hydroxyl, phenolic, carbonyl, and quinone functional groups. On the other hand, humin, which makes up about 50% of the SOM, is mainly composed of aliphatic hydrocarbons such as those found in lipids, waxes, and carbohydrates.[24]

Plants consist of various tissues as well as different molecular components, i.e., approximately 15-40% cellulose, 10-43% hemicellulose, 25-40% lignin, 1-10% waxes, and lipids.[25] Sugars are one of the most important sources of organic carbon in soils because they are the biosphere's most common organic compounds as they are the basic components of all poly-saccharides: cellulose, hemicellulose (polyoses), starch, pectin, fructanes, glucanes, and chitin.[26] Lignin is the major contributor to aromatic moieties as its structure consists of covalently linked (alkyl-aryl ether and C-C) aromatic rings with -OH and -OCH_3 substitutions.

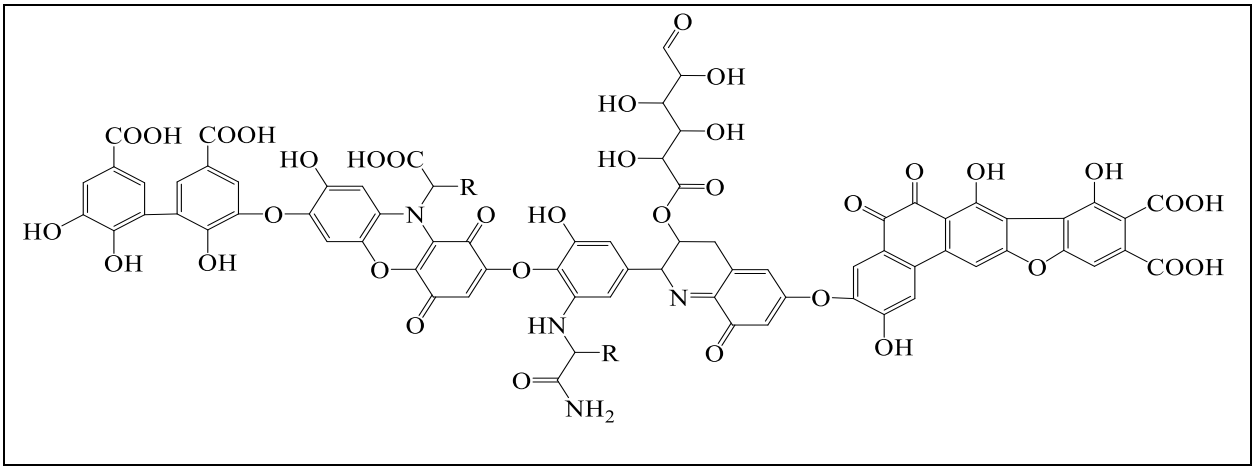

Figure 1.1. Model structure of humic acid.

Based on the chemical makeup of the SOM, it has been proposed that the hydrophilic moieties (sugar moieties) are in contact with the aqueous soil environment, whereas the hydrophobic moieties (aliphatic groups) are far from the aqueous soil environment. The interface between these two moieties contains aromatic moieties, which are both hydrophilic and

hydrophobic.[27] SOM has a significant impact on the sorption of pollutants such as herbicides, fertilizers, etc. SOM is also the storehouse of two-thirds of the global terrestrial carbon.[28] Thus, understanding the interactions of the SOM with pollutants and carbon-sequestration methods is of great interest from an agricultural and environmental viewpoint.

1.1.6 Climate Change, Agricultural Pollution, and Soil

A growing amount of attention is being paid all around the world to the connection between climate change and soil, and more specifically, SOM. Because it acts as both a carbon source and a carbon sink, soil organic matter (SOM) plays a significant part in climate change, even though its precise function in this regard is not completely known. In addition, the SOM helps to lessen the negative consequences of changing climate, such as the increased likelihood of floods and droughts caused by abnormal patterns of rainfall. SOM can hold up to twenty times its weight in water without losing that capacity.[29]

The climate of Earth is impacted by the atmosphere's make-up. Due to the fact that greenhouse gases (GHG) absorb infrared radiation, an increase in GHG concentration in the Earth's atmosphere is associated with a rise in global temperature, which in turn alters rainfall patterns across the world.[30, 31] Among the principal greenhouse gases (CO_2, CH_4, N_2O, O_3, H_2O, and chlorofluorocarbons), carbon dioxide and methane are the most abundant in the Earth's atmosphere. Additionally, methane is 21 times more powerful than carbon dioxide as a greenhouse gas. Consequently, it is of significant concern when human activities or processes result in excessive emissions of these two principal greenhouse gases. Annual GHG emissions are predicted to be 10 billion tonnes (10 Gt), with 15% attributable to land-use changes and the remainder attributable to the usage and production of fossil fuels.[32, 33] As a consequence of forest clearance and soil mechanical tillage, land use change often results in a depletion of carbon from soils and an increase in GHG emissions, particularly CO_2 and CH_4.[34]

Soil is the second largest place on Earth to store carbon after the oceans. It holds about 2-3 x 10^{15} kg of carbon in dead and living matter, about half of which comes from humic acids.[33, 35] Soil organic carbon accounts for around 1550 Gt of the whole soil carbon pool, whereas soil inorganic carbon accounts for roughly 950 Gt of the total soil carbon pool. When compared to the atmospheric C pool (760 Gt), the soil C pool is 3.3 times larger, while the biotic C pool is 4.5 times larger (560 Gt). The SOC pool at 1-meter depth varies from 30 to 800 tons/ha depending on climate, with the average being between 50 and 150 tons/ha.[36]

Thus, the soil has tremendous potential for application in climate change mitigation via the sequestration of atmospheric CO_2 and other greenhouse gases and the prevention of carbon release as powerful greenhouse gases. Due to the soil's abundance, even a little change in the carbon pool from the atmosphere to the soil in a given location may have a significant impact. An extra 1.85 Gt of carbon per year might be sequestered with careful management of the world's croplands. This is equivalent to the amount of carbon emitted annually by the whole transportation industry.[37] Since SOM acts as both a carbon source and carbon sink, it may play a significant role in moderating the growing levels of GHG in the atmosphere.

Since the establishment of an agrarian lifestyle between 10000 and 12000 years ago, the history of human cultures has been inextricably linked to the progress of agricultural techniques.[38, 39] The need to provide food for an ever-increasing population resulted in the extensive application of agricultural chemicals like fertilizers and pesticides to achieve crop yield increases. As the amount of land that could be used for crop production shrank, the use of such chemicals greatly contributed to gains in yields that were achieved on a per-hectare basis. In order to increase the nutritional density of the soil, significant amounts of fertilizers, including mineralized forms of phosphorous and nitrogen were applied. Because of agricultural runoffs, this type of fertilizer can

easily make its way to surface waters. This, in turn, can cause eutrophication or algal blooms, both of which can frequently lead to the death of fish in surface waters (such as streams, rivers, lakes, and fishponds).[40]

It has been demonstrated that the contamination of water with agricultural chemicals like pesticides can have negative effects on aquatic organisms. These negative effects on aquatic organisms can manifest themselves in a variety of ways, including decreased motility and fertility, as well as increased mortality.[41] When animals consume polluted food sources or drink from water systems that have been contaminated, there is a possibility that they may get ill.[42, 43] Moreover, pesticides may have an effect not only on the species for which they were designed but also on non-target creatures, which, in the end, has an impact on biodiversity. The ingestion of tainted water and food puts humans at risk of experiencing the negative effects of pesticides as well. There is growing evidence that some pesticides, including dichlorodiphenyl trichloroethane, atrazine, 2.4-D, and trifluralin, have the potential to operate as endocrine disrupters.[44] Exposure to pesticides has been linked to a variety of other negative health outcomes, including developmental toxicity, teratogenicity, pregnancy loss, neurologic effects, and cognitive disorders.[45, 46] Because of high stability, some agricultural chemicals are resistant to degradation by sunlight and soil microbes, making them difficult to eliminate from the environment. In addition, they may survive in soils for decades, if not longer. Therefore, it is important to study the chemical makeup of the soils and their various interactions with agricultural chemicals.

1.1.7 Agricultural Chemicals

The use of agricultural chemicals (ACs), especially fertilizers, probably started in the Neolithic era when humans began farming instead of the nomadic, hunter-gathering lifestyle. They used both organic and mineral fertilizers, including manure and wood ash. Multiple types of manure, as well as ashes, mud, marl, legumes, and similar things of natural origin, were used during the Roman

and Greek era.[47] In 1840, Justus Liebig set the groundwork for what would become the modern fertilizer business.[48] He was interested in how plants obtained the nutrients they required and what kinds of agricultural methods were most beneficial. The use of ammoniacal liquor from coal gas and the treatment of this liquor with gypsum to fix the ammonia; the use of wood ashes as fertilizer to supply potash, silica, and magnesia; the treatment of ground bones with sulfuric acid to improve the effectiveness of the phosphate and lime; and the ability of superphosphate to fix ammonia were all discussed by Liebig in his work on the chemistry of fertilizers. However, it has now come to light that others had independently come up with the notion of using sulfuric acid to cure bones before Liebig. As regular bone meal had previously failed to provide results, Englishman John B. Lawes tried this kind of fertilizer on an experimental field at Rothamsted in 1839. In 1842, Lawes was granted a patent for his innovation.[49]

Superphosphate was the most widely used kind of phosphorus fertilizer for almost a century. Besides phosphate rock and slag, manures, guano, and basic slag were also often used. Triple superphosphate, nitric and ammonium phosphates and thermal phosphates were among the other materials that had been developed.[48] Concurrently, with the emergence of the phosphorous (P) industry, the potassium (K) industry emerged. After World War II, the nitrogen (N) fertilizer industry, which had trailed so far behind P and K at the beginning of the 19th century, suddenly surged forward.[49] The modern nitrogen industry is predicated on the interaction between hydrogen and atmospheric nitrogen, which results in the production of ammonia. After this came the widespread use of artificial chemical additions as macronutrients (such as nitrogen, phosphorus, and potassium fertilizers), secondary nutrients (such as calcium, magnesium, and sulfur), and micronutrients (B, Cl, Cu, Fe, Mn, and Zn). Fertilizers are now available on the market as both single nutrients and combinations of several nutrients.

It is obvious that the crops that are cultivated will be afflicted with pests and illnesses, which will result in a significant decrease in output and the ever-present potential that the people may starve. Even with the gains that have been made in agricultural sciences, the percentage of potential food and fiber crops that are lost due to pests and diseases ranges from 10 to 90%, with the average being between 35 and 40%.[50] Therefore, there was a significant motivation to investigate potential solutions to the challenges posed by illnesses and insects. Around 4500 years ago, the Sumerians employed sulphur compounds to manage insects and mites. Around 3200 years ago, the Chinese used mercury and arsenical compounds to control body lice. This was the first time that the use of pesticides was documented.[50] Pyrethrum is an insecticide that has been used for over two thousand years. It is obtained by drying the blooms of the Chrysanthemum cinerariaefolium plant, which is also known as "Pyrethrum daisies." Since ancient times, several inorganic compounds have been employed as pesticides The Bordeaux Mixture, which is composed of copper sulfate and lime, is still used in the treatment of a variety of fungal illnesses.[50]

Prior to the 1940s, inorganic compounds like sodium chlorate and sulphuric acid, as well as organic chemicals obtained from natural sources, were frequently utilized in pest management. On the other hand, some pesticides were produced as unintended by-products of other industrial operations like the generation of coal gas. Thus, ammonium sulfate and sodium arsenate were utilized as herbicides, whereas nitrophenols, chlorophenols, creosote, naphthalene, and petroleum oils were used for fungi and insects. The high application rates, lack of selectivity, and phytotoxicity of several of these compounds constituted a major drawback.[50] When the effects of DDT, BHC, aldrin, dieldrin, endrin, chlordane, parathion, captan, and 2,4-D were discovered in the 1940s, the production and use of synthetic pesticides skyrocketed. DDT was the most widely used of these products because of its low cost and high efficiency.[50] Since Dr. Paul Muller

discovered DDT's insecticidal capabilities, he was awarded the Nobel Prize in Medicine in 1949. DDT was extensively utilized, seemed to have little toxicity to mammals, and decreased the incidence of insect-borne illnesses such as malaria, yellow fever, and typhus. Resistance to DDT in house flies was first documented in 1946, and the extensive use of DDT led to reports of damage to non-target flora and animals as well as residues.[50] The improper usage of the chemicals was responsible for some of the injuries, and Rachel Carson brought attention to these issues in her book Silent Spring, which was published in 1962.[42] This brought to light the potential issues that may arise from the indiscriminate use of pesticides and opened the way for the development of solutions that are both safer and less harmful to the environment. In subsequent decades, additional pesticides and herbicides were developed, including imidazolinone, dinitroanilines, aryloxyphenoxypropionate, cyclohexanediones, and glyphosphate, the most widely used herbicide in the world. It has been demonstrated that these new pesticides are less harmful to the environment and pose a lower risk of pest and weed resistance. However, there are a number of potential risks associated with the improper use of these ACs by farmers, their deposition in soil and surface water, and their eventual leaching into groundwater.[50]

Because of their toxicity, persistence, and potential for bioaccumulation, dichlorodiphenyl trichloroethane and a few other polychlorinated compounds were outlawed in the early 1970s. This led to an explosion of research into sorption, with a focus on hydrophobic chlorinated and brominated compounds. As a result, there has been an increase in the number of initiatives taken to manufacture agricultural chemicals and compounds of economic significance that are far less harmful than polychlorinated compounds. One of the results is a rise in the use and synthesis of fluorinated organic chemicals produced synthetically. Aromatic fluorinated chemicals have a broad range of uses, including pesticides and medicines.[51] As industrial waste products, aromatic

fluorinated compound mixtures also infiltrate the environment. As a result, organofluorine compounds have become common xenobiotics in the environment. Between 1980 and 1994, the number of organofluorine agricultural chemicals (AFCs) reached 9% of all ACs, and their production rate surpassed the non-fluorinated agricultural chemicals.[52] There were 9.0 million lbs of trifluralin, 1.2 million lbs of norflurazon, and 0.4 million lbs of acifluorfen used as the herbicide in 2002.[20]

1.1.8 Sorption of ACs in Soil and Previous Sorption Studies

The dynamic interaction that occurs during sorption involves a wide variety of chemicals (for example, ACs), water, and soil. In the environment, sorption is a significant factor that helps determine the bioavailability, transit, and ultimate destiny of ACs. Soil organic matter (SOM), silicate clay, and metal ions in the form of oxides and hydroxides are the primary sorbent components of soil. The sorption properties of a particular soil are very sensitive to variations in the quantity, surface area, and chemical composition of these three sorbents.[53] The physiosorption, which is essentially covalent in nature, is the primary mechanism by which the hydrophobic organic compounds are absorbed by the soil. This category includes hydrogen bonding, quadrupolar interactions, and Van der Waals forces.[18, 54]

A key factor in the distribution of hydrophobic, hydrophilic, and amphiphilic domains within SOM is water, which also functions as a dynamic medium for nutrient transport in soil. Polar domains of amphiphilic structures are localized near the interface of the SOM surface, whereas non-polar domains position themselves in a cluster to reduce their contact with water through hydrophobic interaction. The reduction in SOM's surface area, and hence the decrease in water entrapped in a solvation shell surrounding SOM, is the driving force behind this process, which increases the system's entropy.[55] Hydration has an impact on the sorption characteristics of SOM as well due to the high water holding capacity of SOM, which may keep as much water as

is equal to four times its weight.[9]

SOM is known to be rather malleable and conformationally versatile, depending on its hydration state. Hydrogen bonding with its polar moieties (e.g., -COOH, phenolic), metal-ion complexation, and structural rearrangements are hypothesized as noncovalent factors that allow an initially dry SOM to develop intimate and strongly cross-linked polar connections.[56, 57] It is hypothesized that when SOM is dry, its structure becomes stiffer, and the pore diameters inside it shrink. In order for these pores to open, the aforementioned cohesive forces holding the crosslinks together will need to be disrupted with sufficient energy and kinetic control.[57, 58] Therefore, sorbates cannot freely diffuse to sorption sites. Changing SOM's conformation is possible when the moisture content is increased to above 12%. The polar connections in SOM will become more permeable and flexible when water enters and solvates them, mostly via hydrogen bonding.[57] As a result, new sorption sites are formed. Water is expected to compete effectively for sorption sites; therefore, even under hydrated circumstances, the sorption of nonpolar organic solutes is reduced. Conversely, bipolar chemicals benefit from increased sorption because they may form robust noncovalent interactions with the hydrated SOM. On the other hand, when the water concentration is significantly higher than the saturation limit, water molecules again demonstrate competition for sorption sites, even for bipolar compounds.[56]

Significant factors influencing the activity, mobility, and transformability of AC include adsorption and desorption.[59] However, a molecular-level knowledge of sorption processes, the fate of ACs in various soils, and their sequestration through time is still unclear and debatable. In an effort to overcome this challenge and better comprehend the interactions between AC and soils, the Organization for Economic Cooperation and Development (OECD) produced the first artificial soil test substrate in 1984 to determine the toxicity of compounds toward earthworms. This test

substrate consists of 70% industrial sand (fines in the range of 50-200 microns), 20% kaolin clay (>30% kaolinite), and 10% organic material, which was suggested to be sphagnum peat with a pH close to 5.5-6.0.[60, 61] However, the natural origins of these components vary, resulting in compositional differences that influence sorption. This variability introduces uncertainty into the sorption-desorption behavior evaluation of AC. Bielska et al. demonstrated this when they tested the sorption of cadmium and phenanthrene to 21 artificial soils from various labs generated according to the OECD approach.[62] He showed that variations in phenanthrene sorption could not be well explained by measured soil parameters, even when the total organic carbon content was taken into account.

Instead of using the whole soil sample, humic acid fractions were used in an effort to reduce the SOM's molecular complexity and the potential complications caused by the soil mineral components. Ruggiero conducted his research on the sorption of acifluorfen at a variety of pH levels using two distinct varieties of humic acid standards.[59] He came to the conclusion that the maximum adsorption was seen at pH values that were somewhat near to the pKa of the AC. Both sorption isotherms were nonlinear and had distinct forms, which indicated that the process of sorption was not a straightforward case of partitioning but rather a more complicated one. The various forms of the isotherms demonstrated that other chemical and physical conformational features influence affinity to the same substrate. On the other hand, there was no information concluded concerning the nature of retention relationships or their strength. Martin-Neto used spectroscopic techniques to explore the process of atrazine sorption in humic acids. He came to the conclusion that hydrogen bonding, proton transfer (at low pH), and perhaps hydrophobic bonding mechanisms take place between atrazine and humic acid.[63] The sorption of naphthalene and phenanthrene was investigated by Xing using six distinct humic acid samples taken from

single soil profiles of varying depths. After fitting the data into the Freundlich equation, it was found that all of the isotherms were nonlinear, as indicated by the N values.[64] The aromaticity of the humic acid samples had an increasing effect on the level of nonlinearity. The findings of Xing and colleagues were consistent with the dual-sorption paradigm, which states that partitioning may take place in both extended (flexible) and condensed (rigid) moieties but that nonpartitioning processes can only take place in condensed moieties, which leads to nonlinearity. The sorptive capacity of phenanthrene in humic acids derived from three distinct sources as well as structurally modified humic acids was investigated by Gunasekara.[65] The humic acid was modified by bleaching, which removed hard aromatic moieties, and hydrolysis, which removed flexible carbohydrate moieties. He found that hydrolyzed samples were higher in aromatic moieties and displayed more nonlinear sorption behavior than bleached samples, which were higher in mobile moieties. However, employing these standards of humic acids has its drawbacks, and isolating these standard fractions of SOM may cause the bonds that give SOM its physical structure to be broken. Isolating these standard fractions also overlooks the other components that make up the whole SOM.[66] Atrazine, an organic pesticide, was studied for its sorption behavior on inorganic components like silica and was shown to exhibit nonlinear sorption isotherms.[67] SOM is similar to polymers because humic compounds, like rubbery and glassy polymers, have extended and condensed moieties.[68] Guo and colleagues have used SOM models made of synthetic homopolymers to study the impact of physical conformation on AC sorption, and they have also shown a correlation between the chemical content of synthetic polymers and sorption.[69]

1.1.9 Significance

The complex nature of the soils, along with various unknown and uncontrollable factors, makes analytical studies of soils very challenging. Because of this, comprehensive molecular knowledge of structure/property correlations relevant to soil studies that bridge cutting-edge biochemical and

macromolecular studies is currently beyond reach. Research into the destiny and distribution (e.g., bioavailability) of organic pollutants in soil, such as hydrophobic organic compounds (HOCs) that include agricultural chemicals, is presently based on the characterization of the bulk characteristics of natural soils and the linkage of bulk parameters to the observational data through empirical findings. The quantity of SOM is directly correlated with the sorption capacity for ACs, according to preliminary research.[70] After this discovery, investigations based on the association of additional factors, including oxygen content or polarity indices of SOM based on elemental ratios,[101,102] on sorption capacity followed.[71-73] Several investigations using isotherm-based assessments of non-linear and competitive sorption have shown a correlation between aromatic concentration and sorption capacity of HOC.[68, 74, 75] Nonetheless, aliphatic moieties have also been shown to have a role since identical isotherms have been identified in investigations with soil containing predominantly aliphatic NOM.[58-60, 65, 76] Although these studies are helpful for broad classification of soil and, to a lesser degree, for predicting soil attributes based on bulk characterization, a full mechanistic understanding of the molecular level interactions of soil with HOCs is absent.

To sustain the fertility of soils and to develop sustainable and environmentally friendly agricultural practices, it is important to study the interactions and sorption behavior between anthropogenic compounds and soils. The problem of soil complexity in sorption studies can be solved by the development of soil surrogates, referred to as Engineered Soil Surrogates (ESSs), to mimic the functional structure of the soil. Therefore, the goal of the study was to synthesize a series of ESSs through various techniques such as atom transfer radical polymerization (ATRP), hydrosilylation, grafting reactions, etc. Subsequent observation of the sorption behavior of agricultural chemical (AC), in this case, Norflurazon, on the synthesized ESSs is then possible, and finally, the results can be compared with that of a real soil such as Pahokee peat.

1.2 Design and Synthesis of Engineered Soil Surrogates and Comparison of Sorption Behavior

1.2.1 Engineered Soil Surrogates (ESSs)

The fundamental purpose of the Engineered Soil Surrogate (ESS) synthesis is to recreate, on a controlled and scalable basis, the molecular level composition of the organic matter found in the soil by using a chemical structure that is both straightforward and well-defined. In order to accomplish this goal, the chemical constituents of the building blocks were selected on the basis of previously developed models of SOM, but with some generalizations.[33, 36, 77] On the basis of these models, three primary groups of chemical moieties, namely polar domains, alkyl domains, and O-aryl domains, were deemed to be the fundamental components of SOM. The hydrophobic domains are represented by the alkyl components, while the hydrophilic domains are represented by the polar groups. Because the polarity of aryl groups is determined by the type of the substituent(s) that are present on aromatic rings, these groups may represent both hydrophilic and hydrophobic (amphiphilic) components. The arrangement of these domains or components inside the ESS, which is dependent on hydrophilic, hydrophobic, and other interactions in an aqueous environment, is another issue that should be taken into consideration since it shapes the overall design of the ESS.

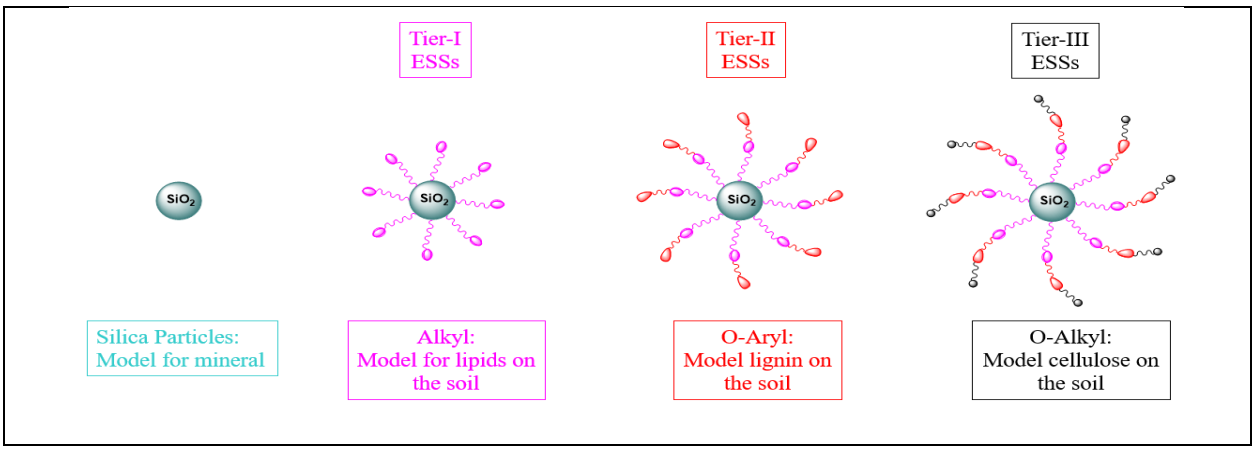

Figure 1.2. Model of the ESSs

The ESSs in this research were synthesized using Controlled Radical Polymerization (CRP) techniques to enable control of molecular size and incorporation of the representative functionalities of polysaccharides, lignin, and lipids, as they are the major components of SOM. Incorporation of these components as blocks or 'tiers' making up the ESS onto silica particles in a stepwise fashion can enable the systematic studies of the soils. Thus, in practice, ESSs have been synthesized, as shown in figure 1.2 are composed of silica particles as minerals, linear hydrocarbons of varying chain length to represent lipids (Tier-I ESS), oligo(O-aryl) groups consisting of hydroxy, methoxy, and acetyl substituted aromatic groups to mimic lignin (Tier-II ESS), and cyclic glucose oligomers (O-alkyl) to represent polysaccharide residues (Tier-III ESS). Using this methodology to tune the content and length of each block allowed the synthesis of a series of ESSs, which is useful for the molecular-level understanding of soil behavior with pollutants.

1.2.2 Atom Transfer Radical Polymerization (ATRP)

Due to its advantages over ionic and coordination polymerization, radical polymerization is the most popular polymerization technique for creating polymeric materials.[78] The benefit of radical polymerization is that it works with many different vinyl monomers. Although it can tolerate water and contaminants in the polymerization mixture, oxygen must be removed from the reaction system. However, a disadvantage of traditional radical polymerization is that it lacks control over the polymer structure, which includes end functionalization, degree of polymerization, polydispersity, chain topologies, and composition.[79]

The development of Controlled Radical Polymerization (CRP) or Reversible-Deactivation Radical Polymerization (RDRP), which is based on the establishment of a rapid dynamic equilibrium between the small amount of growing radicals and the large majority of the dormant species, allows the synthesis of controlled molecular architecture with more precisely controlled

molecular weight and relatively low polydispersities.[80] Due to this equilibrium and faster initiation, only a small percent of the growing chains are terminated, while the remaining dormant chains are capable of reactivation, functionalization, and chain extension. This is in contrast to conventional radical polymerization with slow initiation, fast propagation, and inevitable termination; thus CRP behaves as a 'living system'.[81] Some of the common examples of CRP methods include RAFT[82], nitroxide mediated polymerization[83], degenerative transfer using alkyl halides,[84] Co-based systems,[85] and Ru[86] mediated polymerization.

Atom Transfer Radical Polymerization (ATRP), where atom transfer is the key reaction responsible for uniform polymeric chain growth, is one of the widely used CRP methods.[87] Mild reaction conditions, simple experimental setup, readily available initiators and catalysts, and a wide range of monomers and solvents makes ATRP very promising in polymer synthesis. ATRP produces well-defined polymers with definite end functionalities and low polydispersities (<1.3).[87]

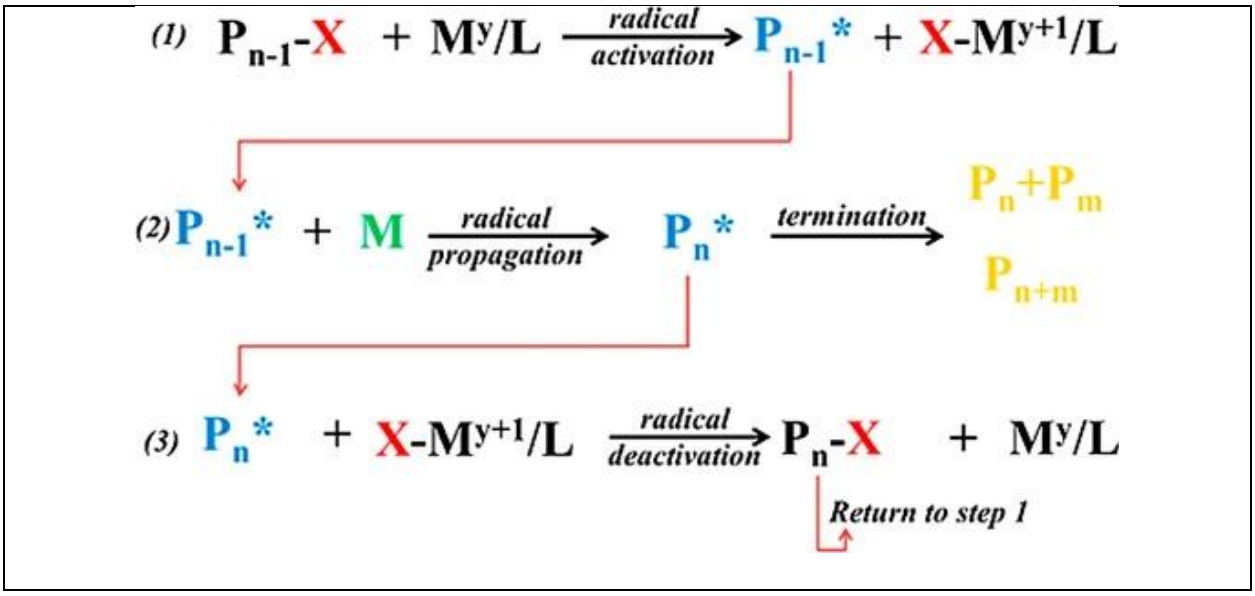

Scheme 1.1. General mechanism of traditional ATRP.[88] *Source:* Plinio Ribeiro Rodrigues and Ronierik Paoli Viera, Advances in atom transfer radical polymerization for drug delivery applications, *European Polymer Journal*, June 1, 2019, p. 14. Reproduced courtesy of Elsevier and the Copyright Clearance Center.

The general mechanism of ATRP is given in scheme 1.1.[88] Here, P_{n-1}-X is the dormant

species that can be either an alkyl halide (R-X) initiator or the growing polymer chain with a halide end cap. ATRP utilizes a catalytic system, where M^y is typically a transition metal catalyst, and L is a ligand, to activate the dormant macro alkyl halide by generating a higher oxidation state complex ($X\text{-}M^{y+}1/L$) and macro-radical living polymer (P_{n-1}*) in step 1. The living polymer then propagates according to step 2, which is directed away from the formation of a dead polymer by chain transfer or bimolecular termination and redirected toward deactivation back to dormant macro alkyl halide (P_n-X), which can return to step 1, thus preventing bimolecular termination. The degree of polymerization is determined by the ratio of the change in monomer concentration to the initial initiator concentration, $DP_n=\Delta[M]/[I]_0$.

ATRP of vinyl monomers like styrenes[89] and methacrylates[90] are readily accessed in the literature. Most of these experiments have been carried out using different transition metal catalysts, for example, copper,[91, 92] iron,[93] ruthenium,[94] and rhenium.[95] Most widely employed systems for the ATRP of styrenes include the heterogeneous mixtures of a copper(I) halide and a neutral chelating amine, imine, or pyridine ligand.[29] These traditional ATRP methods require extremely oxygen-free conditions, which is their major limitation compared to some other recent methods like initiators for continuous activator regeneration (ICAR-ATRP) and activators regenerated by electron transfer (ARGET-ATRP). The Cu(I) activator is continuously regenerated by organic free radicals in ICAR-ATRP, while Cu(II) is converted to Cu(I) and oxygen tolerance is increased in the ARGET ATRP by using an excess reducing agent, such as tin(II) 2-ethylhexanoate or vitamin C.[96]

ATRP is not compatible with the polymerization of monomers containing acidic and phenolic groups such as 4-vinylphenol and methacrylic acid etc. The ligand protonation at low pH, catalyst coordination to the carboxyl group of monomers, and displacement of the halide anion

from the oxidized Cu(II) dormant phase are some of the potential causes of the incompatibility.[97] Therefore, the acidic and phenolic monomers should be converted by protection and deprotection reactions before and after the polymerization, respectively, to be compatible with ATRP. Due to its robustness, mild conditions, and ease of synthesis with controlled molecular weight and low polydispersities; ATRP was chosen as the method of polymerization for this work.

1.2.3 Sorption Batch Equilibrium Studies

Sorption is the process of attachment of one substance (sorbent) to another (sorbate). Various physicochemical mechanisms such as electrostatic interactions, hydrogen bonding, van der Waals forces, covalent bonding, ligand exchange, cation-water bridging, and even physical trapping determine the sorption behavior of agricultural chemicals (AC) with soils.[61] Therefore, studying the sorption of agricultural chemicals (AC) to soils is important to assess the persistence of these agricultural chemicals, as well as to assess the quality of soils.

For carrying out the sorption studies under aqueous conditions, sorbate is equilibrated with sorbent in controlled ionic strength and pH under isothermal conditions. Through batch mode or flow-through tests, sorption parameters such as partitioning coefficient, binding constant, etc., can be identified. Even though the batch equilibration approach is not always optimal in comparison to flow or column tests, soil scientists frequently utilize it because it is a quick and relatively simple operation. Although various protocols have been put forth to ensure uniformity in sorption studies, the Organization for Economic Co-operation and Development (OECD) recommended protocol is the primary methodology that soil scientists around the world have most frequently employed. In this study, the sorption experiments were performed according to the OECD guidelines.[61]

In carrying out adsorption studies, the ideal soil-to-solution ratio and the amount of time needed for sorbent and sorbate to reach equilibrium were required to be calculated first. Every experiment includes a control sample to make sure the test substance doesn't deteriorate or become

adsorbed on the test vessels. In addition, a blank sample that only contains the background solution and soil is utilized to look for analytical method artifacts or soil-related matrix effects. The same testing techniques were used for all the samples, blank and control.

1.2.3.1 Soil-to-solution Ratio

The soil-to-solution ratio experiments are performed to determine the amount of soil required for at least >20% of sorption of the test substance, which is preferred to be >50%.[61] Also, after sorption, the test substance concentration in the aqueous solution should be high enough to be properly detected by the analytical method. To determine the appropriate soil-to-solution ratio, different amounts of soil are mixed with the same concentrations of the test substance, shaking them in a shaker for 2-5 days, and then the sample is centrifuged. After that, High-Performance Liquid Chromatography (HPLC) is used to analyze the extracted supernatant. The calculations are performed according to the following equations:

$$A_t = \frac{m_s}{m_o} \times 100 \qquad \text{Eq. 1.1}$$

$$A_t = \frac{m_o - m_{aq}}{m_o} \times 100 \qquad \text{Eq. 1.2}$$

Where,

A_t = Adsorption percentage of test substance at a specific time t (%);

m_o = Initial mass of test substance at the beginning of the experiment (µg);

m_s = Mass of test substance adsorbed on the soil after time t (µg);

m_{aq} = Mass of test substance remaining in solution after time t (µg).

Based on the percentage sorption of each sample and detection limits of analytical methods, the proper ratio is chosen where the sorption is >50%. The rest of the experiments are conducted using this ratio.

1.2.3.2 Kinetic Experiments

To determine the amount of time needed for the system to reach equilibrium and find a plateau for the sorption, kinetic experiments are carried out before conducting the isotherms. For the kinetic experiments, a series of samples containing the previously determined soil weights from the soil-to-solution ratio experiments and a fixed concentration of the test substance is prepared. The samples are placed in the shaker, and at different intervals (T1, T2, T3, etc.) samples are collected. After centrifugation, the extracted supernatant is analyzed by HPLC to determine the percentage of sorption, which is then plotted versus the time. From there, the equilibration time is determined. An example of sorption kinetic is shown in the Figure 1.3.[61]

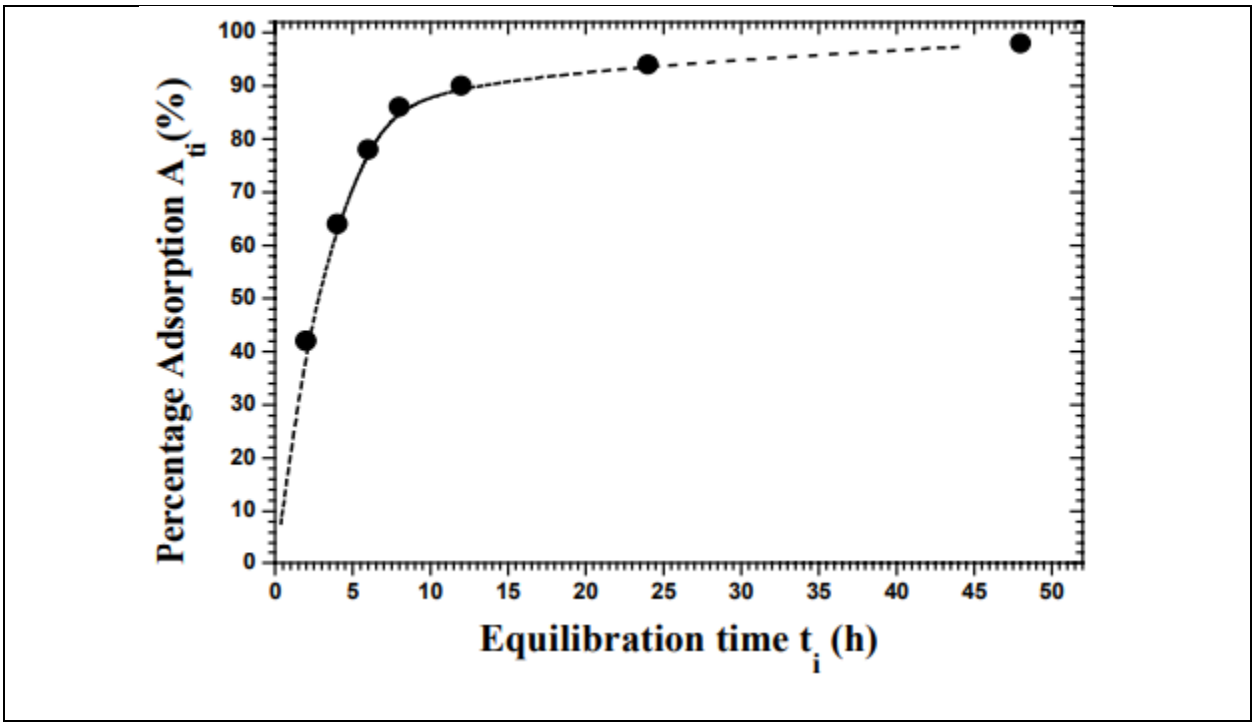

Figure 1.3. Example of sorption kinetics adapted from OECD guidelines.

1.2.3.3 Sorption Isotherms

Sorbate-sorbent interactions such as sorption of organic molecules by soils, their mobility, and distribution between the liquid and solid phases are often described by the distribution

coefficient, K_p (L/Kg), which is the ratio of the concentration of sorbate present on the sorbent C_s (mg/kg) to the concentration of sorbate remaining in the aqueous phase C_{aq} (mg/L).

$$Kp = \frac{C_s}{C_{aq}} \quad \text{Eq. 1.3}$$

Higher K_p values mean the stronger affinities of sorbate to the sorbent. Agricultural chemicals preferentially interact with and adsorb on SOM with increasing hydrophobicity and show increased values of K_p. Whereas hydrophilic molecules show relatively lower Kp values because they are solvated by water and repelled by the hydrophobic moieties of SOM. K_p can be normalized to give the organic carbon distribution coefficient, K_{OC}.[98]

$$K_{OC}^{sor} = K_p^{sor} \times \frac{100}{\text{fraction of organic carbon, } F_{OC}} \quad \text{Eq. 1.4}$$

Sorption can be mathematically modeled by different sorption isotherms such as Langmuir, Freundlich, etc. Freundlich model is the most widely used to study sorption in soil among soil scientists, even though it is purely empirical and does not accurately account for the sorption process in soil.[99, 100]

$$C_s = K_F \cdot C_{aq}^N \quad \text{Eq. 1.5}$$

$$\log C_s = \log K_F + N \log C_{aq} \quad \text{Eq. 1.6}$$

Here, K_F is the Freundlich sorption coefficient which depicts the sorption capacity, and the N value denotes the sorption linearity or the heterogeneity of sorption sites. Higher K_F means a larger binding intensity or affinity towards sorbate and sorbent. N values range from 0 to 1, where N = 1 indicates linear sorption and retaining of the compounds by partitioning. N values less than 1 indicate the presence of heterogeneous binding sites. Most soils show a non-linear sorption behavior.

1.2.4 ^{1}H-^{13}C Cross Polarization Magic Angle Spinning Solid State NMR

Solid-state NMR has emerged as one of the most popular analytical techniques for studying the structures and dynamics of solid materials, such as crystals, glasses, proteins, and polymers due to its great resolution and sensitivity. However, in comparison to the solution state NMR, where some interactions are averaged due to the rapid motion of isotropic molecules in solutions, there are peak broadening occurs in solid-state NMR.

Dipolar decoupling (DD) and magic angle spinning (MAS) techniques were used to circumvent the limitations of the solid-state NMR. Dipolar decoupling uses a high-powered radio frequency at 1H frequency to average the coupling to zero while acquiring a ^{13}C signal. In the case of MAS, the sample is rotated in the rotors at a frequency of a few thousand Hz and at an angle of θ=54.74^{o}, which is the magic angle with respect to the surrounding magnetic field.

On the other hand, a weak signal is observed due to the low signal-to-noise ratio of the less abundant nuclei like ^{13}C. To solve this problem, a spinlock is applied to reach a specific match called Hartmann and Hahn. The cross-polarization (CP) approach, which processes both ^{1}H and ^{13}C at the same frequency, transfers magnetization from very abundant ^{1}H to low abundant ^{13}C to improve peak signals.[101]

Since the combination of CP and MAS, the use of solid-state NMR has expanded dramatically due to the benefits it offers, specifically: samples are stable in solid form, require little sample preparation, don't need a solvent, have no concentration limit, can be used to analyze insoluble samples, and can be evaluated whole samples without pretreatment or extractions.[66] The ^{1}H-^{13}C CP MAS NMR is also popular among soil scientists to determine the composition of the soil organic matter by examining its carbon functional groups.[66] Aliphatic carbon (δ 0–50 ppm), methoxy groups (R–O–CH_3), carbohydrates groups (RC–OH or RC–OR), aromatic groups (δ 11–145 ppm), phenolic groups (δ 145–163 ppm), and carbon-containing carboxylic, carbonyl, amine,

and ester groups (δ 163–180 ppm) are examples of typical functional groups found in SOM.[5] The proportion of each functional group influences the characteristics of SOM, including sorption behavior.[102]

The ^{1}H-^{13}C cross-polarization magic angle spinning (CP-MAS) approach used for this study was carried out on an AV 400 MHz Bruker solid-state apparatus with the material packed into a 4 or 2.5 mm ZrO2 rotor. The following parameters were used to collect spectra: 2048 scans, ramp cross-polarization, a 2 ms contact time, and a 2 s delay between scans; A 120 Hz line broadening function was used, with a spinning speed of 12–15 kHz, and a reference signal of yglycine–CH_2 at 43.5 ppm.

1.2.5 Thermogravimetric Analysis (TGA)

In recent years, thermal analysis or thermos-analytical techniques have been used extensively for the characterization of elements, compounds, or mixtures by observing how physico-chemical properties change as temperature rises.[103] The two main techniques are (a) differential thermal analysis[104], which measures "heat content" change in relation to temperature, and (b) thermogravimetric analysis[103], which measures weight change in relation to temperature. TGA analysis is carried out at a controlled temperature change rate under a controlled atmosphere. To maintain the atmosphere, inert (nitrogen, argon), oxidizing (air or oxygen), or reducing (8-10% hydrogen in nitrogen) gas is purged through the balance. Materials composition and thermal stability data can be obtained from this analysis.

In this study, a TA system TGA 2950 was used for the TGA analysis by using 4 to 8 mg of samples with a ramp temperature of 25 ^{o}C to 600 ^{o}C at 10 ^{o}C per minute under a nitrogen atmosphere. The data obtained as the weight loss was plotted against the temperature. Initial mass loss up to 180 ^{o}C was due to the adsorbed moisture and residual solvents, while the mass loss above 180 ^{o}C to 600 ^{o}C was due to the decomposition of the polymeric ESS sample. The %TOF,

the average degree of polymerization, and graft density were calculated from the TGA analysis.

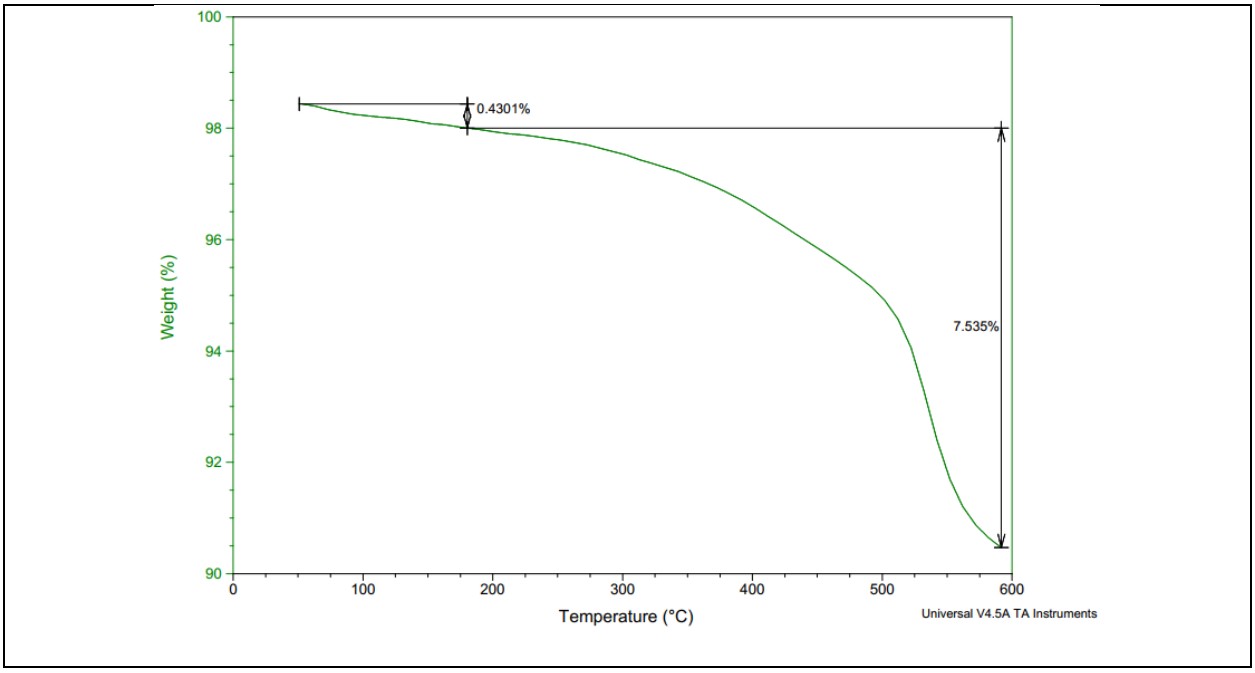

Figure 1.4. TGA thermogram of weight loss from 25 ^{o}C to 600 ^{o}C.

The %TOF can be calculated as follows:

$$Corrected\ W_{180-600} = \left(\left(\frac{W_{180-600}}{100 - W_{25-180}}\right) - \left(\frac{Silica\ W_{180-600}}{100 - Silica\ W_{25-180}}\right)\right) \times 100 \qquad \text{Eq. 1.7}$$

Where,

$Corrected\ W_{180-600}$

$= \%mass\ loss\ corresponding\ to\ the\ organic\ fraction\ decomposition\ in\ the\ sample\ after\ subtracting\ mass\ corresponding\ to\ the\ silica\ blank$

$W_{180-600} =$

$\%mass\ loss\ corresponding\ to\ the\ sample's\ organic\ fraction\ decomposition\ from$ 180^{O} C to 600^{O} C

$W_{25-180} =$

$\%mass\ loss\ corresponding\ to\ the\ adsorbed\ moisture\ and\ residual\ solvents\ from$ 25^{O} C to 600^{O} C

$Silica\ W_{180-600} =$

$\%mass\ loss\ corresponding\ to\ the\ organic\ fraction\ decomposition\ of\ blank\ silica\ from$ 180^{O} C to 600^{O} C

$Silica\ W_{25-180} =$

$\%mass\ loss\ corresponding\ to\ the\ adsorbed\ moisture\ and\ residual\ solvents\ on\ blank\ silica\ from$ 25^{O} C to 600^{O} C

The average degree of polymerization (DP_n) of the second tier and the graft density (δ) were calculated as follows:

$$DP_n = \frac{W_{180-600}^{corr\ P} - W_{180-600}^{corr\ I}}{W_{180-600}^{corr\ I} - (1 - W_{180-600}^{corr\ P})} \times \frac{I_m}{P_m} \quad \text{Eq. 1.8}$$

$Where,$

$W_{180-600}^{corr\ P} = Corrected\ \%loss\ of\ polymer$

$W_{180-600}^{corr\ I} = Corrected\ \%loss\ of\ initiator$

$I_m = molecular\ weight\ of\ the\ initiator\ \left(\frac{g}{mol}\right)$

$P_m = molecular\ weight\ of\ the\ monomer\ (\frac{g}{mol})$

$$\delta = \frac{W_{180-600}^{corr}}{M\ \times\ S_{spec}\ \times 100} \times 10^6 \quad \text{Eq. 1.9}$$

Where,

M = the molar mass (g/mol) of the degradable part of the grafted molecule;

S_{spec}= the specific surface area (m^2/g) of the silica particle before grafting (550 m^2/g)

1.2.6 Results and Discussion

1.2.6.1 Synthesis of Tier-I ESSs

Scheme 1.2 shows the synthesis of the Tier-I aliphatic domain, sometimes referred to as the ATRP surface initiator because the radical initiator is also attached in this synthesis. First, 10-undecen-1-yl-2-bromo-2-methyl propionate alkyl halide ester (**3**) was synthesized by coupling 10-undecen-1-ol (**1**) and 2-bromoisobutyryl bromide (**2**) in the presence of triethylamine (Et_3N) as the base and diethyl ether (Et_2O) as solvent. This alkyl halide ester (**3**) will serve as the initiator for further ATRP polymerization to synthesize Tier-II ESSs. The alkene end of this ester was then hydrosylilated using trichlorosilane ($HSiCl_3$) and Karstedt's catalyst to form (11-(2-Bromo-2-methyl) propionyloxy) undecyltrichlorosilane (**4**). The trichlorosilyl end of compound 4 acts as a tethering point for grafting onto silica gel. Finally, 4 was immobilized onto silica gel by refluxing in toluene. Subsequent washing and drying yields the initiator-functionalized silica gel.

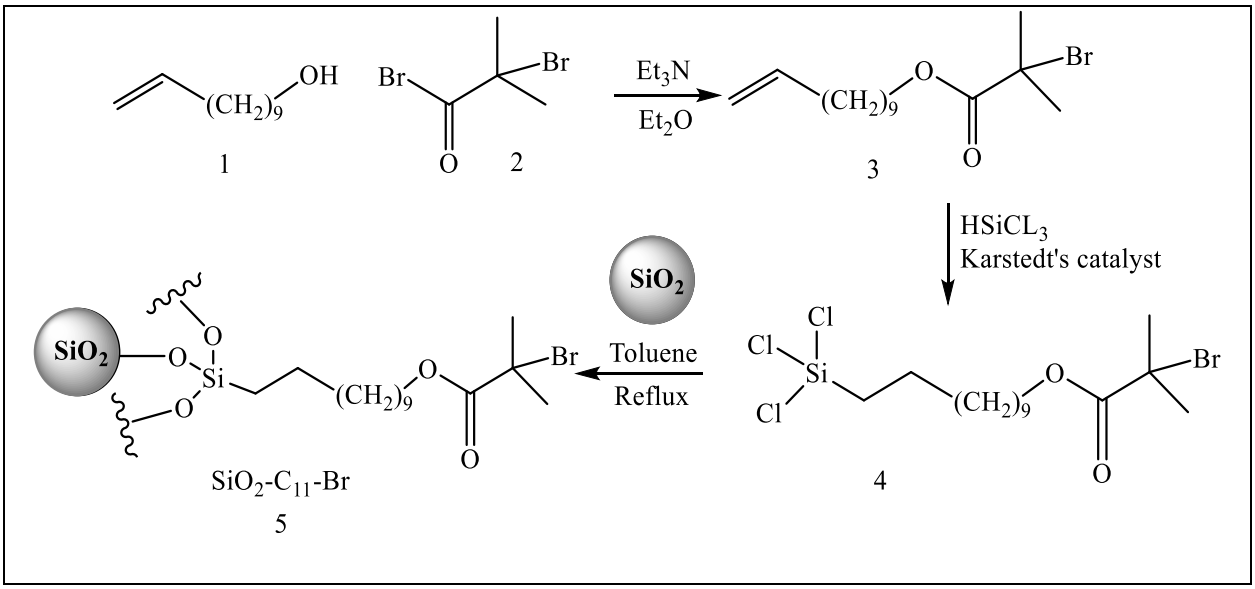

Scheme 1.2 Synthesis of ATRP surface initiator

1.2.6.2 Synthesis of Tier-II ESSs through polymerization of (O-) aryl monomers (4-acetoxy styrene (PAS) and 4-acetoxy-3-methoxy styrene (PAMS))

To mimic the structure of lignin, Tier-II ESSs were synthesized using functionalized silica as the surface-initiator for an ATRP, and 4-acetoxy styrene (PAS) and 4-acetoxy-3-methoxy styrene (PAMS) as monomers as shown in scheme 1.3. Copper (I) bromide was used as catalyst and N,N,N',N'',N''-pentamethyldiethylenetriamine (PMDETA) as ligand. The reactions were refluxed using xylene as a solvent to form the aromatic oligomeric block of 5-10 units. To facilitate the introduction of O-aryl groups as a second tier, an acetyl protected 4-vinyl phenol monomer that is readily accessible on the market was used since ATRP is not possible with the acidic proton of phenolic monomers.[97, 105] To mimic the structure of lignin, which consists of cross-linked polyaryl rings with many hydroxyl substitutions on the aromatic ring, O-aryl groups were added to the aromatic part. Introducing polar groups into the polyaromatic second tier domain is analogous to the humification process (e.g., oxidation) in soil, which converts non-polar structural moieties into comparatively more polar groups. The methoxy substitution on the aromatic ring close to the phenolic -OH groups introduce intermolecular H-bonding and possible polar alterations in the electron density of the ring, and acetyl protected 2-methoxy 4-vinyl phenol was the monomer of choice for this.

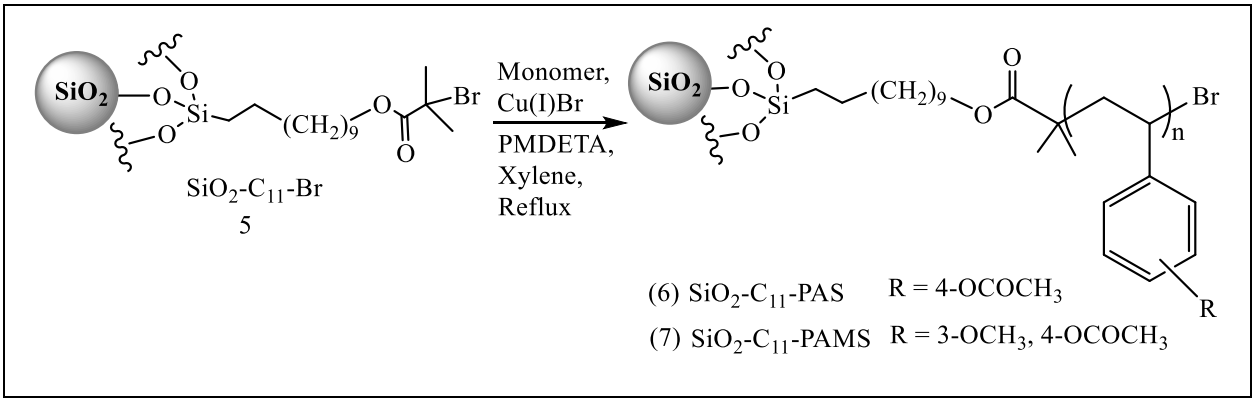

Scheme 1.3. Synthesis of Tier-II ESSs.

1.2.6.3 Hydrolysis of Acetoxy Group of Tier-II ESSs

The acetyl protecting groups present in the Tier-II blocks after polymerization were hydrolyzed to expose the phenolic -OH in aromatic rings (Scheme 1.4) that are found with great frequency in soils. The selective hydrolysis of acetyl ester was achieved by stirring Tier-II ESSs in hydrazine hydrate ($NH_2.NH_2$) and THF for 24 hours. Solid-state ^{13}C NMR and TGA confirmed the successful hydrolysis of the acetyl groups.

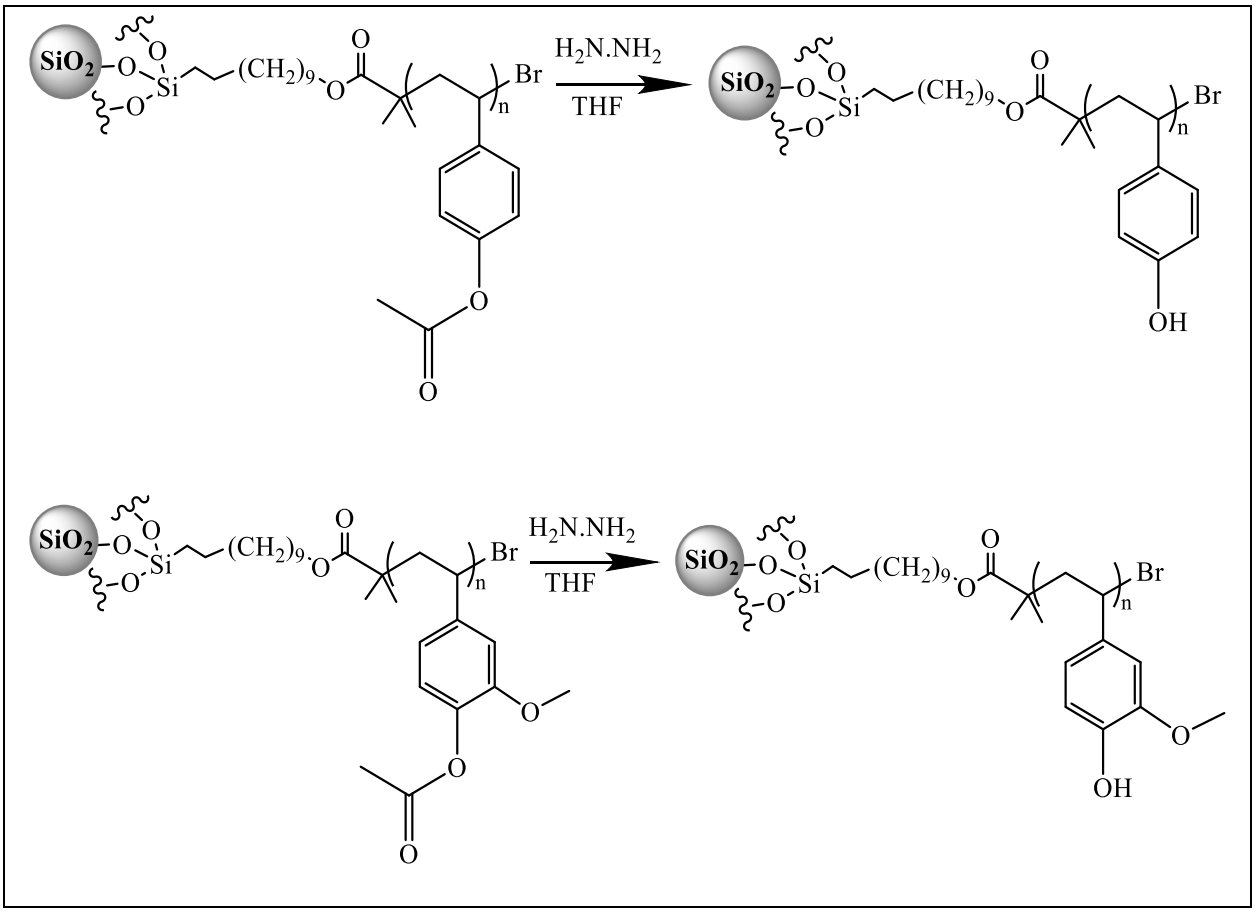

Scheme 1.4. Hydrolysis of Tier-II ESSs.

1.2.6.4 TGA Results

The TGA analysis was performed to determine the total organic fraction, graft density, and average degree of polymerization of the synthesized ESSs. In the TGA thermogram, with increasing temperature ESSs showed a steep mass loss from around 100 ^oC to 180 ^oC, remains somewhat

stable around 180 ^{o}C, then started to fall again above 200 ^{o}C. The initial weight loss from 25 ^{o}C to 180 ^{o}C was due to the water and solvent residues, while the weight loss above 200 ^{o}C was due to the loss of the organic matter grafted onto silica because silica remains intact in this temperature range. TGA data were used to confirm the formation of the organic layer Tiers grafted onto over the inorganic core, implicated as the main active component in the sorption studies. TGA was also used to validate the synthesized ESSs tiers met targeted total organic fractions and average degree of polymerization.

Table 1.1 TGA analysis of ESSs for total organic fraction, graft density, and average degree of polymerization

Entry	ESSs	%TOF	Graft density, mmol/g	DP_{avg}
ESS1	SiO_2-C11-PAS	18.36	0.141	7.427
ESS2	SiO_2-C11-PAMS	18.50	0.136	6.524
ESS3	SiO_2-C11-PASH	13.94	0.148	6.001
ESS4	SiO_2-C11-PAMSH	17.65	0.148	7.062

(Note: The work in this table was contributed by Arjun Pandey)[39]

1.2.7 Acetylation of Real Soil (Pahokee Peat)

To compare the results of the ESSs with real soils, Pahokee peat and Elliot soil were acetylated. Pahokee peat is a peat soil that is found in the Florida everglades, while Elliot soil is a typical agricultural soil, both of which are referenced by the International Humic Substances Society (IHSS). Elliot soil is usually found in Indiana, Illinois, and Iowa. Pahokee peat has very high organic content compared to the Elliot soil.

Table 1.2. Elemental composition of bulk Pahokee peat and Elliot soil.[a]

Soil	**%C**	**%H**	**%O**	**%N**	**%S**	**%P**	**H20**	**Ash**
Pahokee	45.7	4.74	nd	3.13	nd	nd	7.1	15
Elliot	2.9	nd	nd	0.25	nd	nd	1.52	nd

[a] IHSS

The reaction conditions for acetylation of the soils are shown in scheme 5. In a round-bottom flask was added around 2g of soil, 30 mL acetic anhydride, and six drops of concentrated H_2SO_4 followed by stirring at 70^o C for 5 hours. The control reaction was carried out using the same process, where DMSO was used instead of acetic anhydride. DMSO was chosen because it is a similarly polar solvent but not reactive as of acetic anhydride. The samples were purified by subsequent washing with ice water and dried under vacuum. ^{13}C NMR did not show any significant extent of acetylation of the dried Elliot soil, most likely due to a lower percentage of total organic fraction (%TOF). On the other hand, ^{13}C solid-state NMR confirmed the successful acetylation of Pahokee peat by showing an enhanced carbonyl C peak (around 180 ppm), while TGA analysis indicated a 5% increased TOF.

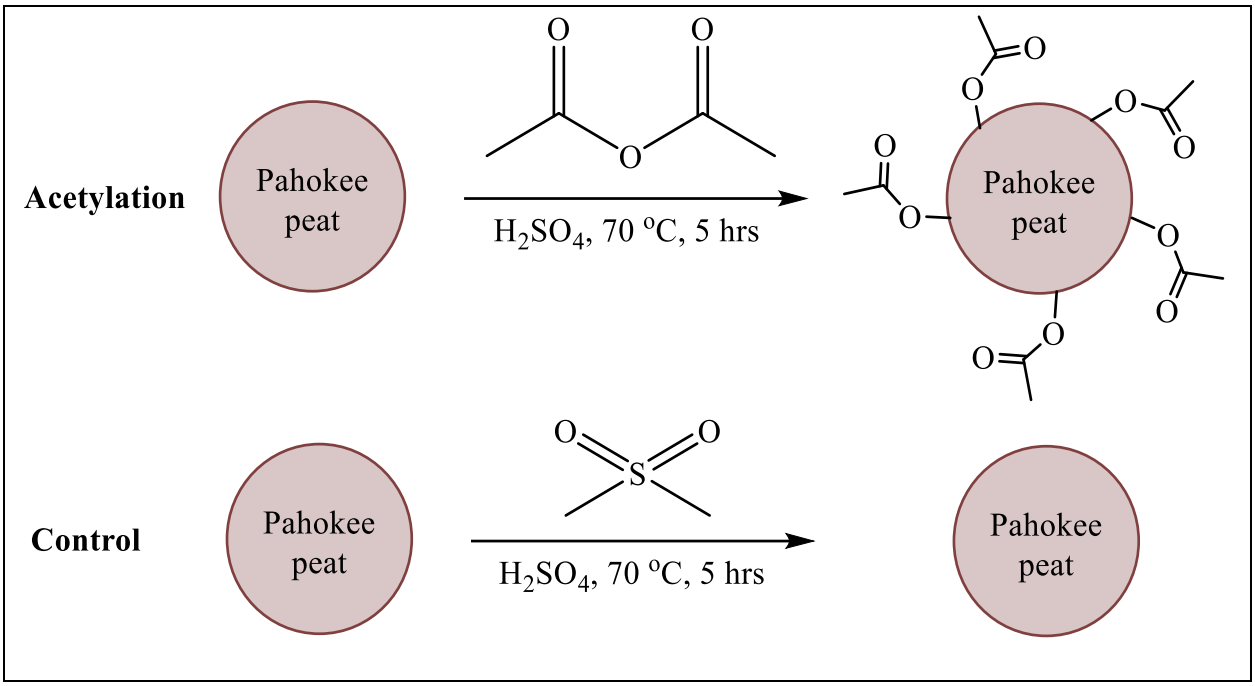

Scheme 1.5. Acetylation and control reaction of Pahokee peat

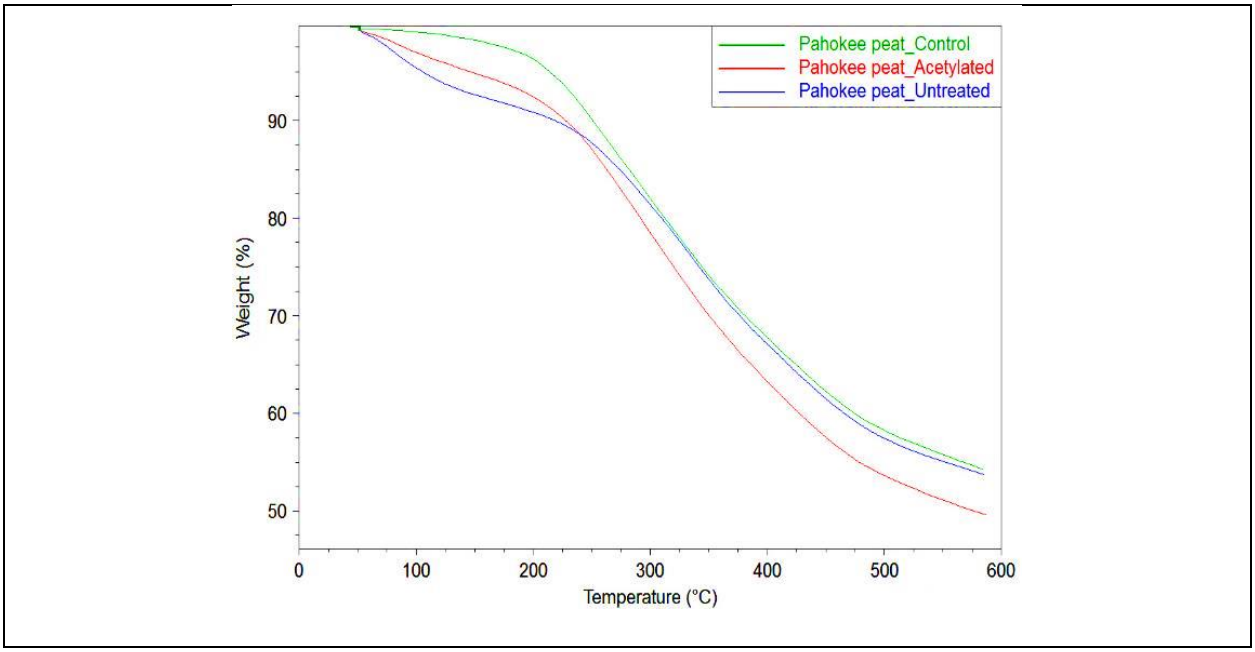

Figure 1.5. TGA thermogram of Pahokee peat.[39]

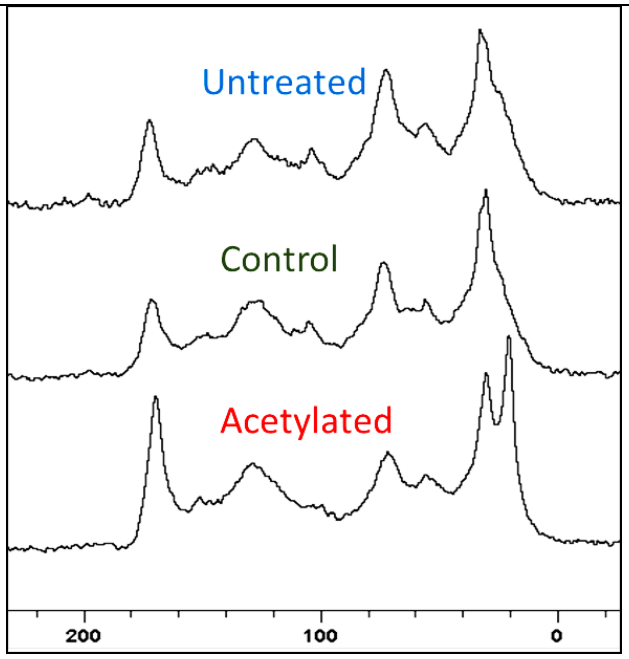

Figure 1.6. CP-MAS ^{13}C NMR of Pahokee peat.[39]

1.2.8 Sorption Study of ESSs and Acetylated Pahokee Peat Using Norflurazon

The sorption studies of synthesized ESSs and acetylated Pahokee peat were carried out using Norflurazon as the model agricultural chemical. Norflurazon is a widely used herbicide, with approximately 500,000 Kg applied in the United States annually, to control many broadleaf and grass weeds as brand names Zorial or Evital.[106] Norflurazon has been shown to form various kinds of expected and proven interactions with soil, such as Van der Waals, π-π interactions, and hydrogen bonding.[107-110]

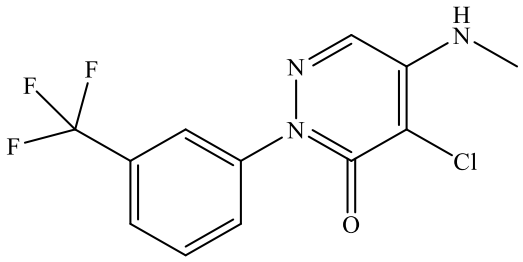

Figure 1.7. Structure of Norflurazon.

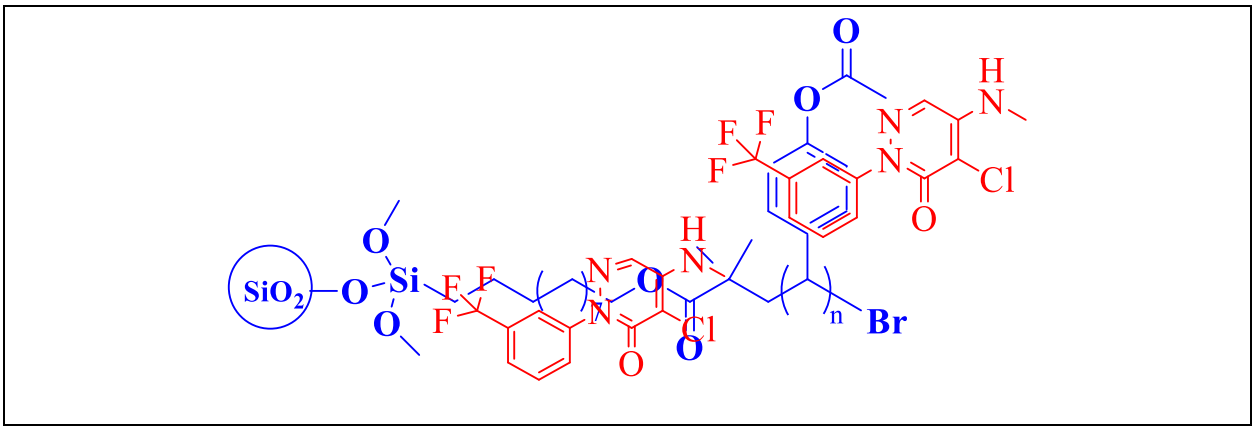

Figure 1.8. Possible binding interactions of Norflurazon with ESSs

The sorption studies were performed in Dr. Cook's research lab following the methods developed by Cook Research Group. The norflurazon concentrations in supernatants were quantified using an 1100 series Agilent HPLC system with UV-VIS detection. The optimal parameters of the methods are a mobile phase of 70/30 (%V/V) of acetonitrile/water, a flow rate of 0.6 mL/min, a sample volume of 20 µL, a C18 column heated at 25 ^{o}C, and detection at 235 nm using diode array detector. The Freundlich parameters were determined, and the Freundlich sorption coefficient, K_F values are highlighted in the following table for comparison between ESSs and acetylated Pahokee peat.

The sorption data can be understood through various approaches, such as the nature and amount of organic carbon, physical availability of the binding sites, and partitioning of sorbent in the aqueous and solid phase, while the extent of hydration was expected to be a major factor in sorption as it influences the morphology of the oligomeric chains in aqueous conditions.

Table 1.3. Comparison of the Freundlich sorption coefficient of ESSs and Pahokee peat

Non-acetylated ESSs/Soil (-OH)	$\log K_F^{sor}$		Acetylated ESSs/Soil (-OAc)
ESS3 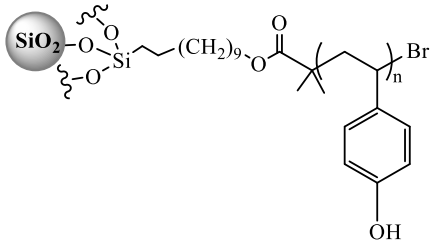	2.699 ± 0.010	2.837 ± 0.022	ESS1 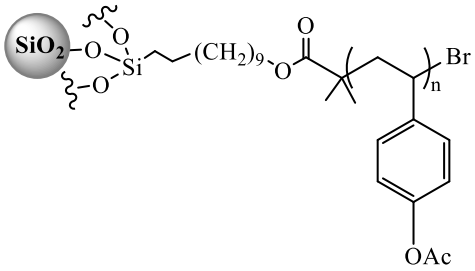
ESS4 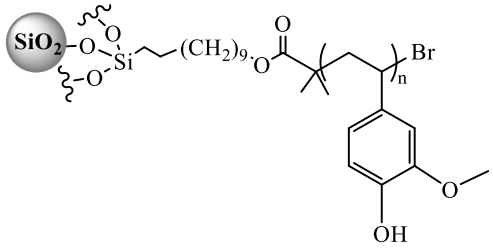	2.543 ± 0.018	2.246 ± 0.052	ESS2 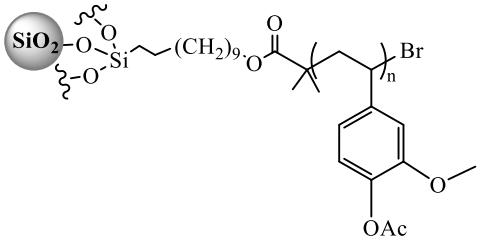
Pahokee Peat 	2.334 ± 0.032	2.515 ± 0.067	Acetylated Pahokee Peat 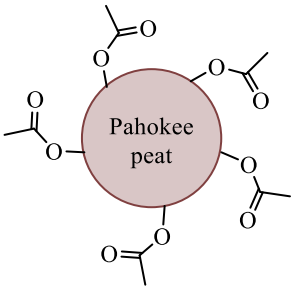

[a]Units of K_F = (µg/g)/(µg/l)^n

(Note: The work in this table was contributed by Ghada Abdalla and Charisma Latto)

Taking a look at ESS1, it contains a polar acetyl group on the para position of the aromatic ring, and it has a $\log K_F^{sor}$ value of 2.837. The $\log K_F^{sor}$ values are supposed to decrease with increasing polarity due to the hydration of the polar block. This is shown by ESS2 exhibiting a reduced $\log K_F^{sor}$ value of 2.246 due to the additional methoxy group on the adjacent carbon to the

acetyl group in the aromatic ring.

The acetyl groups in ESS1 and ESS2 were hydrolyzed to give -OH substitution on aromatic rings of ESS3 and ESS4, which is expected to increase the polarity and, thus the extent of hydration. The $\log K_F^{sor}$ value decreased from 2.837 to 2.669 upon hydrolysis, as expected. The phenolic group in ESS3 is capable of hydrogen bonding; however, the phenol is still protonated at the buffer pH of 5.75, which may provide a small increase in the polarity of the aromatic region. Another possibility is that the addition of the acetoxy groups in ESS1, sterically blocks the access of the hydrophobic Norflurazon binding to the hydrophobic portion of the soil. On the other hand, the hydrolyzed ESS4 did not follow the trend by showing a slight increase in $\log K_F^{sor}$ value from 2.246 to 2.543.

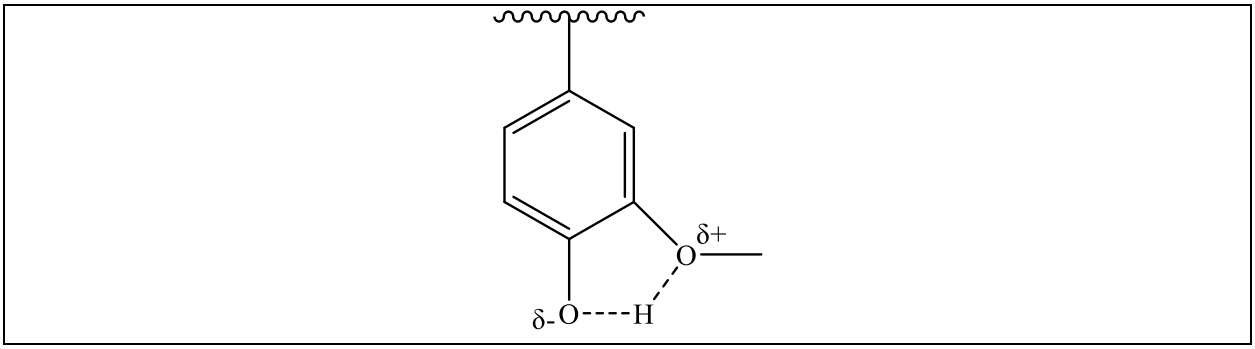

Figure 1.9. Intramolecular hydrogen bonding in ESS4.

This can be explained by the formation of intermolecular hydrogen bonding between the -OCH_3 group and the phenolic -OH group in the aromatic ring (Figure 1.9). The increased negative ionic character of the oxygen of the phenolic group affords electron donation into the ESS4 aromatic ring, which promotes π-π interactions with the electron-deficient aromatic ring of Norflurazon. Also, this intramolecular hydrogen bonding prevents the phenol to form hydrogen bonding with water. The amine groups of Norflurazon are also capable of electrostatic interactions with this partially ionized aromatic ring. These binding interactions between ESS4 and norflurazon

overcome the effect of the predicted higher polarity of the ESS4.

The $\log K_F^{sor}$ value of acetylated Pahokee peat was found to be higher than the non-acetylated or un-modified Pahokee peat. The majority of the phenol and almost all of the alcohols are in the protonated form, while the carboxylic acids may be in both protonated and deprotonated form in the unmodified Pahokee peat at pH 5.75 of the sorption experiment.[111] The acetylation of the Pahokee peat blocks the hydroxyl groups in phenols and alcohols along with some of the carboxylic acid groups, which makes the acetylated Pahokee peat less polar. This reduction in polarity decreased its affinity toward the water, which is corroborated by early reports that esterification significantly decreases the water-sorbing capacity of the hydroxyl groups in cellulose.[112] In the unmodified Pahokee peat, the sorption of hydrophobic Norflurazon from an aqueous solution is hindered by the presence of abundant polar groups that hydrate the soil, which repels the hydrophobic Norflurazon. Conversely, increased sorption of Norflurazon is observed in the acetylated Pahokee peat due to the decreased polarity by the acetylation reaction.

1.3 Effect of Changing Lignin Monomer Structure and Cross-linking in the ESSs; Ongoing and Future Goals of this Project

1.3.1 Change in lignin monomer structure

One of the primary goals of ESSs design for modeling soils is to incorporate the chemical structures that show comparable bulk properties to the real soils and eliminate those which show opposite behavior. The O-aryl groups were introduced into the aromatic ring to model the structure of lignin, which contains crosslinked polyaryl rings with abundant hydroxyl substitutions. Furthermore, the presence of phenolic and methoxy groups in ortho positions to each other in ESSs 4 also shows a close relationship with the structure of lignin. However, ESSs 4 did not show the expected sorption behavior, which suggested that the particular arrangement of the native structure may affect the binding of ACs. Therefore, one interesting factor could be to change the position of

the methoxy group in the meta position relative to the hydroxyl group instead of the ortho position, as is the case in the current ESS models.

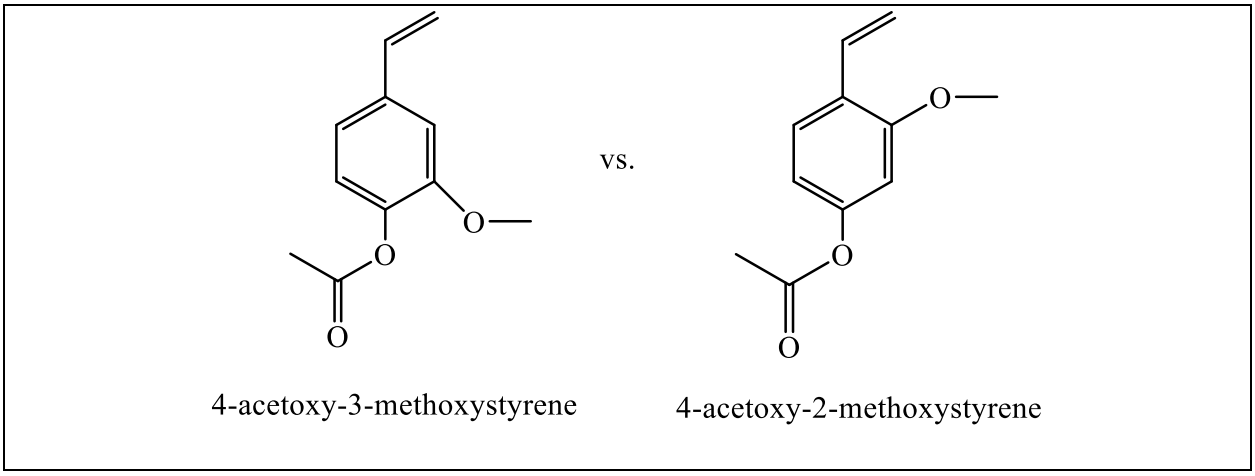

Figure 1.10. Different monomer structure

At this point, the synthesis of 4-acetoxy-2-methoxystyrene is underway to replace 4-acetoxy-3-methoxystyrene in the previous ESS structure(s) to see if this change in molecular structure will change the binding properties of ESS4. This will then be introduced into the Tier-II ESSs, and sorption data will be obtained to compare the results with ESSs 4 and acetylated Pahokee peat to aid in understanding the connection between chemical structure and molecular level interactions of the soils and soil mimics.

1.3.2 Synthesis of 4-acetoxy-2-methoxystyrene (PAMS) monomer

The synthesis of the 4-acetoxy-2-methoxy styrene monomer was initiated according to a published protocol that follows Knoevenagel condensation reaction conditions.[113] According to Knoevenagel condensations, alkylidene-dicarbonyls or analogous compounds are formed by the reactions of aldehydes or ketones in the presence of the weak base with active methylene compounds. Malonic acid is usually utilized as the active methylene compound, and the reaction is accompanied by decarboxylation to produce the corresponding α,β-unsaturated monocarboxylic acid.

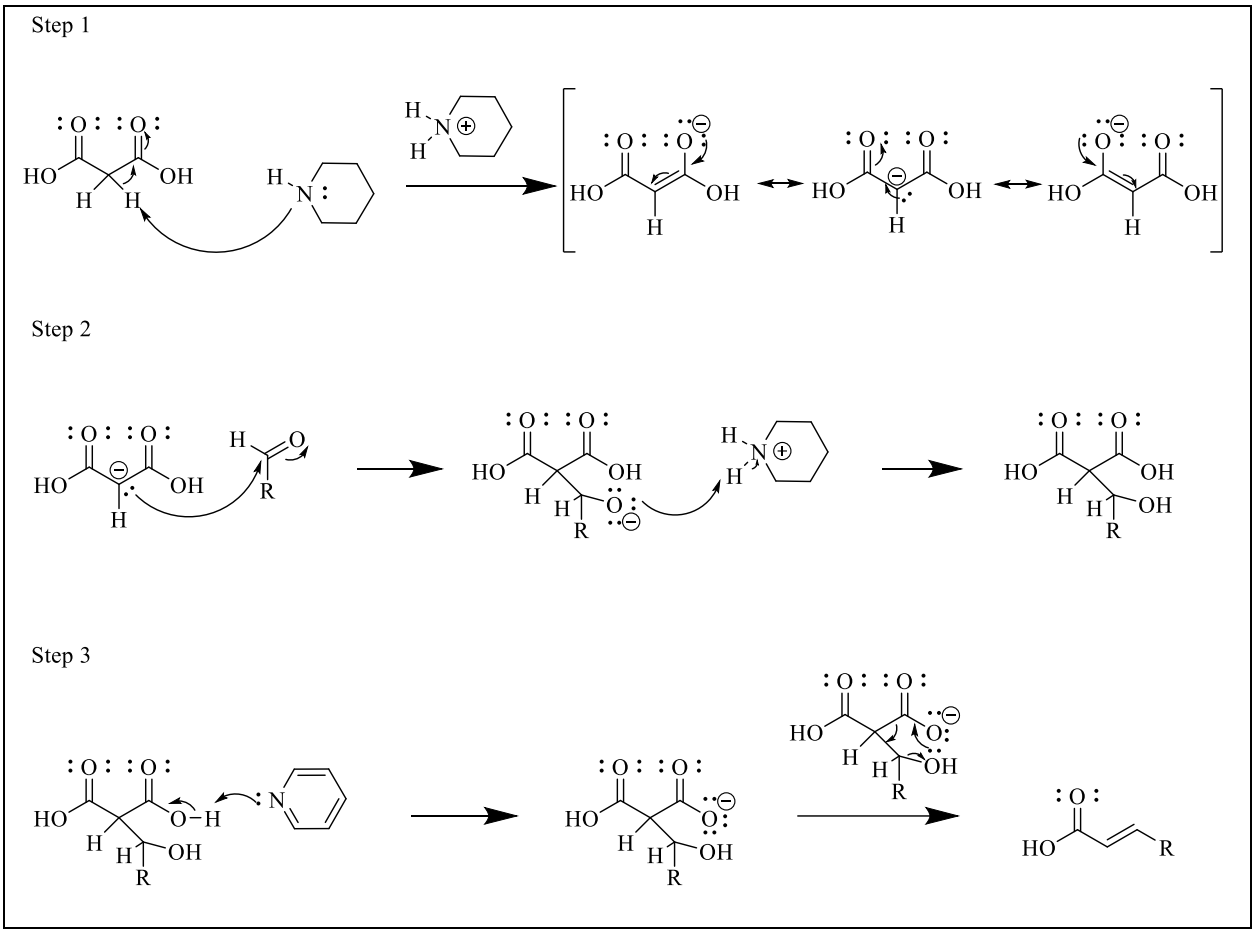

Scheme 1.6. Mechanism of the Knoevenagel condensations reactions for the formation of α,β-unsaturated compound

When condensations with malonic acid are carried out in the presence of aromatic aldehydes, only trans-cinnamic acid is produced. However, Simpson et al. observed the formation of a new compound with the characteristic of styrene while trying to synthesize the 4-hydroxy-trans-cinnamic acid directly from the corresponding aldehydes. The reaction condition employed was similar to the classical Knoevenagel condensation, except for the workup steps where the reaction was quenched by removing the pyridine in vacuo in the presence of toluene instead of pouring it into the concentrated HCl on ice. They concluded the formation of the styrene compounds only occurs in reactions involving 2- or 4-hydroxybenzaldehyde substrate and the new work-up conditions.[113]

In this study, 4-hydroxy-2-methoxybenzaldehyde was used as the starting material. The reaction was carried out using malonic acid as the methylene compound, piperidine as the catalyst, and pyridine as the solvent. The reaction was stirred at 115^{O} C for either 5 hrs or 24 hrs. Even though the crude ^{1}H NMR showed the characteristic styrene peak, the yield was pretty low, and the product couldn't be purified by column chromatography. This leds to the synthesis of the monomer by an alternate approach- the Wittig reaction.

The Wittig reaction is a widely used technique for the conversion of aldehydes and ketones into alkenes by using the Wittig reagents with the formula $R_3P{=}CHR'$.[114] Here, R is mainly a phenyl group. The first step is the formation of the Wittig reagents or ylides. Generally, various strong bases, like butyllithium, sodium hydride, alkoxides, etc., are used for making the nonstabilized ylides.[115] There also have been some reports on the use of amidine bases such as 1,8-diazabicyclo[5.4.0]undec-7-ene (DBU) for the synthesis of the phosphorus ylides.[116] In this work, n-butyllithium and DBU were selected as the bases while keeping the rest of the materials constant. Even though n-butyllithium is a strong base than the DBU, it is moisture sensitive and requires water-free conditions. On the other hand, DBU requires only distilled solvents.[117]

In this work, the synthesis of the 4-acetoxy-2-methoxy styrene monomer started with protecting the -OH group of the 4-hydroxy-2-methoxy benzaldehyde. The protection reaction was carried out using acetyl chloride in the presence of triethylamine as the base. ^{1}H NMR confirmed the successful reaction with more than 80% yields.

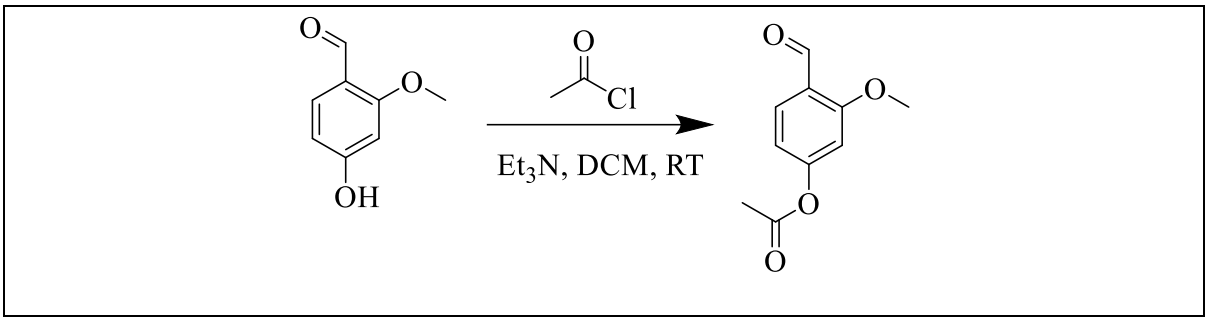

Scheme 1.7. Protection reaction of 4-hydroxy-2-methoxy benzaldehyde

Next, methylenetriphenylphosphorane was made by reacting methyltriphenylphosphonium bromide with either n-butyllithium or DBU under refluxing conditions in toluene. This methylenetriphenylphosphorane act as the Wittig reagent, which reacts with the 4-acetoxy-2-methoxybenzaldehyde to give the styrene monomer. However, no product was obtained from the reaction with the n-butyllithium, probably due to the presence of moisture in the reaction system. On the other hand, 4-acetoxy-2-methoxystyrene monomer was obtained from the reaction with DBU, but the yield was low. The reason for the low yield could be the presence of the electron-donating group on the aldehyde, which slowed down the reaction.[117] None the less, future work could use the low yielding synthesis to provide enough material for synthesizing the desired tier on an ESS.

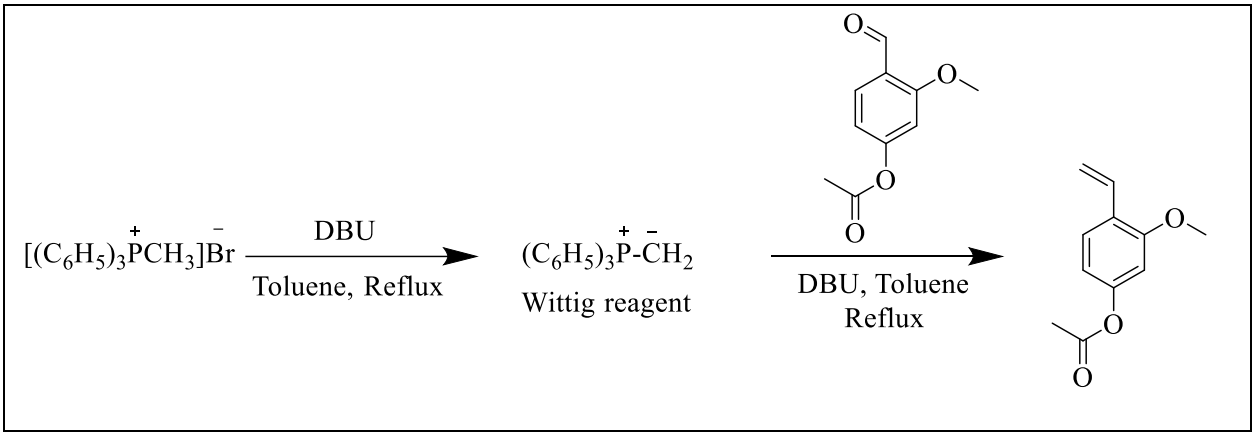

Scheme 1.8. Wittig reaction of 4-acetoxy-2-methoxybenzaldehyde to form 4-acetoxy-2-methoxystyrene

1.3.3 Crosslinking in the ESSs

Cross-linking is an important phenomenon in polymer chemistry and other materials, to create a robust structure that prevents deformation. Crosslinked polymers tend to have increased molecular weight, higher physical and chemical stability, decreased solubility, and biodegradability.[118] The evidence for crosslinking in geosolids is considerable and rising.[119] Brown coals have a tightly crosslinked, supramolecular structure.[120] The presence of matrix-bound α, ω-dicarboxylic acids in peat humin and humic acid has been interpreted as evidence that those units are involved in alkyl chain crosslinking via ester linkages.[121] Polysulfides, ammonia, and amino acids have been shown to integrate S or co-incorporate S and N into organic matter through crosslinking processes in marine sediments. Such reactions may be important in the diagenetic production of protokerogen and humics in marine settings.[122] During early diagenesis, both S and O crosslinking processes integrate algal alkenones into kerogen. The non-hydrolyzable organic component of deep tropical soil, ^{14}C dated at around 8300 years, exhibited a high degree of crosslinking and an abundance of melanoidin.[123] Piccolo et al. hypothesized that crosslinking occurs as a result of biomimetic oxidation of humic compounds.[124]

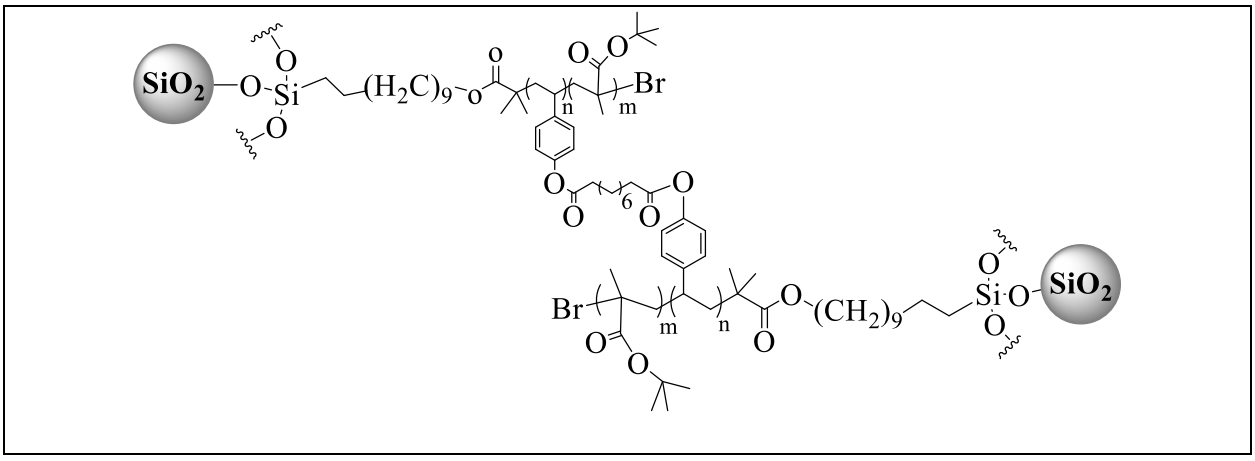

Figure 1.11. An illustrative of possible cross-linking in Tier-III ESSs. (*vide infra*)

Crosslinking may occur through covalent bonds or via coordination bonds between

polyvalent cations and (typically) oxyl groups that have negative charge. Although the molecular size distribution of humic compounds is debatable, solid-state crosslinking may occur regardless of molecular size.[125] Crosslinking by polyvalent cations, as revealed by the findings of several research reports, is dynamic and may be reversed when environmental circumstances change.[126] Crosslinking by covalent organic groups lasts longer and may be the result of increased plant metabolism or abiotic or microbial degradation. Crosslinking may alter the properties and functions of organic matter, although thus far, this has only been hypothesized. It has been hypothesized that soil organic matter may be maintained and preserved by crosslinking, which increases molecular weight and lowers bioavailability,[127] however, there is currently no concrete evidence to support this claim. It has been shown that Ca^{2+}-induced crosslinking of humics accelerates the fouling of ultrafiltration membranes used in water treatment.[128] Modifying humic acids with formaldehyde crosslinking reduces their solubility and increases their sorption capacity for Ca^{2+} cations while maintaining their average ionization constant.[129] Increases in both static exchange capacity and acid characteristics of weak acid groups result from formaldehyde crosslinking's redistribution of electron density in the condensed humic acid system.[130] Curing of humic phenol-formaldehyde segments is another interesting route for regulated crosslinking of humic compounds, which has been shown to increase their detoxifying activity towards heavy metals. Incorporating new phenolic and quinonoid moieties into the humic backbone is possible through those processes. The water-absorbing properties of leonardite potassium humate were significantly improved by N, N'-methylene bisacrylamide crosslinking.[131] Cross-linking has also been discussed in relation to the sorption of organic pollutants to natural organic matter; for example, complexation of a soil humic acid with Al^{3+} decreased the linearity of the sorption of hydrophobic compounds, which was attributed to an increase in the glassy character of the humic

acid due to cross-linking.[132]

The physical characteristics, biological stability, and sorption properties of humic compounds after covalent crosslinking have not been well studied. The chemical properties and ecological function will depend on the specifics of the crosslinking process and the composition of the connecting group. Crosslinks can create new binding sites within SOM, which increases the affinity of the sorbent towards sorbate molecules. Also, increased heterogeneous binding sites lead to non-linear sorption. Thus, crosslinking soil may be important in the future to adjust the sorption properties of ACs and other compounds in farming soils. However, too large of an extent of cross-linking in the soil can reduce the sorption of organic compounds such as norflurazon as the model agricultural chemicals. Therefore, the introduction of crosslinking in the design of ESSs would be exciting to investigate in order to understand the causes and effects of crosslinking on sorption behavior. Phenolic -OH groups present in the tier-II ESSs, and the poly(acrylic) acid or poly(methyl methacrylate) in tier-III ESSs are possible sites for crosslinking, and these crosslinks can be easily formed using various bifunctional molecules such as diacids, diamines, etc.

1.3.4 Grafting from vs. Grafting onto

Surface functionalization and modification of materials are important for various applications, and grafting is one of the versatile methods for such modifications. Grafting-from and grafting-to are the two most prevalent grafting techniques. Grafting from a surface (also known as surface-initiated polymerization) entails the in-situ formation of a polymer layer via chain propagation via the sequential addition of monomer units at surface-initiating sites. In contrast, grafting-to a surface entails the attachment of a premade polymer with the desired functionality to reactive sites on the surface via covalent or physical means. Since grafting allows for the easy and controlled introduction of polymer chains with a high surface density, precise localization of the chain at the surface, and the possibility of grafting several different polymers to the same substrate, it is

superior to other methods, such as polymer deposition and polymer adsorption.[133] The grafting density, the length of the grafted polymer chain, and the composition of the grafted polymer chain all play significant roles in determining the final properties of the grafted polymer chain.

Since small monomers diffuse with less steric hindrance than polymer chains, the grafting-from method is thought to result in a higher grafting density than the grafting-to strategy, in which the polymer chains may shield the reactive regions on the surface.[134] Although grafting-from has been shown to result in higher grafting densities in the vast majority of research, there have been reports of instances where grafting-to has yielded equivalent or even higher results.[135]

The grafting-to approach is advantageous because the preformed polymer used can be easily analyzed using typical solution-based methods versus the lack of solid-based analytical methods, allowing the molar mass and molar-mass dispersity to be identified prior to the grafting reaction; thus, the grafting-to method is favored from an industrial standpoint

Even though the grafting from technique resulted in high grafting density polymers, the characterization is challenging as the polymerization occurs on a solid substrate. Synthesis of tethered polymer layers on solid substrates by grafting from was achieved using anionic, cationic, controlled, and conventional free-radical polymerizations.[136]

Grafting onto or from methods can be accomplished by modifying the substrate surface. Covalent grafting of ω-functional alkoxy- or chloro-silanes is the most general method. Inorganic surface modification, such as silica, often relies on the chemical grafting of alkoxysilane or chlorosilane molecules via interaction with surface hydroxyl groups. This is accomplished by hydrolyzing alkoxysilane or chlorosilane with traces of water in the grafting solvent and then reacting with OH groups on the substrate surface.

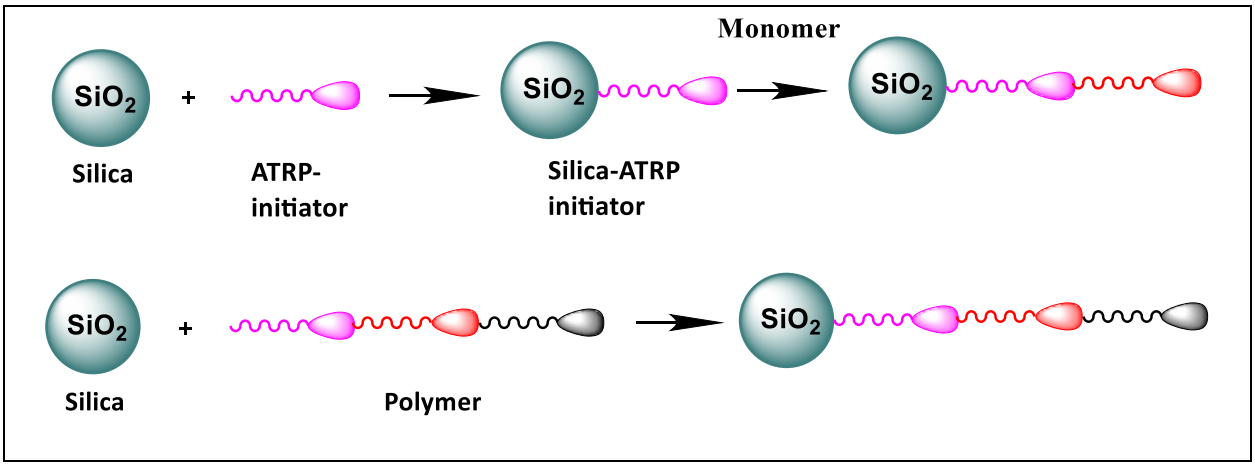

Figure 1.12. Illustration of 'Grafting from' (top) vs 'Grafting onto' technique (bottom)

Initially, ESS synthesis was carried out utilizing the grafting from approach, as detailed in detail in the previous section. In this approach, silica was functionalized with a C11-ATRP initiator, which is utilized to initiate polymerization of the second tier, resulting in homopolymers grafted onto silica gel. The first set of ESSs was successfully synthesized using the grafting from approach, however, there were certain downsides to this strategy. One of these disadvantages was that a high excess of monomer was required to attain the targeted molecular weights. In addition, the inclusion of silica gel in the polymerization process adds an additional variable to the ATRP reaction parameters that is uncontrollable. The full list of drawbacks includes a poor monomer conversion rate, which necessitated employing large monomer concentrations to produce the requisite DPn, a sluggish rate of polymerization, difficulties in characterization, and steric congestion of the immobilized initiator on silica.[137] The gradual characterization during solid-phase synthesis (grafting from) presented another difficulty. Due to the presence of silica, solid-state methods such as thermogravimetric analysis and solid-state ^{1}H-^{13}C CP MAS NMR were the only techniques available that could be used to analyze the materials. These methods were tedious, time-consuming, and solid-state NMR is regarded as semi-quantitative in comparison to solution-phase ^{1}H NMR.

As a result, progress was made toward a more advantageous synthesis by the use of the grafting onto method. In this method, homopolymers are synthesized in solution, which makes it possible for solution-phase ^{1}H NMR to verify and quantify the stepwise synthesized ESS polymers accurately. After that, the oligomers are grafted onto the silica to create silica gel that is functionalized with polymers, namely ESSs, in this instance. The primary disadvantage of using this method is that it may result in a reduced grafting percentage due to steric hindrance. However, grafting onto technique was followed for the synthesis of the cross-linked Tier-II ESS.

1.3.5 Experimental for the Synthesis of the Cross-linked ESSs

1.3.5.1 Synthesis of the Tier-I ESSs (ATRP initiator)

The synthesis of the Tier-I aliphatic domain is shown in Scheme 1.9. 10-undecen-1-ol and 2-bromoisobutyryl bromide were coupled in the presence of triethylamine (Et_3N) as a base and THF as a solvent to produce 10-undecen-1-yl-2-bromo-2-methyl propionate alkyl halide ester. To create Tier-II ESSs, this alkyl halide ester will be used as an initiator in an ATRP polymerization step.

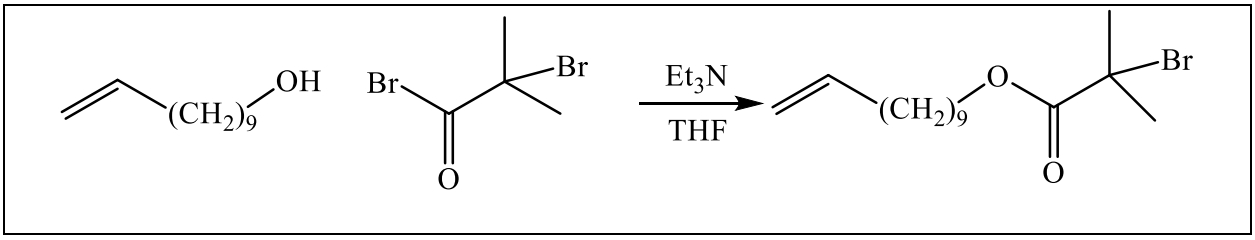

Scheme 1.9. Synthesis of the Tier-I ESSs

1.3.5.2 Synthesis of the Tier-II ESSs (ATRP of 4-acetoxystyrene)

Using 10-undecen-1-yl-2-bromo-2-methyl propionate alkyl halide ester as the initiator for ATRP and 4-acetoxystyrene (PAS) as monomers, Tier-II ESSs were synthesized to resemble the structure of lignin. The ligand employed was N,N,N',N''-pentamethyldiethylenetriamine (PMDETA), and the catalyst was copper (I) bromide. To make the aromatic oligomeric building block, the reactions were carried out in a refluxing xylene solvent.

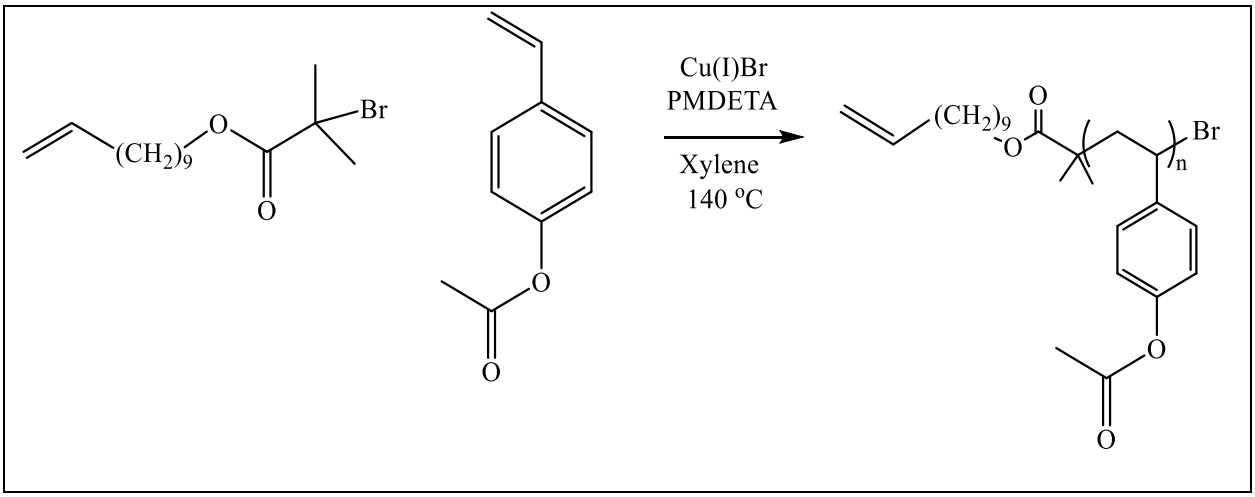

Scheme 1.10. Synthesis of the Tier-II ESSs by ATRP of 4-acetoxystyrene

1.3.5.3 Hydrolysis and Hydrosilylation of the Tier-II ESSs

Hydrolysis of acetyl protecting groups in tier-II building blocks revealed phenolic -OH groups in aromatic rings. Tier-II ESSs were stirred in hydrazine ($H_2N.NH_2$) and THF for 24 hours to accomplish selective hydrolysis of acetyl ester. The alkene end of the Tier-II ESSs was then hydrosilylated using the triethoxysilane and Karstedt's catalyst. But the ^1H did not confirm the successful hydrosilylation reaction, probably due to the triethoxysilane was reacting with the phenolic -OH group present in the Tier-II ESSs instead of the alkene end. However, when the Hydrosilylation reaction of the Tier-II ESSs was performed first, and then the hydrolysis reaction on the hydrosylated Tier-II ESSs, ^1H confirmed the successful synthesis. The triethoxysilyl end will act as the tethering point while grafting onto silica gel.

Due to the strong reactivity of trichlorosilane and its high sensitivity to hydrolysis and crosslinking, the formation of a three-dimensional network (gel slug) that cannot be grafted onto silica was a difficulty.[138] For this reason, a silane-coupling reagent that was less reactive was necessary in order to successfully carry out the hydrosilylation procedure. Triethoxysilane was selected for the hydrosilylation process rather than trichlorosilane because it is active enough to

hydrosilylate the alkene end of the oligomers, but it is not too sensitive to moisture and has a higher propensity to crosslink than trichlorosilane does.

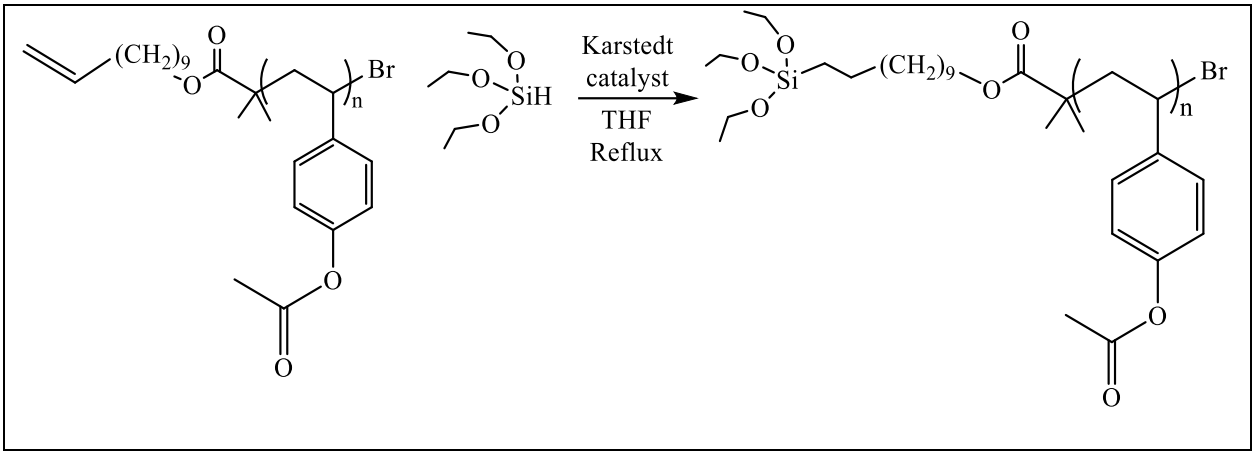

Scheme 1.11. Hydrosilylation of the Tier-II ESSs

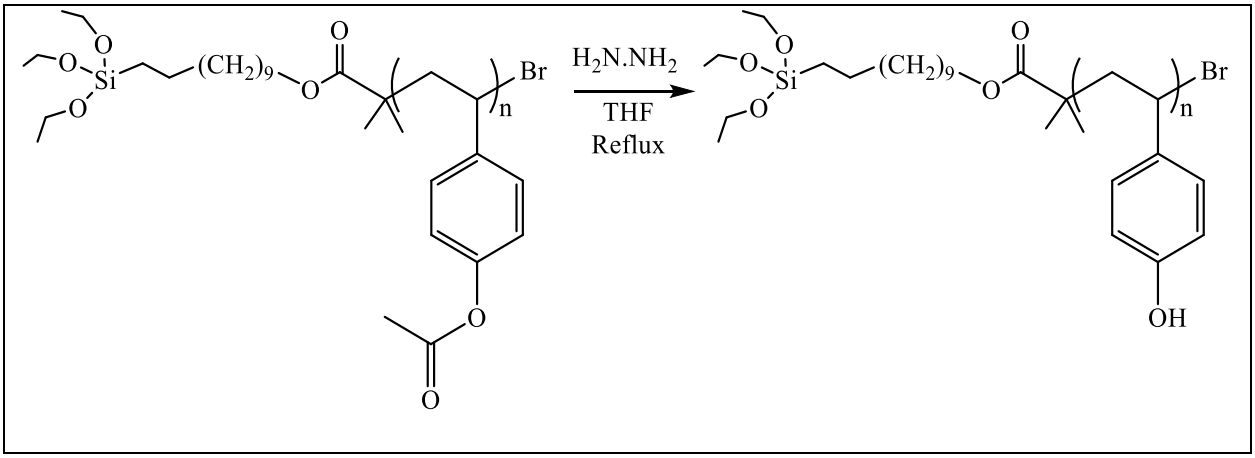

Scheme 1.12. Hydrolysis of the Tier-II ESSs

1.3.5.4 Crosslinking reactions of the hydrolyzed Tier-II ESSs

To impart cross-linking into the soil surrogates, Tier-II ESSs were then stirred with dodecanedioyl dichloride in THF under refluxing conditions. Cross-linking reaction happened on the phenolic -OH site of the Tier-II ESSs, which was confirmed by the ^{1}H NMR and FTIR.

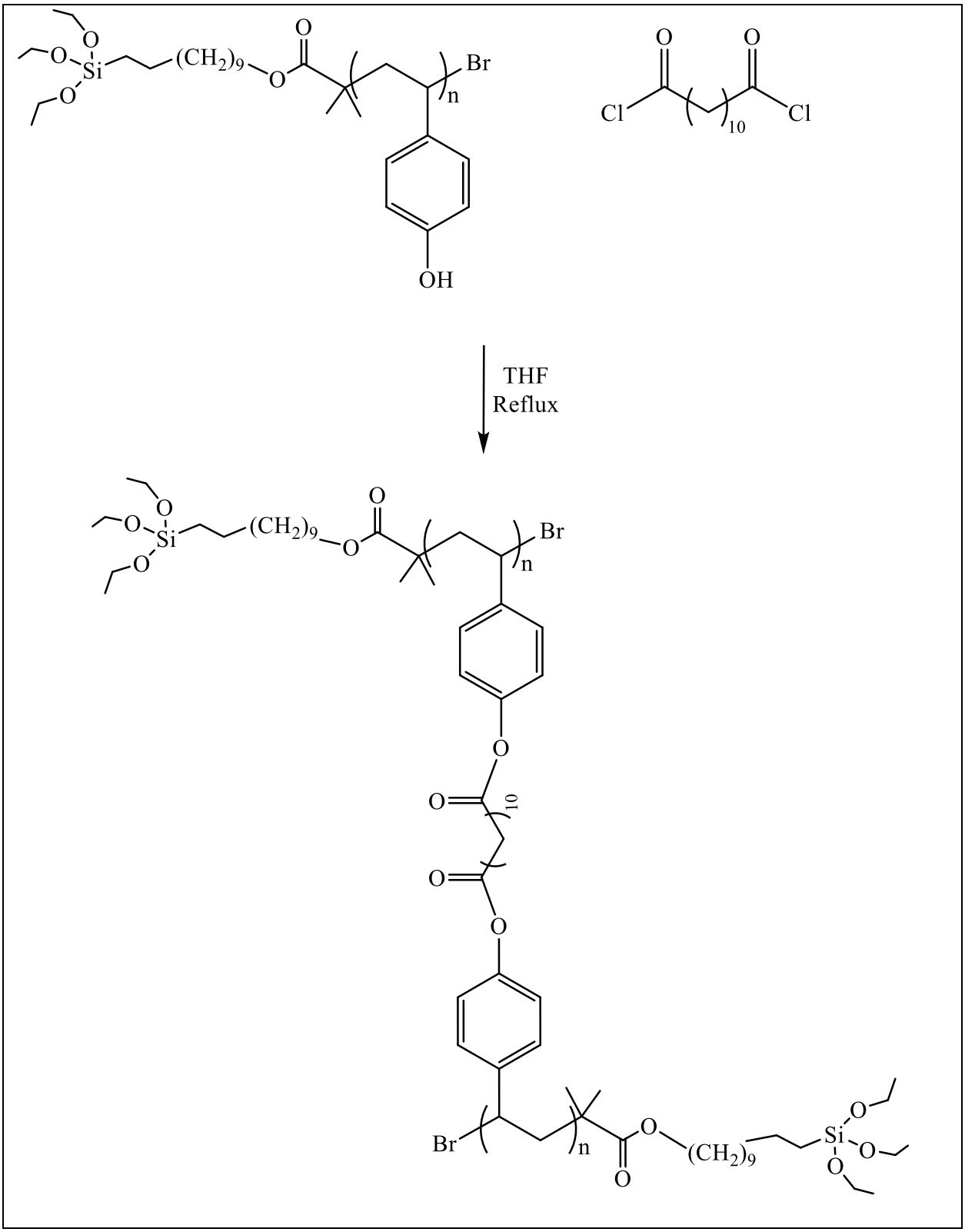

Scheme 1.13. Crosslinking reactions of the hydrolyzed Tier-II ESSs

1.3.5.5 Grafting of the crosslinked Tier-II ESSs onto silica

Hydrosilylated Tier-II were grafted onto silica gel by reacting the silyl end of the oligomers with the silanol groups of the silica particle. There is a strong link formed between organic and inorganic materials by using silane coupling agents.[1] Triethoxy-silane coupling agents have ethoxy groups that are hydrolyzed by water (added or unintended), forming silanol groups that may condense with silanol groups on silica, anchoring the oligomer to the silica particle.

The cross-linked ESSs were dissolved in toluene and refluxed overnight with activated (heated in the oven) silica gel to accomplish the grafting reactions. After separating the supernatant, a series of solvents with changing polarity, such as toluene, acetonitrile, and ethanol were used to wash the grafted product on silica. After drying overnight at 80^{O} C in an oven, the total organic fraction (TOF) grafted was determined by the TGA analysis. To mimic natural soils, the TOF was aimed at between 5% and 25%. However, in the case of cross-linked ESSs, the %TOF was found to be 4.25%, probably due to the limited availability of the polymer end to be tethered because of steric hindrance.[139]

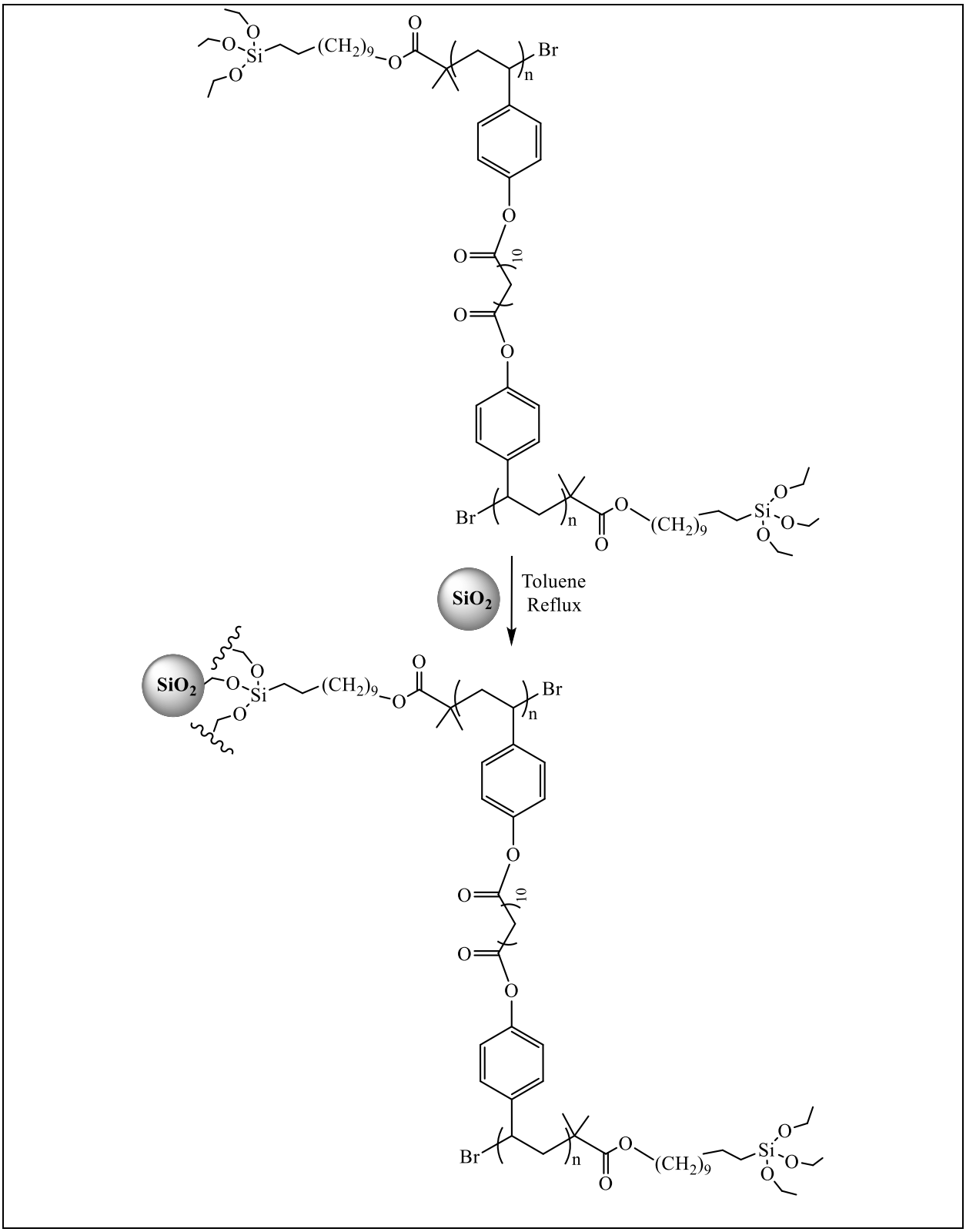

Scheme 1.14. Grafting of the crosslinked Tier-II ESSs onto silica

1.4 Conclusion

A series of ESSs have been synthesized to mimic the natural soils. 13C solid-state NMR and TGA analysis confirmed the successful synthesis of the ESSs. To compare the results with the real soil, acetylation reaction was done on the Pahokee peat. Sorption studies of the ESSs and acetylated Pahokee peat using Norflurazon as the model agricultural chemical showed that the ESS1, ESS2, ESS3, and acetylated Pahokee peat followed the expected trends in the sorption behavior, while ESS4 showed an opposite trend, likely due to the intermolecular hydrogen bonding between the phenolic -OH and nearby -OCH_3 groups in the aromatic ring. To see how the change in molecular structure affects the binding properties of Norflurazon, a different monomer where the -OCH_3 group in the aromatic ring present in the ortho position instead of the meta position relative to the -OH group was synthesized by using Wittig reactions. This monomer can be used to synthesize different Tiers of ESSs. Finally, a cross-linked ESS was synthesized to observe the effects of cross-linking on the sorption behavior of agricultural chemicals. A solution phase synthesis approach was utilized instead of the solid phase synthesis. However, the %TOF found from the cross-linked ESS was 4.25% which is a little low than the aimed value of at least 5%. The probable reason of low grafting was due to the limited availability of the polymer end to be tethered because of steric hindrance.

Chapter 2. Molecularly Imprinted Polymers (MIPs) for the Detection of Fentanyl

2.1 Introduction and Significance

2.1.1 Drug Overdose Epidemic

Since the middle of the 1990s, there has been a significant rise in the number of drug-related hospital emergency department visits, admissions to treatment for substance misuse, and deaths caused by drug overdoses in the United States. Since 2010, there has been a particularly high increase in the number of deaths caused by drug overdoses, and this trend has maintained up to the current day.[140] Prescription opioids, especially OxyContin, were major contributors to the epidemic's initial spread.[141] Since the emergence of OxyContin's abuse-deterrent formulations in 2010[142, 143] and the public's increased awareness of the prescription opioid pandemic, heroin and other synthetic opiates like fentanyl have carried a disproportionate share of the blame for overdose deaths.[140, 142, 144]

Overdose deaths caused by both legal and illegal opioids killed approximately half a million individuals in the United States between 1999 and 2019.[145] The overdose epidemic in the United States has hit an all-time high, with preliminary statistics from 2020 showing that more than 90,000 lives were lost to drug overdoses in the 12 months ending in December 2020.[146] The upward trend in the number of people dying from opioid overdoses may be broken down into three separate waves. The first wave started with a rise in the prescribing of opioids in the 1990s. Since at least 1999, the number of overdose fatalities involving prescription opioids (natural and semi-synthetic opioids and methadone) has been growing.[141] The second wave started in 2010 when there was a sharp rise in the number of fatalities caused by heroin overdoses.[147] The start of the third wave was in 2013, and it was marked by considerable rises in the number of fatal overdoses utilizing synthetic opioids, most notably those containing fentanyl that was produced illegally.[148,

[149] The black market for illicitly produced fentanyl is constantly evolving, and it is increasingly being sold in conjunction with other illicit substances such as heroin, counterfeit medicines, and cocaine.[150]

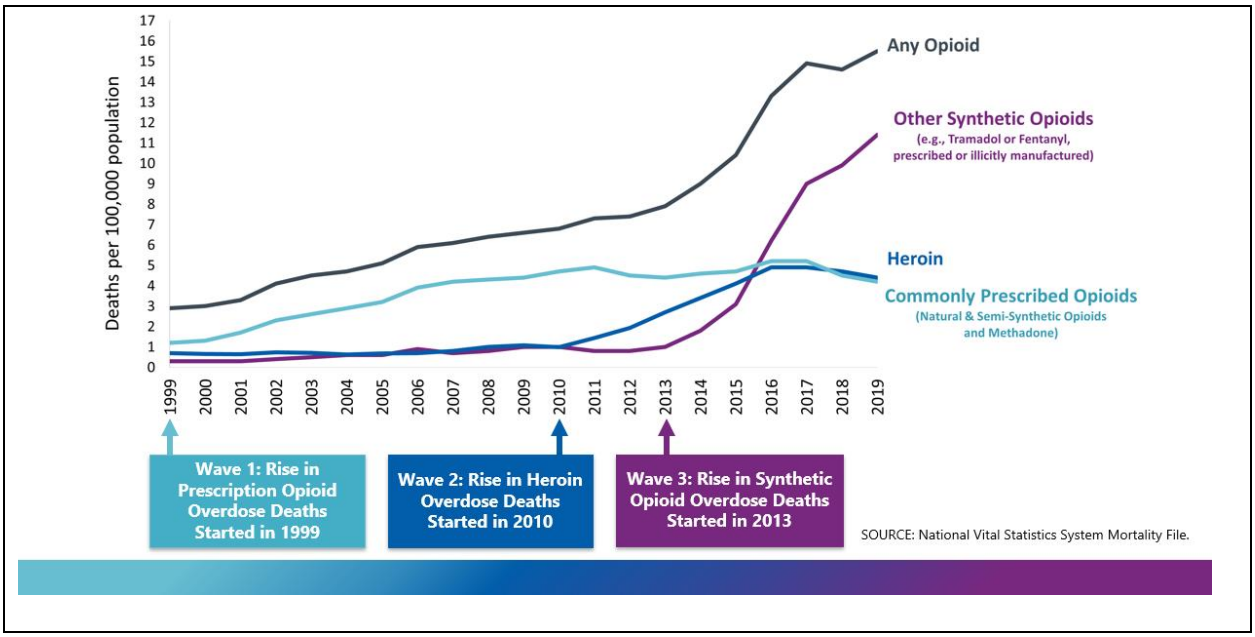

Figure 2.1. Three waves of the rise in opioid overdose deaths.[146]

Even though the United States has been through drug epidemics in the past, the present drug pandemic is notable for three important differences. To begin, the current epidemic's scale, in terms of the projected number of people using the drug and the fatalities it has caused, is far greater than that of earlier outbreaks. Second, while illegal drugs (heroin in the 1970s and cocaine in the 1980s to early 1990s) were the primary cause of the earlier epidemics, legal drugs (prescription opioids) were the primary cause of the contemporary epidemic until the most recent decade. Third, the death toll from drug overdoses used to be concentrated in major cities such as New York, Philadelphia, Baltimore, and San Francisco. However, the current epidemic has encompassed dramatic increases in the death toll from drug overdoses in nontraditional locations, especially in midsize cities, suburbs, and rural areas.[151, 152] This has led to a convergence in drug overdose mortality rates, such that drug overdose death rates in rural regions and urban areas do

not vary much from one another at the national level, despite the fact that there is a significant degree of regional variability in these patterns.[152]

2.1.2 Fentanyl and Fentanyl Analogs

Fentanyl is a synthetic opioid that is 50-100 times more potent than morphine and 50 times more than heroin.[153] In 1960, Paul Janssen of Belgium developed fentanyl and began selling it as a pain reliever.[154] The US Food and Drug Administration (FDA) authorized its use as an intravenous anesthetic in 1972; the drug was subsequently sold under the brand name Sublimaze®.[154] After fentanyl lost its patent protection in 1981, sales skyrocketed by a factor of 10. Abuse and illegal use by physicians, particularly anesthesiologists and surgeons who had access to the medication, was initially recorded in the 1980s and persisted until the early 2000s.[155, 156] When fentanyl transdermal patches were first released in the 1990s, they were primarily used by professionals, but eventually, people gained access. Therefore, beginning in the 1990s and continuing into the early 2000s, there was an increase in the number of reports of overdoses attributed to the abuse of fentanyl transdermal patches.[157-159] The Food and Drug Administration (FDA) issued a warning in 1994 about the risks of fentanyl patches, stating that they should only be supplied to those with severe pain that cannot be handled by less strong opioids.[160] In the middle of the millennium, the number of fatal overdoses caused by NPF (nonpharmaceutical fentanyl- fentanyl produced outside of a pharmaceutical setting) increased dramatically. Most NPF was traced back to tainted heroin or cocaine sold on the streets and injected by users. While urban Chicago, Detroit, and Philadelphia accounted for the bulk of NPF-related mortality, some deaths were also recorded from suburban and rural locations in the Midwest and the East.[161] The DEA was able to track the origins of the lethal NPF down to a single underground laboratory in Toluca, Mexico. This epidemic finally ended in 2007 when the DEA seized the laboratory where the fentanyl was being produced and scheduled the precursors for fentanyl. NPF-laced heroin and cocaine resurfaced in the mid-2010s,

and counterfeit medications containing NPF also increased at that time. There was a near threefold increase in the number of fatalities attributed to NPF between 2012 and 2014 in the United States.[149] The first counterfeit fentanyl tablets were discovered in the United States in 2014.[162] Although NPF-adulteration is most often associated with heroin and other illicitly manufactured opioid analgesics, it has also been detected in cocaine. Because many cocaine users are probably not used to using opioids, this presents a serious threat to their health. In June of 2016, thirteen people in Connecticut overdosed on fentanyl after using cocaine that had been laced with the synthetic opioid.[163] Since the necessary precursors are easily obtained and often transported from China, the manufacture of counterfeit medications and NPF-laced heroin and cocaine is projected to continue to grow.

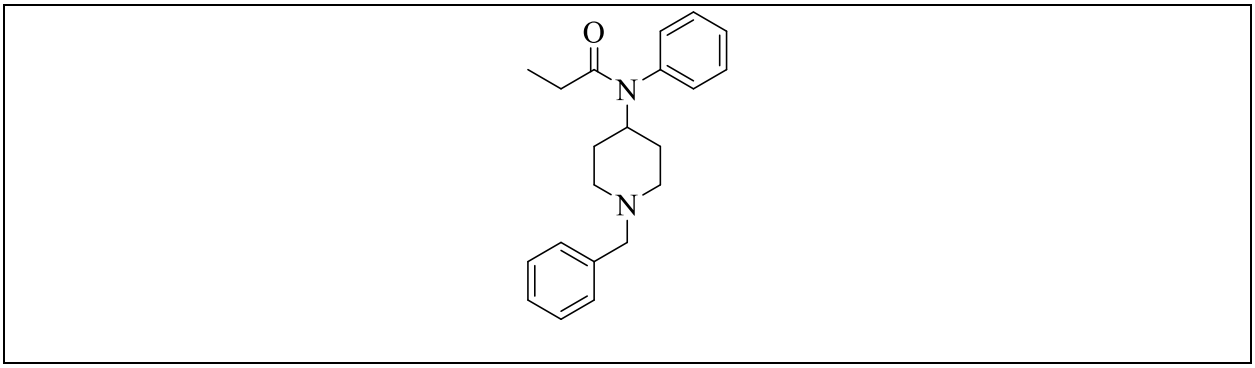

Figure 2.2. Structure of fentanyl

Fentanyl is a complete agonist of the μ-opiate receptor. Fentanyl, like other opioids, has a wide range of effects, from euphoria and sleepiness to analgesia and relaxation to negative side effects such as respiratory depression, gastrointestinal issues, nausea, itching, rashes, orthostatic hypotension, and stiff chest.[164] Fentanyl is rapidly absorbed by tissues and membranes and easily crosses the blood-brain barrier. Because of the molecule's lipophilicity, it was discovered that 98.6% of Fentanyl's plasma permanence was attained in 60 minutes, whereas its total elimination happens after 219 minutes.[164] Due to its degradation in the liver by cytochrome CYP into its

primary metabolites, norefentanyl and depropionylfentanyl, the original structure of fentanyl is only detected in 8-10% of urine samples.[165]

After the production of fentanyl in 1960, numerous other fentanyl analogs were produced for application in medicine and veterinary medicine. In addition, illegal drug makers regularly modify the structural framework of fentanyl to generate unique and stronger fentanyl analogs. Some of these fentanyl analogs include sufentanil, alfentanil, remifentanil, and carfentanil. The Drug Enforcement Administration (DEA) has placed fentanyl analogs that are analgesics or veterinary medications under the Schedule II category of narcotics. Beginning in the winter of 1979, many cases of opioid overdose were reported in the state of California as a result of the usage of "China White," also known as synthetic heroin; nevertheless, the toxicology report did not reveal the presence of heroin or any other recognized opioids. In the end, alpha-methylfentanyl, abbreviated as AMF, was shown to be the agent responsible for the overdoses.[166] Another derivative, 3-methylfentanyl, was discovered in 1984 in Allegheny County, Pennsylvania. It was linked to 16 fatal overdoses during that time period.[167] Following this, both alpha-methyl and methylfentanyl were placed on the schedule I list of controlled substances in 1981 and 1986, respectively. The development of these two analogs led to the passage of the Federal Analogue Act in 1986, which is a subsection of the Controlled Substances Act in the United States. This act allows any chemical that is "substantially similar" to a controlled substance that is listed in Schedule I or II to be treated as if it were also listed in those schedules. The only caveat to this is that the chemical must be intended for consumption by humans in order to qualify for this treatment. Because it is necessary to establish that a designated substance is truly "substantially comparable" and that it was intended for human consumption, this act has proved to be difficult to implement in particular instances that have been tried in the judicial system of the United States.[154]

In the middle to the latter part of the 1980s, at least eleven new analogs were discovered on the black market. These analogs were alleged to be responsible for overdoses that were caused by heroin that included NPF. The emergence of acetylfentanyl as a potent fentanyl analog in 2013 led to a rise in overdose deaths in Rhode Island, Pennsylvania, and North Carolina.[168] Clinical and forensic toxicology labs do not frequently monitor acetylfentanyl, hence it is suspected that the severity of this epidemic is being underestimated. In 2015, the CDC issued a public health warning suggesting more in-depth toxicological study in the event of unexpected spikes in opioid overdoses. Acetylfentanyl was classified as a Schedule I narcotic by the DEA in 2015. The DEA categorized butyryl fentanyl and betahydroxythiofentanyl as Schedule I drugs in 2016 after concluding that they were involved in multiple deaths in 2015.[162] Despite being a general anesthetic for big animals, carfentanil, which was first manufactured in 1974 by Janssen Pharmaceutica, has already found its way into the heroin supply in the United States. The first spread was seen in August/September 2016 in the Midwest and Appalachian regions. Over 300 carfentanil overdoses were predicted by the DEA over this time period.[154] Carfentanil, the most powerful derivative of fentanyl that has been found in the United States, is 10,000 times stronger than morphine.[169]

Several modifications are possible to the fentanyl's core structure, as shown in figure 2.3, which demonstrates the possibility of creating a range of new potent analgesics.[170] Changes with significant practical implications include the substitution of the piperidine ring for the pyrrolidine or azepine rings; the production of open chain compounds; the substitution of the phenyl group in the phenethyl-part of the molecule for various aromatic heterocycles, namely for thiophene and tetrazole; the insertion of carbomethoxy- or methoxymethyl- into the fourth position of the fentanyl's 4-anilino- group, which can be modified by exchanging hydrogen atoms in the aromatic

ring for fluorine atoms or by exchanging the whole benzene ring for an aromatic heterocycle; insertion of several methyl groups in different positions on the piperidine ring; replacing the propionyl- group in the 4-anilido-fragment with several other acyl groups, etc.

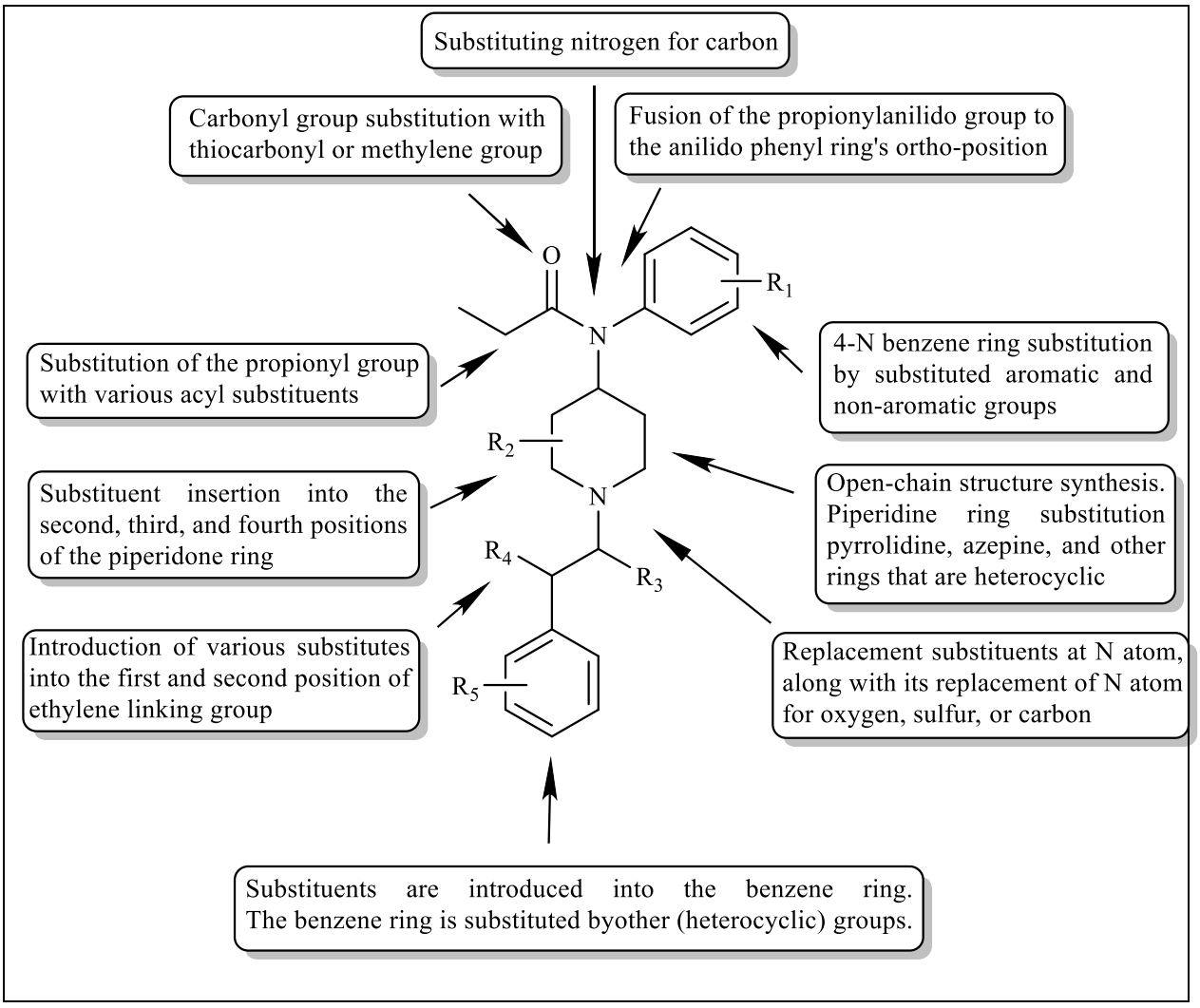

Figure 2.3. Modifications of the fentanyl structure. Reproduced from ref[170]

2.1.3 Previous Studies for the Detection of Fentanyl

According to the CDC, fentanyl overdose deaths have increased from 57,834 in 2020 to 71,238 in 2021.[171] Fentanyl is often mixed with other drugs, such as heroin, to increase its euphoric effects, with or without the knowledge of the end users. With the lethal dose of only 2 mg, fentanyl has become the deadliest synthetic opioid to date.[172] Therefore, several studies have already been

developed for detecting fentanyl using chromatographic and/or spectral techniques.

Zhang et al. created a spectrum library of synthetic opioids by using liquid chromatography-high resolution mass spectrometry (LC-HRMS) and a data collection strategy based on information-dependent acquisition of product ion spectra, all utilizing the CDC's fentanyl analog screening (FAS) kit.[173] The synthetic opioids in the FAS kit (n = 150) were analyzed for their chromatographic retention periods, limits of detection, and matrix effects in urine and serum. In order to assess the prevalence of fentanyl analogs and other synthetic opioids, the FAS LC-HRMS library was applied to all urine and serum specimens supplied to a clinical toxicology laboratory for complete drug testing in 2019 (n = 856) and 2021 (n = 878) respectively (2021).[173] In urine, the LOD for each opioid was between 1 and 10 ng/mL (median, 2.5 ng/mL), whereas in serum, it was between 0.25 and 2.5 ng/mL (median, 0.5 ng/mL). From 2019 to 2021, the prevalence of fentanyl and fentanyl analogs in serum samples rose somewhat, but the prevalence in urine did not change significantly.[173] In order to aid in the structural elucidation and drug identification of future fentanyl analogs, analysis of the developed MS/MS spectrum library showed distinctive fragmentation patterns in most fentanyl analogs.[173] Benchtop ion mobility spectroscopy (IMS) was used to create a technique to detect diluted N-phenylpropanamide (NPPA), a degradant of fentanyl, by Smith et al.[153] They took a semi-quantitative approach using secondary electrospray ionization-ion mobility spectroscopy (SESI-IMS), where NPPA was ionized by IMS in solution and vapor phase, and from fentanyl headspace before being detected on a Faraday plate detector. This is a non-contact detection method, where NPPA in the vapor phase was detected above 5 mg of NPPA.[153] Vaughan et al. studied undiluted pharmaceutical grade fentanyl using solid-phase microextraction followed by gas chromatography-mass spectrometry (SPME-GC-MS) to generate a vapor signature. N-phenethyl-4-piperidone (NPP) and N-

phenylpropanamide (NPPA), two of the three most prevalent chemicals, were positively identified and remained unaffected when contaminated with lactose, mannitol, or initosol.[174] Additionally, NPPA was discovered in the headspace of seized fentanyl compounds. As a means of rapid, on-site testing for fentanyl analogs, Kang et al. created a technique based on the use of a dual ion trap portable mass spectrometer.[175] Sensitive study of numerous fentanyl compounds was made possible via optimization of different direct sample approaches, such as paper capillary spray cartridge with a tiny mass spectrometry equipment footprint. In order to test the efficacy of this approach, they analyzed several beverages for traces of fentanyl and its derivatives. It has also been used to detect fentanyl molecules on a dirty plastic bag's surface, with limits of detection (LODs) as low as 1 ng/cm^2. In addition, a precursor ion scan technique was created for rapid screening of numerous fentanyl compounds. This method has also been used to detect fentanyl in human urine. Six fentanyl derivatives, including fentanyl, cis- and trans-methylfentanyl, sufentanil, alfentanil, and carfentanil, were separated and identified using a nonaqueous capillary electrophoresis-electronspray-tandem mass spectrometry (NACE)-ESI-MS^n method by Rittgen et al.[176] An innovative method for the simultaneous qualitative and quantitative analysis of twenty-four fentanyl analogues, including seven sets of positional isomers, was presented by Buchalter et al., in which gas chromatography (GC) is interfaced with both cold electron ionization mass spectrometric (cold EI MS) and vacuum ultraviolet (VUV) detection by means of a flow splitter.[177] Sisco et al. investigated the use of ion mobility spectrometry (IMS) and thermal desorption direct analysis in real-time mass spectrometry (TD-DART-MS) as tools for the rapid and sensitive detection (nanogram to picograms) of fentanyl, 16 fentanyl analogs, and five additional opioids.[178] Studies on competitive ionization have shown that identifying these compounds in the presence of heroin is easily attainable using TD-DART-MS, even at concentrations of fentanyl that are as low

as 0.1% by mass.[178] When using IMS, it is possible to detect nanogram amounts of fentanyl in a binary combination of fentanyl and heroin; however, this task may be more challenging due to lower resolution in some commercial instrument types. In addition, they had shown that the detection of these substances is not significantly hindered by the presence of three complex background matrices, namely fingerprint residue, dirt, and plasticizers. Wipe sampling of the outside of bags containing questioned powders has proved to be a safe alternative approach for field screening and identification. This method removes the need to handle potentially fatal amounts of material, making it an ideal choice for the purpose.[178] Other analytical techniques used for fentanyl detection include Raman spectroscopy,[179] gas chromatography-infrared spectroscopy (GC-IR),[180] capillary gas chromatography-electron capture detector (GC-ECD),[181] liquid chromatography-ultraviolet detection (LC-UV),[182] liquid chromatography-mass spectrometry (LC-MS),[183] etc.

Lin et al. provided a surfactant-based colorimetric test for the visible and sensitive detection of fentanyl.[184] It has been discovered that sodium dodecyl sulfate (SDS) simultaneously strengthens the halogen-bonding contact between Rose Bengal (RB) as the probe and fentanyl and stabilizes the RB-fentanyl complex. This molecular recognition triggers an intermolecular charge transfer, resulting in a substantial redshift in the RB absorption band and a pronounced color shift from red to purple. This assay has a very fast reaction time (within 1 minute), and the limit of detection is predicted to be as low as 0.1 mgL^{-1}.[184] He et al. developed a visual colorimetric test based on the TCPO-H_2O_2-TMB chemically initiated electron exchange chromogenic (CIEEC) reaction system to take advantage of the catalytic effect of fentanyl and norfentanyl and found that the resultant sensitivity is equivalent to that of the published colorimetric assays for fentanyl. Furthermore, their assay can identify fentanyl and norfentanyl in human urine samples.[185] For the

detection of fentanyl and fentanyl in combination with cocaine and hydrocodone, Kangas et al. developed a novel colorimetric test based on eosin Y, which produces a pink color when reacted with fentanyl.[18620] Several studies were performed for detecting fentanyl using electrochemical sensors.[187, 188]

At present, there are a few immunoassay methods that allow for the detection of fentanyl and its analogs at very low doses. Enzyme-linked immunosorbent assays (ELISAs), enzyme multiplied immunoassay methods (EMITs), and lateral flow immunoassays (LFAs) are the three most often used methods. ELISA is a 96-well plate containing a set quantity of a particular antibody.[189] ELISA may be used to target various kinds of fentanyl/fentanyl analogs by using different antibodies. The plate is incubated with a set quantity of enzyme-labeled free fentanyl and samples to detect the presence of fentanyl or its derivatives. The enzymatic activity will provide a signal that is inversely proportional to the quantity of fentanyl or fentanyl analogs present. ELISA targeting carfentanil and fentanyl was shown to be very selective, with little cross-reactivity with anything but its metabolites.[189] Norfentanyl-targeting kits, on the other hand, have low cross-reactivity with other fentanyl analogs. This is not unexpected given that hepatic cytochrome P450 converts several fentanyl analogs to norfentanyl. As a consequence, it is advised that ELISA kits that target various compounds be used together or that the results be confirmed using mass spectrometry. Aside from its specificity, ELISA is also sensitive enough to detect fentanyl in urine with a detection limit of 0.25 ng/mL and in plasma with a detection limit of 60 pg/mL.[190] Because of its sensitivity, ELISA is often employed in forensic and clinical laboratories. EMIT is most often used for in vitro analysis, and the results are frequently analyzed using a clinical chemistry analyzer. EMIT included enzyme-conjugated fentanyl as well as a particular antibody. Unlabeled fentanyl/fentanyl analogs will bind to the antibody competitively. The change in enzyme activity

is used to calculate the rate of reaction. In comparison to ELISA, the cross-reactivity of carfentanil and 3-methylfentanyl with this technique is quite poor.[189] In addition to the high expense of hiring an analyzer, EMIT is less sensitive than ELISA, making it a less attractive alternative for screening fentanyl/fentanyl analogs. The majority of urine test strips are LFAs. Through capillary action, LFAs quickly transfer the liquid samples across several test strip zones where they will compete to bind with antibodies against dye-labeled fentanyl/fentanyl analogs.[189] A favorable outcome is shown by the absence of a signal on the test line. This test's cross-reactivity was low, making it possible for analogs with the same presence or lack of certain substituents to provide false positive results. The accuracy of the fentanyl test strip (FTS) is increased by the fact that the cutoff concentration is set at 20 ng/mL and that only fentanyl and norfentanyl are tested. However, with high concentrations of 3,4-methylenedioxymethamphetamine (MDMA), diphenhydramine, and methamphetamine, false positives are rather frequent. Since other FTS have detection limits as low as 50 ng/mL, dilution of samples with 10 mL to 50 mL of water would guarantee that only fentanyl would be detected. FTSs have high acceptability among young adult drug users who may be at risk for accidental fentanyl overdose since it is extremely simple to use.[191] Park et al. validated the lateral flow chromatographic immunoassays for detecting fentanyl by collecting illicit drugs from law enforcement.[192] Angelini et al. evaluated the lateral flow immunoassay for detecting fentanyl in urine and saliva.[193]

The methods used so far for the detection of fentanyl by employing chromatographic-spectroscopic techniques are costly, tedious, and require experienced personnel for conducting the tests. Additionally, the equipment cannot be miniaturized into a hand-held device for on-the-spot forensic or real-time medical detection.[194] On the other hand, the semi-quantitative methods using the enzyme-mediated immunoassays have numerous disadvantages. Transport and storage of

antibodies must take place in a refrigerated environment. The synthesis of antibodies is characterized by a lengthy manufacture time, which may range from 6 to 9 weeks in the case of polyclonal antibodies.[195] Cost is another factor to take into consideration. Also, false-positive or false negative results were reported. In the end, due to these problems, neither mass spectrometry nor immunoassays are appropriate for real-time blood monitoring in clinical applications, nor are they good for in-place forensic testing. However, only a few works have been done for the detection of fentanyl by using molecularly imprinted polymer (MIP) based sensors. Liu et al. developed molecularly imprinted nanoparticles based optical fibre grating sensors for the detection of carboxyl-fentanyl, which is one of the two metabolites of butyrylfentanyl.[194, 196, 197] Grillo used the carboxyl-fentanyl molecularly imprinted polymer as the synthetic antibody for the development of an assay.[198] Consequently, the creation of a point-of-care sensor for fentanyl that is not only affordable, which MIPs are, but also simple to use would be advantageous.

2.1.4 Molecularly Imprinted Polymer

Sensing the surrounding environment has become commonplace in the contemporary world. Molecular recognition is crucial to biological processes and is now the subject of considerable chemical study owing to its relevance in processes such as catalysis, separations, and sensing. While natural systems may develop antibodies against a variety of foreign entities, using such receptors in chemical processes confronts a number of challenges, including cost and environmental sensitivity.[199] The development of synthetic receptors that imitate natural antibody-antigen activity with comparable selectivity and sensitivity is a focus of contemporary sensor research. This molecular recognition, when combined with contemporary methods for monitoring changes in the recognition components, holds the possibility of selective, sensitive sensors capable of detecting and monitoring targets noninvasively. Molecularly imprinted polymers (MIPs) are best characterized as synthetic counterparts of biological antibody-antigen systems. As such, they

use a "lock and key" mechanism to selectively attach the target molecule as a template. MIPs have the potential to provide the specificity and selectivity of biological receptors with the added benefits of environmental resilience and cheap cost.[199, 200]

Molecular imprinting is a methodology to engineer synthetic polymers with very specific recognition sites. This technique involves the co-polymerization of functional and cross-linking monomers in the presence of the analyte of interest. This analyte of interest serves as a template molecule or imprint molecule. Molecular imprinting may be accomplished in two distinct ways: through covalent interactions and via non-covalent interactions.[201] The term 'imprinted polymer' was first reported in literature in 1984 by K. Mosbach and B. Sellergren, although G. Wulff had been publishing articles since 1973 using a different title 'Enzyme-Analog Built Polymers'.[202, 203] The Mosbach group concentrated on the utilization of noncovalent interactions between the host and target to form the imprint, while the Wulff group preferred to employ covalent binding as their primary method. It was anticipated that the covalent synthesis would result in a more uniform collection of rebinding cavities as well as the possibility of more target-specific MIPs, however, non-covalent imprinting seems to be the more effective strategy for simulating natural interactions between molecules (hydrogen bonding, electrostatic interactions, etc.), and can provide equal or better binding selectivity.[199, 204]

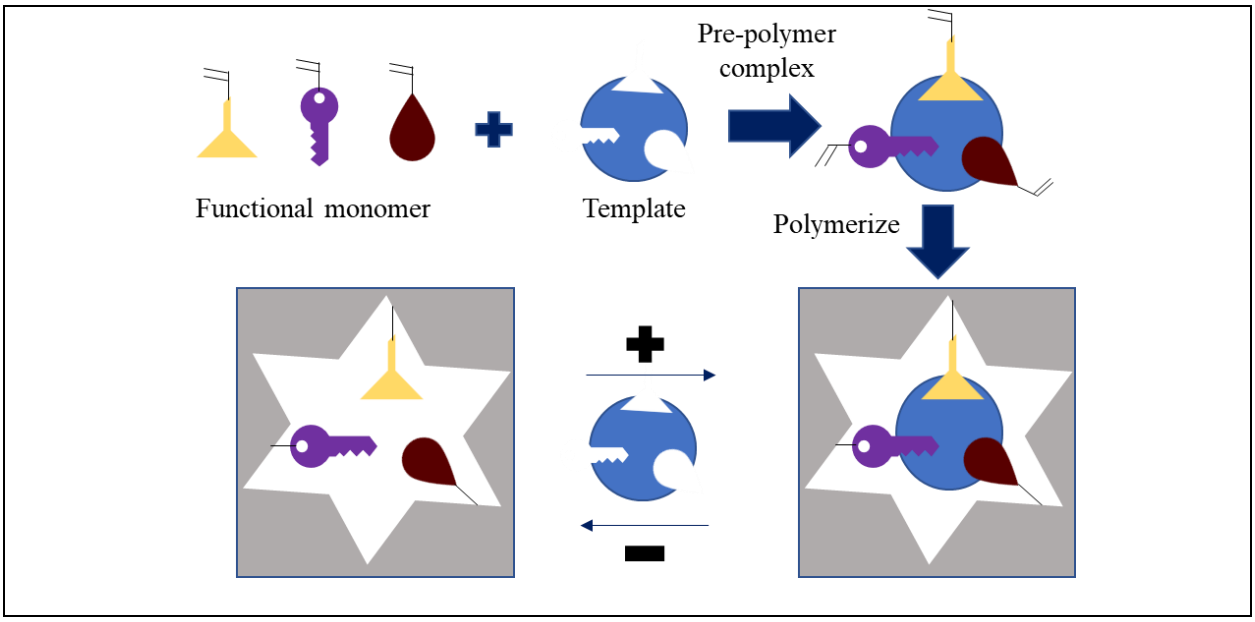

Figure 2.4. Traditional MIP scheme

The molecular imprinting technique begins with a pre-polymer complex (PPC) generated by non-covalent interactions between the imprint molecule and functional monomers as shown in figure 2.4. To create highly cross-linked polymers, the PPC is copolymerized with cross-linker monomer(s). Following the removal of the imprint molecule by solvent extraction, the analyte-specific binding sites are revealed. This gives the polymer a molecular memory, which means it can now rebind the analyte with high selectivity. Free radical polymerization,[205] electropolymerization,[206] controlled/living polymerization,[207] or sol gel synthesis[208] are all viable options for the synthesis of MIPs for a broad variety of analytes, beginning with ions[209] and progressing all the way up to entire cells.[210] MIPs are available in a variety of morphologies, such as monoliths, thin films, or nanoparticles, depending on the purpose for which they are intended.[211] The development of separation and sensing materials was detailed by Mosbach and Sellergren, while Wulff made considerable use of imprinted polymers in catalytic processes.[212, 213] Beginning in 1993, K. Shea reported on fairly unusual biological uses, such as the insertion of a plastic antibody into living mice.[204, 214] The advantages of imprinted polymers include durability, ease of

formation, requiring no special storage conditions, applicability to a much wider temperature range, and cheap cost. This makes the imprinted polymers suitable for various applications such as drug delivery,[215] catalysis,[216] solid-phase extraction,[217] sensing,[218] detecting illegal substances,[219] etc. In fact, several publications have recently reported on MIPs based sensors for the detection of SARS-CoV-2.[220-222]

2.1.5 Components of the Molecularly Imprinted Polymer

2.1.5.1 Monomer

Selection of functional monomer(s) is very crucial for creating highly specific sites for the template molecule. Common functional monomers include carboxylic acids like acrylic acid (AA), methacrylic acid (MAA), trifluoromethacrylic acid (TFMAA), and vinylbenzoic acid, sulphonic acids like 2-acrylamido-2-methylpropane sulphonic acid, and heteroaromatic bases like 4-vinylpyridine, 2-vinylpyridine, and N-vinylimidazole.[202, 223, 224] Monomers with a higher degree of basicity, such as those produced from amines, have also been employed effectively. Hydroxoethylmethacrylate and methacrylamide are examples of functional monomers that employ a neutral functionality to create binding sites through hydrophobic and hydrogen bonding interactions.[225] Furthermore, metal coordination interactions were used to create more potent functional monomers to bind certain sequences of amino acids.[226] A new class of functional monomers based on polymerizable amidines and ureas has been created as a stoichiometrically imprinted polymeric receptor for β-lactam antibiotics.[227] However, methacrylic acid (MAA) is widely used because it may function as a hydrogen bond donor, proton donor, and hydrogen bond acceptor.[228]

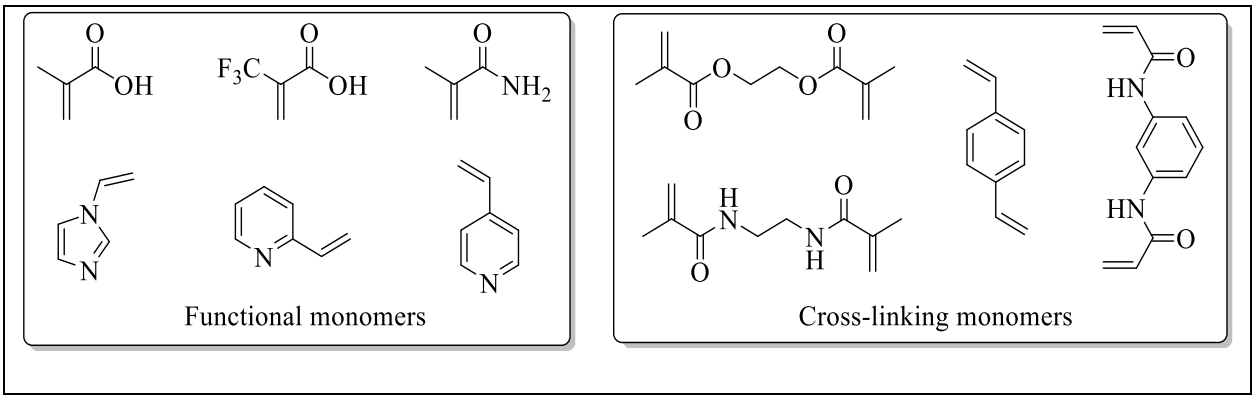

Figure 2.5. Common monomers used for molecular imprinting

The cross-linking monomer helps create a three-dimensional structure that retains its shape even after the template is removed. So, for excellent selectivity, the cross-linker type and concentration in the polymeric matrix are crucial. It was believed that the cross-linking monomer served mostly as a passive component of the polymeric matrix, one that did not engage with the template-binding functional groups. In this way, the imprinted polymer's specificity is enhanced by reducing the impact of non-selective interactions. However, reports from the Spivak group have shown that crosslinkers can also serve as interactive monomers with the template provided excellent molecular recognition.[229-232] Ethyleneglycol dimethylacrylate (EGDMA) is typically the most effective cross-linking monomer in most situations. The usage of similar acrylates compounds has not resulted in any noticeable improvement over EGDMA.[233] Amino acid-based (N,O-bisacryloyl-L-phenylalaninol) cross-linking monomers were the first to be utilized in molecular imprinting because of the variety of polymerizable functions they integrate.[202] Crosslinking amino acid-based monomers that offered reversible covalent bonding to the templates through a Schiff's base have also been used by Wulff and colleagues.[234]

In this work, methacrylic acid (MAA) and ethyleneglycol methacrylate (EGDMA) was used as the functional monomer and cross-linking monomer, respectively.

2.1.5.2 Solvent

The molecular imprinting process is also affected by the kind and amount of solvent used. Toluene, chloroform, dichloromethane, and acetonitrile are the most frequently used solvents in the production of MIPs.[228] Macroporous polymers owe their pore structure to the solvent, which also helps to bring together the other polymerization components (monomer, template, initiator, cross-linker). As the solvents' volume increases, the pore volume of the polymer expands, which is desirable for ensuring adequate flow through the resulting MIP. Therefore, the solvent is often called the "porogen." Less polar solvents, like chloroform or toluene, promote complex formation by facilitating polar non-covalent interactions like hydrogen bonds, whereas more polar solvents, such as protic solvents, tend to dissociate the non-covalent interactions in the prepolymer complex.[228] In this work, chloroform is used as the solvent.

2.1.5.3 Template

The template molecule, in the case of the MIPs, is the target of interest. It has been possible to effectively employ a wide variety of template molecules, including drugs, nucleotide bases, carbohydrates, proteins, amino acids, insecticides, hormones, and coenzymes, amongst others.[38-45] The capacity to effectively engage in non-covalent interactions, such as hydrogen bonding and electrostatic interactions, is a crucial characteristic that the template should possess. The size of the template should also be taken into consideration. The molecular weight of the template may vary from amino acids and medicines to bigger molecules such as proteins; nevertheless, imprinting becomes increasingly difficult as size rises.[235] A too-large template size might result in the template being permanently enclosed in the imprinted cavity. In addition, the size of big templates hinders their capacity to diffuse into the imprinted cavity during rebinding.[236]

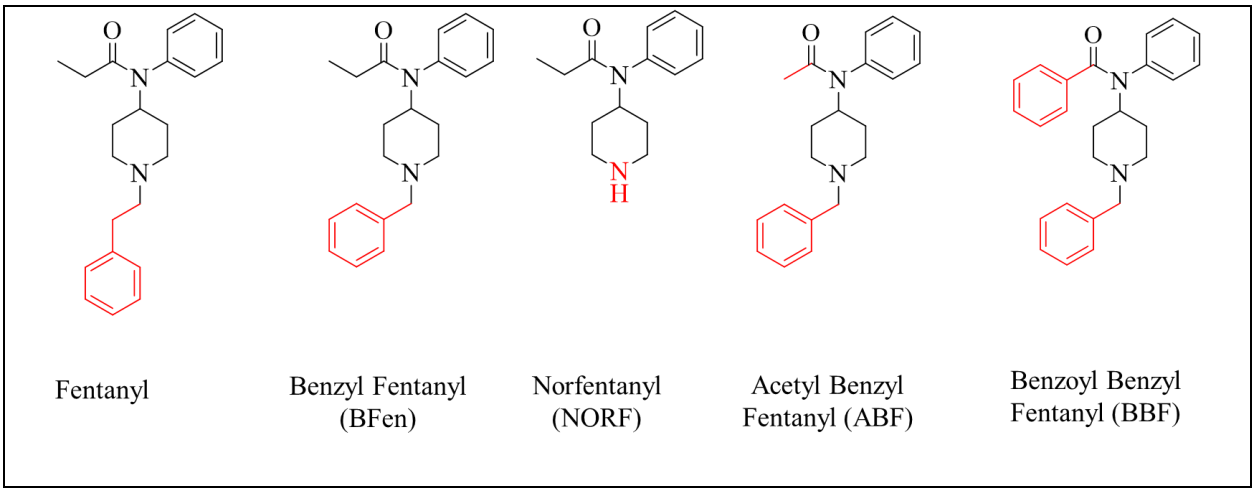

Figure 2.6. Structure of fentanyl and other structurally closely resembled analogs

In this work, fentanyl is the target of interest, and with a molecular weight of 336.47 g/mol, it is small enough to be imprinted, as well as having functional groups capable of hydrogen bonding and electrostatic interactions. But fentanyl is highly toxic to handle, with a lethal dose of only 2 mg. Therefore, the use of a template that closely resembles the structure of the fentanyl but is less toxic would be beneficial. Thus, benzylfentanyl (Bfen) is used as the template in this work. The main difference between fentanyl and benzylfentanyl is a single carbon atom in the N-2-phenylethyl group. Benzylfentanyl does not have any physiological effects as a narcotic, but it is a necessary precursor in the production of fentanyl.[237]

2.1.6 Significance

The long-term research goal of this work is to develop molecularly imprinted polymers (MIPs) based sensors which can selectively detect fentanyl and its analogs. At first, fentanyl and a few of its analogs, especially benzyl fentanyl (Bfen), were synthesized, and the molecularly imprinted polymers were made using different ratios of functional monomer (MAA) to template (benzylfentanyl) while keeping the amounts of cross-linking monomer (EGDMA) constant. Then the MIP parameters such as monomer to template ratio, particle size, mobile phase composition, and flow rates were optimized. Finally, the selectivity of the MIP was evaluated by comparing the

cross-binding selectivity of various drugs such as heroin, cocaine, and methamphetamine.

2.2 Results and Discussion

2.2.1 Synthesis of the Fentanyl and Fentanyl Analogs

Synthesis of the fentanyl and its analogs, especially benzyl fentanyl, was performed according to the previously published protocol with slight modifications.[238] At first, the reductive amination of N-boc-4-piperidone was carried out with aniline in the presence of Sodium triacetoxyborohydride and acetic acid by using dichloroethane as the solvent. The resultant product 1-Boc-4-(phenylamino) piperidine was obtained in good yield (95%). The acylation reaction of 1-Boc-4-(phenylamino) piperidine with propionyl chloride in the presence of triethylamine was carried out to form N-boc-norfentanyl in good yield (91%). Then, the deprotection of the boc protecting group of N-boc-norfentanyl was performed by using ethereal HCl in dry chloroform. The resultant norfentanyl, which is a fentanyl analog and also the primary metabolite, was obtained in good yield (85%).

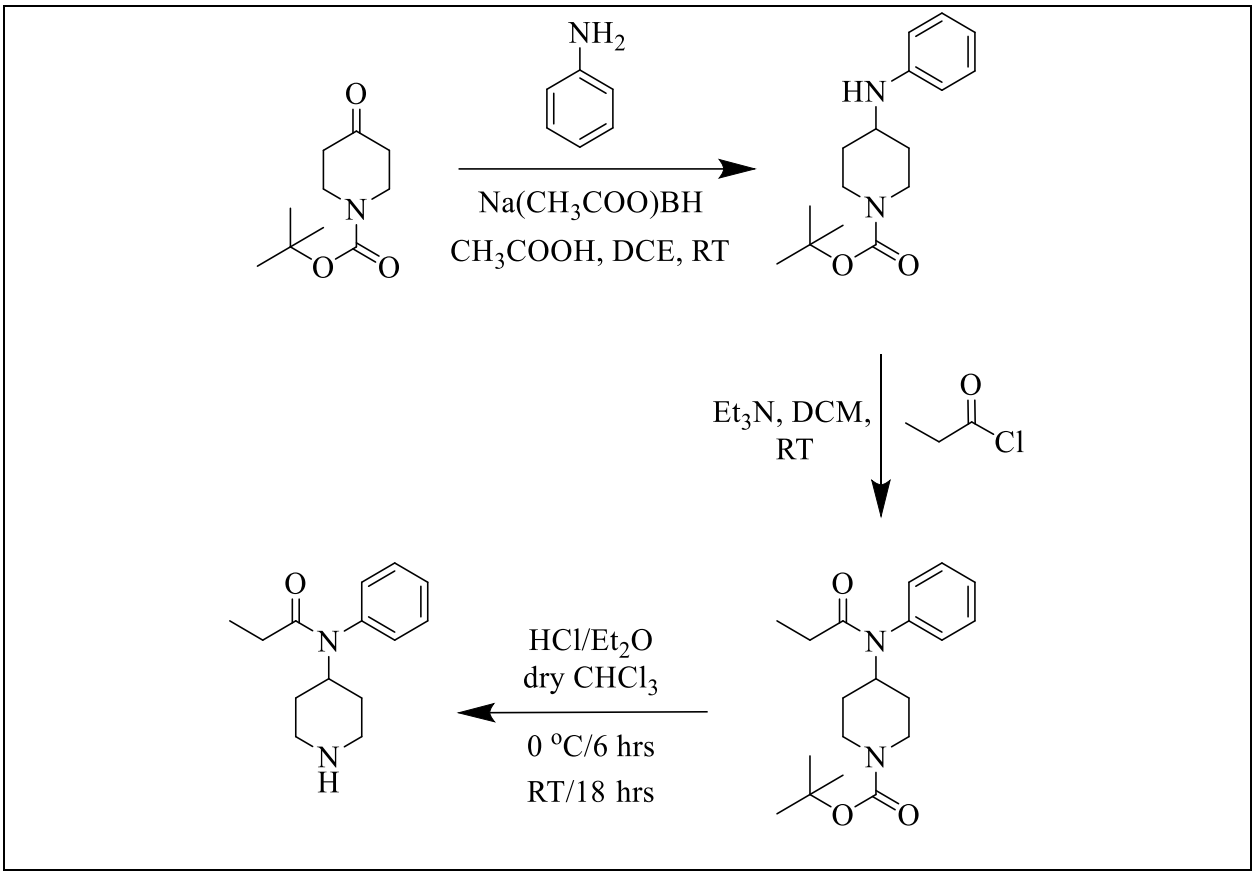

Scheme 2.1 Synthesis of the norfentanyl

Lastly, the alkylation reaction of norfentanyl was carried out with benzyl bromide in the presence of potassium carbonate as a base to form the benzylfentanyl. An extra methylene peak was seen in the ^{1}H NMR, and at first, it was thought that some unreacted benzyl bromide was present. Several purification steps, such as recrystallization, trituration, and column chromatography, were performed, but in each case, similar ^{1}H NMR spectra were obtained with the extra methylene peak. Later, MALDI-TOF analysis revealed the formation of a double substitution product because the molecular weight of the double substitution product matches the molecular weight obtained from the analysis. Both ^{1}H NMR and MALDI-TOF analysis confirmed the formation of the double substitution product, which is a new fentanyl analog.

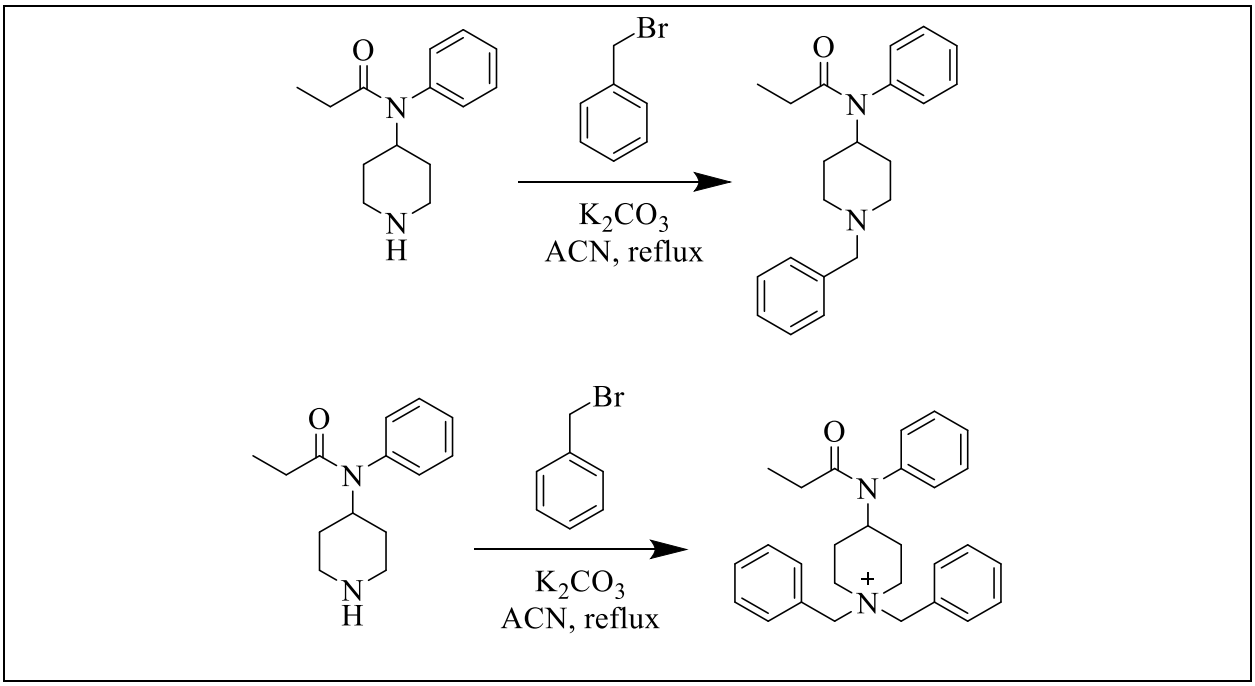

Scheme 2.2. Alkylation of 4-(*N*-propionylaniline) piperidine. Expected reaction (top) vs actual reaction (bottom)

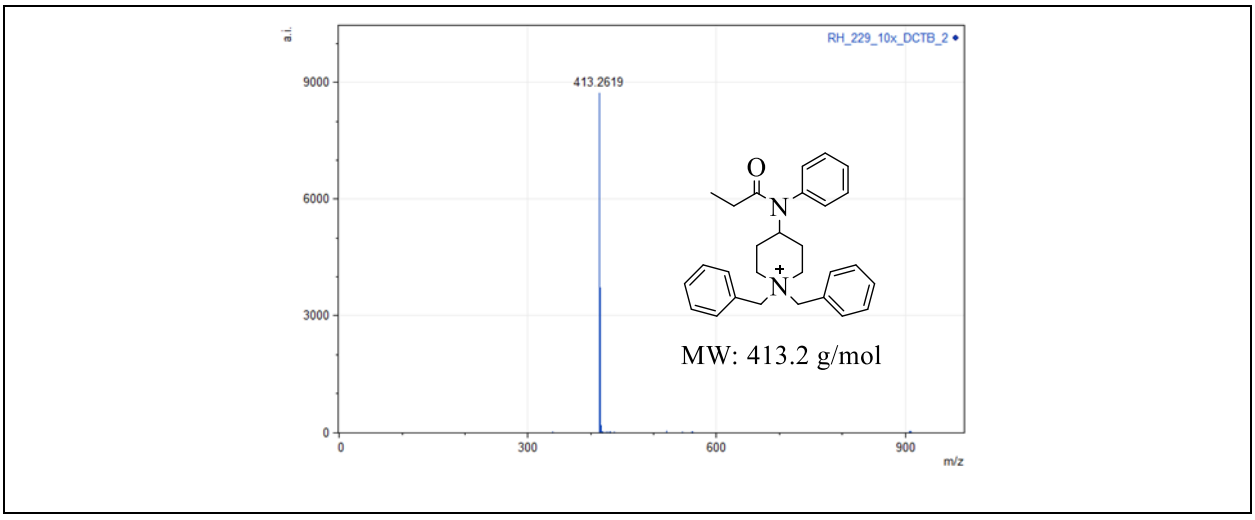

Figure 2.7. MALDI-TOF analysis of the double substituted product

On the other hand, the alkylation reaction of norfentanyl by using phenethyl bromide in the presence of potassium carbonate resulted in the formation of fentanyl. Benzyl bromide is far more reactive than the phenethyl bromide due to the benzylic stabilization of the partial cationic charge on the reacting benzylic carbon in the reaction transition state, which promotes the

formation of the double substituted product. Fentanyl was synthesized only in analytical amounts due to toxicity and controlled substance laws.

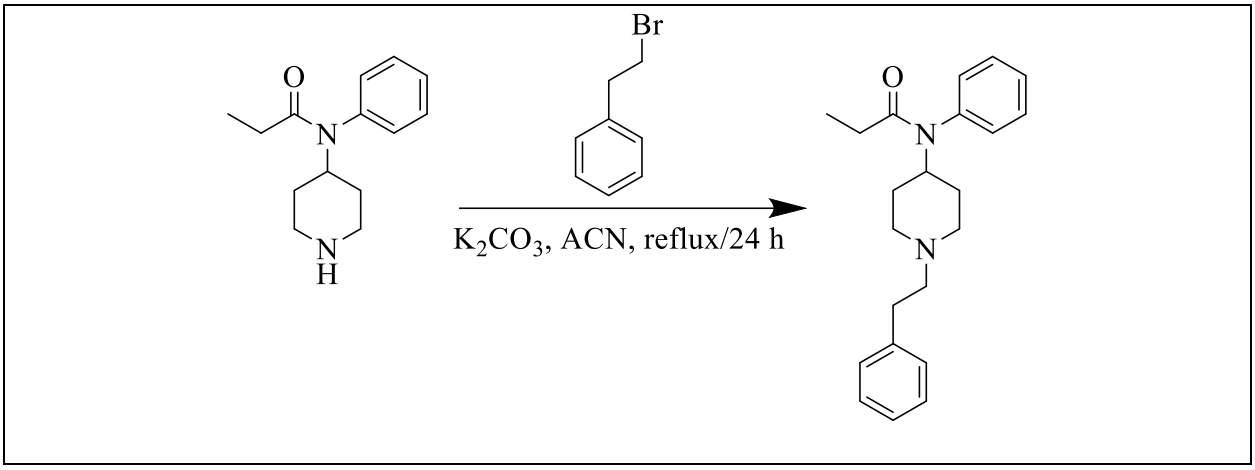

Scheme 2.3. Synthesis of the fentanyl

An alternative approach was then followed to form the benzyl fentanyl, where 1-benzyl-4-piperidone was used as the starting material, as shown in Scheme 2.4. 1-Benzyl-4-(phenylamino) piperidine was formed by the reductive amination of 1-benzyl-4-piperidone with aniline in the presence of sodium triacetoxyborohydride and acetic acid. Lastly, the acylation reaction of 1-Benzyl-4-(phenylamino) piperidine with propionyl chloride in triethylamine resulted in the formation of benzylfentanyl.

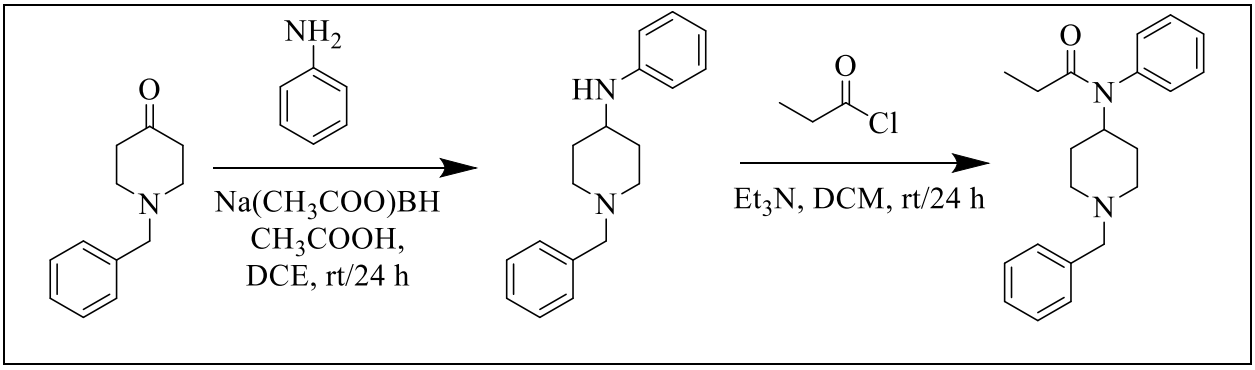

Scheme 2.4. Synthesis of the benzylfentanyl

1-Benzyl-4-(phenylamino) piperidine was used as the starting material for the synthesis of

the acetylbenzylfentanyl (ABF) and benzoylbenzylfentanyl (BBF) (Scheme 2.5). Acylation reaction of 1-Benzyl-4-(phenylamino) piperidine with acetyl chloride and benzoyl chloride resulted in the successful formation of ABF and BBF, respectively.

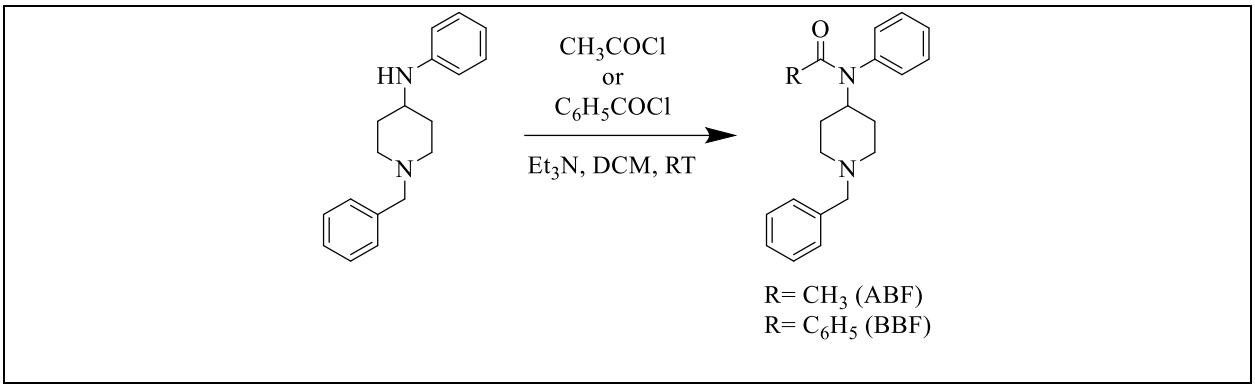

Scheme 2.5. Acylation of 1-Benzyl-4-(phenylamino) piperidine to form ABF and BBF

2.2.2 Polymer Preparation and Chromatographic Analysis

To prepare the imprinted polymer, in a 13 x 100 mm test tube, Benzyl fentanyl (2.7 mmol) was dissolved in 4 mL of chloroform. To this solution was added EGDMA (21 mmol), MAA (5.4 mmol), and AIBN (0.54 mmol). For comparison to the results, a control polymer was prepared similarly without the introduction of the template molecule. The solution was purged for 5 min by bubbling nitrogen gas and then capped and sealed with parafilm. The samples were put into a home-made photochemical reactor, which was immersed in a constant temperature bath. A standard laboratory UV light source (medium pressure 450 W mercury arc lamp) jacketed in a borosilicate double-walled immersion well was inserted in the reactor. At 20 ^{o}C, the polymerization was initiated photochemically, and the temperature was maintained by both the cooling jacket surrounding the lamp and the constant temperature bath holding the entire apparatus. The polymerization was allowed to proceed for 8 h.

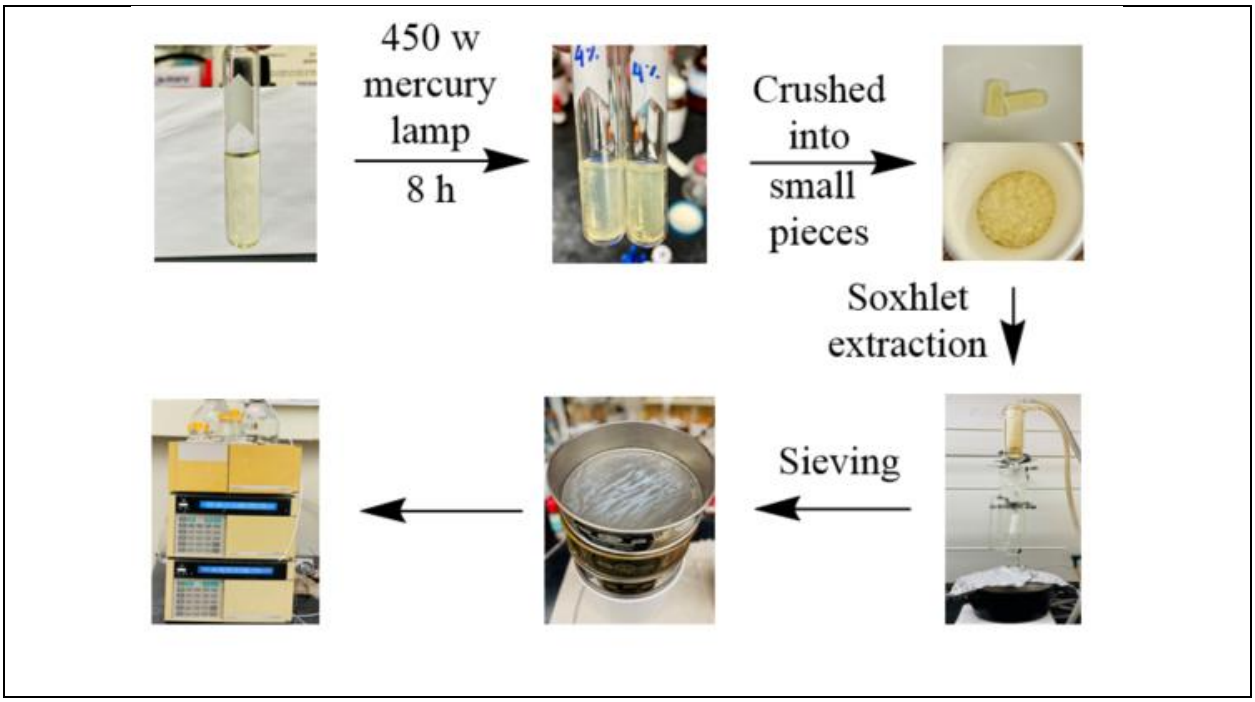

Figure 2.8. Polymer preparation for chromatographic test

The template was removed from the polymer by using Soxhlet extraction with methanol for 24 h. The polymers were then ground using a mortar and pestle. USA Standard Testing Sieves (VWR) were used to size the particles, and the fraction between 25-37 μm was collected. The particles were slurry-packed using a Beckman 1108 Solvent Delivery Module, into the stainless-steel columns (10cm long x 4.1mm inner diameter) to full volume for chromatographic experiments. The columns were equilibrated with the desired mobile phase. A Hitachi L-7100 pump with Hitachi L-7400 detector was used for the HPLC analysis and was accomplished isocratically at room temperature (22 ◦C). A substrate concentration of 0.1 mM in acetonitrile was used, and the wavelength was set at 254 nm. The void volume was determined using acetone as an inert substrate. The capacity factors, imprinting factor (IF), and cross-binding selectivity are calculated according to the equations below.

$$Capacity\ factors,\ k' = \frac{(t_R - t_V)}{t_V} \quad \text{Eq. 2.1}$$

Where, t_R = Retention time of the analyte

t_V = Void volume

$$Imprinting\ factor,\ IF = \frac{k'_1}{k'_2} \quad \text{Eq. 2.2}$$

Where, k'_1 = Capacity factors from imprinted column

k'_2 = Capacity factors from non − imprinted column

$$Cross - binding\ Selectivity = \frac{k'_{MIP}}{k'_{BFIP}} \quad \text{Eq. 2.3}$$

Where, k'_{MIP} = Capacity factors of the analyte

k'_{BFIP} = Capacity factor of the benzyl fentanyl

2.2.3 Monomer to Template Ratio Optimization

The ratio of the template to the monomer, the size of the particles, the makeup of the mobile phase, and the flow rate are some of the factors that need to be investigated in order to achieve the goal of optimizing the selective binding of the BFen-MIP. The first variable that needed to be determined was the optimal monomer to template ratio. This was accomplished by synthesizing five distinct BFen-MIPs with varying amounts of BFen template, all while maintaining the formulation of crosslinker (EGDMA), functional monomer (MAA), and initiator (AIBN) at the value 78:20:2. It is important to note that these polymer components sum up to a total of one hundred percent of the MIP material. This does not include the template, however, since the template is removed during the last phase of MIP synthesis. The ratios of Template to Functional Monomer that were examined were 1:10, 1:5, 1:2.5, 1:2, and 1:1, which provides a fair range of data to analyze the performance trend. The imprinting factor (IF) was calculated according to the

equation discussed in the previous section. The IF shows the difference in BFen binding between the imprinted and non-imprinted polymers, which is a measure of the "imprinting effect," with higher values indicating greater imprinting.

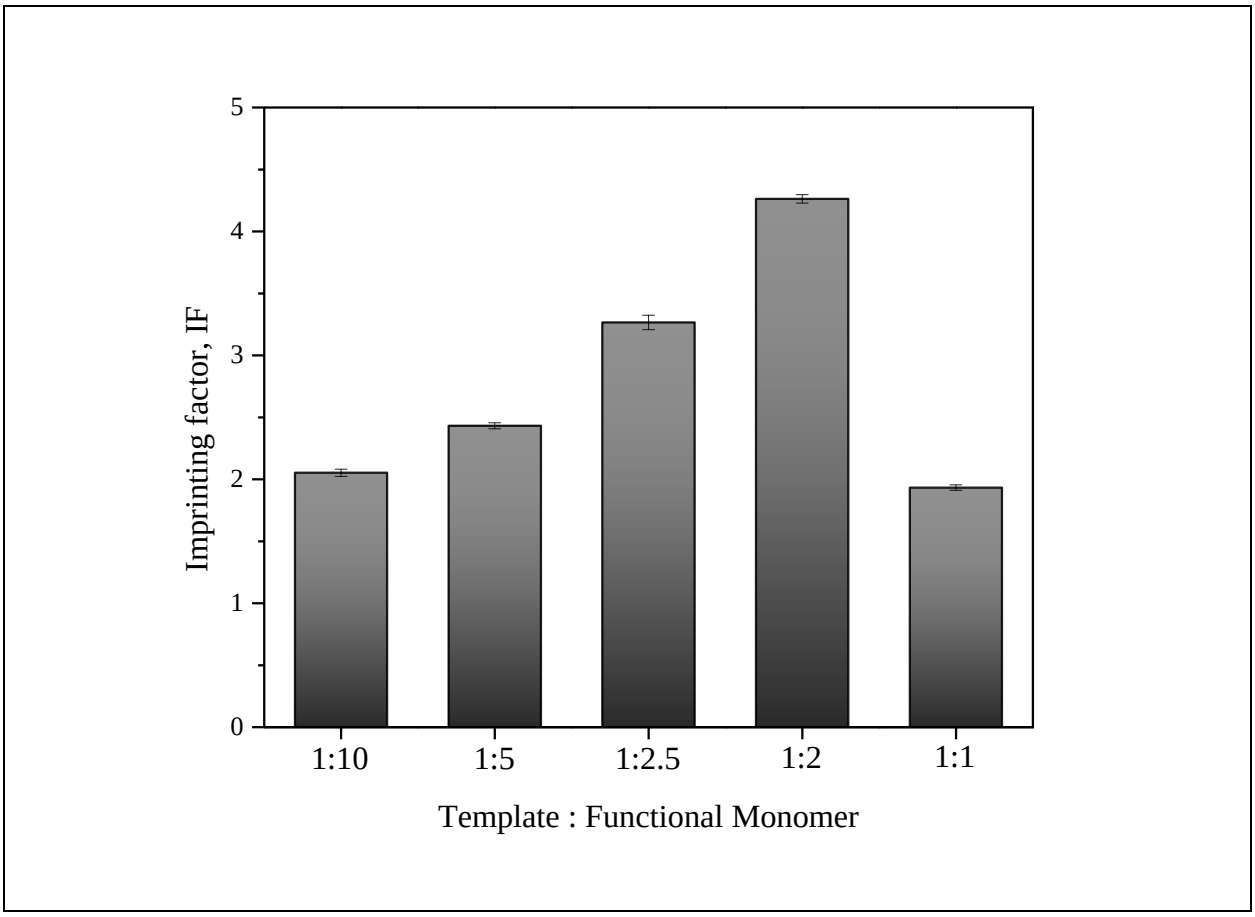

Figure 2.9. Imprinting factor data of the MIPs with different Template:Functional monomer ratio

The imprinting factor data indicated that the optimal Template:Functional Monomer ratio is 1:2 as shown in figure 2.9. This may be explained by referring to Scheme 2.6, which depicts the processes in the formation of Template/Monomer complexes as the amount of template increases. There is an excess of the MAA functional monomer in the first step, which saturates the template complex with MAA, leaving uncomplexed surplus MAA; this fits the data displayed in figure 2.9 for the 1:10, 1:5, and 1:2.5 complexes. The rise in IF when the ratio lowers from 1:10 to 1:5, then to 1:2.5 is due to an increase in the absolute number of imprinted binding sites as the template

amount increases. As the density of imprinted binding sites grows (per gram), so does the quantity of template bound by the imprinted polymer; hence, the "imprinting effect" increases as the density of binding sites increases. As the ratio is reduced from 1:25 to 1:2, the density of binding sites grows to the maximum number conceivable, resulting in the greatest "imprtinting effect" recorded. As the ratio is reduced from 1:2 to 1:1, the number of high affinity sites (1:2 Template:Functional Monomer) that are replaced by low affinity sites drops (1:1 Template:Funtional Monomer). Hence, the overall "imprinting impact" decreases as high affinity sites are replaced by low affinity sites. As a result, the ratio 1:2 Template:Functional Monomer is employed in further studies since it delivers the greatest "imprinting effect."

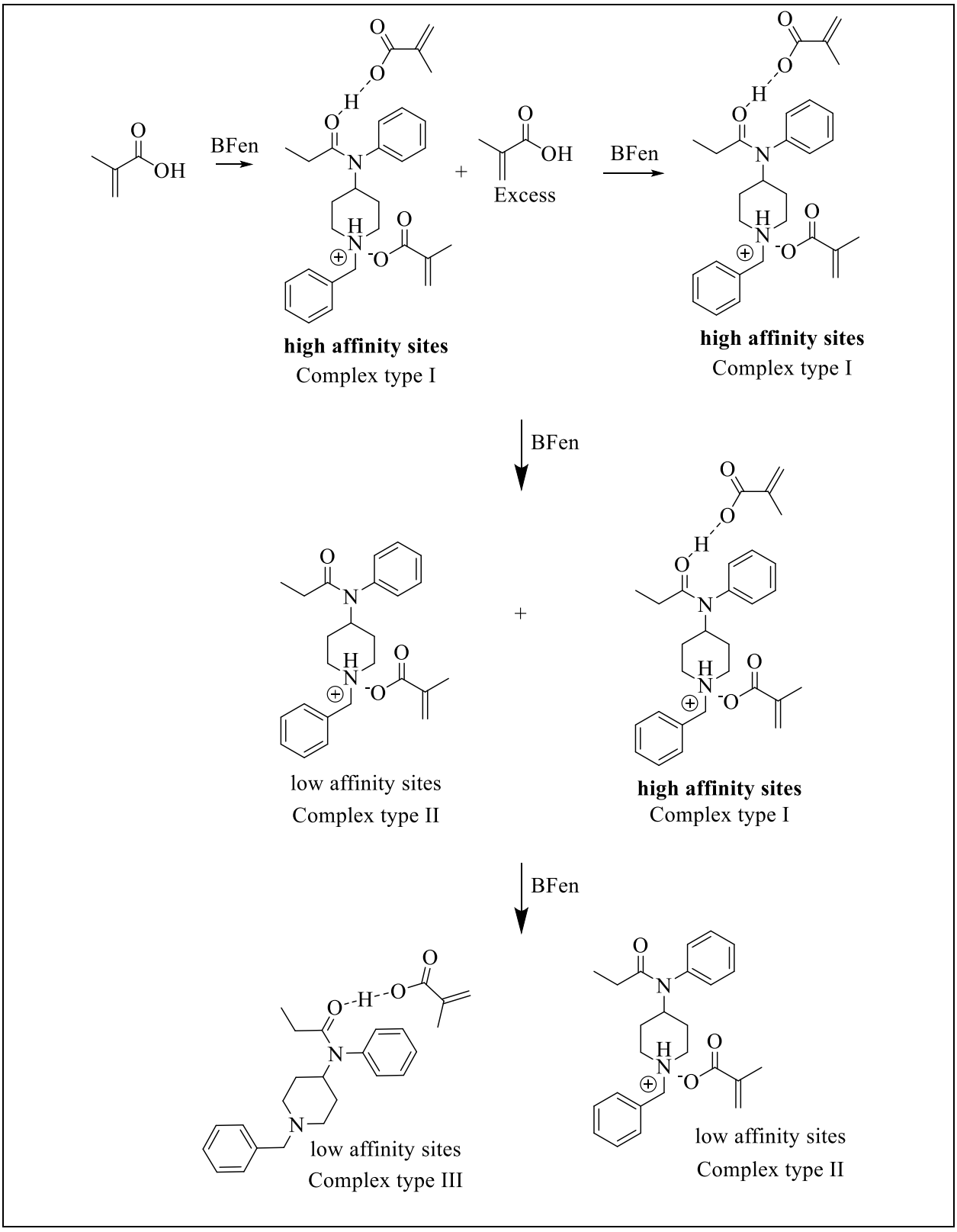

Scheme 2.6. Illustration of the formation of high-affinity sites and low-affinity sites

2.2.4 Selection of the Particle Size

Bulk-processed MIP materials are typically ground and sized prior to packing in columns and assessed for template and other analyte retention. Particle sizing is often done using sieves that come in conventional sizes, with the lowest size accessible being 20 µm. Whatman number 1 filter paper was utilized to filter away particles smaller than 11 µm to achieve smaller sizes.

Several publications have been published that evaluate the performance of various sized MIPs, allowing some conclusions to be drawn. One of the most obvious observations is that MIP sizes bigger than 63 m exhibit poor selectivities and reduced retention times owing to solute mass transfer difficulties via the larger particles. MIP particles crushed to smaller sizes, on the other hand, have shown conflicting results. Despite the higher number of theoretical plates and less concerns with mass transfer for smaller particles, particle size ranges above 25m have produced better outcomes than particle size ranges below 25µ. With this information, two distinct particle size ranges were studied, with the bigger size produced using standard sieves in the 25-37 µm range and the smaller size obtained using standard sieves in the 11-25µ range. MIPs were generated using a template:functional monomer ratio of 1:2, found to be optimum in the previous, to undertake the first optimization of MIP processing and analytic parameters. Two independent columns were slurry packed with various sized MIPs and analyzed using a non-optimized MeCN/H_2O mobile phase system with the ratio 99.9/0.1.

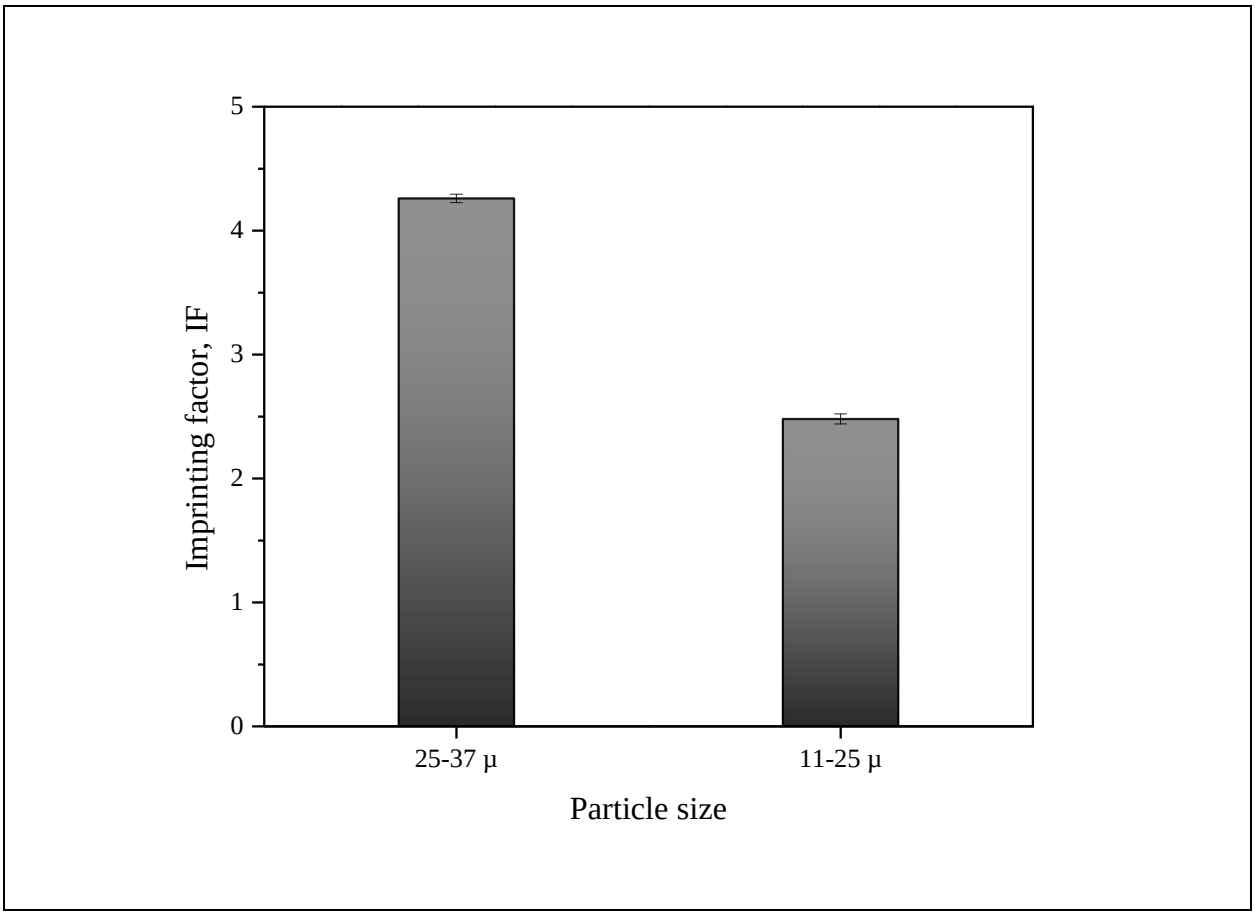

Figure 2.10. Imprinting factor data for the particles of different sizes

The results shown in figure 2.10 indicated that the particle sizes of 25-37 µ have better imprinting factor values than the particle sizes of 11-25 µ, which correlates with the findings of previous studies.[239, 240] Smaller particles may provide increased surface accessibility, shorter path-length diffusion distances for quicker mass-transfer kinetics of substrates, and access to more buried binding sites. However, a considerable number of high-affinity sites may have been destroyed during grinding, which may account for the decreased selectivity of particles smaller than 25 microns. Two additional potential causes are the destruction of a significant number of binding sites with average selectivity, specifically in the 25 µ range, and higher density of polymer in the smaller particles that restrict substrate access to binding sites. Therefore, 25-37 µ sized particles were used for further studies.

2.2.5 Composition of Mobile Phase

The optimum mobile phase conditions were determined using a 10cm long x 4.1mm inner diameter stainless steel column filled with MIP particles ranging in size from 25 to 37 microns. A study was done using various acetonitrile and water proportions, and it was discovered that elution of benzyl fentanyl in 95/5 (v/v): MeCN/H_2O yielded retention values near the void volume, suggesting that the mobile phase was excessively polar. Systematically lowering the water component in acetonitrile to 1% and subsequently to 0.1% indicated longer elution durations, with 100% MeCN producing the longest eluting peak. Mobile phases containing 1% and 0.1% formic acid in acetonitrile were examined to see whether the protonation state of the BFen affected binding; nevertheless, retention durations were reduced. Therefore, it was decided that 100% MeCN was the best mobile phase.

2.2.6 Flow Rate Determination

The effect of flow rate on binding in MIPs was examined by evaluating the impact of three different flow rates on the IF. Flow rates of 0.1, 0.5, and 1.0 mL/min were tested on a 10cm long x 4.1mm inner diameter stainless steel column filled with 25 to 37 micron sized particles. It was unexpected to see that the k' values for all three flow rates were almost identical. Slower flow rates, on the other hand, not only required longer wait periods but also contributed to the broadening of the chromatographic peak; hence, the 1.0 mL/min flow rate was the optimum option for further studies.

2.2.7 Determination of Selectivity

The Cross-Binding Selectivity was used to assess the selectivity of the improved MIP with a 1:2 Template:Functional Monomer ratio. The selectivity of binding for the template, BFen, and more crucially, fentanyl was compared to other regularly encountered substances known to be contaminated with fentanyl, such as heroin, cocaine, and methamphetamine. Furthermore, two

fentanyl analogs, acetylbenzylfentanyl (ABF) and benzoylbenzylfentanyl (BBF), with structural similarities to fentanyl, were also examined.

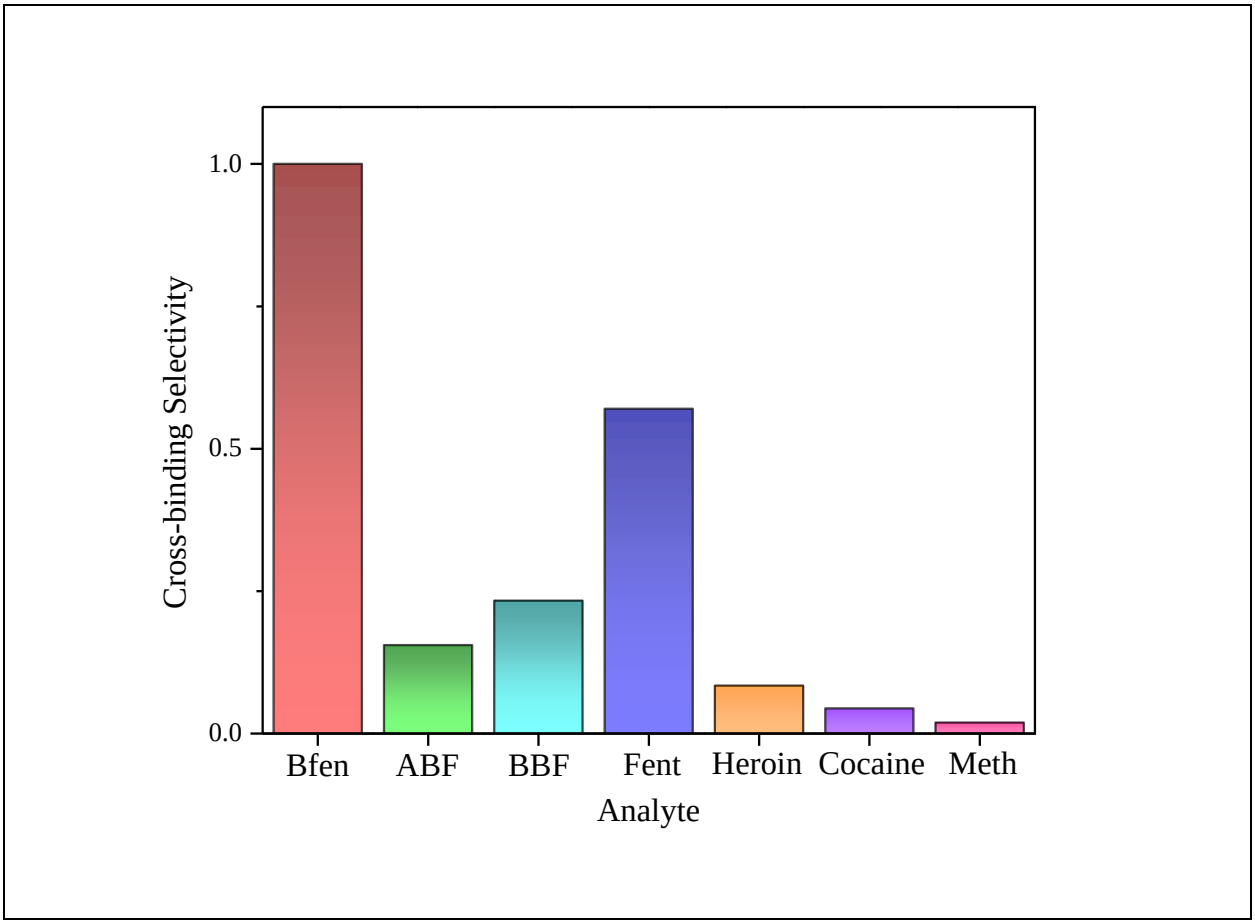

Figure 2.11. Cross-binding selectivity of the synthesized MIP with Template: Functional Monomer ratio of 1:2

The results of the chromatographic tests are given in figure 2.11, with the best selectivity achieved for the BFen as the template to produce the MIP. Despite the fact that ABF and BBF are structurally close in identity to Bfen, they had less binding to the MIP, suggesting the MIP selectivity is due in part to shape selectivity. Higher binding for BBF than ABF was probably due to some non-specific binding to the more hydrophobic benzene group. On the other hand, fentanyl (Fent) shows better binding affinity compared to the other analytes, which suggests binding is controlled more towards ‘moiety A’ than “moiety B’ as shown in figure 2.12.

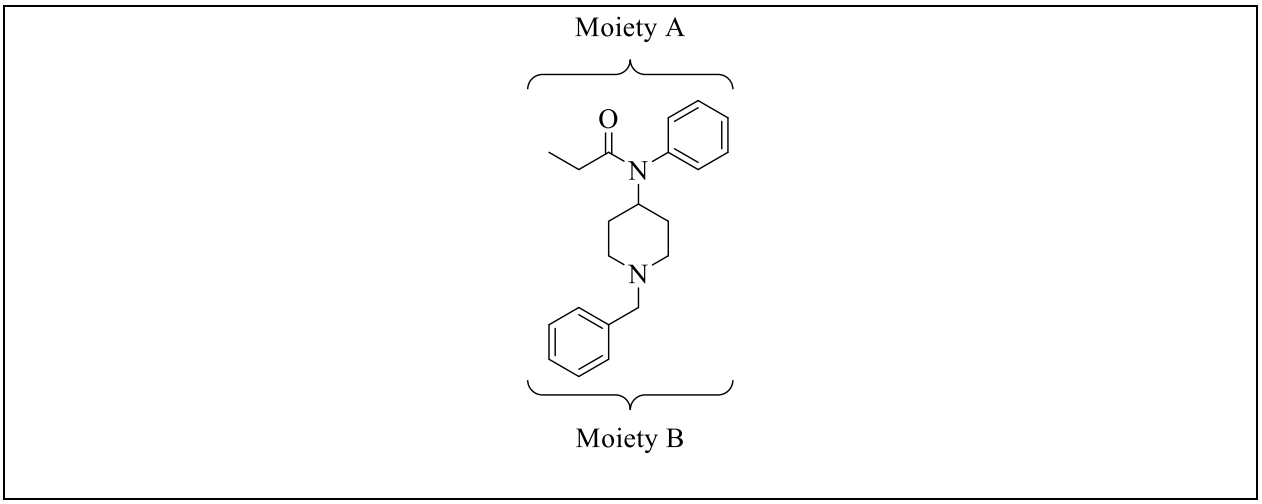

Figure 2.12. Possible binding sites of the Bfen

Heroin, cocaine, and methamphetamine (Meth) showed no binding affinity towards the imprinted polymer indicated by elution close to the void volume, as expected. Applications of this MIP material include separation of fentanyl from other narcotics such as methamphetamine, shown in the chromatogram (Figure 2.13) below. A possible more advance application can be envisioned where the MIP can be used on a tainted methamphetamine sample laced with fentanyl, whereupon the fentanyl is essentially "neutralized" by binding to the MIP, and this will not be metabolized by the human body. Instead, the MIP particles will be eliminated via the excretory system.

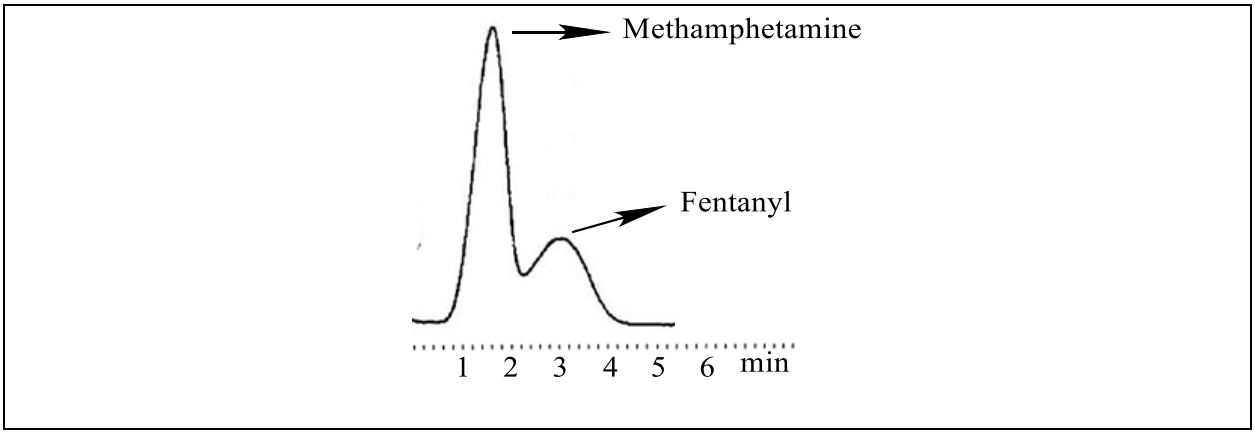

Figure 2.13. An example chromatogram showing the separation between methamphetamine and fentanyl while eluting through the column.

2.3 Conclusion

Fentanyl and various of its analogs, especially benzylfentanyl, acetylbenzylfentanyl, and benzoylbenzylfentanyl, have been successfully synthesized. The alkylation reaction of norfentanyl with benzyl bromide resulted in a double substituted product, which is a new fentanyl analog to the best of our knowledge. MIP was synthesized using MAA as the functional monomer, EGDMA as the crosslinking monomer, AIBN as the initiator, and benzylfentanyl as the template molecule. Different ratios of Template to Functional monomer were used while keeping the crosslinking monomer, and initiator amounts constant.

The chromatographic test revealed that the optimal Template: Functional Monomer ratio is 1:2. The particle sizes of 25-37 μ have better imprinting factor values than the particle sizes of 11-25 μ. It was determined that the 100% ACN at a flow rate of 1.0 mL/min provided the best imprinting factor data. By using these optimized conditions, the selectivity of the synthesized MIP was determined by comparing to other substances such as heroin, cocaine, and methamphetamine. The cross-binding selectivity data revealed that the MIP with Template: Functional Monomer ratio of 1:2 selectively binds the Bfen over the other analytes but is closely followed by actual fentanyl.

2.4 Future/Ongoing Work

The molecularly imprinted polymer synthesized by using MAA as the functional monomer, EGDMA as the cross-linker, and benzylfentanyl (Bfen) as the template provided a very good cross-binding selectivity. However, it would be wise to explore other monomers and template to obtain the best possible MIP that can detect fentanyl and its analogs.

Two major components for MIP synthesis are the functional monomer and cross-linking monomer. Spivak research group has developed a novel monomer, NOBE, that act as both the functional and cross-linking monomer. Historically, NOBE has shown a better imprinting effect over other systems such as MAA/EGDMA through forming hydrogen bonds by amide group.[241]

NOBE was synthesized according to the previously published protocol[242] and MIP was synthesized by using benzylfentanyl as the template. Initial studies showed an improvement in the imprinting factor values. The work is currently in progress to verify the initial data and then cross-binding selectivity will be determined by comparing it with drugs such as heroin, cocaine, and methamphetamine.

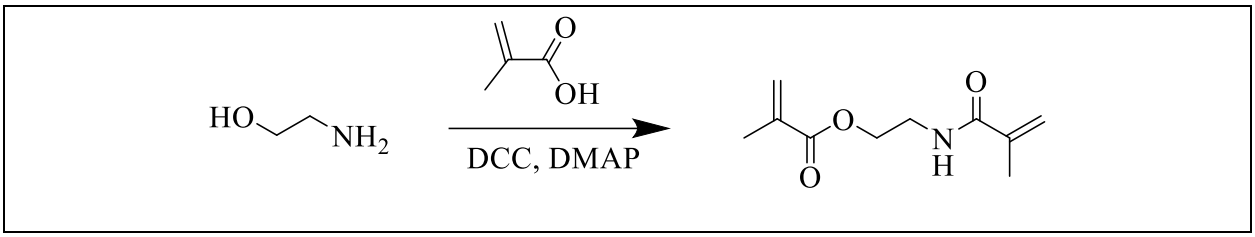

Scheme 2.7. Synthesis of the NOBE monomer

Future work will also investigate how changing the functional monomer such as vinyl sulfonic acid instead of MAA, affects the binding affinity of the materials. Although, benzylfentanyl closely resemble the structure of fentanyl, using other templates, especially norfentanyl which is the primary metabolite of fentanyl, would be interesting to explore. Therefore, an MIP was synthesized by using norfentanyl as the template. Chromatographic tests will be performed to evaluate its binding efficiency.

Chapter 3. Imprinted Hydrogel for Nucleoside Detection

3.1 Introduction

3.1.1 Biosensors

The capability to detect even the tiniest physiologic change in the human body with great sensitivity and correctly monitor processes that affect human nature and their surrounding environment has led to an enormous increase in the quality of life. Research into the detection, measurement, and sensing of biological substances, including viruses, bacteria, DNA, RNA, and proteins, is vital and expanding rapidly, resulting in the development of tiny analytical tools known as biosensors. Biosensors have been around for a long time. In 1906, Cremer observed that the concentration of an acid suspended in an aqueous solution is comparable to the electric potential formed between parts of the solution when divided by a glass membrane, which led to the first recorded notion of a biosensor.[243] Thus, in 1909, Soren Peder Lauritz Sorensen came up with the notion of pH, and in 1922, Hughes came up with an electrode to detect pH.[244] This cleared the way for Leland C. Clark, Jr., the "father of biosensors," to create the first "real biosensor" in 1959.[245] Clark invented a sensor that uses a glucose oxidase electrode to detect the presence of oxygen or hydrogen peroxide in biological samples. Biosensing technologies that are both sensitive and selective have come a long way since then.[246, 247] Biosensors have the potential to be used in a wide variety of fields, from medical diagnostics and drug development to food safety and process control to environmental monitoring and even defense and security.[248]

A biosensor is a device that generates an output signal in response to an applied physical or chemical stimulus. They combine the high precision of biological systems with the high specificity of physicochemical transducers to provide complicated bioanalytical measurements in accessible, user-friendly forms.[249] In most cases, biosensors are made up of three primary parts, the biological sensing element, the physicochemical detector or transducer, and the signal

processing system, all of which are represented in figure 3.1.[250]

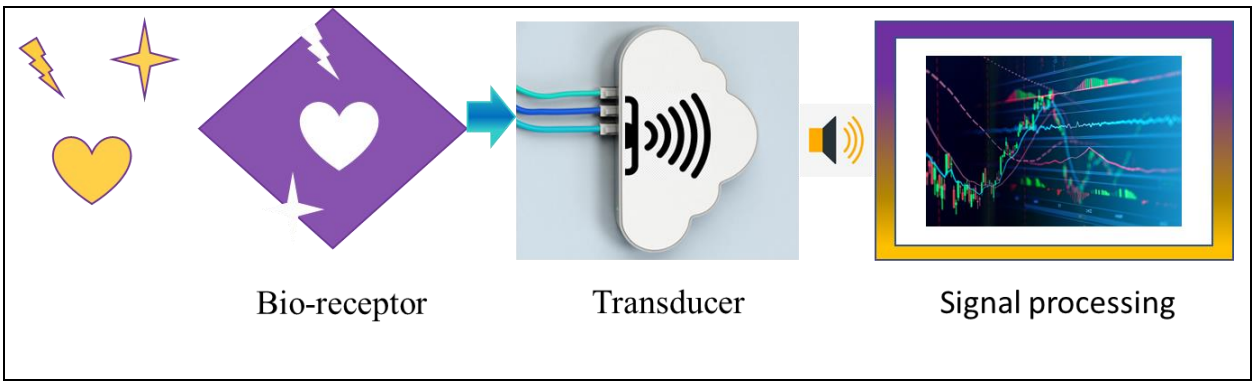

Figure 3.1. Components of the biosensors

To create a signal, biological sensing components are brought into interaction with the analyte of interest. Materials such as bacteria, tissues, cell receptors, enzymes, organelles, antibodies, and nucleic acids are typical examples of sensing elements. The signal that is produced as a result of the interaction between the sensing element and the analyte of interest is then converted by the transducer into an electrical signal that is measurable and quantifiable. Then, the electrical signal is amplified by the signal processing system, and it is sent to a data processor, which generates a quantifiable signal in the form of a digital display, color change, or printout.[251]

When designing a biosensor for a certain purpose, it's important to keep a few things in mind. To build the sensor's target recognition capabilities, a good bioreceptor must be chosen. Second, it is necessary that the bioreceptors be well immobilized to the matrix. Third, the transducer's selection and design should be carefully thought out so that it can effectively convert the binding event between the target and the bioreceptor into observable output signals.[252] A biosensor must be able to precisely distinguish the target at aberrant biological concentrations inside a high background matrix (containing numerous samples other than the analyte). In addition to this, it should be able to endure being washed and used several times without being quickly deteriorated.

Today's medical diagnostic system relies heavily on commercially available devices. The identification, transduction, amplification, and detection abilities of contemporary instrumental sensors have been considerably improved as a result of the success of current analytical procedures. In turn, this method may provide very reliable quantitative data, with a detection limit that is much lower than with other approaches. Despite the fact that advancements in all types of current instrumental sensors are hailed as one of humanity's greatest triumphs, there are a few drawbacks that must be highlighted. One of the biggest problems is that achieving such a high level of sensitivity typically necessitates the use of expensive equipment such as mass spectrometry (MS), surface plasmon resonance (SPR), etc., the collection of highly accurate data, the comparison of results with pure standard reagents, the employment of highly skilled personnel, and the maintenance of an extremely sterile working environment.[253] As a result, there is still a significant need to investigate new avenues in order to develop methods that are very specific, ultrasensitive, affordable, and user-friendly while still adaptable to a wide range of conditions.

Biosensors may be developed using materials whose chemical or physical characteristics can be altered in response to an applied stimulus. These materials are able to selectively perceive specific types of environmental stimuli, such as temperature, light, pH, magnetic and electrical field, and so on, while also being capable of transducing a detectable output signal by modifying its chemical or physical characteristics. There are a number of benefits to using these substances. First, they are simple to use; consumers can often examine the results of the readout without any special equipment. Naked-eye detection sensors are also a promising area of research. Second, they cost less than comparable alternatives because they need less complex instrumental components. Third, because of their simple construction and sturdy qualities, they are convenient for travel and storage. Hydrogels are attractive biosensors because they can combine the functions

of a conventional biosensor, recognition, signal translation, and readable detection, into a single device. In recent years, the approach of molecular imprinting using supramolecular interactions to produce polymerizable target-ligand complexes has garnered increasing interest.[254-257]

3.1.2 Hydrogels as the Biosensor

Hydrogels are insoluble polymer networks that are crosslinked and may be formed of hydrophilic homo- or hetero-co-polymers. They have the potential to absorb substantial quantities of water.[258] Due to their hydrophilic nature, they may expand in water to several hundred times their dry mass. Since the discovery of hydrogels in the 1960s by Wichterle and Limand, they have received a significant amount of attention for their use as scaffolds in a variety of applications, including sensors, drug delivery carriers, adhesives, cancer treatment, and tissue engineering.[259-261] Because of their high biocompatibility, versatility in synthesis, and the ability to have their physical and chemical characteristics altered, hydrogels are widely regarded as one of the most promising possibilities for use in the fabrication of biosensors.

Hydrogels are a great scaffold for a polymeric detection device because, depending on the hydrogel's structural components, they have the capacity to alter characteristics in response to stimuli such as changes in pH, chemical, ionic strength, heat, light, or temperature.[262, 263] Changes in hydrophilic/hydrophobic ratio, small molecule release, or gel conformational changes like swelling/shrinking may all contribute to the overall effect.[264] A hydrogel modified with poly(N,N-dimethylaminoethyl methacrylate) (PDMA) or poly(ethylene glycol) (PEG) to exhibit pH-dependent activity is an example of a stimuli-responsive material. Hydrogels with thermo-responsive properties may be created by adding a monomer such N-isopropylacrylamide (NIPAAm). A hydrogel system that is both temperature and pH-sensitive may be created by the copolymerization of groups like poly(hydroxyethyl methacrylate-coacrylic acid) or poly(acrylamide-co-acrylic acid).[265]

One of the most crucial and vital aspects of biosensor fabrication and design is using a dependable technique for the immobilization of bioreceptors on a hydrogel surface. There are several factors to consider when choosing an immobilization technique, including the bioreceptor's degradation and viability, the accessibility of reactive groups, and the binding type (covalent or noncovalent).[266] Adsorption and entrapment, noncovalent or covalent binding, crosslinking, or a mix of these processes are all viable options for immobilizing bioreceptors on the hydrogel surface. A method of immobilization may be either reversible or irreversible, depending on the methodology used.[267] In recent years, molecular imprinting using supramolecular interactions to produce polymerizable target-ligand complexes has garnered increasing interest. Molecular imprinting provides a straightforward and efficient method for generating the recognition of biomolecules, such as proteins that can readily form complexes with ligands via noncovalent template-functional monomer interactions such as hydrogen bonding, hydrophobic interactions, ionic interactions, etc. Protein imprinted polyacrylamide MIP material that can selectively recognize template protein was first developed by Hjerten's group.[268] Since then, many examples of successfully imprinting biological targets like epitopes, proteins, viruses, and so on have been published, and this number is rapidly increasing.[269-273]

Simple bioresponsive networks using imprinted hydrogels have been developed by the Spivak research group. They were able to effectively imprint the proteins thrombin and PDGF-ββ in the form of capillary hydrogels for detection using the naked eye.[274] Their findings demonstrated that the limits of detection might be as low as femtomolar quantities of the target protein. This was ascribed to the complicated interplay that occurred between the aptamers and the supramolecular protein crosslinks (making use of noncovalent interactions), in addition to the lowering of excluded volume in their gels. In addition, the Spivak group imprinted the apple stem pitting virus (ASPV)

in order to demonstrate that other biological templates of interest can be used.[275] A novel approach, known as the double imprinting technique, was devised so that hydrogels could be synthesized and measured without the need to make the hydrogels in capillaries as was previously done. The process of double imprinting consisted of the imprinting of the target virus at the molecular scale, as well as the imprinting of an additional pattern at the macromolecular scale, which was achieved by polymerizing the hydrogel in a lithographic mold. This resulted in the creation of a diffraction-grating sensor with shorter reaction times, which enabled the shrinkage of the hydrogel to ASPS to be monitored by the change in the diffraction pattern. In this work, the double imprinted hydrogels technique was employed by focusing on a microRNA as the target of interest.

3.1.3 miR-21 DNA as the Target

MicroRNAs (miRNAs) are a kind of short noncoding RNA (~22 nucleotides) that play an important regulatory function in gene expression by inhibiting translation and hastening the decay of specific messenger RNAs (mRNAs).[276, 277] More than 60% of human protein-coding genes are controlled by miRNAs, and over 2600 mature miRNAs have been discovered and annotated so far in Homo sapiens.[278] miRNA expression levels that are abnormal are linked to a variety of human illnesses, notably cancer.[278, 279] As a result, miRNAs have been identified as potential molecular biomarkers, and aberrant miRNA expression has been used in cancer diagnosis, classification, and prognosis.[280, 281] The quantitative identification of miRNAs is critical for both the research of miRNA biological activities and illness diagnosis. miR-21, a 22 base pair sequence, was one of the first miRNAs discovered, and it was found as a cancer-promoting 'oncomiR', targeting several tumor suppressor genes involved in proliferation, apoptosis, and invasion.[282, 283]

The ability to quickly and quantitatively identify miRNAs has implications for both early cancer diagnosis and the tracking of cancer's development over time. It is, however, exceedingly difficult to construct a quick, low-cost, and sensitive platform for the detection of miRNA due to

their inherent features, such as their low quantity, short, and highly homologous sequences. Extensive work has been done over the last several decades to develop methods of quick and sensitive miRNA identification.[284] Despite being the gold standard, Northern blotting is laborious and has poor sensitivity. Complex equipment and the risk of a false positive plague other methods, such as RT-PCR and Surface Enhanced Raman Spectroscopy (SERS). Only a few studies have been performed for miRNA using MIPs.[285, 286] Rather than RNA, DNA was selected as the target because RNA is both more costly and cumbersome to work with due to its rapid degradation.

DNA is a phosphodiester-linked block copolymer made up of just four different kinds of monomeric units such as adenine (A), thymine (T), cytosine (C), and guanine (G). The sequence of bases in DNA can be accurately controlled, in contrast to the majority of synthetic polymers. DNA was long thought of as nothing more than a genetic material; however, recent research has shown that it also has functional capabilities such as molecular recognition and catalysis.[287] Because of its chemical and physical stability, biocompatibility, and tunable nature, DNA has attracted a lot of attention as a potential analytical sensor. The miR-21 DNA sequence and RNA sequence are identical, with the exception of the presence of the nucleic acid thymine in lieu of the nucleic acid uracil. As a result, it is not difficult to produce a mimic sequence using DNA in place of RNA. Functional aptamers were used to bind the target into the polymer matrix.

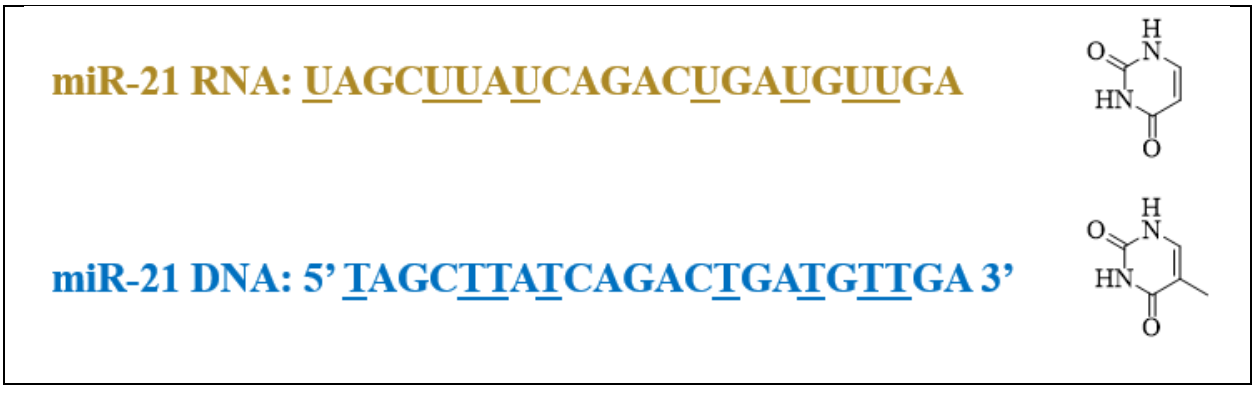

Figure 3.2. Sequences of miR-21 RNA (top) and miR-21 DNA (bottom)

Aptamers, which are one of the more recent classes of bio-receptors, are seen to be a viable alternative for developing or strengthening the recognition capacity of hydrogels. Aptamers are oligonucleotides, which are either DNA or RNA molecules, that have the ability to attach to a broad variety of target molecules such as proteins, drugs, ions, vitamins, peptides, surfaces, etc., with a high affinity and a high level of specificity.[288] It was developed primarily in the early 1990s with the creation of SELEX (Systematic Evolution of Ligands by Exponential enrichment), an in vitro selection and amplification technology.[289-291] Aptamers' exceptional selective binding capacity is due to the stable structure created between the aptamers and the target. The sequence-specific, three-dimensional structure of the aptamer ligand that serves as a stiff scaffold for the assembly of the aptamer's functionalities helps to enable the precise interactions that occur between amino acids. Aptamers have various benefits due to the fact that they are chemically manufactured, unlike other bio-receptors such as antibodies and cells. First, since aptamers do not need animal processing, they are very simple and inexpensive to get. Second, they tend to be more stable than antibodies. Furthermore, they are readily modifiable, meaning that more functions may be added to serve a variety of purposes.[290, 291] It is possible to incorporate DNA into a hydrogel network by modifying the DNA using phosphoramidite or acrydite, which allows for covalent conjugation to the backbones of the polymer networks. The addition of an 18-atom hexa-ethylene glycol spacer (iSp18) to the sequence makes it more flexible, which has been exploited to make rebinding the aptamer-functionalized hydrogel to the template molecule easier.[289]

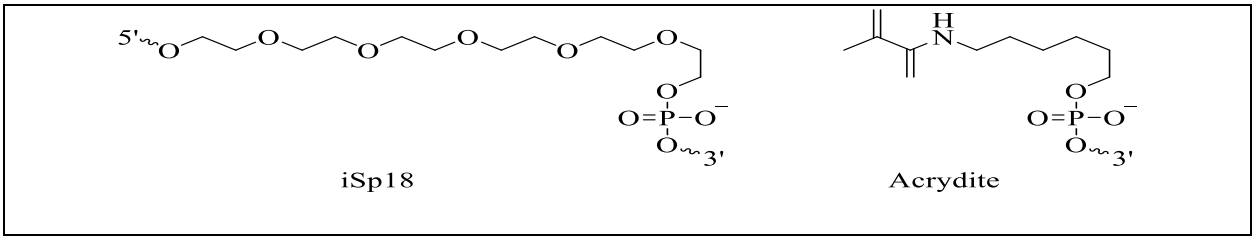

Figure 3.3. Aptamer functional modifications

Various investigations on DNA integrated into hydrogels have been conducted because of DNA's durability and capacity to be modified.[292-295] The smallest target sequences studied so far in DNA sensors have had 26 bases. To accomplish this, a bio-responsive hydrogel suspension array was tagged with quantum dots. Hydrogel contraction in response to target DNA strand addition led to a blue change in Bragg diffraction peak location, with a 10 nM detection limit (LOD).[296] Several steps are needed to make the quantum-dot beads, but the example demonstrates that it is feasible to detect small DNA sequences. Imprinted hydrogels have also been used in other types of DNA detection technologies. Tierney et al. provide an example of using functionalized aptamers in a hydrogel that is bonded to the tip of an optical fiber for high-resolution interferometric reading. At the micromolar concentration level, their 35-base-pair target sequences could be detected.[297] Gel electrophoresis was used by Ogiso et al. to immobilize their double-stranded DNA target sequence (for 5 µM samples) by creating binding sites for it in the MIP gel.[298]

3.1.4 Significance

In this work, a diffraction grating imprinted hydrogel was employed for the detection of 22-base pair miR-21 DNA. Complementary DNA aptamers were employed to hybridize the DNA with the target sequence. The size of the DNA target, the quantity imprinted, and its subsequent use in detecting RNA sequences set the current work apart from earlier studies. Advantages of the diffraction grating design include the gratings' responsiveness to changes in pH and temperature as well as the size and shape of individual molecules (through target addition and removal). In our hypothesis, the insertion and removal of the miR-21 target was anticipated to cause the grating to distort, and the subsequent shrinking/swelling response can be seen through laser diffraction.

3.2 Materials and Methods

3.2.1 Materials

miR-21 DNA mimic, Aptamer1, and Aptamer2 were purchased from Integrated DNA Technologies (IDT). Acrylamide (Am), N,N'-methylenebisacrylamide (MBAm), N-isopropylacrylamide (NIPAAm), ammonium persulphate (APS), N,N,N',N'-Tetramethylethylenediamine (TEMED), pentaerythiol triacrylate (PETA), Trimethylolpropane tris(3-mercaptopropionate) (TMPTMP) were purchased from Sigma-Aldrich and used without further purification.

3.2.2 Preparation of the Thiol-Acrylate (TA) Mold

The substrate that was employed to imprint the grating pattern onto the hydrogel was crucial to the success of the diffraction hydrogels. Poly(dimethylsilaxane) (PDMS) is often utilized as the hydrogel stamp or mold because it can accurately reproduce the grating master.[275, 299-301] Other benefits of PDMS include its elastomeric nature, cheap cost of manufacture, and moldability to submicrometer details. The hydrophobic nature of PDMS complicates the introduction of aqueous solutions in applications like microfluidics and hydrogel. Thiol-acrylate materials are an option that was presented by Bounds et al.[302] To create stable hydrophilic microfluidic devices, they used pentaerythritol triacrylate (PETA) and trimethylolpropane tris(3-mercaptopropionate) (TMPTMP) catalyzed by diethylamine in a Michael Addition reaction. The diffraction-grating gels in this work were fabricated employing the thiol-acrylate (TA) composite as a mold. The mold was prepared in the Pojman research group by employing a 1:1 ratio of PETA to TMPTMP, which cures in one hour at room temperature. After peeling off the TA from the grating master, the mold was ready to be used for the hydrogel preparation, as illustrated in figure 3.4.

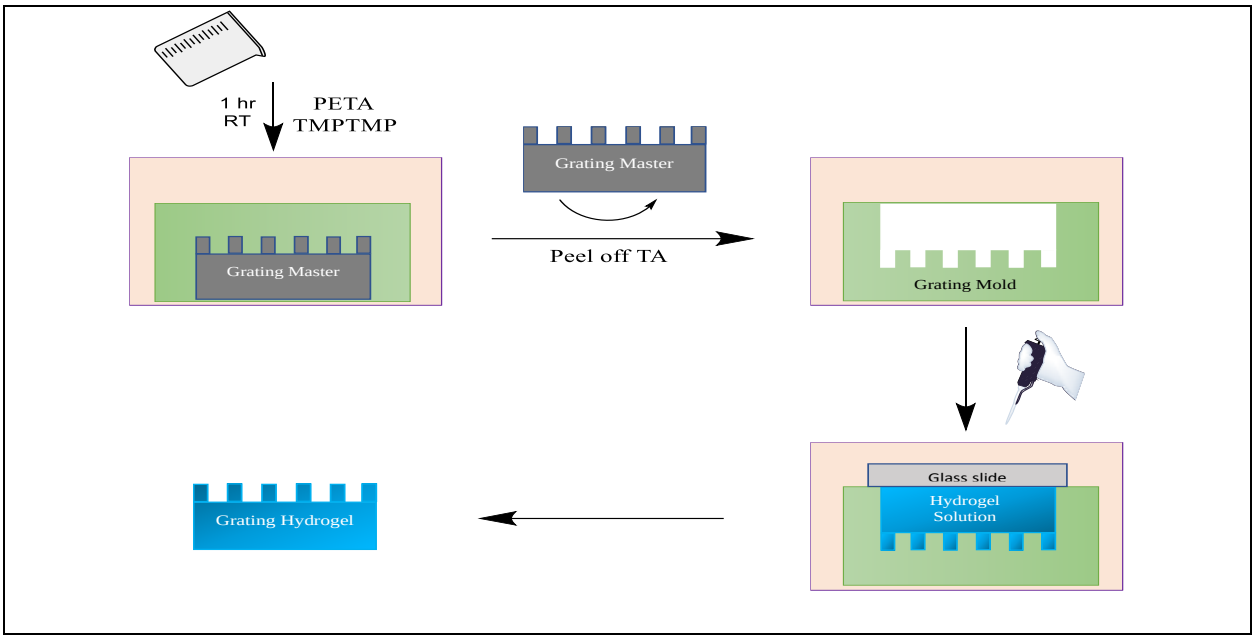

Figure 3.4. Illustration of the TA mold and hydrogel preparation

3.2.3 Preparation of the Double-Imprinted Hydrogel

The target of interest in this work was the short 22-mer sequence miR-21 DNA. Two 11- base pair aptamers, both of which are modified at the 5' end, were used as the biomimetic receptors. The aptamers are complimentary with the DNA mimic, as shown in figure 3.5.

Aptamer1	3' – ATC GAA TAG TC	/iSp18//5Acryd/5'
miR-21 DNA	5' – TAG CTT ATC AG	A CTG ATG TTG A – 3'
	3' – T GAC TAC AAC T	/iSp18//5Acryd/5' Aptamer2

Figure 3.5. The sequence of miR-21 DNA mimic and the aptamers

The melting temperature (Tm) of DNA was used to determine the optimal temperature for hybridization and dehybridization (Eq. 3.1). The salt concentration (M) has an effect on the melting temperature; the electrostatic repulsion between the phosphate groups along the backbone of the DNA strands is diminished by the salt, effectively controlling the annealing of DNA.[303] The melting temperature can be adjusted depending on the salt concentration (M). This, of course, is

also reliant on the amount of thymine and adenosine present in the strands. This is because thymine and adenosine give less hydrogen bonding than guanine and cytosine do, which in turn causes guanine and cytosine to produce stronger bonds.

$$T_m = 16.6 \log M + 0.41 \left(\frac{G}{C}\right) + 81.5 \qquad \text{Eq. 3.1}$$

Table 3.1. Formulation of the components for a 200 µL hydrogel

Chemical	Molecular weight	Mass (g)	Mole ratio	moles
Aptamer1	3931.8	1.30E-05	1	3.31E-09
Aptamer2	3891.7	1.29E-05	1	3.31E-09
miR-21 DNA	6702.4	2.22E-05	1	3.31E-09
MBAm	154	0.000122	240	7.92E-07
NIPAAm	113	0.01798	48000	1.59E-04
Am	71	0.0112	48000	1.58E-04

The formulation for the preparation of a 200 µL gel is shown in table 3.1. The synthesis of the hydrogel started with the annealing of the DNA. For this purpose, 10 µL of Aptamer1 (3.31 nmol), 10 µL of Aptamer2 (3.31 nmol), 10 µL of miR-21 DNA mimic (3.31 nmol), and 59 µL of PBS buffer were added in a plastic vial and vortexed. The plastic vial containing the solution was placed in a 90 ^{O}C water bath for 2 minutes. After 2 minutes, the plastic vial was removed from the water bath, and the solution was vortexed every 2 minutes for about 10 minutes. Then 100 µL of the monomer stock solution was added to the vial and vortexed. A 10 mL monomer stock solution was prepared beforehand by dissolving 11.20 mg of Am, 17.98 mg of NIPAAm, and 0.12 mg of MBAm in PBS buffer. 10 µL of ammonium persulphate (APS) solution (10 wt% in PBS buffer) which was then added to the plastic vial, and the solution was vortexed. Finally, 1 µL of TEMED was added to initiate the polymerization; the mixture was vortexed for 2 seconds and immediately

transferred to the TA mold and covered with a clean glass slide. After 8 hrs, the hydrogel was removed from the mold and transferred to a culture dish with PBS buffer to equilibrate. The overall scheme is shown in figure 3.6.

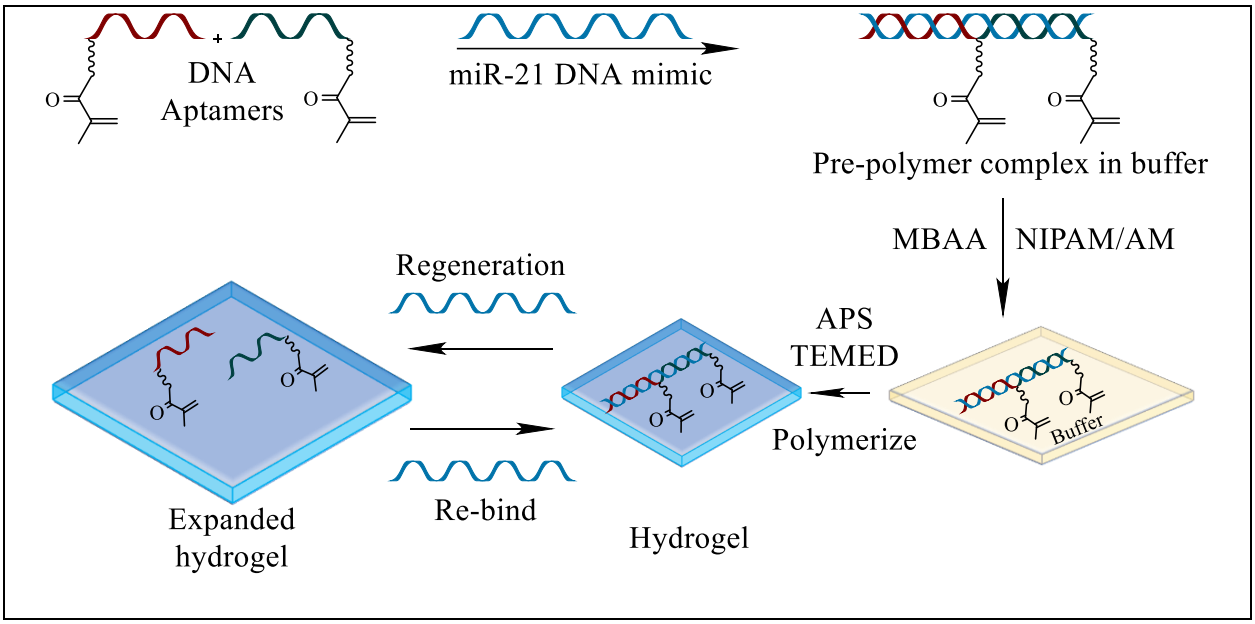

Figure 3.6. Illustration of the hydrogel preparation. Reproduced from ref [304]

3.2.4 Regeneration/Rebinding Process

The removal of the miR-21 DNA was carried out by putting the hydrogel in a 0.5 mM NaCl solution and heating it at 70 ^{O}C overnight. Then, the hydrogel was transferred to a culture dish containing PBS buffer. The PBS buffer solution was replaced every 3-6 hours until the volume changes in the hydrogel reached equilibrium. After the regeneration, the hydrogel was placed in the 50 µL rebinding solution of miR-21 DNA or other analytes. This cycle was repeated several times with each hydrogel.

3.2.5 Measurements of the Diffraction Grating Hydrogel

Gratings, e.g. in hydrogels, are influenced by physical properties such as shrinking or swelling in response (by addition and removal of a target) and changes in pH and temperature. The hydrogel recognition activated molecular trigger causes a modification to take place in the light beam pattern

as it travels through the grating hydrogel. This change was measured by using a ruler as shown in the figure and the percentage shrinkage of the hydrogel after each cycle was measured according to the equation.

$$Percent\ Shrinkage = \frac{d_0 - d}{d_0} \times 100\% \quad \text{Eq. 3.2}$$

Where, $d_0 = distance\ without\ DNA$

$d = distance\ with\ DNA$

It is worth mentioning that there is an inversely proportional relationship between the hydrogel shrinking/swelling response and the diffraction pattern distance, as explained by the equations below:[64]

$$\theta = \sin^{-1}(\frac{\lambda}{d}) \quad \text{Eq. 3.3}$$

$$\theta = \tan^{-1}(\frac{D}{h}) \quad \text{Eq. 3.4}$$

$$D = h \tan[\sin^{-1}(\frac{\lambda}{d})] \quad \text{Eq. 3.5}$$

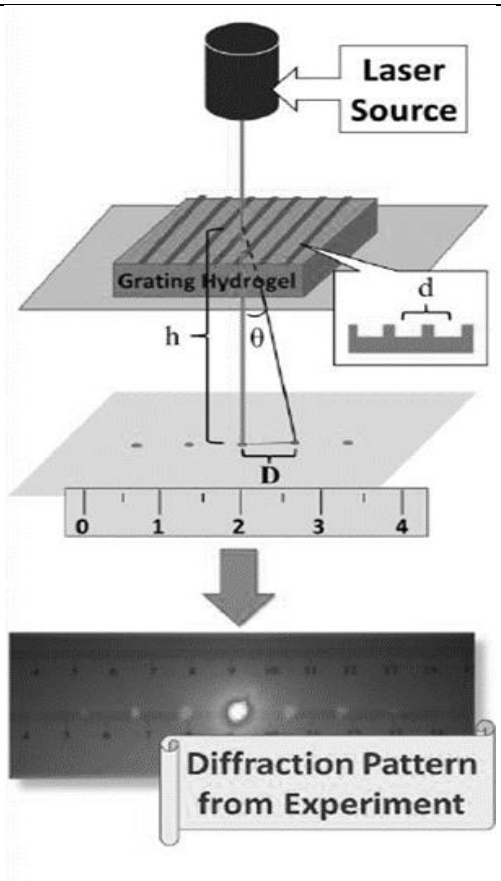

Figure 3.7. Diffraction pattern measurements.[275] *Source:* David A. Spivak and Wei Bai, A Double-Imprinted Diffraction-Grating Sensor Based on a Virus Responsive Super-Aptamer Hydrogel Derived from an Impure Extract, *Angewandte Chemie International Edition,* January 22, 2014, p. 4. Reproduced courtesy of John Wiley and Sons and the Copyright Clearance Center.

The angle of diffraction (θ) for the transmitted laser light may be calculated from the diffraction pattern's distance (d), where (λ) is the wavelength of the laser source (532 nm for the green laser pointer used here). As θ increases, the separation between the diffraction patterns becomes tighter. As shown in the equation, θ is a function of both the height (h) of the laser source and the distance (D) between two consecutive projected laser points. The combined equations show that when the hydrogel expands, the distance (D) between the laser spots reduces (lower grating period), and vice versa because of the inversely proportional relationship between the grating period (d) and the distance (D).

3.3 Results and Discussion

3.3.1 Reproducibility of the Grating Hydrogel

One of the most crucial aspects of biosensing is the biosensor's reproducibility, or its capacity to provide identical output signals or findings in repeated experimental runs. Reproducible signals give excellent reliability and resilience to biosensor response inferences. To check the reproducibility of the miR-21 DNA imprinted hydrogel, the percent shrinkage of a gel over three cycles of adding the miR-21 DNA target, removing it with the regenerating solution, and then re-addition of the miR-21 DNA target was measured. The average percentage shrinking response over multiple cycles, as shown in figure 3.8, was 4.40 ± 0.06%. This data demonstrates the reproducibility of the hydrogel and, in turn, system's stability across multiple cycles. To further verify the reproducible nature of the miR-21 DNA imprinted hydrogels, four hydrogels were made using the same formulations. The average percentage shrinking upon addition of the DNA target obtained was 3.80 ± 0.80%, as shown in figure 3.9, which further demonstrates the repeatability of the response.

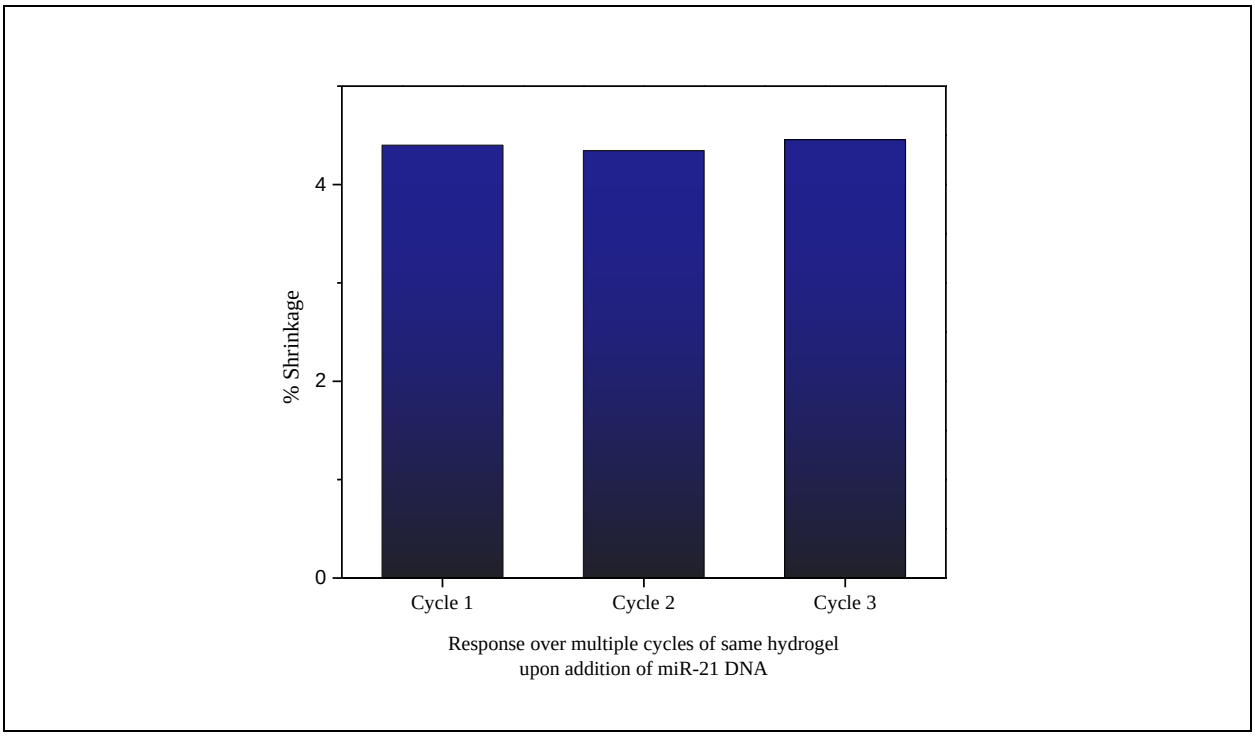

Figure 3.8. Shrinking response of hydrogel over multiple cycles. Contributed from ref [304]

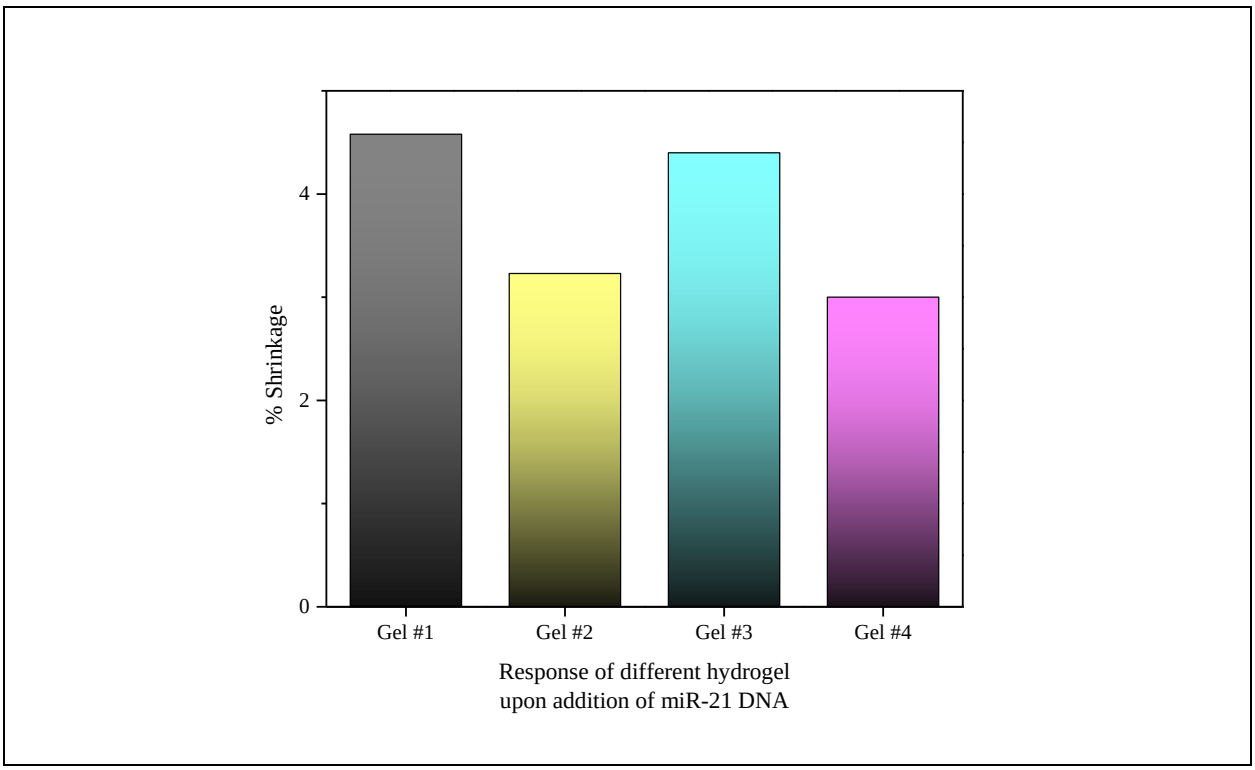

Figure 3.9. Reasonably reproducible shrinking response from different hydrogel with identical formulations

3.3.2 Control Studies

Several control studies were performed to verify whether it was critical to include both the aptamers and the DNA target inside the imprinted complex. While keeping the monomers, crosslinker, and initiator amounts the same, other components (Aptamer1, Aptamer2, and miR-21 DNA) were changed, as shown in Table 3.2. The percentage shrinkage response upon the addition of miR-21 DNA is shown in figure 3.10.

Table 3.2. Change in the components of the hydrogel for control studies

Entry	Components of the Hydrogel
miR-21 DNA MIP	Aptamer1 + miR-21 DNA + Aptamer2
Control 1	Aptamer1 + miR-21 DNA
Control 2	mir21-DNA
Control 3	Aptamer1 + Aptamer 2

It was hypothesized that both aptamers would be necessary to efficiently hybridize the target DNA mir21 and elicit the maximal response. Prior work by Bai et al. demonstrates that pre-complexation of both aptamers to their respective targets is an essential component of the response mechanisms for their hydrogels since many complexation locations are necessary for imprinting polymers.[37,64] miR-21 DNA MIP is composed of the full complex and showed a percentage shrinking response of 3.80 ± 0.80%, which is the average shrinking response from 4 different hydrogels as shown in figure 3.9. When the hydrogels were made with Aptamer 1 and miR-21 DNA (Control 2), the percentage shrinking response got reduced to 1.50 ± 0.65% due to the reduction in the number of receptors present.

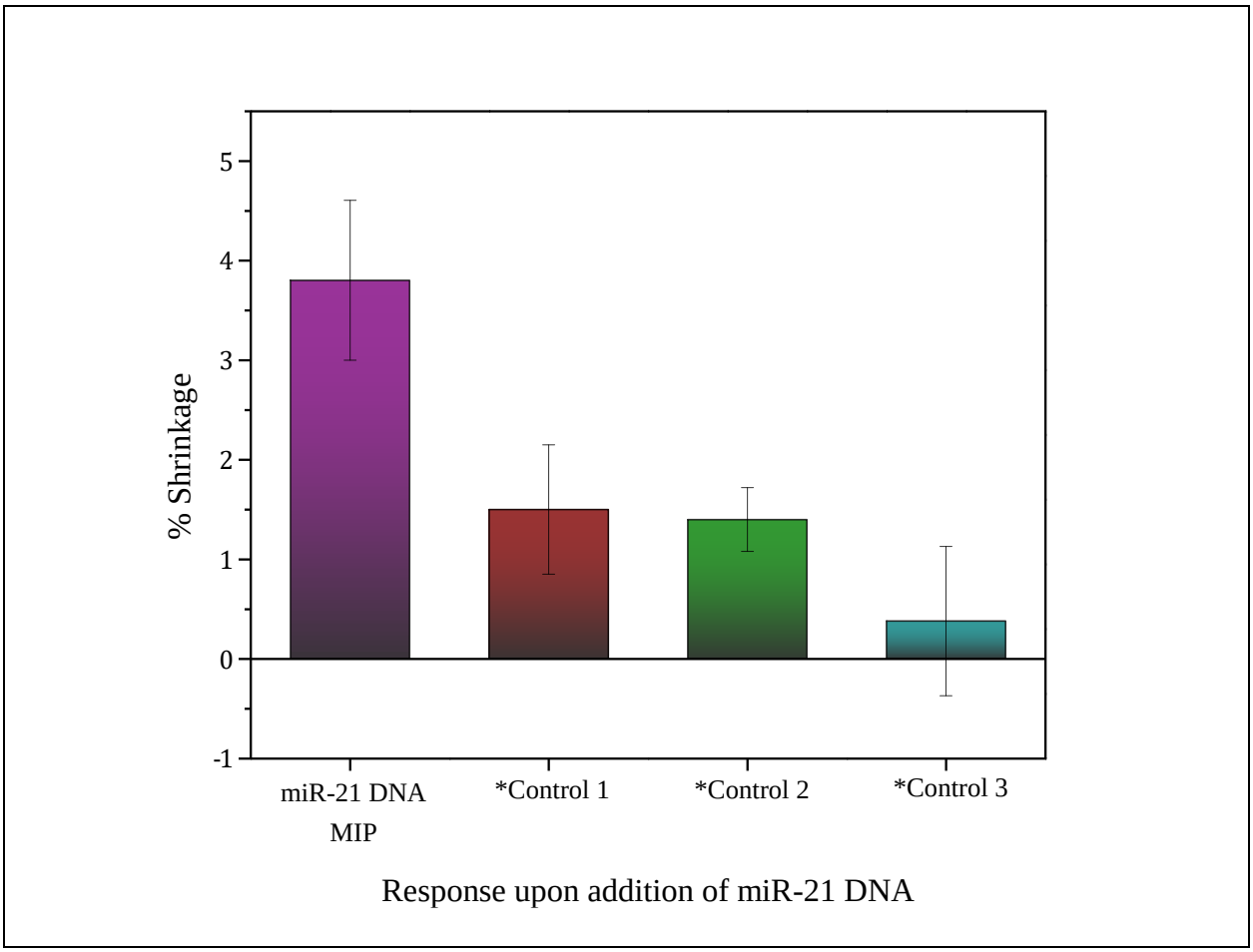

Figure 3.10. Shrinking response of control hydrogels. MiR-21 DNA MIP is the average data from figure 3.9. *Contributed by Britney Hebert from ref[304]

A gel was prepared without the aptamers, imprinting just the target mir-21 DNA (Control 2) to further demonstrate the significance of including the aptamers into the hydrogel for the DNA target identification. This hydrogel depended completely on the macromolecular memory established during polymerization inside the network since there were no recognition components present. Hydrogel lacking both aptamers (Control 2) showed a percentage shrinking response of 1.40 ± 0.32%, which is lower than that seen with single aptamer imprints. Control 1 and Control 2 demonstrate the dependence of hydrogel response on the hybridization of the miR-21 DNA target to its complementing aptamers.

To determine whether an imprinting system in which the aptamers and target are integrated into the polymerization is required, a hydrogel was made without the miR-21 DNA target, creating a non-imprinted polymer (Control 3). This polymer depended only on the hybridization of the aptamer/DNA complex formation after polymerization since the aptamers remained inside the hydrogel network. Control 4 showed a percentage shrinking response of 0.38 ± 0.75% when exposed to mir21-DNA. This is because aptamers, when polymerized in the absence of the target, are randomly distributed rather than creating a pre-organized complex of Aptamer 1-miR21 DNA-Aptamer 2. When the target miR-21 DNA is included in the polymerization process, the aptamers are ordered in an optimal fashion for rebinding. These findings substantiated the need to assemble the whole complex of Aptamer 1-miR21 DNA-Aptamer 2 since omitting any one component diminished the hydrogels' response.

3.3.3 Selectivity and Specificity of the Grating Hydrogel

The most significant aspect of a biosensor is its selectivity. For a bioreceptor to be selective, it must be able to distinguish between the target analyte and any background substances present in the sample. To check for the selectivity, miR-21 DNA imprinted hydrogels were incubated in different analytes. The difference(s) in the base pair sequence of different analytes compared to the miR-21 DNA target is highlighted in yellow and shown in the table. Mismatch 1 has only one change in the base pair sequence, cytosine (C) instead of guanine (G), in the middle. Mismatch 7 has seven differences in the 5' end of the nucleotide. In the case of ‘5-spacer’, five thymine (T) group was inserted in the middle of the sequence. While 'Random' has some complementary in the base pair sequence, 'Anti' has a completely opposite base pair sequence compared to the miR-21 DNA. The miR-21 DNA imprinted hydrogel was incubated into each of the analytes separately, and the percent shrinking response was recorded.

Table 3.3. Sequences of different analytes

Oligonucleotide	Base pair sequence
miR-21 DNA	5’ – TAG CTT ATC AGA CTG ATG TTG A – 3’
Mismatch 1	5’ – TAG CTT ATC ACA CTG ATG TTG A – 3’
Mismatch 7	5’ – ATC GAA TTC AGA CTG ATG TTG A – 3’
5-spacer	5’ – TAG CTT ATC AGT TTT TA CTG ATG TTG A – 3’
Random	5' – GAT TCA CTG AGT CTA CGA TAG C– 3'
Anti	5' – ATC GAA TAG TCT GAC TAC AAC T – 3'

The percentage shrinking response for different analytes is shown in figure 3.11. Even though Mismatch 1 has the maximum complementarity in the base pair sequence, very small shrinking response was observed upon multiple cycles of its addition to the imprinted hydrogel. This result indicated the high selectiveness of the hydrogels in responding to the miR-21 DNA target only. A similar response was expected for the rest of the analytes as they have more differences in the base pair sequence. Although, some response was observed for Mismatch 7, 5-spacer, Random, and Anti sequence, the shrinking response was lower than 2% in all cases. The lack of response was probably due to some non-specific binding and changes in the total hydrodynamic volume of the gel due to the presence of some unbound analytes in the hydrogel. Another possible reason for the lack of response was most likely due to the pre-complexed binding during the hydrogel preparation, which allowed the aptamers to be ordered specifically to the miR-21 DNA target only.

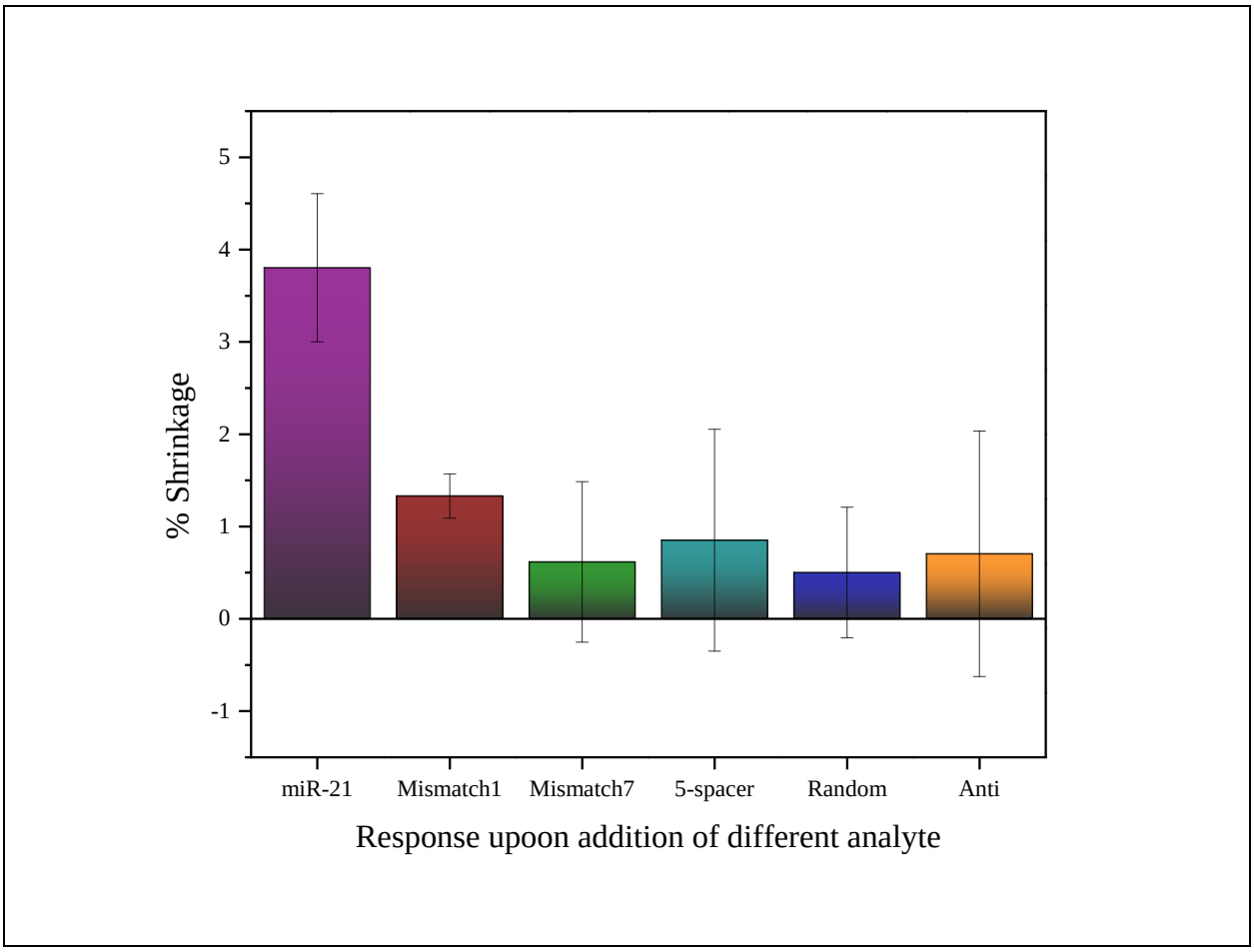

Figure 3.11. Shrinking response of hydrogel upon addition of different analyte.

3.3 Conclusion

The molecularly imprinted polymer gel laser diffraction sensor (MIP-GLaDiS) was investigated in this work by using the 22-base pair miR-21 DNA as the target, which has never been used in such systems to the best of our knowledge. MIP-GLaDiS, which involved both the micro- and macro- imprint technique, was made using the Thiol-Acrylate (TA) mold. Due to the greater hydrophilicity of the TA composite material, the gel was successfully and reliably imprinted with the TA mold's pattern. The hydrogel shrank or swelled upon the addition or removal of the miR-21 DNA target, respectively, which altered the diffraction pattern on the gel. This alteration was observed by shining a laser pointer through the hydrogel. The shrinking of hydrogel was due to

the hybridization of the miR-21 DNA target with the aptamers. The diffraction hydrogel showed a percentage shrinking response of 3.80 ± 0.80, which was reproducible over multiple cycles. The control studies indicate that the full Aptamer 1- miR-21 DNA- Aptamer 2 complex during hydrogel preparation is crucial for binding of the target mir-21 DNA since omitting any one component diminished the hydrogels' response. A very low shrinking response was observed when the base pair sequences of the analytes were changed compared to the miR-21 DNA, which indicated the high selectivity of the MIP-GLaDiS. During the hydrogel preparation process, the aptamers were ordered specifically to the miR-21 DNA target only.

Appendix A. Experimental and Spectra for Chapter 1

Materials and Methods

Materials

The 4-vinylphenyl acetate monomer was obtained from Aldrich and put through an alumina column to get rid off the inhibitor. 4-vinyl-2-methoxy phenol, 4-vinyl-3-methoxy phenol, silica gel (Merck grade 9385, pore size 60 Å, 230-400 mesh), 2-bromoisobutyryl bromide, 10-undecane-1-ol, Copper(I)bromide, N,N,N',N'',N''-pentamethyldiethylenetriamine (PMDETA), triethylamine, trichlorosilane, triethoxysilane, Platinum(0)-1,3-divinyl-1,1,3,3-tetramethyldisiloxane complex (Karstedt catalyst), acetic anhydride, pyridine, dimethylaminopyridine (DMAP), malonic acid, methyltriphenylphosphonium bromide, DBU, dodecanedioyl dichloride, hydrazine were obtained from either Sigma-Aldrich or VWR. All the solvents such as toluene, xylene, diethylether, THF, ethyl acetate, hexane, acetonitrile, ethanol were obtained from VWR and used without further purification.

Synthesis of 10-undecan-1-yl 2-bromoisobutyrate

10-undecen-1-yl-2-bromoisobutyrate was made by making a few small changes to a method that had been described before.43 In a 500mL round bottom flask (RBF), triethylamine was added to a solution of 10-undecen-1-ol 1 (4.08 mL, 20.36 mmol) in 100 mL diethyl ether (3.13 mL, 22.40 mmol). The flask was cooled to 0 ^{o}C, and a solution of 2-bromoisobutyryl bromide 2 (2.8 mL, 22.4 mmol) in dry diethyl ether (50 mL) was added drop by drop through a dropping funnel while stirring for 10 minutes. The reaction mixture was left at room temperature for 15 hours while it was stirred. After the reaction was done, 50 mL of hexanes was added, and the precipitate (Triethylammonium bromide ($Et_3N^+Br^-$)) was taken out with a gravity filtration. Under reduced pressure, the solvent was removed, leaving a clear liquid that was purified with a 25:1 mixture of hexane and ethyl acetate by column chromatography. ^{1}H NMR was used to prove that the product

was made.

Synthesis of 11-(2-Bromo-2-methyl)propionyloxy undecyltrichloriosilane

10-undecen-1-yl 2-bromoisobutyrate 3 (7.11 g, 22.27 mmol) and trichlorosilane (11.33 mL, 112 mmol) were added to a 100 mL RBF at 0 ^{o}C under a nitrogen atmosphere. This was followed by Karstedt catalyst ((140 µL, 12µmol), and the reaction mixture was stirred for 24 hrs at room temperature in xylene. Under reduced pressure, the excess reagent ($HSiCl_3$) was taken out, and the remaining product was dissolved in 50 mL of hexanes and quickly filtered through a silica plug to get rid of the catalyst. The final product was a clear liquid, and its purity was shown by the disappearance of vinyl signals in ^{1}H NMR.

Surface grafting of Tier-I ESSs on silica

In order to prepare the SiO_2 gel, it was heated overnight at 120 °C in an oven. Silica was functionalized by heating the trichlorosilyl-end group containing compounds with 6.0 g SiO_2 in Toluene (50 mL) at 80 °C. In a typical procedure, toluene is added to an RBF charged with SiO_2, then the trichlorosilyl-end functionalized compound (0.45 mL) is injected dropwise using a syringe, followed by 18 hours of heating at 80 °C. Once allowing the reaction mixture to cool to ambient temperature, the toluene was decanted after the product had completely settled. The product was washed with toluene, acetonitrile, and methanol (2 x 50 mL each). The resultant substance was dried in an oven for 48 hrs at 50 ^{o}C. The product was confirmed by means of TGA and ^{13}C CP-MAS NMR analysis.

Synthesis of the Tier-II ESSs (ATRP of 4-acetoxystyrene)

In a 250 mL RBF, was added 2.28g of SiO2-C11-Br in 17 mL of xylene. After purging with N_2 gas for 5 minutes, Cu(I)Br (182mg, 1.27 mmol) catalyst and N,N,N',N'',N''-pentamethyldiethylenetriamine (PMDETA) ligand (0.32 mL, 1.53 mmol) was added. The 4-acetoxystyrene monomer (7.8g, 48 mmol) was added while the reaction mixture was purged with

N_2 gas, and the RBF was fitted with a condenser. The reaction mixture was purged for another 5 minutes and then placed in the oil bath at 140 ^oC for 24 hrs. After cooling to ambient temperature, the resulting mixture was washed with 2 x 50 mL portions of toluene, acetonitrile, ethanol, half-saturated EDTA solution, water, and ethanol before being heated to 50 ^oC in an oven while being stirred under positive N_2 pressure for 48 hours. TGA and solid-state NMR were used to analyze the produced tan powder.

Synthesis of the Tier-II ESSs (ATRP of 4-acetoxy-3-methoxystyrene)

In a 250 mL RBF, was added 2.26g of SiO2-C11-Br in 17 mL of xylene. After purging with N_2 gas for 5 minutes, Cu(I)Br (184mg, 1.28 mmol) catalyst and N,N,N',N'',N''-pentamethyldiethylenetriamine (PMDETA) ligand (0.32 mL, 1.53 mmol) was added. The 4-acetoxy-3-methoxystyrene monomer (10g, 52 mmol) was added while the reaction mixture was purged with N_2 gas, and the RBF was fitted with a condenser. The reaction mixture was purged for another 5 minutes and then placed in the oil bath at 140 ^oC for 24 hrs. After cooling to ambient temperature, the resulting mixture was washed with 2 x 50 mL portions of toluene, acetonitrile, ethanol, half-saturated EDTA solution, water, and ethanol before being heated to 50 ^oC in an oven while being stirred under positive N_2 pressure for 48 hours. TGA and solid-state NMR were used to analyze the produced tan powder.

Hydrolysis of Acetoxy Group of Tier-II ESSs

A 250 mL RBF was filled with the Tier-II ESSs (SiO_2-C11-PAS and SiO_2-C11-PAMS) (approximately 2.0 g), and then 40 mL (per gram of the polymer) THF was added and stirred. After adding the hydrazine (1.165mL/g polymer functionalized silica) drop by drop, the RBF was flushed with N_2 gas, sealed with a stopper, and stirred at room temperature for 10 hrs. The resultant mixture was then washed twice with 50mL each of THF, ethyl acetate, and ethanol before being oven dried for 48 hours at 50 °C under N_2. TGA and solid-state NMR were used to examine the

resultant solid.

Protection reaction of 4-hydroxy-2-methoxybenzaldehyde

In a 250 mL RBF, 4-hydroxy-2-methoxybenzaldehyde (2.0 g, 13.1 mmol) was added in 40 mL of DCM, and then triethylamine (5.5 mL, 39.4 mmol) was added. Finally, acetyl chloride (2.8 mL, 39.4 mmol) was added dropwise, and the reaction mixture was stirred at room temperature for 24 hrs. Then the reaction mixture was filtered and washed with 2 x 50 mL of 1M NaOH and brine solution. The product was purified by column chromatography by using 80:20 of hexane: ethyl acetate.

Wittig reaction of 4-acetoxy-2-methoxybenzaldehyde to form 4-acetoxy-2-methoxystyrene

To a refluxing solution of methyltriphenylphosphonium bromide (13.2 mL, 2.7 mmol) in toluene (50 mL) was added DBU (4.4 mL, 2.9 mmol). After refluxing for 30 minutes, 4-acetoxy-2-methoxybenzaldehyde (3.1 mL, 1.3 mmol) in toluene was added to the solution, and the reaction mixture were refluxed for 24 hrs. Then the reaction mixture was washed with water (3 x 50 mL) and dried over magnesium sulphate. The product was purified by column chromatography by using 70:30 hexane: dichloromethane.

Crosslinking reactions of the hydrolyzed Tier-II ESSs

In a 100 mL RBF, hydrolyzed Tier-II ESS (0.5 g, 0.3 mmol) was added to 25 mL of THF, and then triethylamine (47 µL, 0.3 mmol) was added. Finally, dodecanedioyl dichloride (0.7 mL, 2.7 mmol) was added dropwise, and the reaction mixture was stirred under reflux conditions for 24 hrs. Then the reaction mixture was filtered and washed with 2 x 50 mL of 1M NaOH and brine solution. The product was purified by column chromatography by using 50:50 hexane: ethyl acetate.

Norflurazon sorption isotherm

For all of the experiments, the background solution consisted of 18 Ωm water with 0.01 M $CaCl_2$ (96.0%, Sigma-Aldrich St. Louis, MO), 100 ppm NaN_3 (99%, Acros), and 0.05 M MES (high purity, VWR) at a pH of 5.75. These components were added to keep the ionic strength constant, suppress biological activity, and keep the pH stable, respectively. In addition, reagent-grade methanol with a v/v of 0.1% that was purchased from VWR was used to assist in the dissolution of NOR into the background solution in order to produce a stock solution of NOR.

Table A.1. Soil-to-solution (S2S) ratio and sorption kinetics of ESSs and acetylated Pahokee peat with 20 ppm of Norflurazon

	S2S ratio			Sorption kinetics		
Entry	Weight	%sorption	sd	days	%sorption	sd
ESS1	20 mg	74.88	0.91	5	74.03	0.12
ESS2	40 mg	51.95	0.16	6	45.09	0.21
ESS3	20 mg	53.01	0.21	5	52.89	0.16
ESS4	40 mg	51.95	0.15	6	53.82	0.21
Acetylated Pahokee peat	80 mg	55.61	0.09	6	57.8	0.98

sd= standard deviation

Table A.2. Freundlich adsorption isotherm binding parameter (KF), linear regression constant (N), and goodness to fit (R2) for Norflurazon with ESSs and acetylated Pahokee peat

	Sorption		
Entry	$\log K_F^{sor}$	N^{sor}	R^2
ESS1	2.837±0.022	0.974±0.041	0.990
ESS2	2.246±0.052	0.993±0.080	0.963
ESS3	2.699±0.010	0.909±0.016	0.998
ESS4	2.543±0.018	0.785±0.029	0.992
Acetylated Pahokee peat	2.515±0.067	0.530±0.090	0.979

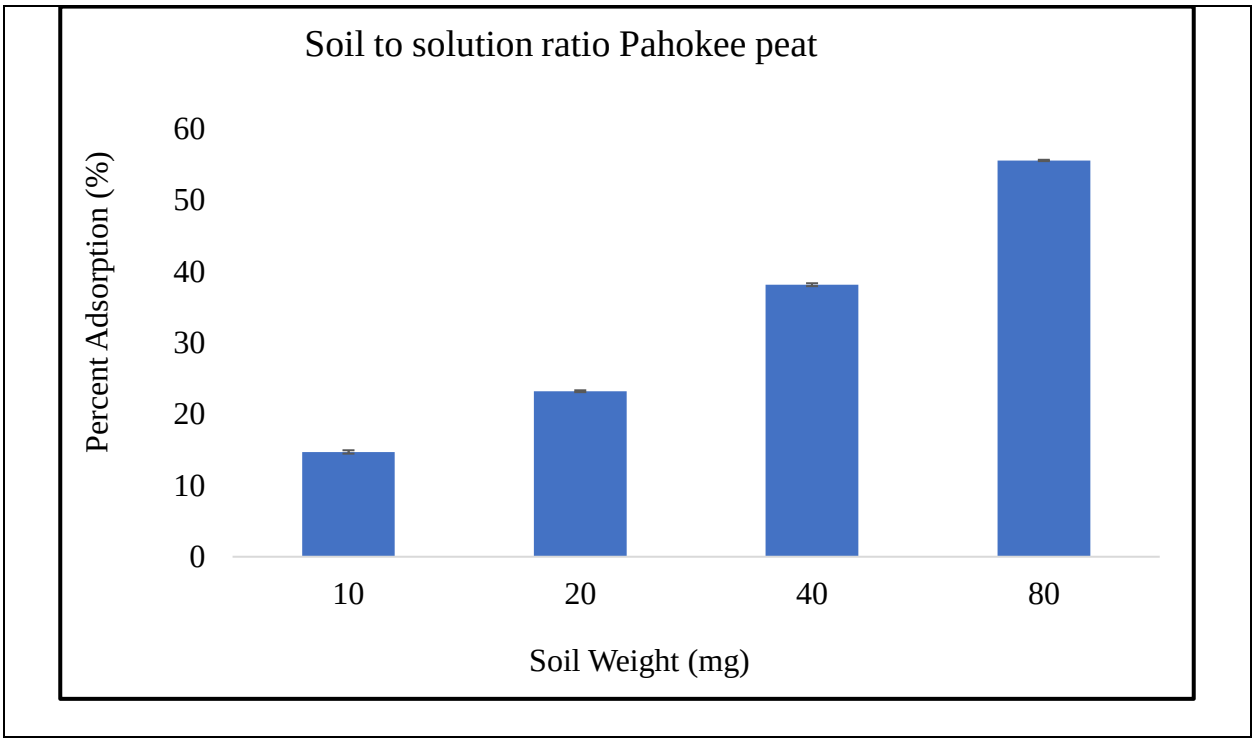

Figure A.1. Soil to solution ratio of Pahokee peat

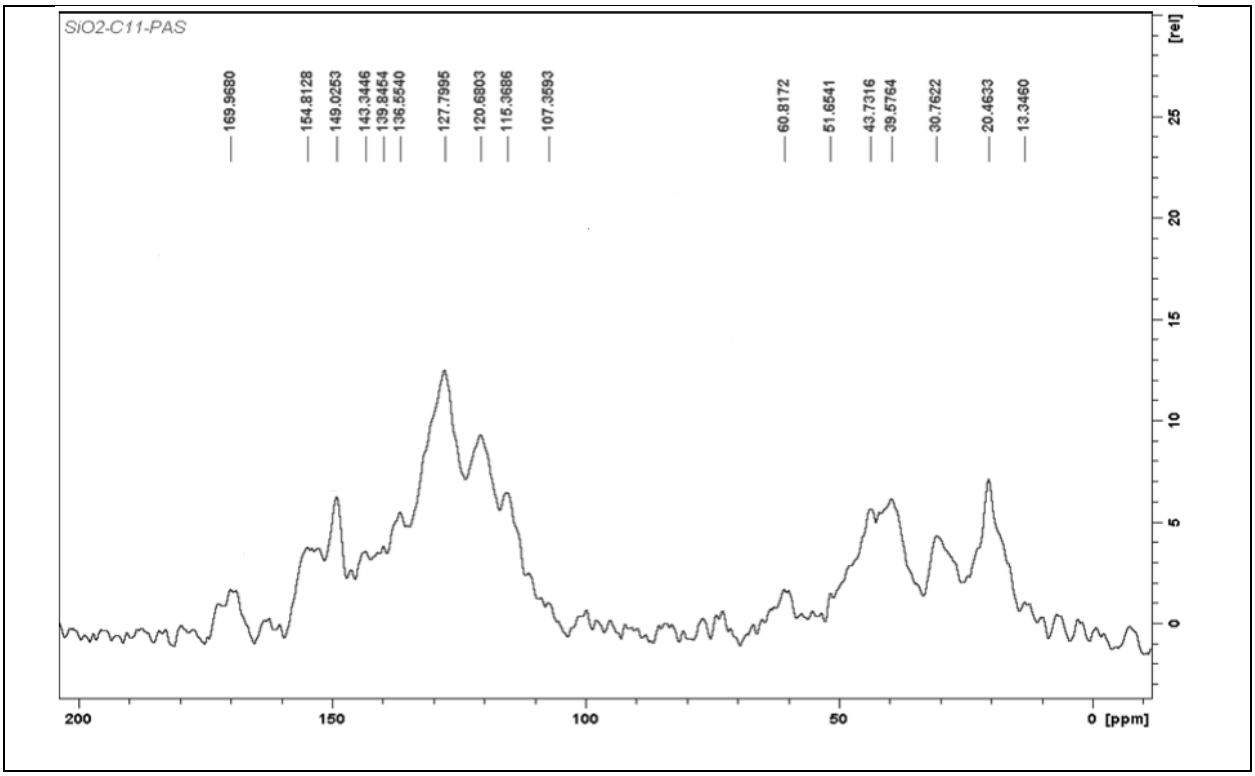

Figure A.2. CP-MAS ^{13}C solid-state NMR of ESS1.

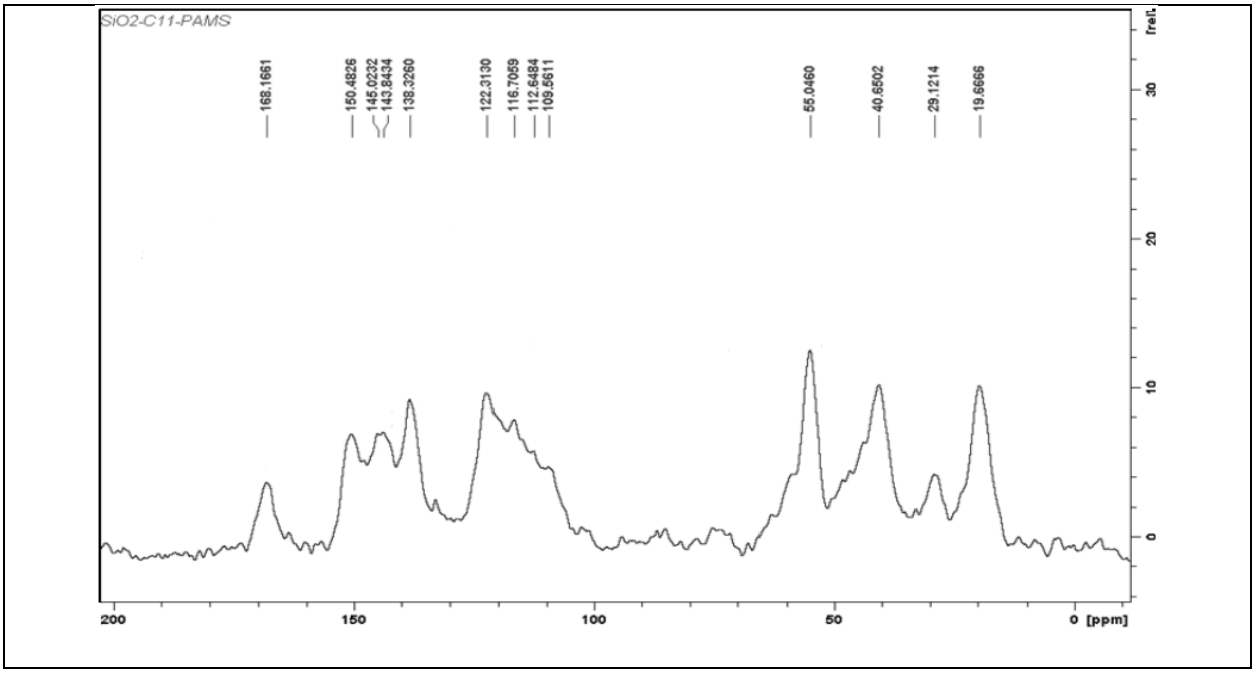

Figure A.3. CP-MAS ^{13}C solid-state NMR of ESS2.

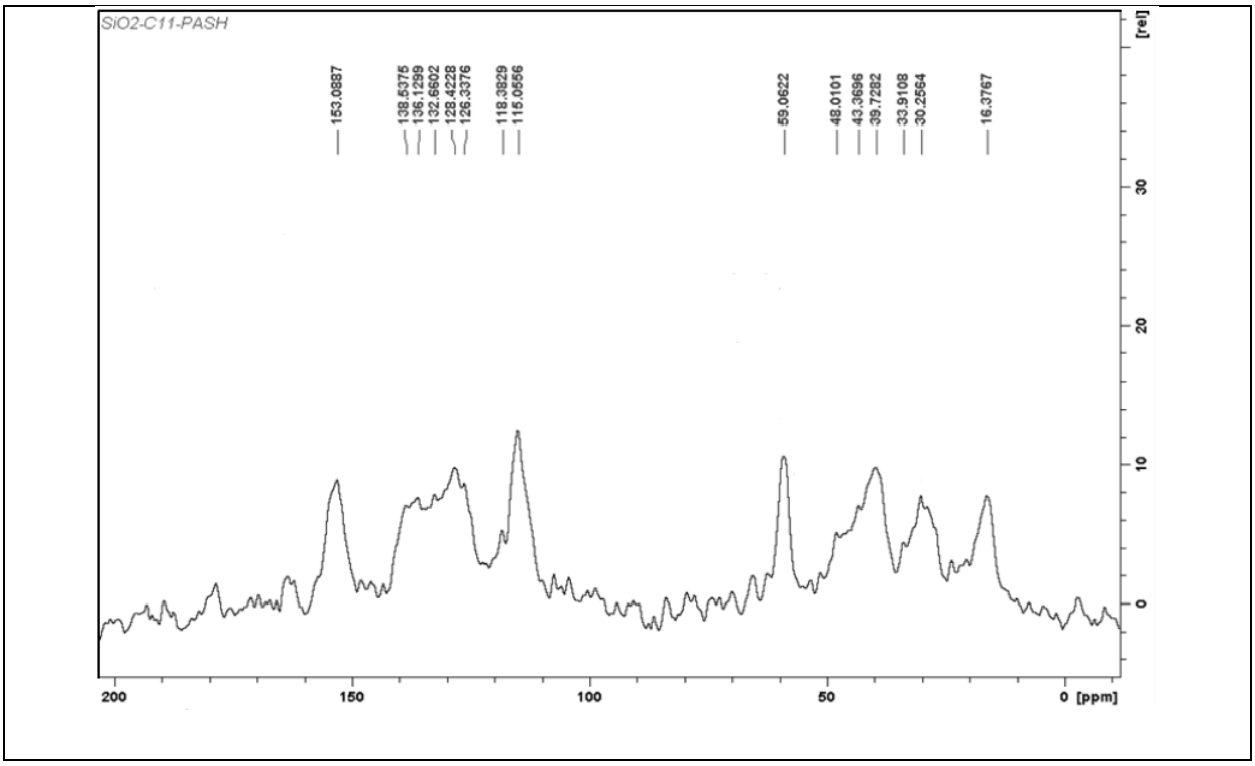

Figure A.4. CP-MAS ^{13}C solid-state NMR of ESS3.

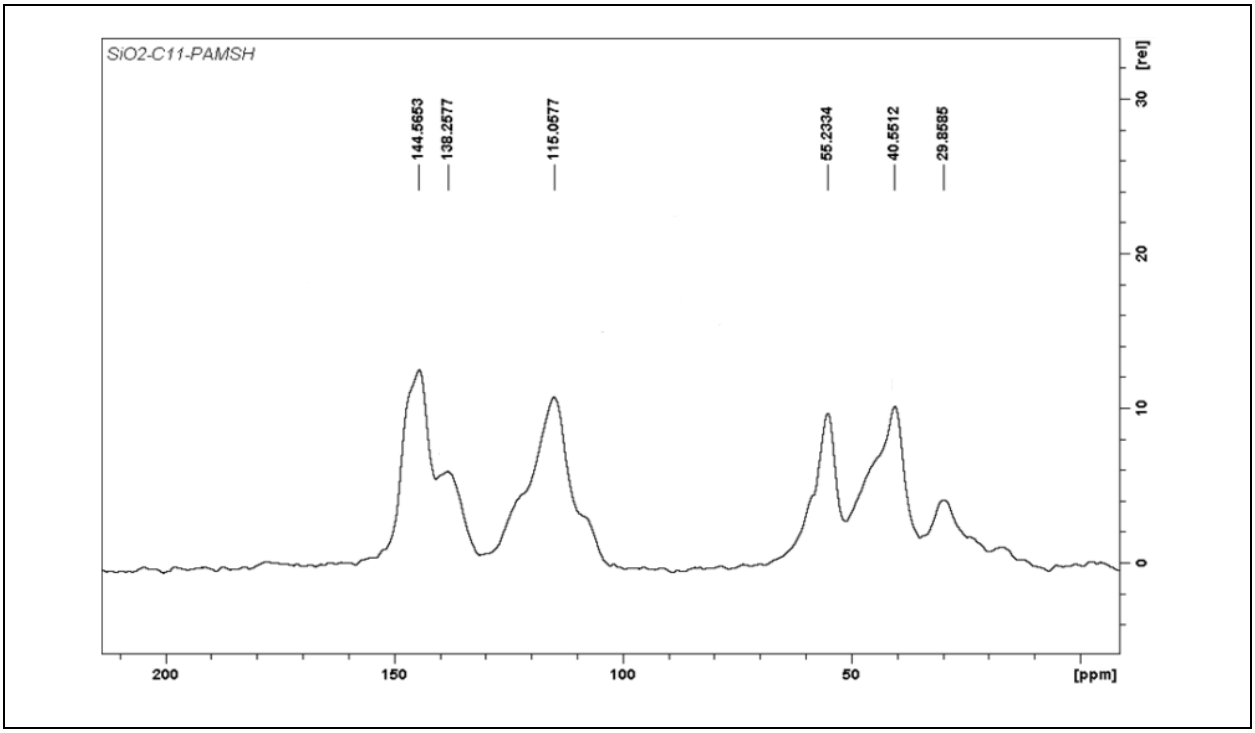

Figure A.5. CP-MAS ^{13}C solid-state NMR of ESS4.

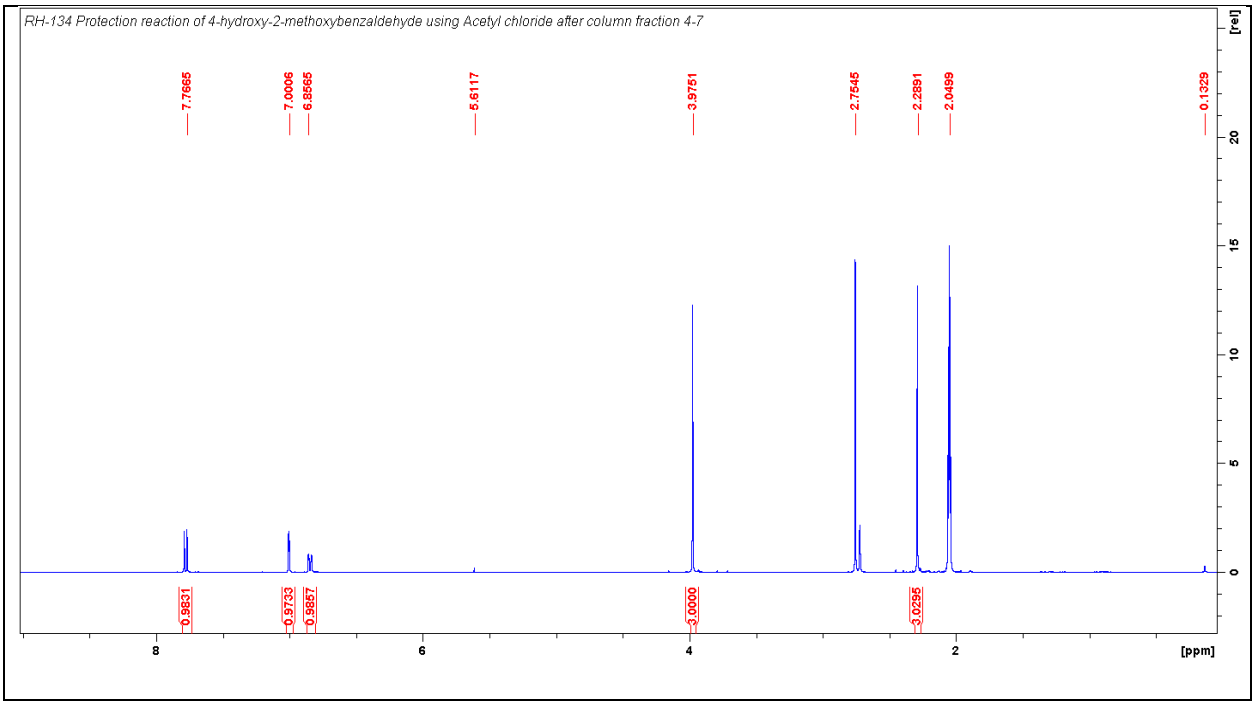

Figure A.6. ^{1}H NMR of protection reaction of 4-hydroxy-2-methoxybenzaldehyde

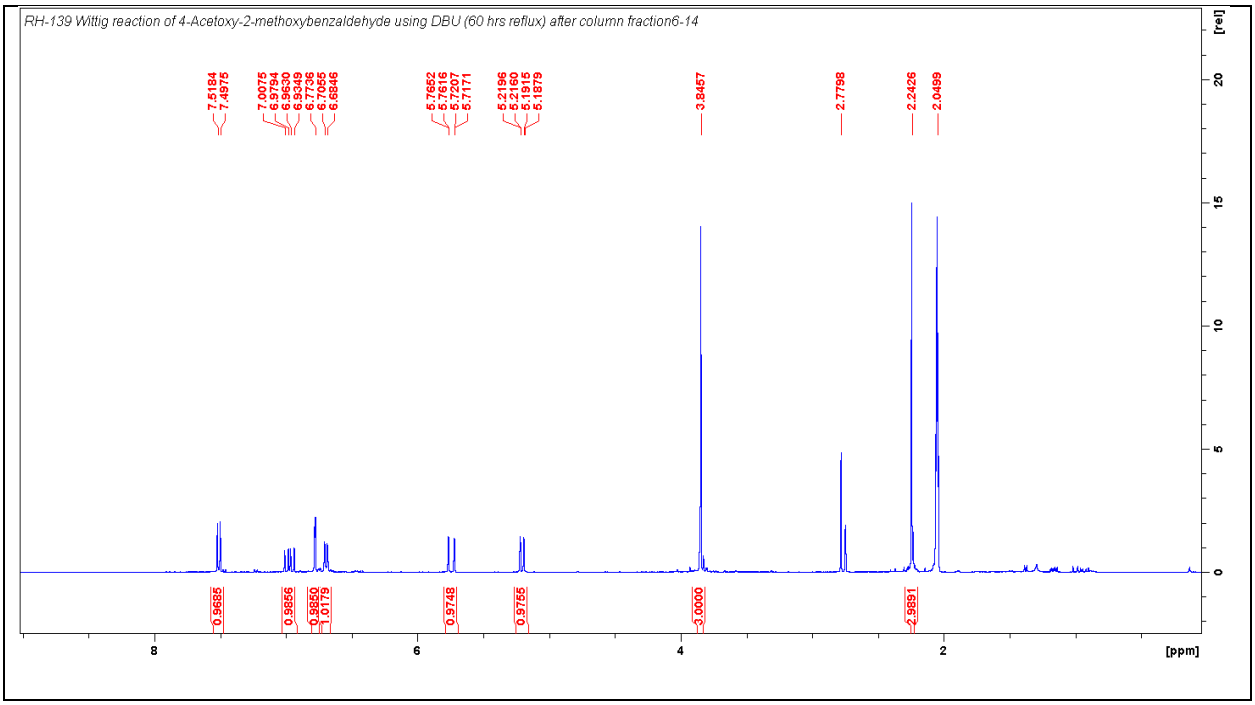

Figure A.7. ^{1}H NMR of Wittig reaction of 4-acetoxy-2-methoxybenzaldehyde

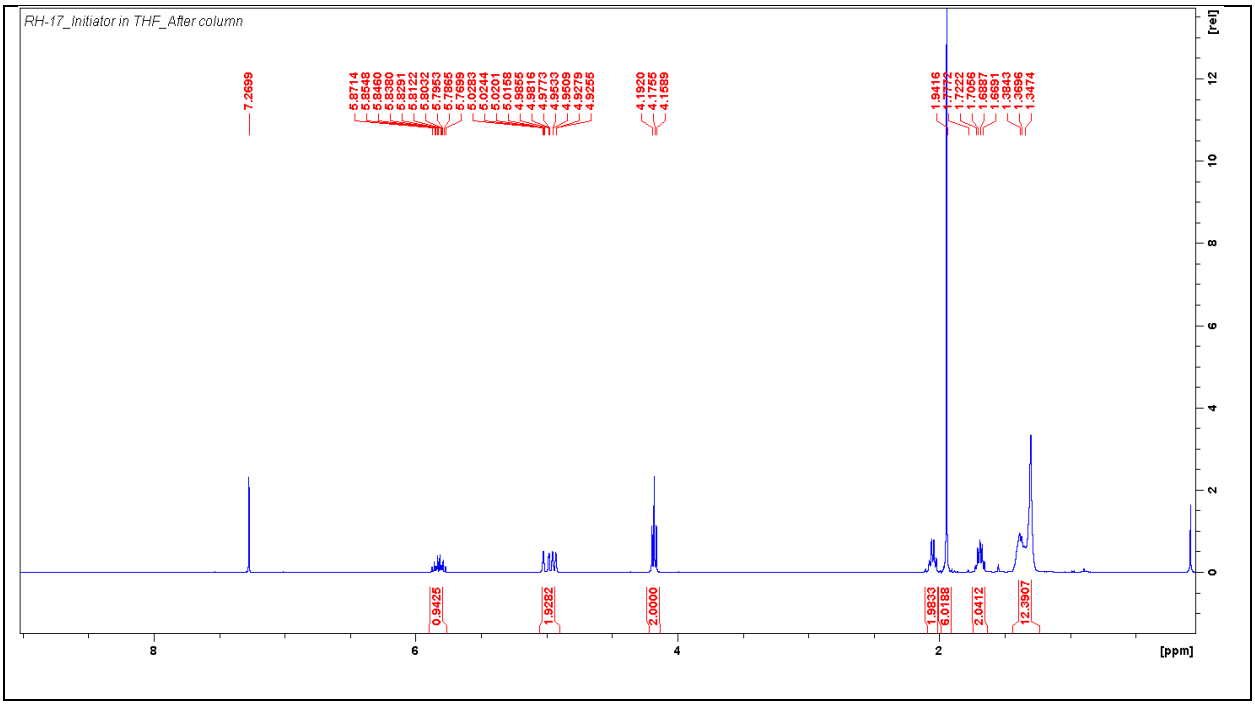

Figure A.8. ^{1}H NMR of ATRP initiator synthesis

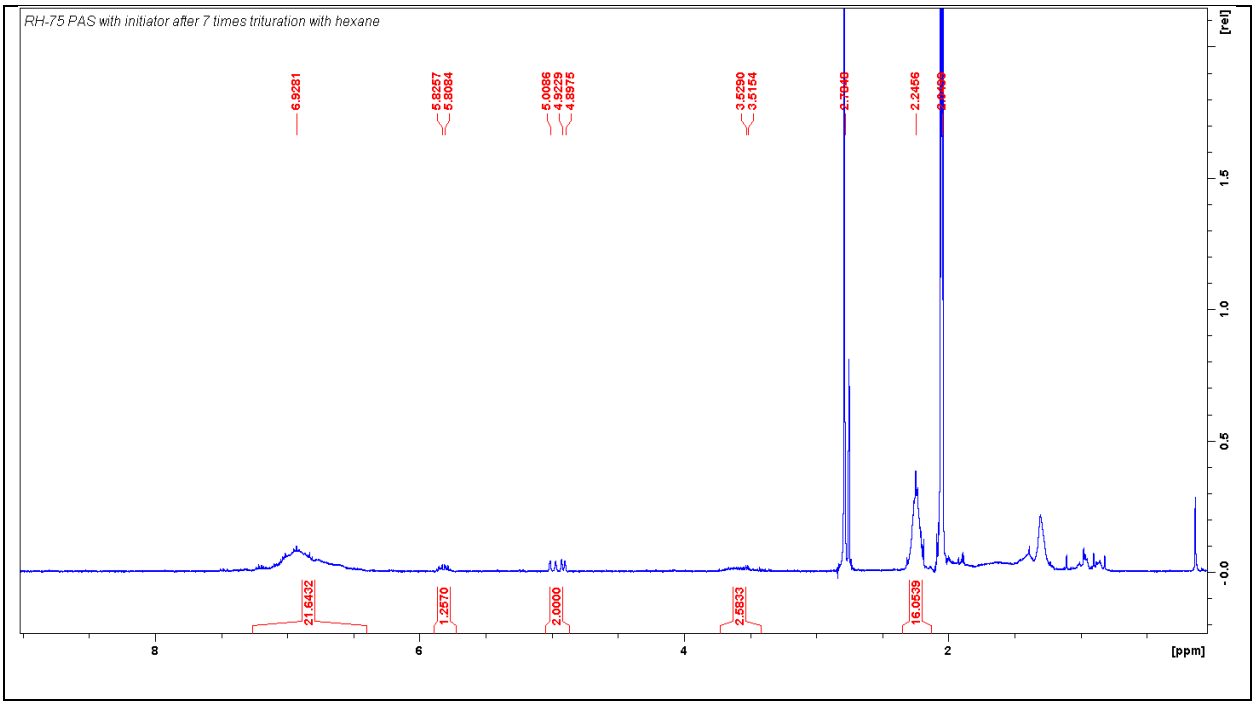

Figure A.9. ^{1}H NMR of ATRP of 4-acetoxystyrene

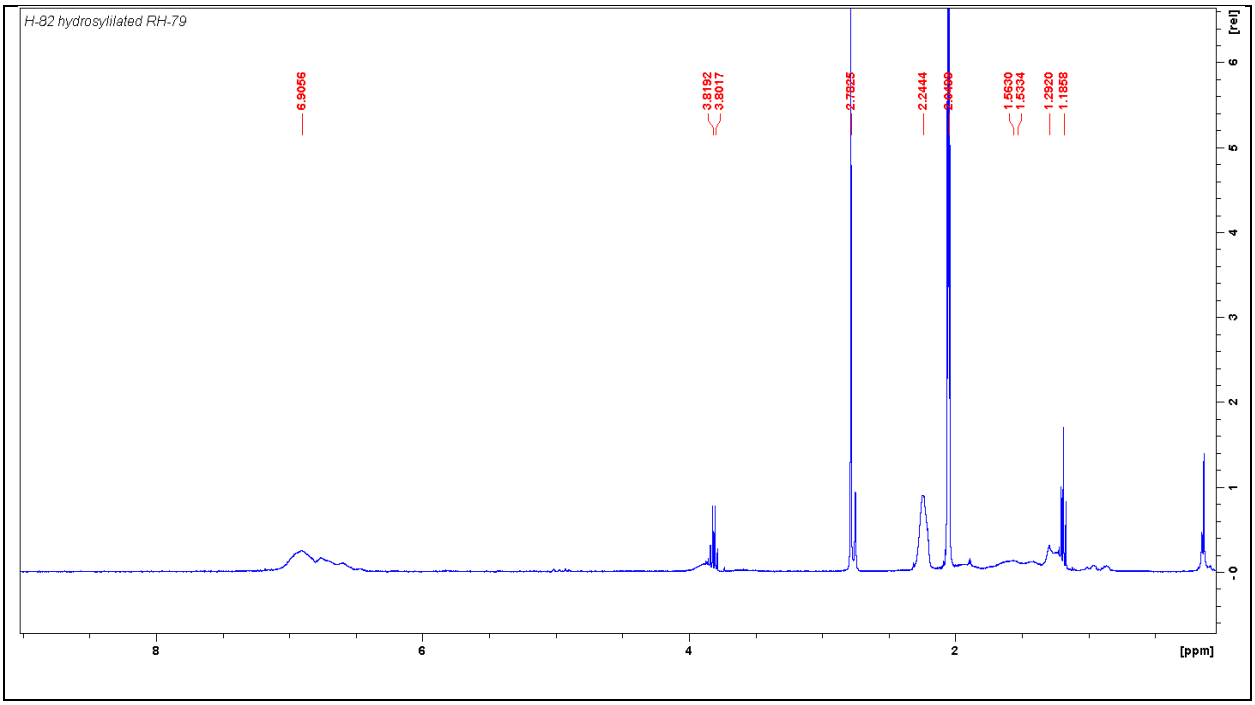

Figure A.10. ^{1}H NMR of PAS-Si

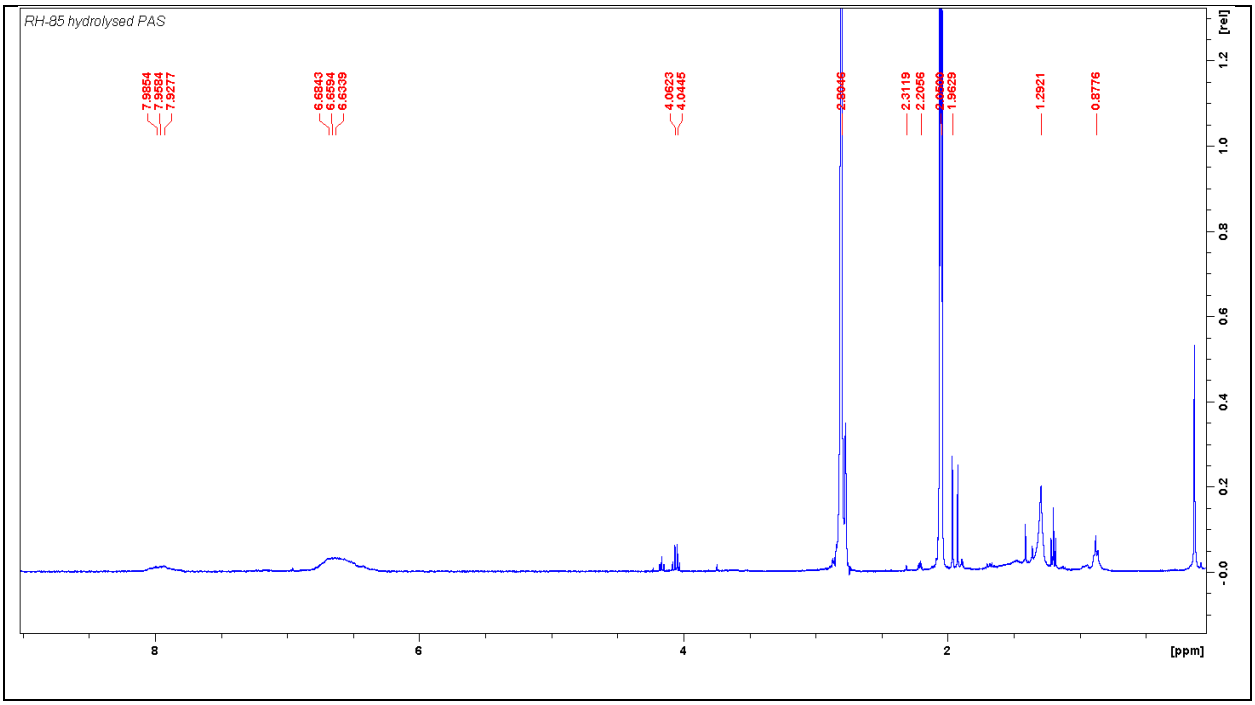

Figure A.11. ^{1}H NMR of PASH-Si

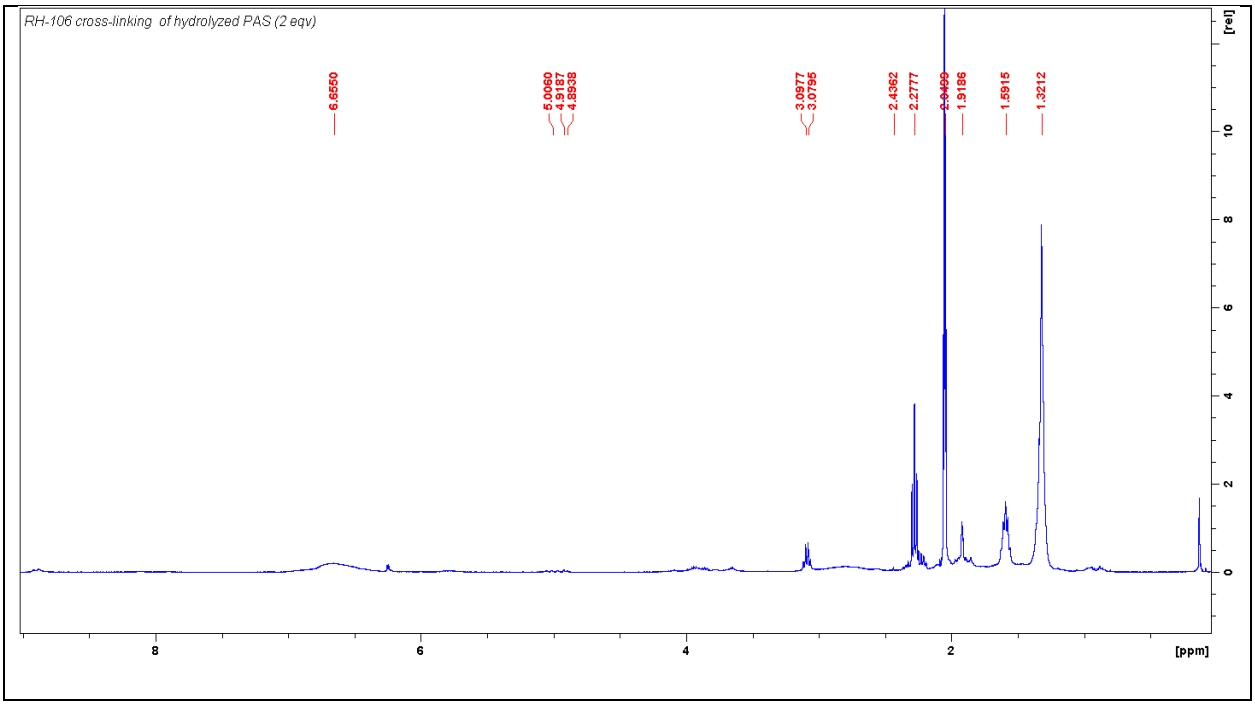

Figure A.12. ^{1}H NMR of cross-linked ESS

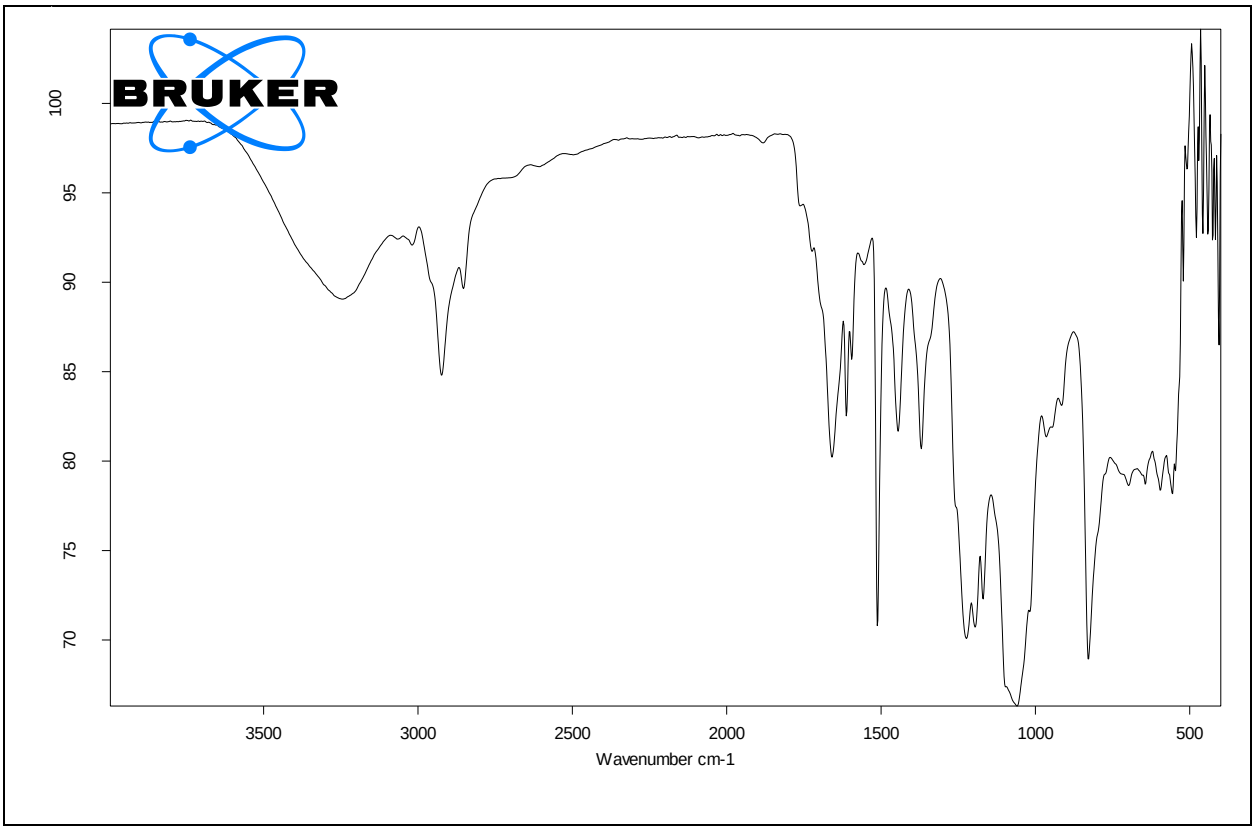

Figure A.13. FTIR spectra of PASH-Si (before cross-linking reaction)

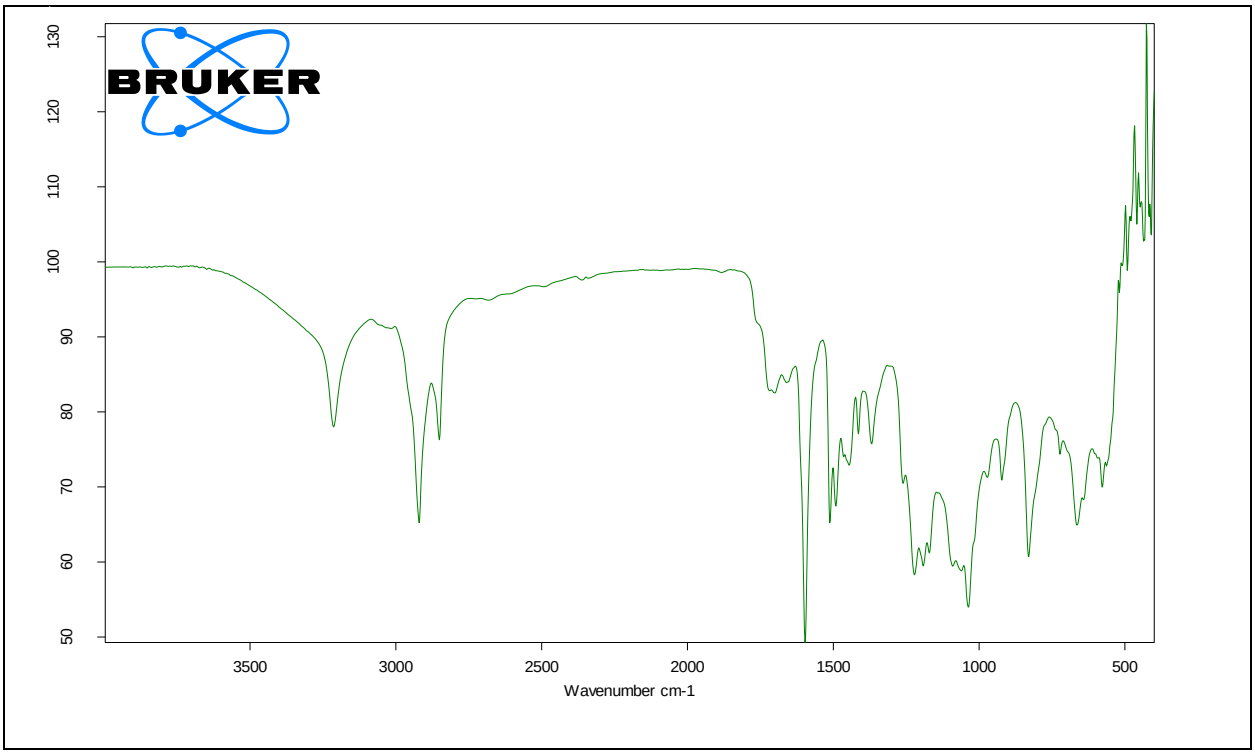

Figure A.14. FTIR spectra of cross-linked ESS (after cross-linking reaction)

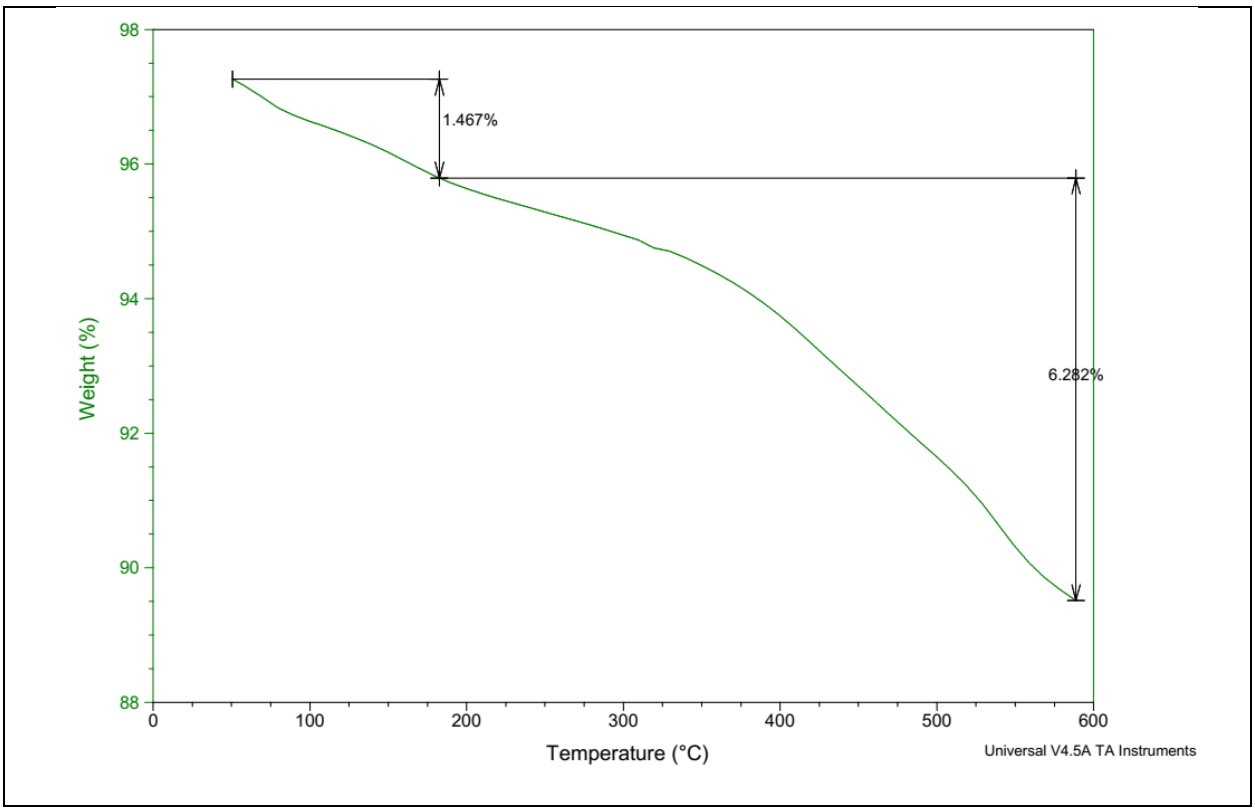

Figure A.15. TGA thermogram of cross-linked ESS after grafting reaction

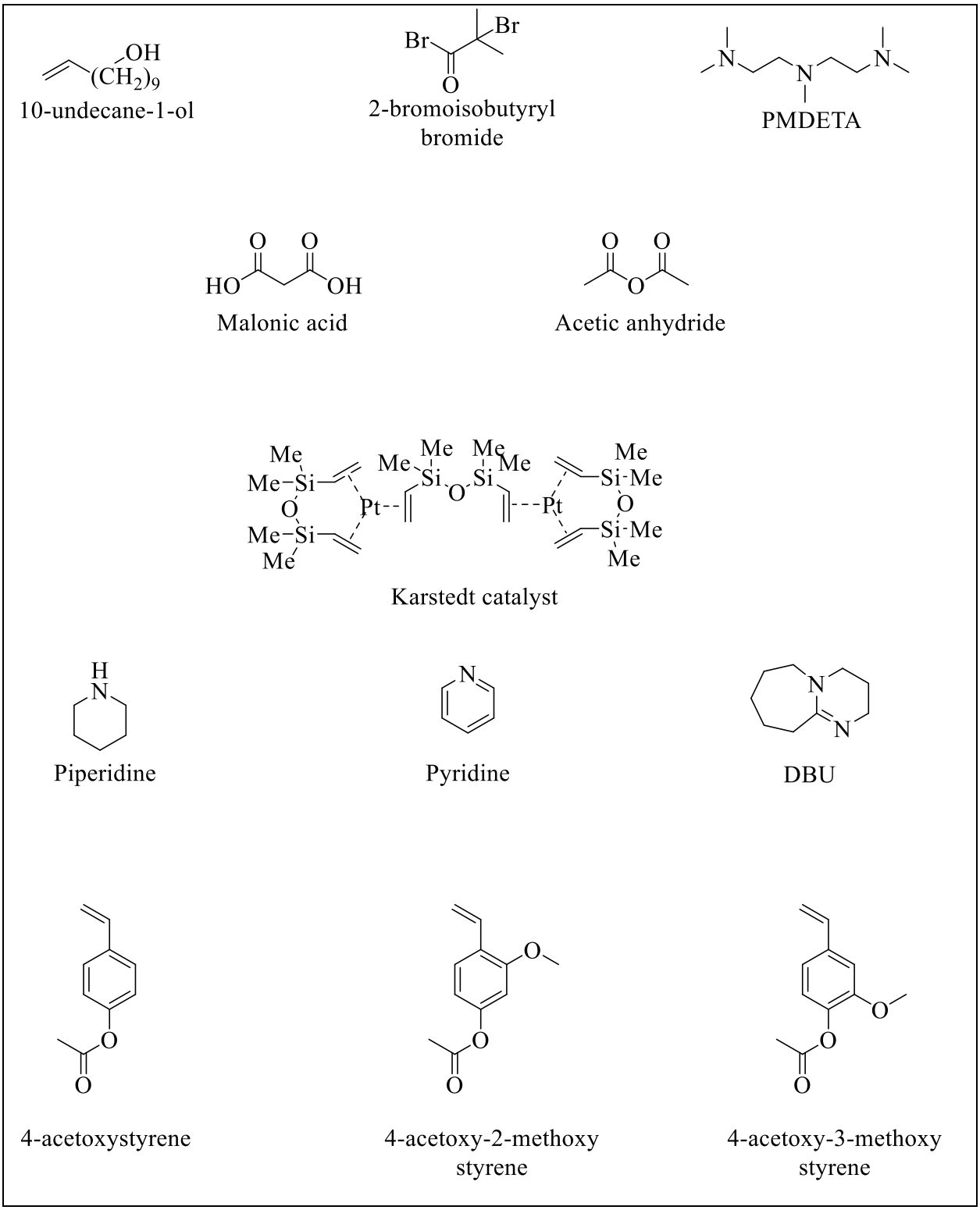

Figure A.16 Structure of some of the chemicals used in chapter 1

Appendix B. Experimental and Spectra for Chapter 2

Materials and Methods

Materials

Unless otherwise indicated, Benzyl fentanyl, fentanyl, heroin, cocaine, and methamphetamine were purchased from the Toronto Research Chemicals. Ethyleneglycol dimethacrylate (EGDMA) and Methacrylic acid (MAA) were obtained from Aldrich and distilled in vacuo under boiling conditions before polymerization. Solvents obtained from commercial suppliers such as VWR or Sigma-Aldrich were HPLC grade and used as-is. Reactions that need anhydrous conditions were performed in dry glassware under N_2 atmosphere. Reactions were monitored by thin-layer chromatography. Column chromatography was carried out with flash silicagel.

Measurements

^{1}H NMR was measured in $CDCl_3$, $(CD_3)_2CO$ or $(CD_3)_2SO$ on an AV 400 MHz Bruker instrument. MALDI-TOF MS was performed on a commercial instrument (Bruker UltrafelXreme MALDI TOF/TOF) available at the Mass Spectrometry Facility of the Department of Chemistry at Louisiana State University. MS samples were prepared by resuspended in methanol at 1 mg/mL concentration and mixed 1:1 (v/v) with DCTB (20 mg/mL in DCM) and also 1:1 (v/v) with CHCA (10 mg/mL in DCM). A 1 µL aliquot of each mixture was deposited on the target. A range of 500-2500 Da was used to collect the spectra and data were analyzed with flexAnalysis 3.3.

Synthesis of Benzyl Fentanyl, Fentanyl, Norfentanyl, Acetyl Benzyl Fentanyl, and Benzoyl Benzyl Fentanyl

Reductive Amination of *tert*-Butyl 4-oxopiperidine-1-carboxylate (N-Boc-4-piperidone)

N-Boc-4-piperidone (4.0 g, 20 mmol) and aniline (4.64 g, 50 mmol) were mixed in 1,2-dichloroethane (50 mL) and then AcOH (1.21 g, 20 mmol) was added. Finally, the reaction mixture was treated with sodium triacetoxyborohydride (6.38 g, 30 mmol). The mixture was stirred at rt

for 24 h. The reaction mixture was quenched by adding 1 N NaOH, and the product was extracted with dichloroethane. The organic layer was dried over $MgSO_4$ and concentrated under vacuum to give either yellow solid or oil. The product was then purified either by recrystallization in hexane or column chromatography using EtOAc: $CHCl_3$ 50:50 to obtain a 90% yield.

Acylation of 1,1-Dimethylethyl 4-(phenylamino)-1-piperidinecarboxylate (1-Boc-4-(phenylamino) piperidine)

1-Boc-4-(phenylamino)piperidine (1.0 g, 3.6 mmol) was dissolved in dichloromethane (15 mL) and Et_3N (1.1 g, 11 mmol) was added. Then propionyl chloride (1.0 g, 11 mmol) was added and the mixture was stirred at rt for 24 h. The reaction mixture was washed with 1 N NaOH (3 X 15 mL) and 5 N NaOH (2 X 15 mL) and extracted with dichloromethane. The organic layer was dried over $MgSO_4$ concentrated under vacuum to give either yellow solid or oil. The product was then purified either by recrystallization in hexane or column chromatography using EtOAc: $CHCl_3$ 50:50 to obtain a 90% yield.

Deprotection of 4-[(1-oxopropyl)phenylamino]-1-piperidinecarboxylic acid, 1,1-dimethylethyl ester (N-Boc norfentanyl)

4-[(1-oxopropyl)phenylamino]-1-piperidinecarboxylic acid, 1,1-dimethylethyl ester (1.0 g, 3 mmol) was dissolved in 3 mL of dry $CHCl_3$, cooled at 0ºC under N_2 atm. Then 10 mL of 2M HCl in ethyl ether were added dropwise. The temperature was kept at 0ºC/6 h, increased to room temperature, and stirred for 18 h. HCl and ether were purged under a current of N_2 with further removal under vacuum. The off-white sticky solid residue was washed with ethyl ether (3 x 20 mL) and dried under vacuum. Yield 94%.

Alkylation of 4-(*N*-Propionylaniline) piperidine (Norfentanyl)

In a 100 mL RBF, norfentanyl (0.5 g, 2.15 mmol) was mixed with K_2CO_3 (0.74 g, 5.38 mmol) in 15 mL of ACN. Then, benzyl bromide (0.38 mL, 3.22 mmol) was added dropwise, and the reaction mixture was stirred for 24 h under refluxing condition. After 24 h, the reaction mixture was filtered,

and solvent was removed under reduced pressure. Several purification techniques such as column chromatography, recrystallization, trituration was performed to purify the product but, in each case, a double substituted product was obtained.

Reductive amination of 1-Benzyl-4-piperidone

1-Benzyl-4-piperidone (4.0 g, 21 mmol) and aniline (4.92 g, 53 mmol) were mixed in 1,2-dichloroethane (50 mL) and then AcOH (1.27 g, 21 mmol) was added. Finally, the reaction mixture was treated with sodium triacetoxyborohydride (6.72 g, 32 mmol). The mixture was stirred at rt for 24 h. The reaction mixture was quenched by adding 1 N NaOH, and the product was extracted with dichloroethane. The organic layer was dried over $MgSO_4$ and concentrated under vacuum to give either yellow solid or oil. The product was then purified either by recrystallization in hexane or column chromatography using EtOAc: $CHCl_3$ 50:50 to obtain a 90% yield.

Acylation of 1-Benzyl-4-(phenylamino) piperidine

1-Benzyl-4-(phenylamino) piperidine (1.0 g, 3.8 mmol) was dissolved in dichloromethane (15 mL) and Et_3N (1.14 g, 11 mmol) was added. Then propionyl chloride (1.04 g, 11 mmol) was added and the mixture was stirred at rt for 24 h. The reaction mixture was washed with 1 N NaOH (3 X 15 mL) and 5 N NaOH (2 X 15 mL) and extracted with dichloromethane. The organic layer was dried over $MgSO_4$ concentrated under vacuum to give either yellow solid or oil. The product was then purified either by recrystallization in hexane or column chromatography using EtOAc: $CHCl_3$ 50:50 to obtain a 90% yield.

Polymer Preparation

Table B.1. Composition of the different MIP

%Template	Bfen (mmol)	EGDMA (mmol)	MAA (mmol)	AIBN (mmol)
0	0	21	5.4	0.54
2	0.54	21	5.4	0.54
4	1.1	21	5.4	0.54
8	2.2	21	5.4	0.54
10	2.7	21	5.4	0.54
20	5.4	21	5.4	0.54

Spectra for Chapter 2

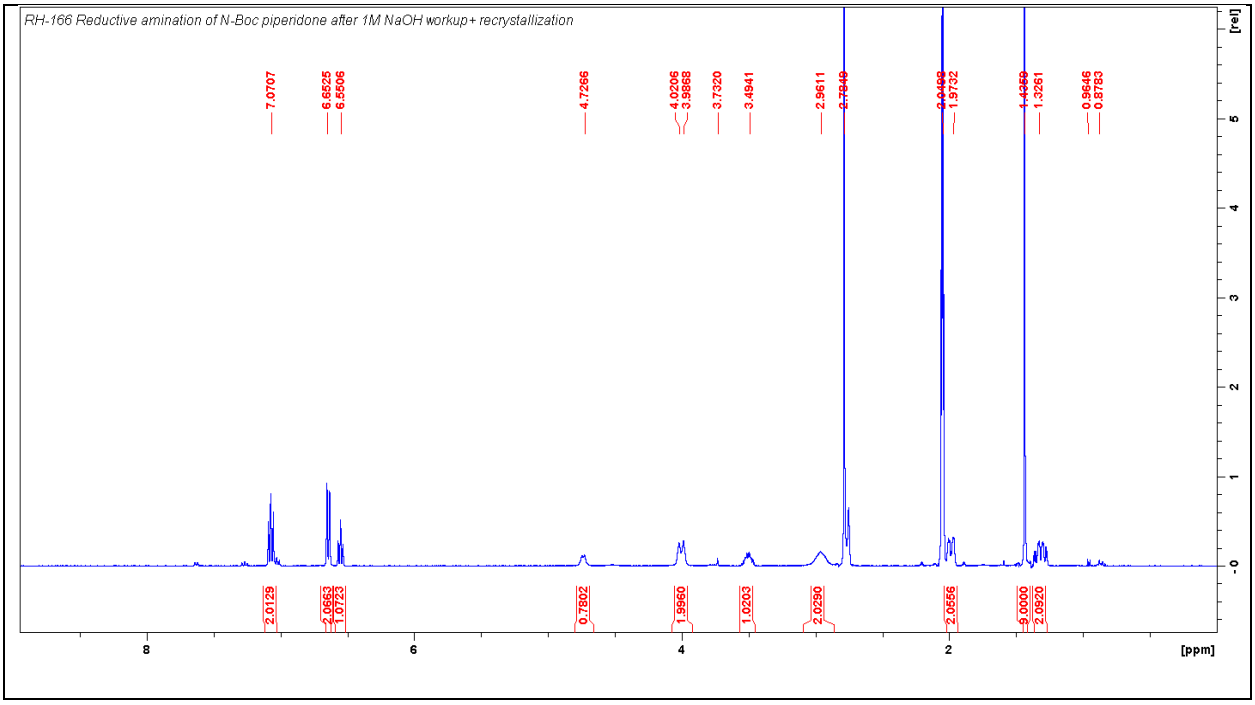

Figure B.1. ^{1}H NMR of reductive amination of N-boc piperidone

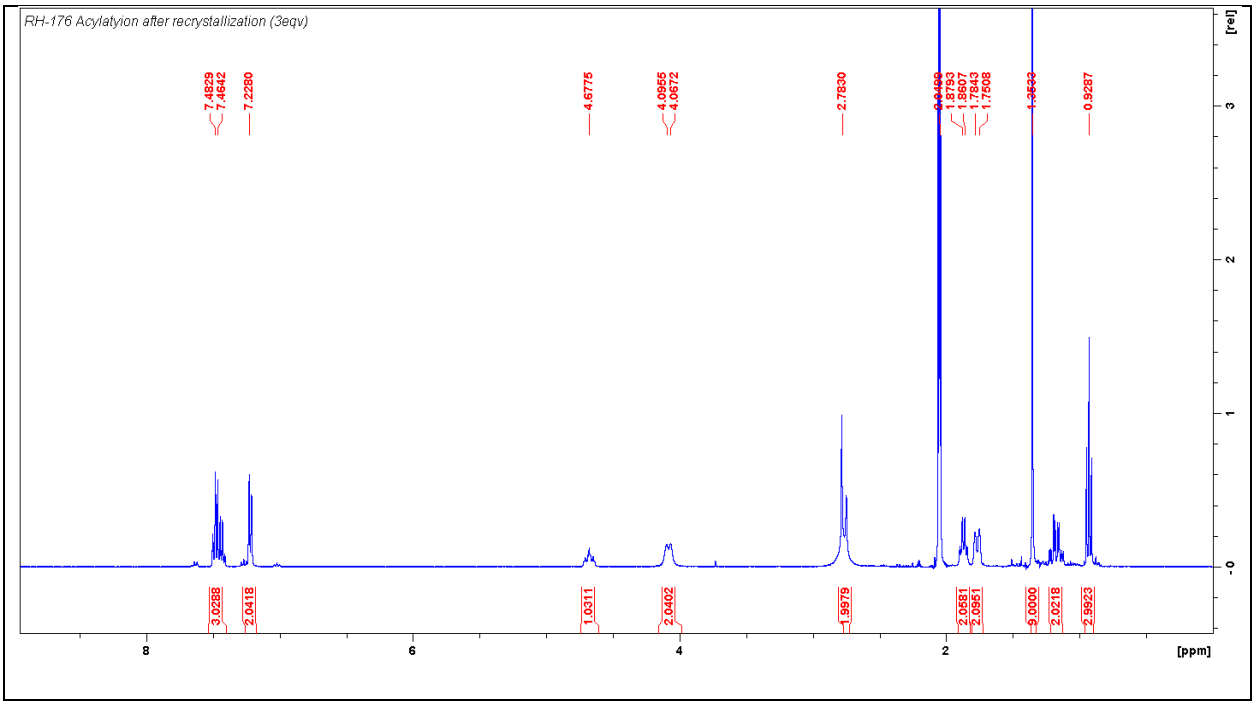

Figure B.2. ^{1}H NMR after acylation reaction of N-boc piperidine

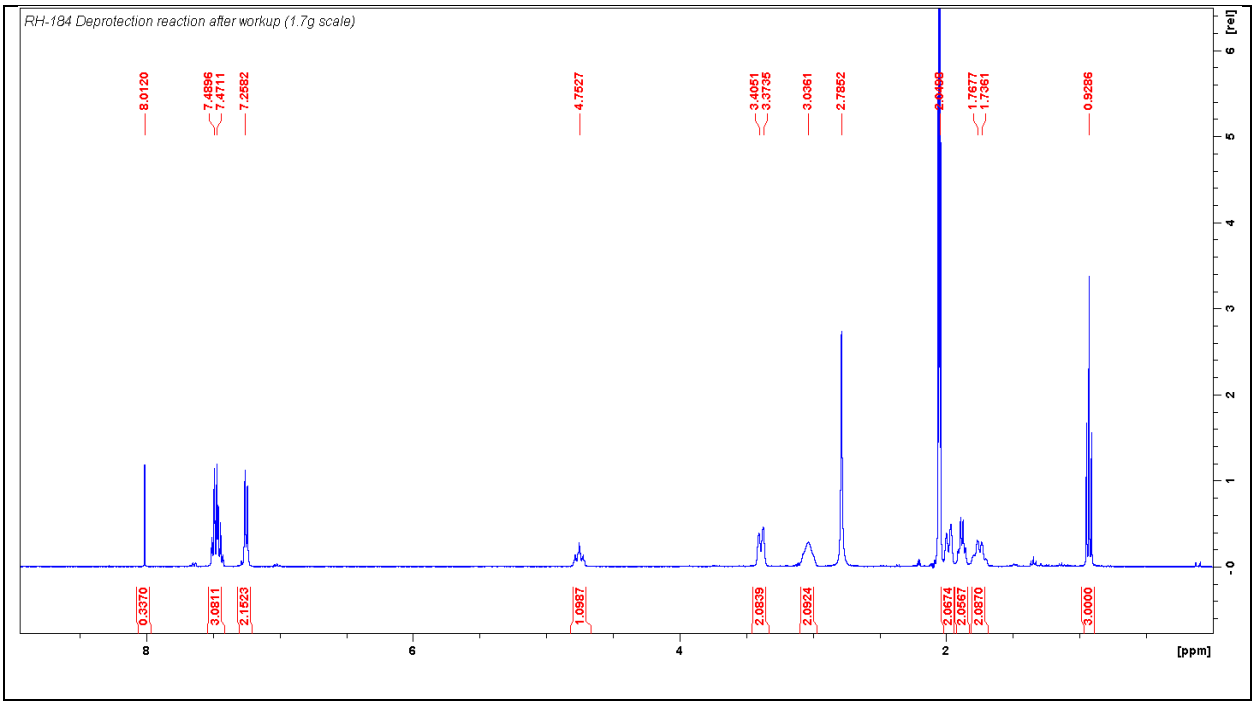

Figure B.3. ^{1}H NMR of norfentanyl

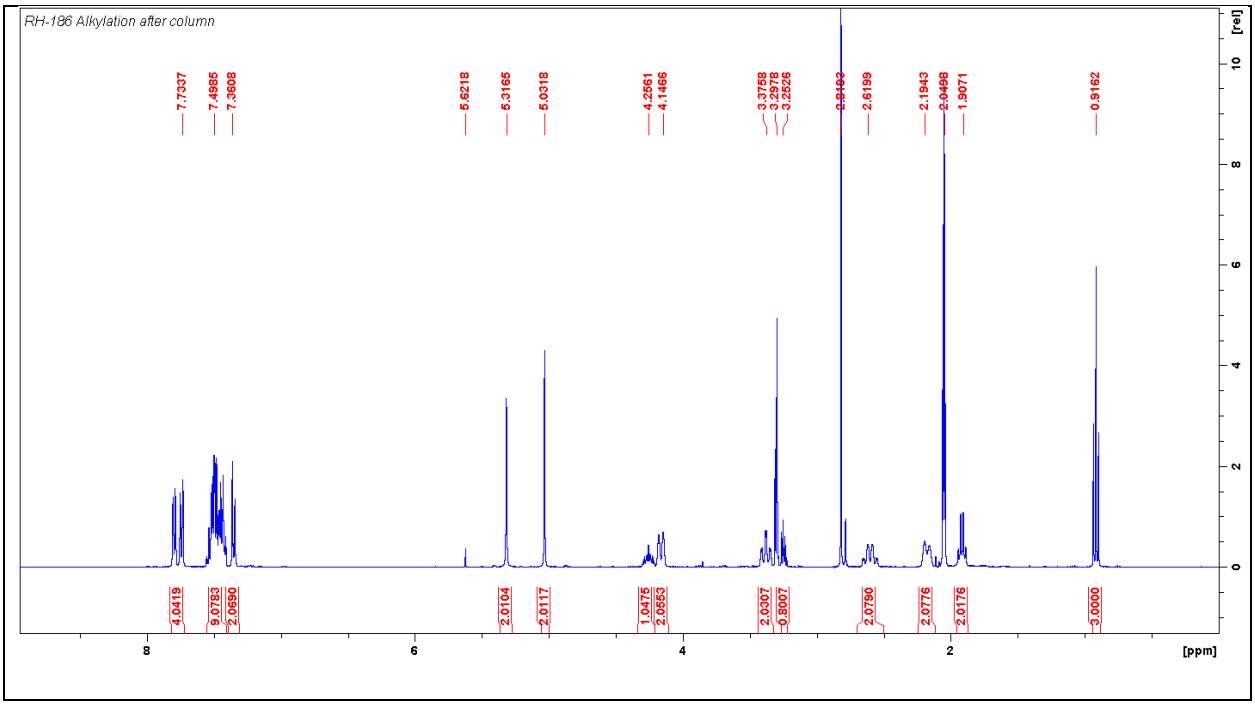

Figure B.4. ^{1}H NMR after alkylation reaction of norfentanyl

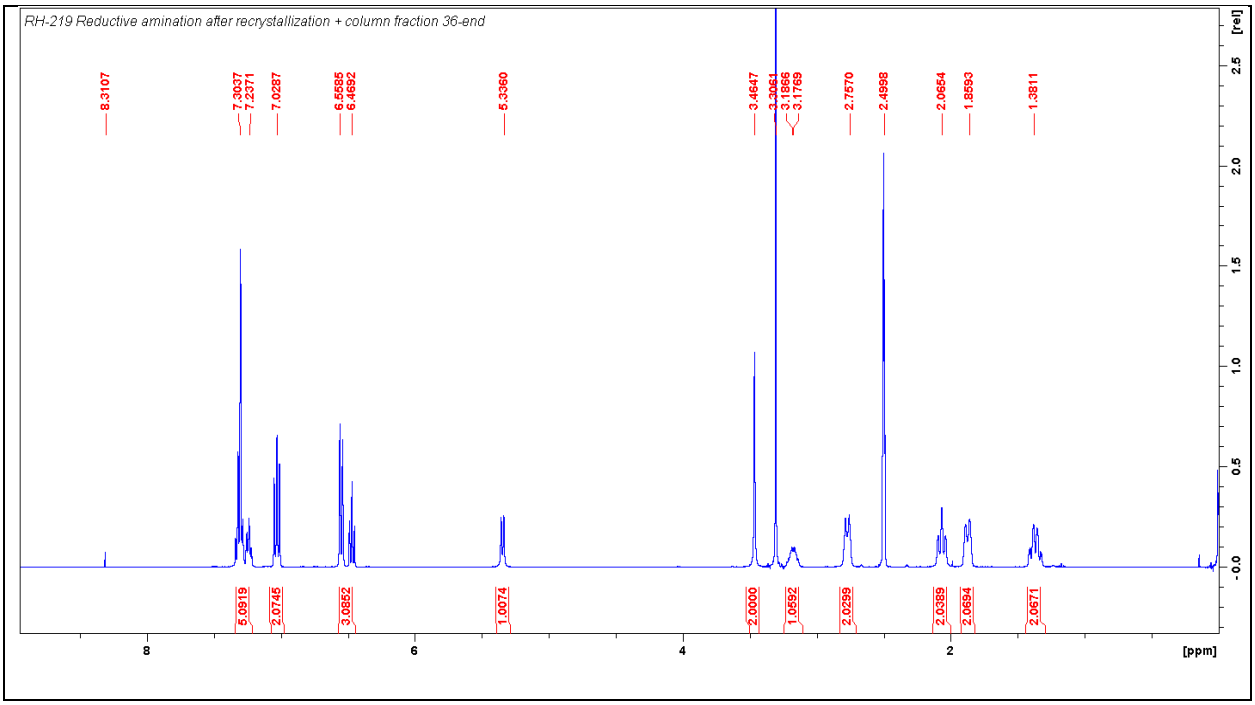

Figure B.5. ^{1}H NMR after reductive amination of 1-benzyl-4-piperidone

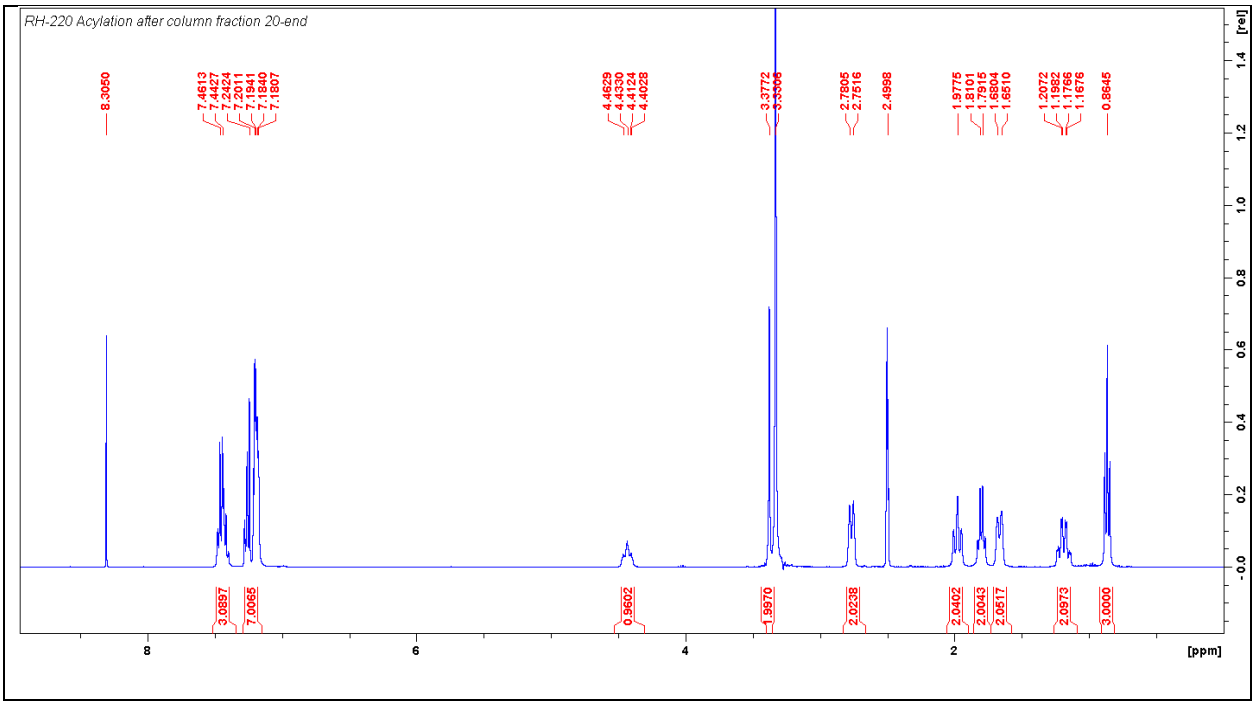

Figure B.6. ^{1}H NMR after acylation reaction of 1-Benzyl-4-(phenylamino) piperidine

Appendix C. Experimental for Chapter 3

Preparation of the Grating Master

Master micrograting molds with gratings 5 μm in width and 10 μm in spacing were prepared by spin-coating 5 μm of negative photoresist SU-8 (MicroChem Corp., Newton, MA) onto a pre-cleaned silicon wafer. The wafer was then placed for UV exposure (Quintel Ultraline 7000 series mask aligner, Morgan Hill, CA), followed by conventional developing and hard-baking processes. The grating master was cut to a size of 1.0 cm^2 and then put in an upside-down orientation in a culture plate. After degassing for 15 minutes in a vacuum, a combination of Sylgard 184 silicone elastomer base and Sylgard 184 silicone elastomer curing agent (10:1, w:w) was carefully poured into the culture dish that contained the template. The elastomer was cured in an oven at a temperature of 80 degrees Celsius for a period of ten hours. Finally, the grating master was removed from the elastomer replica.

Preparation of PBS Buffer

The PBS buffer stock solution was prepared by dissolving NaCl (2.0 g), KCl (0.05 g), Na_2HPO_4 (0.36 g), and KH_2PO_4 (0.06 g) in DI water by using a volumetric flask.

Table C.1. The formulation for the preparation of 250 mL PBS buffer solution

Chemical	Weight (g)	MW	Moles	[mM]
NaCl	2.0	58.5	0.0342	136.75
KCl	0.05	74.5	0.0007	2.68
Na_2HPO_4	0.36	142	0.0025	10.14
KH_2PO_4	0.06	136	0.0004	1.76

Appendix D. Copyright Permissions

Scheme 1.1

Figure 3.7

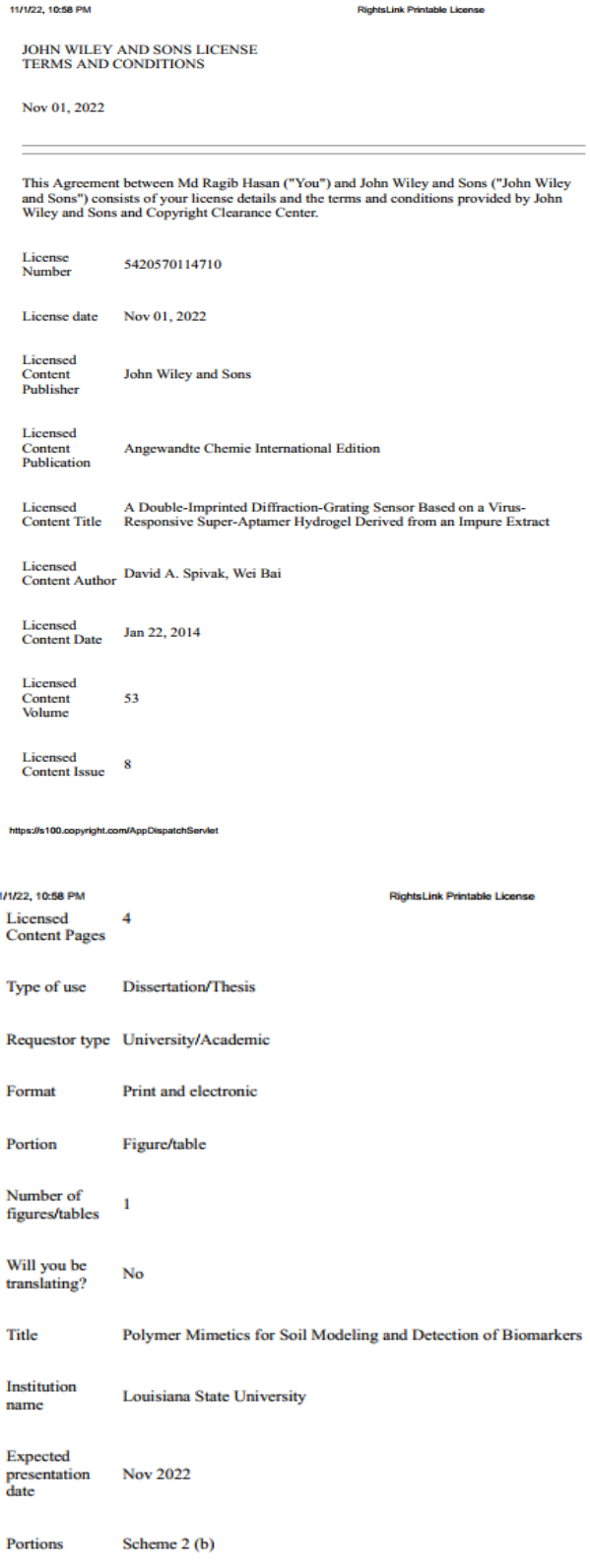

11/1/22, 10:58 PM RightsLink Printable License

JOHN WILEY AND SONS LICENSE
TERMS AND CONDITIONS

Nov 01, 2022

This Agreement between Md Ragib Hasan ("You") and John Wiley and Sons ("John Wiley and Sons") consists of your license details and the terms and conditions provided by John Wiley and Sons and Copyright Clearance Center.

License Number	5420570114710
License date	Nov 01, 2022
Licensed Content Publisher	John Wiley and Sons
Licensed Content Publication	Angewandte Chemie International Edition
Licensed Content Title	A Double-Imprinted Diffraction-Grating Sensor Based on a Virus-Responsive Super-Aptamer Hydrogel Derived from an Impure Extract
Licensed Content Author	David A. Spivak, Wei Bai
Licensed Content Date	Jan 22, 2014
Licensed Content Volume	53
Licensed Content Issue	8

https://s100.copyright.com/AppDispatchServlet

11/1/22, 10:58 PM RightsLink Printable License

Licensed Content Pages	4
Type of use	Dissertation/Thesis
Requestor type	University/Academic
Format	Print and electronic
Portion	Figure/table
Number of figures/tables	1
Will you be translating?	No
Title	Polymer Mimetics for Soil Modeling and Detection of Biomarkers
Institution name	Louisiana State University
Expected presentation date	Nov 2022
Portions	Scheme 2 (b)

References

1. Kopittke, P. M.; Menzies, N. W.; Wang, P.; McKenna, B. A.; Lombi, E., Soil and the intensification of agriculture for global food security. *Environment International* **2019,** *132*, 105078.

2. FAO Statistical Databases. http://apps.fao.org/ (accessed 08/12).

3. FAOSTATE: Land use. https://www.fao.org/faostat/en/#home (accessed 08/12/2022).

4. Verwer, C.; van der Meer, P.; Nabuurs, G.-J. *Review of carbon flux estimates and other greenhouse gas emissions from oil palm cultivation on tropical peatlands-Identifying the gaps in knowledge*; 1566-7197; Alterra: 2008.

5. Kalev, S. D.; Toor, G. S., The composition of soils and sediments. In *Green Chemistry*, Elsevier: 2018; pp 339-357.

6. Plaster, E. J. I., Soil science and management. Delmar Publ.: New York, 1992; pp 340-341.

7. Cranberry Field Decline Information. https://www.bccranberries.com/growers/cranberry-field-decline-information/ (accessed 08/12/2022).

8. Ridgman, W. J., Practical Pedology. By S. G. McRae. 253 pages. Chichester: Ellis Horwood Ltd.1988. Price £35.00 (hard covers). ISBN 0 85312 918 5. *The Journal of Agricultural Science* **1989,** *112* (2), 283-284.

9. Sposito, G., *The Chemistry of Soils*. Second Edition ed.; Oxford University Press: New York, 2008.

10. Howe, J. A.; Smith, A. P., 2 - The soil habitat. In *Principles and Applications of Soil Microbiology (Third Edition)*, Gentry, T. J.; Fuhrmann, J. J.; Zuberer, D. A., Eds. Elsevier: 2021; pp 23-55.

11. Fuhrmann, J. J., 3 - Microbial metabolism. In *Principles and Applications of Soil Microbiology (Third Edition)*, Gentry, T. J.; Fuhrmann, J. J.; Zuberer, D. A., Eds. Elsevier: 2021; pp 57-87.

12. Oliver, J. E., CLIMATE CHANGE AND THE GLOBAL HARVEST: POTENTIAL IMPACTS OF THE GREENHOUSE EFFECT ON AGRICULTURE, by C. Rosenzweig and D. Hillel, Oxford University Press, New York, 1998. No of pages: 324. Price: £49.50, US$65.00. ISBN 0-19-508889-1. *International Journal of Climatology* **2000,** *20* (8), 934-934.

13. Soil Water. https://www.ctahr.hawaii.edu/mauisoil/a_comp03.aspx (accessed 08/14/2022).

14. Modern Soil Microbiology. 2nd Edition ed.; Jan Dirk van Elsas, J. T. T., Janet K. Jansson,

Paola Nannipieri, Ed. CRC Press: 2006.

15. Dunnivant, F. M.; Anders, E., *A basic introduction to pollutant fate and transport: an integrated approach with chemistry, modeling, risk assessment, and environmental legislation*. John Wiley & Sons: 2006.

16. Ehrlich, H. L.; Newman, D. K.; Kappler, A., *Geomicrobiology*. M. Dekker: 2002.

17. Osman, K. T., *Soils: Principles, Properties and Management*. Springer: Berlin, 2012.

18. Rene P. Schwarzenbach, P. M. G., Dieter M. Imboden, *Environmental Organic Chemistry*. Wiley- Interscience: New Jersey, 2003.

19. Gillman, G., Using variable charge characteristics to understand the exchangeable cation status of oxic soils. *Soil Research* **1984,** *22* (1), 71-80.

20. Lattao, C. V., Studies on the Effect of Natural Organic Matter and Hydration on the Sorption and Desorption of Trifluorinated Pesticides. **2009**.

21. Loffredo, E.; Senesi, N., The role of humic substances in the fate of anthropogenic organic pollutants in soil with emphasis on endocrine disruptor compounds. In *Soil and water pollution monitoring, protection and remediation*, Springer: 2006; pp 69-92.

22. MacCarthy, P.; Clapp, C.; Malcolm, R.; Bloom, P. In *Humic substances in soil and crop sciences: selected readings. Proceedings of a symposium cosponsored by the International Humic Substances Society; Chicago, Illinois, 2 December 1985*, Humic substances in soil and crop sciences: selected readings. Proceedings of a symposium cosponsored by the International Humic Substances Society; Chicago, Illinois, 2 December 1985., American Society of Agronomy, Inc.: 1990.

23. Osman, K. T., Plant nutrients and soil fertility management. In *Soils*, Springer: 2013; pp 129-159.

24. Hayes, M. H.; Mylotte, R.; Swift, R. S., Humin: its composition and importance in soil organic matter. *Advances in agronomy* **2017,** *143*, 47-138.

25. Ismail-Meyer, K.; Stolt, M. H.; Lindbo, D. L., Soil organic matter. In *Interpretation of micromorphological features of soils and regoliths*, Elsevier: 2018; pp 471-512.

26. Gunina, A.; Kuzyakov, Y., Sugars in soil and sweets for microorganisms: review of origin, content, composition and fate. *Soil Biology and Biochemistry* **2015,** *90*, 87-100.

27. Kleber, M.; Sollins, P.; Sutton, R., A conceptual model of organo-mineral interactions in soils: self-assembly of organic molecular fragments into zonal structures on mineral surfaces. *Biogeochemistry* **2007,** *85* (1), 9-24.

28. Batjes, N. H., Batjes, NH 1996. Total carbon and nitrogen in the soils of the world. European Journal of Soil Science, 47, 151–163. Reflections by NH Batjes. *European Journal of Soil Science* **2014,** *65* (1), 2-3.

29. Stevenson, F. J., *Humus chemistry: genesis, composition, reactions*. John Wiley & Sons: 1994.

30. Schwedt, G., *The essential guide to environmental chemistry*. John Wiley & Sons Incorporated: 2001.

31. Pachauri, R. K.; Reisinger, A., Climate change 2007. Synthesis report. Contribution of Working Groups I, II and III to the fourth assessment report. **2008**.

32. Canadell, J. G.; Le Quéré, C.; Raupach, M. R.; Field, C. B.; Buitenhuis, E. T.; Ciais, P.; Conway, T. J.; Gillett, N. P.; Houghton, R.; Marland, G., Contributions to accelerating atmospheric CO2 growth from economic activity, carbon intensity, and efficiency of natural sinks. *Proceedings of the national academy of sciences* **2007,** *104* (47), 18866-18870.

33. Trumper, K., *The natural fix?: the role of ecosystems in climate mitigation: a UNEP rapid response assessment*. UNEP/Earthprint: 2009.

34. Mann, L., Changes in soil carbon storage after cultivation. *Soil Science* **1986,** *142* (5), 279-288.

35. Clapp, C.; Hayes, M.; Simpson, A.; Kingery, W., Chemistry of soil organic matter. *Chemical processes in soils* **2005,** *8*, 1-150.

36. Lal, R., Soil carbon sequestration impacts on global climate change and food security. *science* **2004,** *304* (5677), 1623-1627.

37. Zomer, R. J.; Bossio, D. A.; Sommer, R.; Verchot, L. V., Global sequestration potential of increased organic carbon in cropland soils. *Scientific Reports* **2017,** *7* (1), 1-8.

38. Montgomery, D. R., Soil erosion and agricultural sustainability. *Proceedings of the National Academy of Sciences* **2007,** *104* (33), 13268-13272.

39. Pandey, A., *Development of a Tunable Platform for the Study of Geomacromolecular Matrices Using Controlled Radical Polymerization*. Louisiana State University and Agricultural & Mechanical College: 2019.

40. Connell, D. W.; Miller, G. J., *Chemistry and ecotoxicology of pollution*. John Wiley & Sons: 1984; Vol. 65.

41. Berenzen, N.; Kumke, T.; Schulz, H. K.; Schulz, R., Macroinvertebrate community structure in agricultural streams: impact of runoff-related pesticide contamination. *Ecotoxicology and Environmental Safety* **2005,** *60* (1), 37-46.

42. Carson, R., Silent Spring III. *New Yorker* **1962,** *23*.

43. Elliott, J. E.; Harris, M. L.; Wilson, L. K.; Whitehead, P. E.; Norstrom, R. J., Monitoring temporal and spatial trends in polychlorinated dibenzo-p-dioxins (PCDDs) and dibenzofurans (PCDFs) in eggs of great blue heron (Ardea herodias) on the coast of British Columbia, Canada, 1983–1998. *AMBIO: A Journal of the Human Environment* **2001,** *30* (7), 416-428.

44. Bridges, J.; Bridges, O., Integrated risk assessment and endocrine disrupters. *Toxicology* **2004,** *205* (1-2), 11-15.

45. Boxall, A. B.; Hardy, A.; Beulke, S.; Boucard, T.; Burgin, L.; Falloon, P. D.; Haygarth, P. M.; Hutchinson, T.; Kovats, R. S.; Leonardi, G., Impacts of climate change on indirect human exposure to pathogens and chemicals from agriculture. *Environmental health perspectives* **2009,** *117* (4), 508-514.

46. Dolk, H.; Vrijheid, M., The impact of environmental pollution on congenital anomalies. *British Medical Bulletin* **2003,** *68* (1), 25-45.

47. Russel, D. A.; Williams, G. G., History of chemical fertilizer development. *Soil Science Society of America Journal* **1977,** *41* (2), 260-265.

48. Liebig, J. v., Organic chemistry in its applications to agriculture and physiology. **1840**.

49. Soil, U. S. A. R. S.; Division, W. C. R.; Agricultural, T. V. A. O. o.; Development, C., *Superphosphate: its history, chemistry, and manufacture*. Agricultural Research Service, US Depart of Agriculture: 1964.

50. Unsworth, J., History of pesticide use. IUPAC (International Union of Pure and Applied Chemistry). *Mai2010Available online: http://agrochemicals. iupac. org/index. php* **2010**.

51. Rao, N. S.; Baker, B. E., Textile finishes and fluorosurfactants. In *Organofluorine Chemistry*, Springer: 1994; pp 321-338.

52. Cartwright, D., Recent developments in fluorine-containing agrochemicals. *Organofluorine Chemistry* **1994**, 237-262.

53. Channarayappa, C.; Biradar, D., *Soil basics, management, and rhizosphere engineering for sustainable agriculture*. CRC Press: 2018.

54. Pignatello, J. J., Interaction of anthropogenic organic chemicals with organic matter in natural particles. In *Molecular Environmental Soil Science at the Interfaces in the Earth's Critical Zone*, Springer: 2010; pp 181-181.

55. Rezus, Y.; Bakker, H., Observation of immobilized water molecules around hydrophobic groups. *Physical Review Letters* **2007,** *99* (14), 148301.

56. Graber, E.; Tsechansky, L.; Borisover, M., Hydration-assisted sorption of a probe organic compound at different peat hydration levels: the link solvation model. *Environmental science & technology* **2007,** *41* (2), 547-554.

57. Schaumann, G. E.; LeBoeuf, E. J., Glass transitions in peat: their relevance and the impact of water. *Environmental science & technology* **2005,** *39* (3), 800-806.

58. Todoruk, T. R.; Langford, C. H.; Kantzas, A., Pore-scale redistribution of water during wetting of air-dried soils as studied by low-field NMR relaxometry. *Environmental science & technology* **2003,** *37* (12), 2707-2713.

59. Ruggiero, P.; Crecchio, C.; Mininni, R.; Pizzigallo, M., Adsorption of the herbicide acifluorfen on humic acids. *Science of the total environment* **1992,** *123*, 93-100.

60. Hayes, M., Chemical nature and reactivities of soil organic polymers. In *Pollutants in Porous Media*, Springer: 1984; pp 126-142.

61. OECD, T. N., 106: Adsorption–Desorption Using a Batch Equilibrium Method. *Organisation for Economic Co-operation and Development, Paris* **2000**.

62. Bielská, L.; Hovorková, I.; Komprdová, K.; Hofman, J., Variability of standard artificial soils: physico-chemical properties and phenanthrene desorption measured by means of supercritical fluid extraction. *Environmental pollution* **2012,** *163*, 1-7.

63. Martin-Neto, L.; Vieira, E. M.; Sposito, G., Mechanism of atrazine sorption by humic acid: a spectroscopic study. *Environmental Science & Technology* **1994,** *28* (11), 1867-1873.

64. Xing, B., Sorption of naphthalene and phenanthrene by soil humic acids. *Environmental Pollution* **2001,** *111* (2), 303-309.

65. Gunasekara, A. S.; Simpson, M. J.; Xing, B., Identification and characterization of sorption domains in soil organic matter using structurally modified humic acids. *Environmental science & technology* **2003,** *37* (5), 852-858.

66. Cook, R. L., Coupling nmr to nom. *Analytical and bioanalytical chemistry* **2004,** *378* (6), 1484-1503.

67. Xing, B.; Pignatello, J. J.; Gigliotti, B., Competitive sorption between atrazine and other organic compounds in soils and model sorbents. *Environmental science & technology* **1996,** *30* (8), 2432-2440.

68. Xing, B.; Pignatello, J. J., Dual-mode sorption of low-polarity compounds in glassy poly (vinyl chloride) and soil organic matter. *Environmental science & technology* **1997,** *31* (3), 792-799.

69. Guo, X.; Wang, X.; Zhou, X.; Kong, X.; Tao, S.; Xing, B., Sorption of four hydrophobic

organic compounds by three chemically distinct polymers: role of chemical and physical composition. *Environmental science & technology* **2012,** *46* (13), 7252-7259.

70. Karickhoff, S. W.; Brown, D. S.; Scott, T. A., Sorption of hydrophobic pollutants on natural sediments. *Water research* **1979,** *13* (3), 241-248.

71. Grathwohl, P., Influence of organic matter from soils and sediments from various origins on the sorption of some chlorinated aliphatic hydrocarbons: implications on Koc correlations. *Environmental science & technology* **1990,** *24* (11), 1687-1693.

72. Rutherford, D. W.; Chiou, C. T.; Kile, D. E., Influence of soil organic matter composition on the partition of organic compounds. *Environmental science & technology* **1992,** *26* (2), 336-340.

73. Xing, B.; McGill, W. B.; Dudas, M. J., Sorption of α-naphthol onto organic sorbents varying in polarity and aromaticity. *Chemosphere* **1994,** *28* (1), 145-153.

74. Chefetz, B.; Deshmukh, A. P.; Hatcher, P. G.; Guthrie, E. A., Pyrene sorption by natural organic matter. *Environmental science & technology* **2000,** *34* (14), 2925-2930.

75. Chefetz, B.; Xing, B., Relative role of aliphatic and aromatic moieties as sorption domains for organic compounds: a review. *Environmental science & technology* **2009,** *43* (6), 1680-1688.

76. Chen, B.; Xing, B., Sorption and conformational characteristics of reconstituted plant cuticular waxes on montmorillonite. *Environmental science & technology* **2005,** *39* (21), 8315-8323.

77. Cowie, A. L.; Kirschbaum, M. U.; Ward, M., Options for including all lands in a future greenhouse gas accounting framework. *Environmental Science & Policy* **2007,** *10* (4), 306-321.

78. Dunn, A., The chemistry of free radical polymerization G. Moad and DH Solomon. Elsevier Science, Oxford, 1995. pp. xvi+ 408, price£ 75.00, US $120.00 (hardback),£ 38.00 (paperback). ISBN 0-08-042078-8 (hardback), 0-08-042079-6 (paperback). Wiley Online Library: 1997.

79. Coessens, V.; Pintauer, T.; Matyjaszewski, K., Functional polymers by atom transfer radical polymerization. *Progress in polymer science* **2001,** *26* (3), 337-377.

80. Matyjaszewski, K., Atom transfer radical polymerization (ATRP): current status and future perspectives. *Macromolecules* **2012,** *45* (10), 4015-4039.

81. Braunecker, W. A.; Matyjaszewski, K., Controlled/living radical polymerization: Features, developments, and perspectives. *Progress in polymer science* **2007,** *32* (1), 93-146.

82. Chiefari, J.; Chong, Y.; Ercole, F.; Krstina, J.; Jeffery, J.; Le, T. P.; Mayadunne, R. T.; Meijs, G. F.; Moad, C. L.; Moad, G., Living free-radical polymerization by reversible addition−

fragmentation chain transfer: the RAFT process. *Macromolecules* **1998,** *31* (16), 5559-5562.

83. Bertin, D.; Gigmes, D.; Marque, S. R.; Tordo, P., Kinetic subtleties of nitroxide mediated polymerization. *Chemical Society Reviews* **2011,** *40* (5), 2189-2198.

84. Gaynor, S. G.; Wang, J.-S.; Matyjaszewski, K., Controlled radical polymerization by degenerative transfer: effect of the structure of the transfer agent. *Macromolecules* **1995,** *28* (24), 8051-8056.

85. Zhao, Y.; Yu, M.; Fu, X., Photo-cleavage of the cobalt–carbon bond: visible light-induced living radical polymerization mediated by organo-cobalt porphyrins. *Chemical Communications* **2013,** *49* (45), 5186-5188.

86. Takeshima, H.; Satoh, K.; Kamigaito, M., Bio-based functional styrene monomers derived from naturally occurring ferulic acid for poly (vinylcatechol) and poly (vinylguaiacol) via controlled radical polymerization. *Macromolecules* **2017,** *50* (11), 4206-4216.

87. Matyjaszewski, K.; Xia, J., Atom transfer radical polymerization. *Chemical reviews* **2001,** *101* (9), 2921-2990.

88. Rodrigues, P. R.; Vieira, R. P., Advances in atom-transfer radical polymerization for drug delivery applications. *European Polymer Journal* **2019,** *115*, 45-58.

89. Qiu, J.; Matyjaszewski, K., Polymerization of substituted styrenes by atom transfer radical polymerization. *Macromolecules* **1997,** *30* (19), 5643-5648.

90. Kato, M.; Kamigaito, M.; Sawamoto, M.; Higashimura, T., Polymerization of methyl methacrylate with the carbon tetrachloride/dichlorotris-(triphenylphosphine) ruthenium (II)/methylaluminum bis (2, 6-di-tert-butylphenoxide) initiating system: possibility of living radical polymerization. *Macromolecules* **1995,** *28* (5), 1721-1723.

91. Wang, J.-S.; Matyjaszewski, K., Controlled/" living" radical polymerization. Halogen atom transfer radical polymerization promoted by a Cu (I)/Cu (II) redox process. *Macromolecules* **1995,** *28* (23), 7901-7910.

92. Percec, V.; Barboiu, B., " Living" radical polymerization of styrene initiated by arenesulfonyl chlorides and CuI (bpy) nCl. *Macromolecules* **1995,** *28* (23), 7970-7972.

93. Matyjaszewski, K.; Wei, M.; Xia, J.; McDermott, N. E., Controlled/“living” radical polymerization of styrene and methyl methacrylate catalyzed by iron complexes. *Macromolecules* **1997,** *30* (26), 8161-8164.

94. Kotani, Y.; Kamigaito, M.; Sawamoto, M., Living radical polymerization of para-substituted styrenes and synthesis of styrene-based copolymers with rhenium and iron complex catalysts. *Macromolecules* **2000,** *33* (18), 6746-6751.

95. Kotani, Y.; Kamigaito, M.; Sawamoto, M., Re (V)-mediated living radical polymerization of styrene: ReO2I (PPh3) 2/R− I initiating systems. *Macromolecules* **1999,** *32* (8), 2420-2424.

96. Lau, K. H. A.; Ren, C.; Sileika, T. S.; Park, S. H.; Szleifer, I.; Messersmith, P. B., Surface-grafted polysarcosine as a peptoid antifouling polymer brush. *Langmuir* **2012,** *28* (46), 16099-16107.

97. Fantin, M.; Isse, A. A.; Gennaro, A.; Matyjaszewski, K., Understanding the fundamentals of aqueous ATRP and defining conditions for better control. *Macromolecules* **2015,** *48* (19), 6862-6875.

98. Pignatello, J. J.; Xing, B., Mechanisms of slow sorption of organic chemicals to natural particles. *Environmental science & technology* **1995,** *30* (1), 1-11.

99. Wauchope, R. D.; Yeh, S.; Linders, J. B. H. J.; Kloskowski, R.; Tanaka, K.; Rubin, B.; Katayama, A.; Kördel, W.; Gerstl, Z.; Lane, M., Pesticide soil sorption parameters: theory, measurement, uses, limitations and reliability. *Pest management science* **2002,** *58* (5), 419-445.

100. Carmo, A. M.; Hundal, L. S.; Thompson, M. L., Sorption of hydrophobic organic compounds by soil materials: application of unit equivalent Freundlich coefficients. *Environmental Science & Technology* **2000,** *34* (20), 4363-4369.

101. Hennel, J. W.; Klinowski, J., Magic-angle spinning: a historical perspective. *New techniques in solid-state NMR* **2005**, 1-14.

102. Matilainen, A.; Gjessing, E. T.; Lahtinen, T.; Hed, L.; Bhatnagar, A.; Sillanpää, M., An overview of the methods used in the characterisation of natural organic matter (NOM) in relation to drinking water treatment. *Chemosphere* **2011,** *83* (11), 1431-1442.

103. Coats, A.; Redfern, J., Thermogravimetric analysis. A review. *Analyst* **1963,** *88* (1053), 906-924.

104. Mackenzie, R.; Mitchell, B., Differential thermal analysis. A review. *Analyst* **1962,** *87* (1035), 420-434.

105. Jain, P.; Dai, J.; Baker, G. L.; Bruening, M. L., Rapid synthesis of functional polymer brushes by surface-initiated atom transfer radical polymerization of an acidic monomer. *Macromolecules* **2008,** *41* (22), 8413-8417.

106. Key, B. D.; Howell, R. D.; Criddle, C. S., Fluorinated Organics in the Biosphere. *Environmental Science & Technology* **1997,** *31* (9), 2445-2454.

107. Sun, K.; Gao, B.; Ro, K. S.; Novak, J. M.; Wang, Z.; Herbert, S.; Xing, B., Assessment of herbicide sorption by biochars and organic matter associated with soil and sediment. *Environmental Pollution* **2012,** *163*, 167-173.

108. Sun, K.; Keiluweit, M.; Kleber, M.; Pan, Z.; Xing, B., Sorption of fluorinated herbicides to plant biomass-derived biochars as a function of molecular structure. *Bioresource Technology* **2011,** *102* (21), 9897-9903.

109. Keiluweit, M.; Kleber, M., Molecular-Level Interactions in Soils and Sediments: The Role of Aromatic π-Systems. *Environmental Science & Technology* **2009,** *43* (10), 3421-3429.

110. Sheng, G.; Yang, Y.; Huang, M.; Yang, K., Influence of pH on pesticide sorption by soil containing wheat residue-derived char. *Environmental Pollution* **2005,** *134* (3), 457-463.

111. Mikita, M. A.; Steelink, C.; Wershaw, R. L. J. A. C., Carbon-13 enriched nuclear magnetic resonance method for the determination of hydroxyl functionality in humic substances. **1981,** *53* (11), 1715-1717.

112. Hoover, S. R.; Mellon, E. F. J. T. R. J., Effect of acetylation on sorption of water by cellulose. **1947,** *17* (12), 714-716.

113. Simpson, C. J.; Fitzhenry, M. J.; Stamford, N. P. J., Preparation of vinylphenols from 2- and 4-hydroxybenzaldehydes. *Tetrahedron letters* **2005,** *46* (40), 6893-6896.

114. Maercker, A., The wittig reaction. *Organic reactions* **2004,** *14*, 270-490.

115. Fieser, M., *Reagents for organic synthesis*. John Wiley & Sons: 1990; Vol. 2.

116. Taira, S. i.; Danjo, H.; Imamoto, T., A facile synthesis of 2-substituted indoles from (2-aminobenzyl) triphenylphosphonium salts. *Tetrahedron letters* **2002,** *43* (16), 2885-2888.

117. Okuma, K.; Sakai, O.; Shioji, K., Wittig reaction by using DBU as a base. *Bulletin of the Chemical Society of Japan* **2003,** *76* (8), 1675-1676.

118. Hiemenz, P. C.; Lodge, T. P., *Polymer chemistry*. CRC press: 2007.

119. Schneckenburger, T.; Lattao, C.; Pignatello, J. J.; Schaumann, G. E.; Thiele-Bruhn, S.; Cao, X.; Mao, J., Preparation and characterization of humic acid cross-linked with organic bridging groups. *Organic Geochemistry* **2012,** *47*, 132-138.

120. Kuznetsov, P.; Kuznetsova, L., Effect of the mineral components of brown coals on the properties of organic matter in the interaction with solvents. *Solid Fuel Chemistry* **2008,** *42* (6), 373-381.

121. Grote, M.; Klinnert, S.; Bechmann, W., Comparison of degradation state and stability of different humic acids by means of chemolysis with tetramethylammonium hydroxide. *Journal of Environmental Monitoring* **2000,** *2* (2), 165-169.

122. Kok, M. D.; Schouten, S.; Damsté, J. S. S., Formation of insoluble, nonhydrolyzable, sulfur-rich macromolecules via incorporation of inorganic sulfur species into algal carbohydrates.

Geochimica et Cosmochimica Acta **2000,** *64* (15), 2689-2699.

123. Poirier, N.; Derenne, S.; Balesdent, J.; Rouzaud, J.-N.; Mariotti, A.; Largeau, C., Abundance and composition of the refractory organic fraction of an ancient, tropical soil (Pointe Noire, Congo). *Organic Geochemistry* **2002,** *33* (3), 383-391.

124. Piccolo, A.; Conte, P.; Tagliatesta, P., Increased conformational rigidity of humic substances by oxidative biomimetic catalysis. *Biomacromolecules* **2005,** *6* (1), 351-358.

125. Piccolo, A., The supramolecular structure of humic substances. *Soil science* **2001,** *166* (11), 810-832.

126. Kunhi Mouvenchery, Y.; Kučerík, J.; Diehl, D.; Schaumann, G. E., Cation-mediated cross-linking in natural organic matter: a review. *Reviews in Environmental Science and Bio/technology* **2012,** *11* (1), 41-54.

127. Monreal, C. M.; Sultan, Y.; Schnitzer, M., Soil organic matter in nano-scale structures of a cultivated Black Chernozem. *Geoderma* **2010,** *159* (1-2), 237-242.

128. Hao, Y.; Moriya, A.; Maruyama, T.; Ohmukai, Y.; Matsuyama, H., Effect of metal ions on humic acid fouling of hollow fiber ultrafiltration membrane. *Journal of membrane science* **2011,** *376* (1-2), 247-253.

129. Cihlář, Z.; Vojtová, L.; Conte, P.; Nasir, S.; Kučerík, J., Hydration and water holding properties of cross-linked lignite humic acids. *Geoderma* **2014,** *230*, 151-160.

130. Ryabova, I.; Mustafina, G., Modification of coal humic acids with formaldehyde. *Russian journal of applied chemistry* **2003,** *76* (2), 261-263.

131. Li, W.; Wang, J.; Zou, L.; Zhu, S., Synthesis and characterization of potassium humate–acrylic acid–acrylamide hydrogel. *Journal of Polymer Research* **2008,** *15* (6), 435-445.

132. Lu, Y.; Pignatello, J. J., Sorption of apolar aromatic compounds to soil humic acid particles affected by aluminum (III) ion cross-linking. *Journal of Environmental Quality* **2004,** *33* (4), 1314-1321.

133. Minko, S., Grafting on solid surfaces:"grafting to" and "grafting from" methods. In *Polymer surfaces and interfaces*, Springer: 2008; pp 215-234.

134. Roy, D.; Semsarilar, M.; Guthrie, J. T.; Perrier, S., Cellulose modification by polymer grafting: a review. *Chemical Society Reviews* **2009,** *38* (7), 2046-2064.

135. Nebhani, L.; Schmiedl, D.; Barner, L.; Barner-Kowollik, C., Quantification of Grafting Densities Achieved via Modular "Grafting-to" Approaches onto Divinylbenzene Microspheres. *Advanced Functional Materials* **2010,** *20* (12), 2010-2020.

136. Matyjaszewski, K.; Miller, P. J.; Shukla, N.; Immaraporn, B.; Gelman, A.; Luokala, B. B.; Siclovan, T. M.; Kickelbick, G.; Vallant, T.; Hoffmann, H., Polymers at interfaces: using atom transfer radical polymerization in the controlled growth of homopolymers and block copolymers from silicon surfaces in the absence of untethered sacrificial initiator. *Macromolecules* **1999,** *32* (26), 8716-8724.

137. Pyun, J.; Jia, S.; Kowalewski, T.; Patterson, G. D.; Matyjaszewski, K., Synthesis and characterization of organic/inorganic hybrid nanoparticles: kinetics of surface-initiated atom transfer radical polymerization and morphology of hybrid nanoparticle ultrathin films. *Macromolecules* **2003,** *36* (14), 5094-5104.

138. Song, K.; Sandi, G., Characterization of montmorillonite surfaces after organosilane modification. *Clays and Clay Minerals* **2001,** *49* (2), 119-125.

139. Hansson, S.; Trouillet, V.; Tischer, T.; Goldmann, A. S.; Carlmark, A.; Barner-Kowollik, C.; Malmström, E., Grafting efficiency of synthetic polymers onto biomaterials: A comparative study of grafting-from versus grafting-to. *Biomacromolecules* **2013,** *14* (1), 64-74.

140. Hedegaard, H.; Bastian, B. A.; Trinidad, J. P.; Spencer, M.; Warner, M., Drugs most frequently involved in drug overdose deaths: United States, 2011–2016. **2018**.

141. Control, C. f. D.; Prevention, Vital signs: overdoses of prescription opioid pain relievers---United States, 1999--2008. *MMWR. Morbidity and mortality weekly report* **2011,** *60* (43), 1487-1492.

142. Cicero, T. J.; Ellis, M. S.; Surratt, H. L., Effect of abuse-deterrent formulation of OxyContin. *New England Journal of Medicine* **2012,** *367* (2), 187-189.

143. Evans, W. N.; Lieber, E. M.; Power, P., How the reformulation of OxyContin ignited the heroin epidemic. *Review of Economics and Statistics* **2019,** *101* (1), 1-15.

144. Jones, C. M.; Einstein, E. B.; Compton, W. M., Changes in synthetic opioid involvement in drug overdose deaths in the United States, 2010-2016. *Jama* **2018,** *319* (17), 1819-1821.

145. Wide-ranging online data for epidemiologic research (WONDER). http://wonder.cdc.gov (accessed 09/03/2022).

146. Provisional Drug Overdose Death Counts. https://www.cdc.gov/nchs/nvss/vsrr/drug-overdose-data.htm.

147. Rudd, R. A.; Paulozzi, L. J.; Bauer, M. J.; Burleson, R. W.; Carlson, R. E.; Dao, D.; Davis, J. W.; Dudek, J.; Eichler, B. A.; Fernandes, J. C., Increases in heroin overdose deaths—28 states, 2010 to 2012. *Morbidity and Mortality Weekly Report* **2014,** *63* (39), 849.

148. O'Donnell, J. K.; Gladden, R. M.; Seth, P., Trends in deaths involving heroin and synthetic opioids excluding methadone, and law enforcement drug product reports, by census region—

United States, 2006–2015. *Morbidity and Mortality Weekly Report* **2017,** *66* (34), 897.

149. Gladden, R. M.; Martinez, P.; Seth, P., Fentanyl law enforcement submissions and increases in synthetic opioid–involved overdose deaths—27 states, 2013–2014. *Morbidity and Mortality Weekly Report* **2016,** *65* (33), 837-843.

150. National Drug Threat Assessment. https://www.dea.gov/sites/default/files/2020-01/2019-NDTA-final-01-14-2020_Low_Web-DIR-007-20_2019.pdf (accessed 09/03/2022).

151. Paulozzi, L. J.; Xi, Y., Recent changes in drug poisoning mortality in the United States by urban–rural status and by drug type. *Pharmacoepidemiology and drug safety* **2008,** *17* (10), 997-1005.

152. Rigg, K. K.; Monnat, S. M.; Chavez, M. N., Opioid-related mortality in rural America: Geographic heterogeneity and intervention strategies. *International Journal of Drug Policy* **2018,** *57*, 119-129.

153. Smith, C. D.; Fulton, A. C.; Romanczyk, M.; Giordano, B. C.; Katilie, C. J.; DeGreeff, L. E., Detection of N-phenylpropanamide vapor from fentanyl materials by secondary electrospray ionization-ion mobility spectrometry (SESI-IMS). *Talanta Open* **2022,** *5*, 100114.

154. Armenian, P.; Vo, K. T.; Barr-Walker, J.; Lynch, K. L., Fentanyl, fentanyl analogs and novel synthetic opioids: a comprehensive review. *Neuropharmacology* **2018,** *134*, 121-132.

155. Ward, C.; Ward, G. C.; Saidman, L. J., Drug abuse in anesthesia training programs: A survey: 1970 through 1980. *Jama* **1983,** *250* (7), 922-925.

156. Garriott, J. C.; Rodriguez, R.; Di Maio, V. J., A death from fentanyl overdose. *Journal of analytical toxicology* **1984,** *8* (6), 288-289.

157. Rose, P. G.; Macfee, M. S.; Boswell, M. V., Fentanyl transdermal system overdose secondary to cutaneous hyperthermia. *Anesthesia & Analgesia* **1993,** *77* (2), 390-391.

158. Marquardt, K. A.; Steven Tharratt, R., Inhalation abuse of fentanyl patch. *Journal of Toxicology: Clinical Toxicology* **1994,** *32* (1), 75-78.

159. Teske, J.; Weller, J.-P.; Larsch, K.; Tröger, H. D.; Karst, M., Fatal outcome in a child after ingestion of a transdermal fentanyl patch. *International journal of legal medicine* **2007,** *121* (2), 147-151.

160. Wyman, J., Warning against misusing of fentanyl analgesic skin patch. *Food and Drug Administration news release. January* **1994,** *18*.

161. Nonpharmaceutical Fentanyl-Related Deaths --- Multiple States, April 2005--March 2007. https://www.cdc.gov/mmwr/preview/mmwrhtml/mm5729a1.htm (accessed 09/04/2022).

162. Rules - 2016-Notice of Intent: Temporary Placement of Butyryl Fentanyl and Beta-hydroxythiofentanyl into Schedule I. http://www.deadiversion.usdoj.gov/fed regs/rules/2016/fr032316.htm.

163. Tomassoni, A. J.; Hawk, K. F.; Jubanyik, K.; Nogee, D. P.; Durant, T.; Lynch, K. L.; Patel, R.; Dinh, D.; Ulrich, A.; D'Onofrio, G., Multiple fentanyl overdoses—New Haven, Connecticut, June 23, 2016. *Morbidity and Mortality Weekly Report* **2017,** *66* (4), 107.

164. McClain, D. A.; Hug Jr, C. C., Intravenous fentanyl kinetics. *Clinical Pharmacology & Therapeutics* **1980,** *28* (1), 106-114.

165. Silverstein, J. H.; Rieders, M. F.; McMullin, M.; Schulman, S.; Zahl, K., An analysis of the duration of fentanyl and its metabolites in urine and saliva. *Anesthesia and analgesia* **1993,** *76* (3), 618-621.

166. Kram, T. C.; Cooper, D. A.; Allen, A. C., Behind the identification of China White. *Analytical chemistry* **1981,** *53* (12), 1379A-1386A.

167. Hibbs, J.; Perper, J.; Winek, C. L., AN outbreak of designer drug—related deaths in pennsylvania. *Jama* **1991,** *265* (8), 1011-1013.

168. Rogers, J. S.; Rehrer, S. J.; Hoot, N. R., Acetylfentanyl: an emerging drug of abuse. *The Journal of Emergency Medicine* **2016,** *50* (3), 433-436.

169. O'Donnell, J.; Gladden, R. M.; Mattson, C. L.; Kariisa, M., Notes from the field: overdose deaths with carfentanil and other fentanyl analogs detected—10 states, July 2016–June 2017. *Morbidity and Mortality Weekly Report* **2018,** *67* (27), 767.

170. Vardanyan, R. S.; Hruby, V. J., Fentanyl-related compounds and derivatives: current status and future prospects for pharmaceutical applications. *Future medicinal chemistry* **2014,** *6* (4), 385-412.

171. U.S. Overdose Deaths In 2021 Increased Half as Much as in 2020 – But Are Still Up 15%. https://www.cdc.gov/nchs/pressroom/nchs_press_releases/2022/202205.htm (accessed 09/05/2022).

172. Facts about Fentanyl. https://www.dea.gov/resources/facts-about-fentanyl (accessed 09/05/2022).

173. Zhang, Y.; Tangsombatvisit, C.; Yun, C.; Pang, S.; Hooshfar, S.; Wu, A. H.; Lynch, K. L., Development and application of a High-Resolution mass spectrometry method for the detection of fentanyl analogs in urine and serum. *Journal of Mass Spectrometry and Advances in the Clinical lab* **2022,** *26*, 1-6.

174. Vaughan, S. R.; Fulton, A. C.; DeGreeff, L. E., Comparative analysis of vapor profiles of fentalogs and illicit fentanyl. *Analytical and Bioanalytical Chemistry* **2021,** *413* (28), 7055-7062.

175. Kang, M.; Lian, R.; Zhang, X.; Li, Y.; Zhang, Y.; Zhang, Y.; Zhang, W.; Ouyang, Z., Rapid and on-site detection of multiple fentanyl compounds by dual-ion trap miniature mass spectrometry system. *Talanta* **2020,** *217*, 121057.

176. Rittgen, J.; Pütz, M.; Zimmermann, R., Identification of fentanyl derivatives at trace levels with nonaqueous capillary electrophoresis-electrospray-tandem mass spectrometry (MS n, n= 2, 3): Analytical method and forensic applications. *Electrophoresis* **2012,** *33* (11), 1595-1605.

177. Buchalter, S.; Marginean, I.; Yohannan, J.; Lurie, I. S., Gas chromatography with tandem cold electron ionization mass spectrometric detection and vacuum ultraviolet detection for the comprehensive analysis of fentanyl analogues. *Journal of Chromatography A* **2019,** *1596*, 183-193.

178. Sisco, E.; Verkouteren, J.; Staymates, J.; Lawrence, J., Rapid detection of fentanyl, fentanyl analogues, and opioids for on-site or laboratory based drug seizure screening using thermal desorption DART-MS and ion mobility spectrometry. *Forensic Chemistry* **2017,** *4*, 108-115.

179. Smith, M.; Logan, M.; Bazley, M.; Blanchfield, J.; Stokes, R.; Blanco, A.; McGee, R., A Semi-quantitative method for the detection of fentanyl using surface-enhanced Raman scattering (SERS) with a handheld Raman instrument. *Journal of Forensic Sciences* **2021,** *66* (2), 505-519.

180. Suzuki, S., Studies on fentanyl and related compounds: II. Spectrometric discrimination of five monomethylated fentanyl isomers by gas chromatography/Fourier transform-infrared spectrometry. *Forensic Science International* **1989,** *43* (1), 15-19.

181. Moore, J. M.; Allen, A. C.; Cooper, D. A.; Carr, S. M., Determination of fentanyl and related compounds by capillary gas chromatography with electron capture detection. *Analytical chemistry* **1986,** *58* (8), 1656-1660.

182. Lurie, I.; Allen, A., Reversed-phase high-performance liquid chromatographic separation of fentanyl homologues and analogues: II. Variables affecting hydrophobic group contribution. *Journal of Chromatography A* **1984,** *292* (2), 283-294.

183. Lurie, I. S.; Berrier, A. L.; Casale, J. F.; Iio, R.; Bozenko Jr, J. S., Profiling of illicit fentanyl using UHPLC–MS/MS. *Forensic science international* **2012,** *220* (1-3), 191-196.

184. Lin, Y.; Sun, J.; Xiang, X.; Yu, H.; Shao, B.; He, Y., Surfactants directly participate in the molecular recognition for visual and sensitive detection of fentanyl. *Sensors and Actuators B: Chemical* **2022,** *354*, 131215.

185. He, Y.; Liang, J.; Sun, J.; Zhao, X.; Lin, Y.; Shao, B., A Chemically Initiated Electron Exchange Chromogenic Reaction System for Colorimetric Detection of Fentanyl and Norfentanyl.

186. Kangas, M. J.; Symonsbergen, D.; Holmes, A. E., A new possible alternative colorimetric drug detection test for fentanyl. *Organic & Medicinal Chemistry International Journal* **2017,** *4*

(4), 85-87.

187. Glasscott, M. W.; Vannoy, K. J.; Fernando, P. A. I.; Kosgei, G. K.; Moores, L. C.; Dick, J. E., Electrochemical sensors for the detection of fentanyl and its analogs: Foundations and recent advances. *TrAC Trends in Analytical Chemistry* **2020,** *132*, 116037.

188. Wester, N.; Mynttinen, E.; Etula, J.; Lilius, T.; Kalso, E.; Mikladal, B. F.; Zhang, Q.; Jiang, H.; Sainio, S.; Nordlund, D., Single-walled carbon nanotube network electrodes for the detection of fentanyl citrate. *ACS Applied Nano Materials* **2020,** *3* (2), 1203-1212.

189. Ruangyuttikarn, W.; Law, M. Y.; Rollins, D. E.; Moody, D. E., Detection of fentanyl and its analogs by enzyme-linked immunosorbent assay. *Journal of Analytical Toxicology* **1990,** *14* (3), 160-164.

190. Lockwood, T.-L. E.; Vervoordt, A.; Lieberman, M., High concentrations of illicit stimulants and cutting agents cause false positives on fentanyl test strips. *Harm reduction journal* **2021,** *18* (1), 1-9.

191. Krieger, M. S.; Goedel, W. C.; Buxton, J. A.; Lysyshyn, M.; Bernstein, E.; Sherman, S. G.; Rich, J. D.; Hadland, S. E.; Green, T. C.; Marshall, B. D., Use of rapid fentanyl test strips among young adults who use drugs. *International Journal of Drug Policy* **2018,** *61*, 52-58.

192. Park, J. N.; Sherman, S. G.; Sigmund, V.; Breaud, A.; Martin, K.; Clarke, W. A., Validation of a lateral flow chromatographic immunoassay for the detection of fentanyl in drug samples. *Drug and Alcohol Dependence* **2022,** *240*, 109610.

193. Angelini, D. J.; Biggs, T. D.; Maughan, M. N.; Feasel, M. G.; Sisco, E.; Sekowski, J. W., Evaluation of a lateral flow immunoassay for the detection of the synthetic opioid fentanyl. *Forensic science international* **2019,** *300*, 75-81.

194. Liu, L.; Grillo, F.; Canfarotta, F.; Whitcombe, M.; Morgan, S. P.; Piletsky, S.; Correia, R.; He, C.; Norris, A.; Korposh, S., Carboxyl-fentanyl detection using optical fibre grating-based sensors functionalised with molecularly imprinted nanoparticles. *Biosensors and Bioelectronics* **2021,** *177*, 113002.

195. Leenaars, M.; Hendriksen, C. F., Critical steps in the production of polyclonal and monoclonal antibodies: evaluation and recommendations. *Ilar Journal* **2005,** *46* (3), 269-279.

196. Steuer, A. E.; Williner, E.; Staeheli, S. N.; Kraemer, T., Studies on the metabolism of the fentanyl-derived designer drug butyrfentanyl in human in vitro liver preparations and authentic human samples using liquid chromatography-high resolution mass spectrometry (LC-HRMS). *Drug Testing and Analysis* **2017,** *9* (7), 1085-1092.

197. Staeheli, S. N.; Baumgartner, M. R.; Gauthier, S.; Gascho, D.; Jarmer, J.; Kraemer, T.; Steuer, A. E., Time-dependent postmortem redistribution of butyrfentanyl and its metabolites in blood and alternative matrices in a case of butyrfentanyl intoxication. *Forensic science*

international **2016,** *266*, 170-177.

198. Grillo, F. Development of a novel assay for drugs of abuse based on Molecularly Imprinted Polymers as synthetic antibodies. University of Leicester, 2018.

199. BelBruno, J. J., Molecularly imprinted polymers. *Chemical reviews* **2018,** *119* (1), 94-119.

200. Wulff, G., Molecular imprinting in cross-linked materials with the aid of molecular templates—a way towards artificial antibodies. *Angewandte chemie international edition in English* **1995,** *34* (17), 1812-1832.

201. Mosbach, K., Molecular imprinting. *Trends in biochemical sciences* **1994,** *19* (1), 9-14.

202. Andersson, L.; Sellergren, B.; Mosbach, K., Imprinting of amino acid derivatives in macroporous polymers. *Tetrahedron Letters* **1984,** *25* (45), 5211-5214.

203. Wulff, G.; Sarhan, A.; Zabrocki, K., Enzyme-analogue built polymers and their use for the resolution of racemates. *Tetrahedron Letters* **1973,** *14* (44), 4329-4332.

204. Shea, K. J., Molecular imprinting of synthetic network polymers: the de novo synthesis of macromolecular binding and catalytic sites. *Trends Polym. Sci.* **1994,** *2*, 166-173.

205. Panagiotopoulou, M.; Beyazit, S.; Nestora, S.; Haupt, K.; Bui, B. T. S., Initiator-free synthesis of molecularly imprinted polymers by polymerization of self-initiated monomers. *Polymer* **2015,** *66*, 43-51.

206. Crapnell, R. D.; Hudson, A.; Foster, C. W.; Eersels, K.; Grinsven, B. v.; Cleij, T. J.; Banks, C. E.; Peeters, M., Recent advances in electrosynthesized molecularly imprinted polymer sensing platforms for bioanalyte detection. *Sensors* **2019,** *19* (5), 1204.

207. Beyazit, S.; Bui, B. T. S.; Haupt, K.; Gonzato, C., Molecularly imprinted polymer nanomaterials and nanocomposites by controlled/living radical polymerization. *Progress in Polymer Science* **2016,** *62*, 1-21.

208. Moein, M. M.; Abdel-Rehim, A.; Abdel-Rehim, M., Recent applications of molecularly imprinted sol-gel methodology in sample preparation. *Molecules* **2019,** *24* (16), 2889.

209. Branger, C.; Meouche, W.; Margaillan, A., Recent advances on ion-imprinted polymers. *Reactive and Functional Polymers* **2013,** *73* (6), 859-875.

210. Mujahid, A.; Aigner, S.; Dickert, F. L., Micro-structured interdigital capacitors with synthetic antibody receptors for ABO blood-group typing. *Sensors and Actuators B: Chemical* **2017,** *242*, 378-383.

211. Refaat, D.; Aggour, M. G.; Farghali, A. A.; Mahajan, R.; Wiklander, J. G.; Nicholls, I. A.; Piletsky, S. A., Strategies for molecular imprinting and the evolution of MIP nanoparticles as

plastic antibodies—Synthesis and applications. *International journal of molecular sciences* **2019,** *20* (24), 6304.

212. Mosbach, K.; Haupt, K., Some new developments and challenges in non-covalent molecular imprinting technology. *Journal of Molecular Recognition: An Interdisciplinary Journal* **1998,** *11* (1-6), 62-68.

213. Wulff, G., Fourty years of molecular imprinting in synthetic polymers: origin, features and perspectives. *Microchimica acta* **2013,** *180* (15), 1359-1370.

214. Chen, W.; Meng, Z.; Xue, M.; Shea, K. J., Molecular imprinted photonic crystal for sensing of biomolecules. *Molecular Imprinting* **2016,** *4* (1), 1-12.

215. Luliński, P., Molecularly imprinted polymers based drug delivery devices: A way to application in modern pharmacotherapy. A review. *Materials Science and Engineering: C* **2017,** *76*, 1344-1353.

216. Muratsugu, S.; Shirai, S.; Tada, M., Recent progress in molecularly imprinted approach for catalysis. *Tetrahedron Letters* **2020,** *61* (11), 151603.

217. Turiel, E.; Martín-Esteban, A., Molecularly imprinted polymers-based microextraction techniques. *TrAC Trends in Analytical Chemistry* **2019,** *118*, 574-586.

218. Ramanavicius, S.; Jagminas, A.; Ramanavicius, A., Advances in molecularly imprinted polymers based affinity sensors. *Polymers* **2021,** *13* (6), 974.

219. Bräuer, B.; Unger, C.; Werner, M.; Lieberzeit, P. A., Biomimetic sensors to detect bioanalytes in real-life samples using molecularly imprinted polymers: a review. *Sensors* **2021,** *21* (16), 5550.

220. Dery, L.; Zelikovich, D.; Mandler, D., Electrochemistry of Molecular Imprinting of Large Entities. *Current Opinion in Electrochemistry* **2022**, 100967.

221. Hashemi, S. A.; Bahrani, S.; Mousavi, S. M.; Omidifar, N.; Behbahan, N. G. G.; Arjmand, M.; Ramakrishna, S.; Lankarani, K. B.; Moghadami, M.; Firoozsani, M., Graphene-Based Femtogram-Level Sensitive Molecularly Imprinted Polymer of SARS-CoV-2. *Advanced materials interfaces* **2021,** *8* (24), 2101466.

222. Perri, C.; Cennamo, N.; D'Agostino, G.; Arcadio, F.; Chiaretti, G.; Parisio, E. M.; Camarlinghi, G.; Vettori, C.; Di Marzo, F.; Cennamo, R. In *Detection of SARS-CoV-2 by plasmonic optical fibers and molecularly imprinted polymers*, Presented at the 2nd International Electronic Conference on Applied Sciences, 2021.

223. Kempe, M.; Mosbach, K.; Fischer, L., Chiral separation using molecularly imprinted heteroaromatic polymers. *Journal of molecular recognition* **1993,** *6* (1), 25-29.

224. Matsui, J.; Nicholls, I. A.; Takeuchi, T., Molecular recognition in cinchona alkaloid molecular imprinted polymer rods. *Analytica chimica acta* **1998,** *365* (1-3), 89-93.

225. Yu, C.; Mosbach, K., Molecular imprinting utilizing an amide functional group for hydrogen bonding leading to highly efficient polymers. *The Journal of Organic Chemistry* **1997,** *62* (12), 4057-4064.

226. Hart, B. R.; Shea, K. J., Synthetic peptide receptors: Molecularly imprinted polymers for the recognition of peptides using peptide− metal interactions. *Journal of the American Chemical Society* **2001,** *123* (9), 2072-2073.

227. Urraca, J. L.; Hall, A. J.; Moreno-Bondi, M. C.; Sellergren, B., A stoichiometric molecularly imprinted polymer for the class-selective recognition of antibiotics in aqueous media. *Angewandte Chemie* **2006,** *118* (31), 5282-5285.

228. Vasapollo, G.; Sole, R. D.; Mergola, L.; Lazzoi, M. R.; Scardino, A.; Scorrano, S.; Mele, G., Molecularly imprinted polymers: present and future prospective. *International journal of molecular sciences* **2011,** *12* (9), 5908-5945.

229. Sibrian-Vazquez, M.; Spivak, D. A., Characterization of molecularly imprinted polymers employing crosslinkers with nonsymmetric polymerizable groups. *Journal of Polymer Science Part A: Polymer Chemistry* **2004,** *42* (15), 3668-3675.

230. Sibrian-Vazquez, M.; Spivak, D. A., Improving the strategy and performance of molecularly imprinted polymers using cross-linking functional monomers. *The Journal of Organic Chemistry* **2003,** *68* (25), 9604-9611.

231. Spivak, D. A.; Sibrian-Vazquez, M., Development of improved crosslinking monomers for molecularly imprinted materials. *MRS Online Proceedings Library (OPL)* **2002,** *723*.

232. Spivak, D. A.; Sibrian-Vazquez, M., Development of an aspartic acid-based cross-linking monomer for improved bioseparations. *Bioseparation* **2001,** *10* (6), 331-336.

233. Wulff, G.; Vietmeier, J.; Poll, H. G., Enzyme-analogue built polymers, 22. Influence of the nature of the crosslinking agent on the performance of imprinted polymers in racemic resolution. *Die Makromolekulare Chemie: Macromolecular Chemistry and Physics* **1987,** *188* (4), 731-740.

234. Wulff, G.; Vietmeier, J., Enzyme-analogue built polymers, 25. Synthesis of macroporous copolymers from α-amino acid based vinyl compounds. *Die Makromolekulare Chemie: Macromolecular Chemistry and Physics* **1989,** *190* (7), 1717-1726.

235. Sellergren, B., Imprinted polymers with memory for small molecules, proteins, or crystals. *Angewandte Chemie International Edition* **2000,** *39* (6), 1031-1037.

236. Yan, M., *Molecularly imprinted materials: science and technology*. CRC press: 2004.

237. Henderson, G. L., Designer drugs: past history and future prospects. *J Forensic Sci* **1988,** *33* (2), 569-575.

238. Mayer, B. P.; DeHope, A. J.; Mew, D. A.; Spackman, P. E.; Williams, A. M., Chemical attribution of fentanyl using multivariate statistical analysis of orthogonal mass spectral data. *Analytical Chemistry* **2016,** *88* (8), 4303-4310.

239. Simon, R.; Houck, S.; Spivak, D. A., Comparison of particle size and flow rate optimization for chromatography using one-monomer molecularly imprinted polymers versus traditional non-covalent molecularly imprinted polymers. *Analytica chimica acta* **2005,** *542* (1), 104-110.

240. Cheong, S. H.; Rachkov, A. E.; Park, J. K.; Yano, K.; Karube, I., Synthesis and binding properties of a noncovalent molecularly imprinted testosterone-specific polymer. *Journal of Polymer Science Part A: Polymer Chemistry* **1998,** *36* (11), 1725-1732.

241. Sibrian-Vazquez, M.; Spivak, D. A., Molecular imprinting made easy. *Journal of the American Chemical Society* **2004,** *126* (25), 7827-7833.

242. LeJeune, J. P., Design and development of chiral and achiral molecularly imprinted stationary phases. **2010**.

243. Nikhil, B.; Pawan, J.; Nello, F.; Pedro, E., Introduction to biosensors. *Essays Biochem* **2016,** *60* (1), 1-8.

244. Hughes, W. S., The potential difference between glass and electrolytes in contact with the glass. *Journal of the American Chemical Society* **1922,** *44* (12), 2860-2867.

245. Tetyana, P.; Shumbula, P. M.; Njengele-Tetyana, Z., Biosensors: Design, Development and Applications. In *Nanopores*, IntechOpen: 2021.

246. Clark Jr, L. C.; Lyons, C., Electrode systems for continuous monitoring in cardiovascular surgery. *Annals of the New York Academy of sciences* **1962,** *102* (1), 29-45.

247. Li, Y.-C. E.; Lee, I., The current trends of biosensors in tissue engineering. *Biosensors* **2020,** *10* (8), 88.

248. Turner, A. P., Biosensors: sense and sensibility. *Chemical Society Reviews* **2013,** *42* (8), 3184-3196.

249. Newman, J. D.; Turner, A. P., Home blood glucose biosensors: a commercial perspective. *Biosensors and bioelectronics* **2005,** *20* (12), 2435-2453.

250. Malhotra, S.; Verma, A.; Tyagi, N.; Kumar, V., Biosensors: principle, types and applications. *Int. J. Adv. Res. Innov. Ideas Educ* **2017,** *3* (2), 3639-3644.

251. Grieshaber, D.; MacKenzie, R.; Vörös, J.; Reimhult, E., Electrochemical biosensors-sensor principles and architectures. *Sensors* **2008,** *8* (3), 1400-1458.

252. Vo-Dinh, T.; Cullum, B., Biosensors and biochips: advances in biological and medical diagnostics. *Fresenius' journal of analytical chemistry* **2000,** *366* (6), 540-551.

253. Homola, J., Surface plasmon resonance sensors for detection of chemical and biological species. *Chemical reviews* **2008,** *108* (2), 462-493.

254. Bai, W., Bio-imprinted hydro-gels (BIGS) for protein and virus detection. **2014**.

255. Juric, D.; Rohner, N. A.; von Recum, H. A., Molecular imprinting of cyclodextrin supramolecular hydrogels improves drug loading and delivery. *Macromolecular bioscience* **2019,** *19* (1), 1800246.

256. Chaterji, S.; Kwon, I. K.; Park, K., Smart polymeric gels: Redefining the limits of biomedical devices. *Progress in Polymer Science* **2007,** *32* (8), 1083-1122.

257. Li, Z.; Wulf, V.; Wang, C.; Vázquez-González, M.; Fadeev, M.; Zhang, J.; Tian, H.; Willner, I., Molecularly Imprinted Sites Translate into Macroscopic Shape-Memory Properties of Hydrogels. *ACS Applied Materials & Interfaces* **2019,** *11* (37), 34282-34291.

258. Byrne, M. E.; Park, K.; Peppas, N. A., Molecular imprinting within hydrogels. *Advanced drug delivery reviews* **2002,** *54* (1), 149-161.

259. Buwalda, S. J.; Boere, K. W.; Dijkstra, P. J.; Feijen, J.; Vermonden, T.; Hennink, W. E., Hydrogels in a historical perspective: From simple networks to smart materials. *Journal of controlled release* **2014,** *190*, 254-273.

260. Ahmed, E. M., Hydrogel: Preparation, characterization, and applications: A review. *Journal of advanced research* **2015,** *6* (2), 105-121.

261. Willner, I., Stimuli-controlled hydrogels and their applications. *Accounts of Chemical Research* **2017,** *50* (4), 657-658.

262. Byrne, M. E.; Salian, V., Molecular imprinting within hydrogels II: Progress and analysis of the field. *International journal of pharmaceutics* **2008,** *364* (2), 188-212.

263. White, E. M.; Yatvin, J.; Grubbs III, J. B.; Bilbrey, J. A.; Locklin, J., Advances in smart materials: Stimuli-responsive hydrogel thin films. *Journal of Polymer Science Part B: Polymer Physics* **2013,** *51* (14), 1084-1099.

264. Schmaljohann, D., Thermo-and pH-responsive polymers in drug delivery. *Advanced drug delivery reviews* **2006,** *58* (15), 1655-1670.

265. Dong, L.-c.; Hoffman, A. S., A novel approach for preparation of pH-sensitive hydrogels

for enteric drug delivery. *Journal of Controlled Release* **1991,** *15* (2), 141-152.

266. Bjerketorp, J.; Håkansson, S.; Belkin, S.; Jansson, J. K., Advances in preservation methods: keeping biosensor microorganisms alive and active. *Current opinion in biotechnology* **2006,** *17* (1), 43-49.

267. Fandrich, A.; Buller, J.; Memczak, H.; Stöcklein, W.; Hinrichs, K.; Wischerhoff, E.; Schulz, B.; Laschewsky, A.; Lisdat, F., Responsive Polymer-Electrode Interface—Study of its Thermo-and pH-Sensitivity and the Influence of Peptide Coupling. *Electrochimica Acta* **2017,** *229*, 325-333.

268. Hjerten, S.; Liao, J.-L.; Nakazato, K.; Wang, Y.; Zamaratskaia, G.; Zhang, H.-X., Gels mimicking antibodies in their selective recognition of proteins. *Chromatographia* **1997,** *44* (5), 227-234.

269. Cumbo, A.; Lorber, B.; Corvini, P. F.-X.; Meier, W.; Shahgaldian, P., A synthetic nanomaterial for virus recognition produced by surface imprinting. *Nature communications* **2013,** *4* (1), 1-7.

270. Nishino, H.; Huang, C. S.; Shea, K. J., Selective protein capture by epitope imprinting. *Angewandte Chemie* **2006,** *118* (15), 2452-2456.

271. Yang, J.; Liu, L.; Cao, X., Combination of bioimprinting and silane precursor alkyls improved the activity of sol–gel-encapsulated lipase. *Enzyme and microbial technology* **2010,** *46* (3-4), 257-261.

272. Liu, C.; Kubo, T.; Otsuka, K., Specificity recognition for a target protein, cytochrome c using molecularly imprinted hydrogels. *Journal of Materials Chemistry B* **2022**.

273. Zhou, Q.; Xu, Z.; Liu, Z., Molecularly Imprinting–Aptamer Techniques and Their Applications in Molecular Recognition. *Biosensors* **2022,** *12* (8), 576.

274. Bai, W.; Gariano, N. A.; Spivak, D. A., Macromolecular amplification of binding response in superaptamer hydrogels. *Journal of the American Chemical Society* **2013,** *135* (18), 6977-6984.

275. Bai, W.; Spivak, D. A., A double-imprinted diffraction-grating sensor based on a virus-responsive super-aptamer hydrogel derived from an impure extract. *Angewandte Chemie International Edition* **2014,** *53* (8), 2095-2098.

276. Gebert, L. F.; MacRae, I. J., Regulation of microRNA function in animals. *Nature reviews Molecular cell biology* **2019,** *20* (1), 21-37.

277. Dong, H.; Lei, J.; Ding, L.; Wen, Y.; Ju, H.; Zhang, X., MicroRNA: function, detection, and bioanalysis. *Chemical reviews* **2013,** *113* (8), 6207-6233.

278. Esteller, M., Non-coding RNAs in human disease. *Nature reviews genetics* **2011,** *12* (12),

861-874.

279. Tavazoie, S. F.; Alarcón, C.; Oskarsson, T.; Padua, D.; Wang, Q.; Bos, P. D.; Gerald, W. L.; Massagué, J., Endogenous human microRNAs that suppress breast cancer metastasis. *Nature* **2008,** *451* (7175), 147-152.

280. Lu, J.; Getz, G.; Miska, E. A.; Alvarez-Saavedra, E.; Lamb, J.; Peck, D.; Sweet-Cordero, A.; Ebert, B. L.; Mak, R. H.; Ferrando, A. A., MicroRNA expression profiles classify human cancers. *nature* **2005,** *435* (7043), 834-838.

281. Chen, M.; Calin, G. A.; Meng, Q. H., Circulating microRNAs as promising tumor biomarkers. *Advances in clinical chemistry* **2014,** *67*, 189-214.

282. Jenike, A. E.; Halushka, M. K., miR-21: a non-specific biomarker of all maladies. *Biomarker Research* **2021,** *9* (1), 1-7.

283. Feng, Y.-H.; Tsao, C.-J., Emerging role of microRNA-21 in cancer. *Biomedical reports* **2016,** *5* (4), 395-402.

284. Ye, J.; Xu, M.; Tian, X.; Cai, S.; Zeng, S., Research advances in the detection of miRNA. *Journal of pharmaceutical analysis* **2019,** *9* (4), 217-226.

285. Longo, L.; Scorrano, S.; Vasapollo, G., RNA nucleoside recognition by phthalocyanine-based molecularly imprinted polymers. *Journal of polymer research* **2010,** *17* (5), 683-687.

286. Hashemi-Moghaddam, H.; Kashi, M.; Mowla, S. J.; Nouraee, N., Separation of microRNA 21 as a cancer marker from glioblastoma cell line using molecularly imprinted polymer coated on silica nanoparticles. *Journal of separation science* **2016,** *39* (18), 3564-3570.

287. Zhang, Z.; Liu, J., Molecular imprinting with functional DNA. *Small* **2019,** *15* (26), 1805246.

288. Famulok, M.; Hartig, J. S.; Mayer, G., Functional aptamers and aptazymes in biotechnology, diagnostics, and therapy. *Chemical reviews* **2007,** *107* (9), 3715-3743.

289. Wilson, D. S.; Szostak, J. W., In vitro selection of functional nucleic acids. *Annual review of biochemistry* **1999,** *68* (1), 611-647.

290. Tuerk, C.; Gold, L., Systematic evolution of ligands by exponential enrichment: RNA ligands to bacteriophage T4 DNA polymerase. *science* **1990,** *249* (4968), 505-510.

291. Ellington, A. D.; Szostak, J. W., In vitro selection of RNA molecules that bind specific ligands. *nature* **1990,** *346* (6287), 818-822.

292. Xiong, X.; Wu, C.; Zhou, C.; Zhu, G.; Chen, Z.; Tan, W., Responsive DNA-based hydrogels and their applications. *Macromolecular rapid communications* **2013,** *34* (16), 1271-

1283.

293. Kahn, J. S.; Hu, Y.; Willner, I., Stimuli-responsive DNA-based hydrogels: from basic principles to applications. *Accounts of chemical research* **2017,** *50* (4), 680-690.

294. Iqbal, S.; Ahmed, F.; Xiong, H., Responsive-DNA hydrogel based intelligent materials: Preparation and applications. *Chemical Engineering Journal* **2021,** *420*, 130384.

295. Si, Y.; Xu, L.; Wang, N.; Zheng, J.; Yang, R.; Li, J., Target microRNA-responsive DNA hydrogel-based surface-enhanced Raman scattering sensor arrays for microRNA-marked cancer screening. *Analytical chemistry* **2020,** *92* (3), 2649-2655.

296. Zhao, Y.; Zhao, X.; Tang, B.; Xu, W.; Li, J.; Hu, J.; Gu, Z., Quantum-dot-tagged bioresponsive hydrogel suspension array for multiplex label-free DNA detection. *Advanced Functional Materials* **2010,** *20* (6), 976-982.

297. Tierney, S.; Stokke, B. T., Development of an oligonucleotide functionalized hydrogel integrated on a high resolution interferometric readout platform as a label-free macromolecule sensing device. *Biomacromolecules* **2009,** *10* (6), 1619-1626.

298. Ogiso, M.; Minoura, N.; Shinbo, T.; Shimizu, T., Detection of a specific DNA sequence by electrophoresis through a molecularly imprinted polymer. *Biomaterials* **2006,** *27* (22), 4177-4182.

299. Wang, X.; Liu, X.; Wang, X., Hydrogel diffraction grating as sensor: A tool for studying volume phase transition of thermo-responsive hydrogel. *Sensors and Actuators B: Chemical* **2014,** *204*, 611-616.

300. Wang, X.; Wang, X., Aptamer-functionalized hydrogel diffraction gratings for the human thrombin detection. *Chemical Communications* **2013,** *49* (53), 5957-5959.

301. Ye, G.; Wang, X., Glucose sensing through diffraction grating of hydrogel bearing phenylboronic acid groups. *Biosensors and Bioelectronics* **2010,** *26* (2), 772-777.

302. Bounds, C. O.; Upadhyay, J.; Totaro, N.; Thakuri, S.; Garber, L.; Vincent, M.; Huang, Z.; Hupert, M.; Pojman, J. A., Fabrication and characterization of stable hydrophilic microfluidic devices prepared via the in situ tertiary-amine catalyzed michael addition of multifunctional thiols to multifunctional acrylates. *ACS applied materials & interfaces* **2013,** *5* (5), 1643-1655.

303. Rizzi, G.; Dufva, M.; Hansen, M. F., Two-dimensional salt and temperature DNA denaturation analysis using a magnetoresistive sensor. *Lab on a Chip* **2017,** *17* (13), 2256-2263.

304. Hebert, B. L., Molecularly Imprinted Polymers for Enantiomer Separations and Biomolecular Sensors. **2016**.

Vita

Md Ragib Hasan was born in Bangladesh and completed his bachelor's and master's in Applied Chemistry and Chemical Engineering from the University of Dhaka. During his master's thesis, he worked on the comparison of the structural, magnetic, and transport properties of holmium substituted cobalt ferrite and magnesium ferrite in collaboration with the Atomic Energy Centre, Dhaka under the supervision of Dr. Rafiqul Islam and co-supervision of Dr. Muhammad Nazrul Islam Khan. Ragib worked as an Analytical Chemist at the Bangladesh Material Testing Laboratory Ltd. for nine months. Then he moved to LSU to pursue his Ph.D. in Chemistry in Fall 2017 and joined Dr. David Spivak's research group with a focus in Polymer Chemistry. During the doctoral studies, Ragib worked on several projects including the sorption behavior of agricultural chemicals with the natural mimics of soil, molecularly imprinted polymers for the detection of fentanyl, and imprinted hydrogel for microRNA detection. Ragib has presented several talks and posters at national and regional conferences. Ragib taught several semesters of general, organic, and advanced organic and inorganic laboratories at LSU. Ragib served as an executive committee member of Macromolecular Studies Graduate Students Association, Bangladeshi Students Association at LSU, and volunteered in chemistry demonstrations and outreach events.